TARGETED AND CONTROLLED DELIVERY OF THERAPEUTIC AGENTS USING POLYMERIC MATERIALS: HYDROGELS, NANOFIBERS, NANOGELS AND MICELLES

by
Ismail Altınbaşak
B.S., Chemistry, Boğaziçi University, 2009
M.S., Chemistry, Boğaziçi University, 2015

Submitted to the Institute for Graduate Studies in
Science and Engineering in partial fulfillment of
the requirements for the degree of
Doctor of Philosophy

Graduate Program in Chemistry
Boğaziçi University
2023

ACKNOWLEDGEMENTS

It feels like just yesterday when I asked Professor Amitav Sanyal if I could be a Ph.D. student in their lab at the end of my first year as an MSc student. Many MSc students in the university, including myself, ask the same question: "what is the next step ?" Today, when I consider my choice between pursuing a Ph.D. at the Sanyal Group or abroad and working in the industry, I feel I made the best decision. Nevertheless, I am thrilled to be working at one of the best labs in the world with two wonderful people as my supervisors. Now I am about to submit my doctoral thesis and conclude this 6-year chapter of my life. Science taught me that reactions don't always go as planned, just like life. However, after short breaks on those stubborn projects and brain storming with friends and coworkers, I always regain my determination and excitement to go back and start over. Without these people and a pleasant laboratory environment, finishing this thesis would have been more challenging. I thus used this area as an opportunity to express my gratitude for these lovely folks in a few words.

First and foremost, I would like to express my sincere gratitude to my thesis supervisor. I am genuinely thankful for his motivation which directs me in academic life. I admire the way he treated my silly ideas throughout my undergraduate work in his lab and the encouragement he gave them. I appreciate his confidence in me since it motivated me to pursue a master's in chemistry. He provided unending guidance and support for my master's projects, which inspired my Ph.D. application. The most significant benefit of this Ph.D. opportunity was learning from different perspectives, which in my case, resulted in challenging but thoughtfully planned research projects. To my Ph.D. advisor, I wish to express my gratitude to Prof. Dr. Amitav Sanyal for letting me do my research on this team. Despite having a full schedule, Amitav always tried to make time for suggestions, ideas, and creative solutions to projects that seemed stuck and inspired me to face new challenges.

Secondly, I would like to thank my thesis supervisor Prof. Rana Sanyal. I still recall the day I went to her office to request permission to work as an undergraduate student at Sanyal Group. Even though she didn't regularly meet me in the laboratory, she described my weaknesses as a researcher on the day I began to understand her. She is the one who always

makes the harshest criticisms, and those became my most important guidance throughout the Ph.D. and helped me to shape and refşne my research abilities. Rana Sanyal deserves my tremendous gratitude for teaching us the real purpose of scientists and their science. Although it seems impossible to reach her level in the future for most of the Ph.D. students, including myself, now we know how much work it will take to become an outstanding scientist.

I also want to thank my jury member, Assist. Prof. Özgül Gök and Assist. Prof. Nergiz Cengiz for her valuable revisions and help in improving my thesis. When I joined the Sanyal Group, I was fortunate to work with a well-qualified group of Ph.D. students, including Özgül and Nergis. Then, I was asking to them how to set reactions; now, I am asking how to improve my thesis. I humbly believe that a research group can be kept alive and strong thanks to such enthusiastic researchers willing to help younglings.

Furthermore, this dissertation would not have reached its current quality without suggestions from my jury member: Assoc. Prof. Oktay Demircan and Prof. İlknur Doğan. I appreciate you taking the time to read this dissertation in-depth and providing me with the tools to elevate it to the next level.

I would like to extend my deepest gratitude to my collaborators, Prof. Rabah Boukherroub and Prof. Sabine Szunerits, for their invaluable contributions to my research. Their expertise in the area of graphene oxide helped me to finish one chapter of this dissertation. I would also like to thank another collaborator, Prof. Mark Grinstaff, for his contribution to another chapter of this dissertation. His expertise, insight, and guidance have been instrumental in helping me to elevate the level of my research. I would also like to thank Prof. Aaron Colby for his assistance with the experiments in this chapter.

An academic research group is perhaps one of the places with the highest employee rotation; people around you periodically change. Nonetheless, there are always wonderful people who help me with my projects and accompany me in the laboratory. Sedef is one among them, and I can't express how valuable her assistance has been to me. She completed the drug analysis for most of my projects, allowing me to focus on other things. Therefore,

thank you very much, Sedef. Then, Ali came to the laboratory and took care of duties from Sedef. I want to appreciate his efforts in helping me with the analysis. However, he also became a very good company to me during the launches and our melancholy conversations with Tugay. At this point, I also want to thank him as well for all the game nights, gym mornings, and the launch times when we can't decide what to eat. Another great person Salli deserves these lines. She companied me for years in the teaching lab under our beloved instructor Özge Akdeniz. She also did all of my cell studies and helped me finalize most of the thesis topic. Thank you very much, Salli.

I want to express my sincere appreciation to my former and current colleagues (Mehmet, Burcu, Sadık, Buğra, Özlem, Tuğçe, Laura, Yavuz, Tuba, Nazli, Bianka, Merve, yağmur, Hamida, Başak, Merve, Filiz, Aysun, Büşra, Damla, Enfal, Nora, Sinem, Meltem, Altan, and Ruveyda) for all the hilarious moments both in and outside of the lab. Whether we were working on group projects, sharing ideas and resources, or just taking breaks to de-stress, I always felt welcome and supported. Your friendship and camaraderie meant so much to me during this journey, and I am deeply grateful for your presence in my life. Thank you for being such an important part of my academic experience."

I would like to thank the Presidency of Republic of Turkey Directorate of Strategy and Budget for infrastructure grant no. 2009K120520, RS Research and the European Union Marie Sklodowska-Curie action (H2020-MSCA-RISE-2015, PANG-690836) for financial assistance for the work reported in this thesis.

I am deeply grateful to my wife, Ece, for her unwavering support and encouragement throughout my studies. She has been a constant source of strength and motivation, and I could not have achieved this degree without her love and support. Thank you for being my partner in every sense of the word and for always believing in me. I had a really chaotic and disorganized life before living together due to my horrific time management and midnight living routine. She pulled me out of this chaos and helped me to live a more organized life. She never stopped to use her magic to make my struggles in my Ph.D. disappear and replace them with a big smile. Your love and support mean everything to me.

ABSTRACT

TARGETED AND CONTROLLED DELIVERY OF THERAPEUTIC AGENTS USING POLYMERIC MATERIALS: HYDROGELS, NANOFIBERS, NANOGELS AND MICELLES

Stimuli-responsive polymeric materials have emerged as attractive platforms for controlled drug delivery applications. In this thesis, photothermally active and pH-responsive nanofibers were fabricated for the triggered release of antibiotics and chemotherapeutic drugs, respectively. Alternatively, Redox-responsive hydrogels were designed for therapeutic protein delivery. Additionally, nanogels and micelles were synthesized for controlled and targeted delivery of chemotherapeutic agents. In the first part, reduced graphene-oxide-embedded poly(acrylic acid) nanofibers were prepared for the on-demand release of antibiotics for local infections. Ampicillin and cefepime were loaded to nanofibers, and E. coli K12 and S. epidermis bacterial strains were eradicated with photothermally released antibiotics. In the second part, pH-responsive nanofiber buttresses were fabricated using an acrylate-based copolymer containing acid-sensitive hydrolyzable hydrophobic side chains. Doxorubicin and docetaxel were loaded into the nanofiber buttresses, and selective drug release was observed in an acidic environment. In the third part, fast-forming dissolvable hydrogels were synthesized by crosslinking maleimide-terminated disulfide-containing PEG-based polymer. Various macromolecules were loaded into the hydrogels, and slow and on-demand release under a reductive environment was accomplished. In the fourth part, redox-responsive nanogels were fabricated using self-assembly and subsequent crosslinking of copolymers containing disulfide-linked maleimide side chains. Nanogels were loaded with docetaxel, and their surface was modified with a peptide-based targeting ligand. Enhanced cytotoxicity and internalization of targeted drug-loaded nanogels were observed. In the last part of the thesis, drug-loaded and targeted pH-responsive micellar structures were fabricated using a diblock copolymer composed of 5-fluorouracil and PEG-methacrylate-based blocks. Targeted dual-drug-containing micelles exhibited enhanced toxicity and cell internalization toward oral squamous carcinoma cells.

ÖZET

TERAPÖTİK AJANLARIN POLİMERİK MALZEMELER KULLANARAK HEDEFLİ VE KONTROLLÜ SALINIMI: HİDROJELLER, NANOLİFLER, NANOJELLER VE MİSELLER

Uyaranlara duyarlı polimerik malzemeler, kontrollü ilaç verme uygulamaları için ilgi çekici platformlar olarak ortaya çıkmıştır. Bu tezde, sırasıyla antibiyotiklerin ve kemoterapötik ilaçların bir uyarana cevap olarak meydana gelen salınımı için fototermal olarak aktif ve pH'a duyarlı nanolifler üretildi. Alternatif bir platform olarak, terapötik protein iletimi için redoksa duyarlı hidrojeller tasarlandı. Ek olarak, kemoterapötik ajanların kontrollü ve hedefli iletimi için nanojeller ve miseller sentezlendi. İlk bölümde, bölgesel enfeksiyonlar için kontrol edilebilir antibiyotik salınımı için indirgenmiş grafen oksit gömülü poli (akrilik asit) nanolifler hazırlandı. Ampisilin ve sefepim nanoliflere yüklendi ve *E. coli* K12 ve *S. epidermis* bakteri varyantları fototermal olarak salınan antibiyotiklerle yok edildi. İkinci bölümde, aside duyarlı hidrolize edilebilir hidrofobik yan zincirler içeren akrilat bazlı bir kopolimer kullanılarak pH'a duyarlı nanofiberler üretildi. Nanoliflere doksorubisin ve dosetaksel yüklendi ve asidik ortamda seçici ilaç salımı gözlendi. Üçüncü bölümde, uçlarında maleimid bulunan ve disülfür içeren PEG bazlı polimer çapraz bağlanarak hızlı oluşan ve hızlı çözünebilen hidrojeller sentezlendi. Hidrojellere çeşitli makromoleküller yüklendi ve indirgeyici bir ortam altında yavaş ve kontrollü salınım sağlandı. Dördüncü bölümde, redoks duyarlı nanojeller, belirli bir sıcaklıkta kendi kendine bir araya gelen, disülfid bağı ve maleimid yan zincirleri içeren kopolimerlerin çapraz bağlanmasıyla üretildi. Nanojeller, docetaxel ile yüklendi ve yüzeyleri peptit bazlı bir hedefleme ligandı ile modifiye edildi. Hedeflenen ilaç yüklü nanojellerde yüksek sitotoksisite ve hücre içerisine giriş gözlemlendi. Tezin son bölümünde, 5-florourasil ve PEG-metakrilat bazlı bloklardan oluşan bir diblok kopolimer kullanılarak ilaç yüklü ve hedeflenen pH'a duyarlı misel yapılar üretildi. Hedeflenen ikili ilaç içeren miseller, oral skuamöz karsinom hücrelerine karşı yüksek sitotoksisite ve hücre içerisine giriş sergiledi.

TABLE OF CONTENTS

ACKNOWLEDGEMENTS iii
ABSTRACT vi
ÖZET vii
LIST OF FIGURES xiii
LIST OF TABLES xxv
LIST OF ACRONYMS/ABBREVIATIONS xxvi
1. INTRODUCTION 1
1.1. Smart Polymeric Materials for Drug Delivery 1
1.2. Stimuli-Responsive Polymeric Materials 2
1.2.1. Drug Delivery with Hydrogels 4
1.2.2. Drug Delivery with Stimuli-Responsive Nanofibers 8
1.2.3. Drug Delivery using Micellar Nanoparticles 14
1.2.4. Drug Delivery with Nanogels 14
2. RESEARCH OVERVIEW 23
3. REDUCED GRAPHENE-OXIDE-CONTAINNING POLY(ACRYLIC ACID) NANOFIBER: A PHOTOTHERMALLY CONTROLLED ANTIBIOTIC DELIVERY PLATFORM 25
3.1. Introduction 25
3.2. Experimental 29
3.2.1. Materials 29
3.2.2. Methods 29
3.2.3. Fabrication of rGO-Loaded PAA Nanofiber (PAA@rGO) 31
3.2.4. Loading of Antibiotics onto Nanofibers 32
3.2.5. Photothermal-Triggered Antibiotics Release 32
3.2.6. Wound Healing and Histology 33
3.3. Results and Discussion 34
3.3.1. Fabrication and Characterization of rGO-Containing Nanofibers 34
3.3.2. Loading and Release of Antibiotics into Nanofibers 37
3.3.3. Antibacterial Activity Under Passive and Active Release 40

3.3.4. Infectious Wound-Healing Studies Using rGO Nanofibers....42
3.4. Conclusion....45
4. pH-SENSITIVE POLYMERIC NANOFIBER FOR LOCAL CANCER TREATMENT....46
4.1. Introduction....46
4.2. Experimental....49
4.2.1. Materials....49
4.2.2. Synthesis of Polymer....49
4.2.3. Fabrication and Characterization of Drug-Loaded Nanofibers....50
4.2.4. Hydrolysis of Nanofibers....50
4.2.5. Drug and Fluorescein-Amine Release from Nanofibers....51
4.2.6. Cytotoxicity Assay....51
4.3. Results and Discussion....52
4.3.1. Synthesis of pH-Responsive Polymer....52
4.3.2. Fabrication of Drug-Loaded pH-Responsive Nanofibers....53
4.3.3. pH-Responsiveness of Nanofibers....54
4.3.4. Effect of Fiber Diameter on Release Rate of an Encapsulated Cargo....57
4.3.5. pH-Responsive Drug Release from the Nanofibers....58
4.3.6. Cell Viability Studies....61
4.3.7. Feasibility Testing for Use as a Surgical Buttress....62
4.4. Conclusion....63
5. REDOX-SENSITIVE HYDROGELS FOR ON-DEMAND PROTEIN DELIVERY....64
5.1. Introduction....64
5.2. Experimental....66
5.2.1. Materials....66
5.2.2. Methods....66
5.2.3. Cell lines....67
5.2.4. Synthesis of Masked Maleimide Disulfide Acid....67
5.2.5. Synthesis of Maleimide Disulfide-Terminated PEG Polymer....68
5.2.6. Selectivity in Thiol–Maleimide and Thiol–Disulfide Exchange Reactions....68

5.2.7. Preparation and Characterization of the HGs 69
5.2.8. Degradation of the HG and FITC-Labeled Protein and Dextran Release 70
5.2.9. Cytotoxicity Experiments 70
5.2.10. Live/Dead Cell Viability Assay 70
5.3. Results and Discussion 71
5.3.1. Synthesis and Characterization of Maleimide Disulfide-Terminated Telechelic PEG Polymer 71
5.3.2. Orthogonality of the Thiol–Maleimide, and Thiol–Disulfide Exchange Chemistry 76
5.3.3. Preparation and Characterization of HGs 80
5.3.4. Degradation of HGs 82
5.3.5. Macromolecular Release from HGs 86
5.3.6. Cell Studies 88
5.4. Conclusion 90
6. REDOX-RESPONSIVE NANOGELS FOR DRUG-DELIVERY: THIOL-MALEIMIDE AND DISULFIDE-EXCHANGE CHEMISTRY AS ORTHOGONAL TOOLS FOR FABRICATION AND DEGRADATION 91
6.1. Introduction 91
6.2. Experimental 94
6.2.1. Materials 94
6.2.2. Methods 94
6.2.3. Cell Lines 95
6.2.4. Synthesis of Masked Maleimide-Disulfide-Containing Monomer (FMDSMA) 95
6.2.5. Synthesis of Masked Maleimide-Disulfide-Containing Copolymer 96
6.2.6. Orthogonality of the Thiol-Disulfide Exchange and Thiol-Maleimide Reaction 96
6.2.7. Determination of LCST of Copolymer 97
6.2.8. Preparation of Nanogels 97
6.2.9. Loading and Release of NR 97
6.2.10. Conjugation of cRGDfC to Nanogels 98

6.2.11. Loading and Release of DTX....98
6.2.12. Cell Experiments....98
6.2.13. Internalization Experiments....99
6.3. Results and Discussion....100
6.3.1. Synthesis of Masked Maleimide-Disulfide-Containing Monomer....100
6.3.2. Synthesis of the Redox-Responsive Copolymer....102
6.3.3. The Selectivity of Thiol-Maleimide reaction Over Thiol-Disulfide Exchange Reaction....104
6.3.4. Fabrication of Redox-Responsive NGs....105
6.3.5. NR-Loading and Redox-Responsive NR Release From Nanogels....107
6.3.6. DTX Release, Cytotoxicity, and Cell Uptake....109
6.4. Conclusion....111
7. COMBINATION OF COVALENT AND NON-COVALENT DRUG-LOADING ON pH-RESPONSIVE MICELLAR STRUCTURE FOR TARGETED DRUG-DELIVERY....113
7.1. Introduction....113
7.2. Experimental....116
7.2.1. Materials....116
7.2.2. Method....116
7.2.3. Cell Lines....117
7.2.4. Synthesis of 5-Fluorouracil-Containing Monomer....117
7.2.5. Synthesis of PEG-Based Macro-Initiator....117
7.2.6. Synthesis of 5FMA Containing Diblock Copolymer....118
7.2.7. End Group Modification of Diblock Copolymer With cRGDfK....118
7.2.8. Preparation of Micelles....119
7.2.9. Docetaxel Loading into Micelles....119
7.2.10. DTX Release, Cytotoxicity, and Cell Uptake....120
7.3. Results and Discussion....121
7.3.1. Synthesis and Characterization of 5-Fluorouracil Monomer....121
7.3.2. Synthesis of the Diblock Copolymer....123
7.3.3. Fabrication and Characterization of Micelles....127
7.3.4. pH-Responsive Docetaxel and 5-Fluorouracil Release....129

7.3.5. Cytotoxicity and Internalization Experiments for Drug Conjugates on CAL 27 131
7.4. Conclusion 134
8. CONCLUSION 135
REFERENCES 138
APPENDIX A: ADDITIONAL DATA 186
APPENDIX B: COPYRIGHT NOTICES 188

LIST OF FIGURES

Figure 1.1. Polymeric materials with different stimuli-responsiveness used in this thesis. 2

Figure 1.2. An overview of biochemical, physical, and chemical stimuli used for stimuli-responsive polymers [21]. 3

Figure 1.3. Application of hydrogels in biomedical science [28]. 4

Figure 1.4. Schematic representation of degradation of and protein release from redox-responsive hydrogels [49]. 6

Figure 1.5. Schematic representation of photothermally triggered antibacterial peptide release from cryogel patches [57]. 7

Figure 1.6. Applications of stable hydrophilic nanofibers in the biomedical field [58]. 9

Figure 1.7. SEM images of PAA nanofibers (a) before and (b) after immersing in water [75]. 10

Figure 1.8. Morphology comparison of H9c2 myoblast cells at 20 h of post-seeding on (a) gelatin only, (b) 15:85 polyaniline-gelatin, (c) 30:70 polyaniline-gelatin, (d) 45:55 polyaniline-gelatin fibers, (e) glass matrices [77]. 11

Figure 1.9. Schematic diagram of the production of PAOx-based crosslinked nanofibers employing in-place situ UV-crosslinking during electrospinning and their 12

Figure 1.10. SEM images of PLA fiber mats loaded with paracetamol after 24 hours at 37 °C in pH 7.4 (a), 5.6 (b), and 4.0 (c) buffer solutions, $PLAOE_D$ mats in pH 7.4 (d), 5.6 (e), and 4.0 (f) buffer solutions, and $PLAOE_P$ mats in pH 7.4 (g), 5.6 (h), and 4.0 (i) buffer solutions [84]. 13

Figure 1.11. Different approaches in the synthesis of polymeric nanogels. 15

Figure 1.12. Schematic illustration of redox-sensitive nanogels [99]. 16

Figure 1.13. (a) Synthetic technique, and (b) crosslinking method of PDS-bearing polymers to produce a redox-responsive nanogel-based drug delivery system [103]. 18

Figure 1.14. Formation of micellar structures and loading of functional agents [112]. ... 19

Figure 1.15. Schematic representation of targeted and non-targeted docetaxel-loaded micelles [119]. 21

Figure 1.16. Schematic illustration of the synthesis of core-crosslinked targeted docetaxel-loaded micelles [123]. 22

Figure 3.1. Illustration of the fabrication of antibiotic-loaded PAA@rGO nanofibers: (1) electrospinning of rGO-loaded PAA nanofiber mats followed by (2) loading with different antibiotics and photothermal-triggered antibiotic release. 26

Figure 3.2. (a) HPLC plot of AMP (5, 10, 20 and 50 μg mL-1) in PBS (0.1 M, pH 7.4) together with AMP calibration curve; (b) HPLC plot of CFP 33

Figure 3.3. Characterization of rGO-loaded PAA nanofiber mats formed by electrospinning: (a) photograph of electrospun PAA@rGO; (b) Raman

spectra of rGO (black), PAA (gray), and PAA@GO (red); (c) scanning electron microscopy (SEM) images of nanofiber mats; and (d) stability of β-cyclodextrin cross-linked PAA@rGO nanofibers in water at 37 °C for 60 h 35

Figure 3.4 (a) FTIR and (b) XPS (C1s Scan) spectra of PAA@rGO nanofibers. 36

Figure 3.5. SEM images of fabricated rGO@PAA nanofiber mats at different scales. 36

Figure 3.6. Photothermal properties of cross-linked PAA@rGO: (a) photothermal heating curves of PAA (gray) and PAA@rGO (red) nanofiber patches (4 mg) immersed in PBS (0.1 M, pH 7.4) and irradiated at 980 nm (1 W cm^{-2}) for 10 min and (b) temperature profile of PAA@rGO nanofiber mats upon 10 min irradiation at varying power densities. 37

Figure 3.7. (a) Loading capacity of PAA@rGO nanofiber mats (4 mg) with ampicillin and cefepime upon incubation for 24 h into PBS (0.1 M, pH 7.4) under shaking at different drug concentrations. (b) Passive release from antibiotic-loaded cross-linked PAA@rGO nanofibers when immersed in 0.1 M PBS (pH 7.4) for 24 h at 37 °C. 38

Figure 3.8. Photothermal-triggered antibiotics' release for PAA@rGO nanofibers: (a) release profile of ampicillin from a PAA@rGO nanofiber loaded with ampicillin (25 μg mL^{-1}) when activated at 980 nm at 2 and 1 W cm^{-2} and (b) release profile of cefepime from PAA@rGO nanofibers loaded with cefepime (25 μg mL^{-1}) when activated at 980 nm at 2 and 1 W cm^{-2}.....39

Figure 3.9. (a) Planktonic growth of *E. coli* K12 (1 × 108 cfu mL^{-1}) treated with ampicillin released photothermally from nanofiber mats at different time intervals. (b) Planktonic growth of *S. epidermis* treated with cefepime

released photothermally from nanofiber mats at different time intervals. (c) SEM images of *S. epidermidis* treated with cefepime photothermally released from PAA@rGO nanofiber mats for 5 and 30 min.....41

Figure 3.10. (a) Loading of ampicillin (85 μg mL^{-1}) and the amount of photothermally released ampicillin after 10 min laser irradiation (1 W cm^{-1}). (b) Loading of cefepime (25 μg mL^{-1}) and release of cefepime when activated at 980 nm at 2 W cm^{-2}. 42

Figure 3.11. (a) Photographs of wound scars 24 h after treatment (940 nm, LED array) for 10 min with cefepime-loaded nanofibers mats. Negative control-intact skin; positive control-infected untreated skin. Insert at the top left demonstrates the setup for animal treatment. (b) Photographs of intact mouse skin and three representative skin samples after 48 h of infection under different treatment conditions. 43

Figure 3.12. Controlled heating of meat with PAA@rGO with NIR LED: Heating up to 67°C for 10 min causes meat to burn, but heating skin to 52°C shows no visible tissue damage.....44

Figure 3.13. Histological examination of skin wound healing 48 h after the infection. Sections of skin tissues with Gram staining. Intact mouse skin; untreated skin (after infection); and photothermally treated infected skin part of the wound (PAA-CFP and PAA@rGO-CFP).....45

Figure 4.1. Illustration of pH-dependent drug release from pH-responsive electrospun nanofibers. 48

Figure 4.2. SEC traces of polymers (eluent: DMAC). 52

Figure 4.3. ^{1}H NMR spectrum of polymer. 53

Figure 4.4. SEM images of (a) 350 nm and (b) 800 nm nanofibers with their size distribution histograms, (c) and (d), respectively. Representative confocal image (e) of doxorubicin-loaded nanofibers. 54

Figure 4.5. (a) Schematic of pH-labile polymer cleavage and fiber swelling. Image of the water droplet on a nanofiber buttress incubated in (b) PBS or (c) in pH 5.5 buffer. (d) Contact angle measurements of nanofiber buttresses incubated in different conditions. (e) Change in contact angle of nanofiber buttresses in the acidic buffer. (f) Release kinetics of trimethoxybenzaldehyde during incubation under different pH conditions (N=3). 55

Figure 4.6. (a) SEM image of nanofibers prior to incubation in aqueous solution. (b) Change in fiber diameter as a function of time and buffer pH (N=3). (c) SEM image of nanofibers after incubation for four weeks in pH 7.4 PBS and (d) after four weeks in pH 5.5 aqueous buffer. 56

Figure 4.7. The release of fluorescein amine from nanofiber buttresses as a function of fiber diameter and time while incubated in pH 5.5 aqueous buffer (N=3). 57

Figure 4.8. Release of (a) docetaxel and (b) doxorubicin from nanofiber buttresses as a function of time and pH in an aqueous buffer. (c) Doxorubicin release in RMPI-HEPES media (all data N=3). 59

Figure 4.9. Long-term release of doxorubicin from nanofibers incubated at pH 7.4. 60

Figure 4.10. Doxorubicin release from nanofibers at pH 6.5 phosphate buffer. 60

Figure 4.11. (a) Cytotoxicity of supernatant from unloaded nanofibers incubated at pH 6.5 or 7.4 diluted and incubated with MDA-MB-231 cells. (b)

Cytotoxicity of supernatant from doxorubicin-loaded nanofibers incubated at pH 6.5 or 7.4 diluted and incubated with MDA-MB-231, A549, and NCI-H460 cells. (c) Cytotoxicity of free doxorubicin on MDA-MB-231, A549, and NCI-H460 cells (all data N≥3). 62

Figure 4.12. Demonstration of the feasibility of using pH-responsive nanofiber buttresses as reinforcements for surgical resection margins. 63

Figure 5.1. Schematic illustration of fabrication and protein encapsulation and release from fast-forming dissolvable hydrogels. 66

Figure 5.2. Synthesis of disulfide-containing PEG bis-maleimide precursor. 72

Figure 5.3. (a) ^{1}H NMR and (b) ^{13}C NMR spectra of the masked maleimide-disulfide acid. 73

Figure 5.4. FTIR spectrum of masked maleimide-disulfide acid. 74

Figure 5.5. LC-MS characterization of the masked maleimide-disulfide acid. 74

Figure 5.6. ^{1}H NMR spectrum of disulfide- and furan-protected bis-maleimide containing PEG polymer. 75

Figure 5.7. ^{13}C NMR spectrum of disulfide containing PEG furan-protected bis-maleimide polymer. 76

Figure 5.8. (a) ^{1}H and (b) ^{13}C NMR spectrum of disulfide containing PEG bis-maleimide. 77

Figure 5.9. FTIR spectra of PEG, masked maleimide-disulfide terminated PEG, and maleimide-disulfide terminated PEG. 78

Figure 5.10. Comparison of (a) ^{1}H and (b) ^{13}C NMR spectrums of PEG bis-maleimide polymer and thiol-conjugated bis-maleimide polymers. 79

Figure 5.11. SEC chromatographs of PEG polymers before and after addition of 2-mercaptoethanol. 80

Figure 5.12. (a) Photographic image of a wet hydrogel sample, (b) SEM image of a dry hydrogel sample (scale bar: 100 μm), (c) frequency sweep test, and (d) water uptake swelling profile. 81

Figure 5.13. UV-vis spectra of Ellman's reagent solution incubated with hydrogel (red) and tetra-thiol polymer (blue). 82

Figure 5.14. FTIR spectra of thiol-terminated four arm PEG, maleimide-disulfide terminated PEG, and hydrogel. 83

Figure 5.15. Strain sweep test of hydrogel. 83

Figure 5.16. (a) Frequency sweep test and (b) strain sweep test of the FITC-BSA loaded hydrogel. 84

Figure 5.17. (a) Behavior of disulfide-containing hydrogel in PBS and DTT (200 mM) solutions, and (b) rheological analysis of the degradation of hydrogel in DTT solutions (10 and 100 mM). 85

Figure 5.18. Time sweep test of hydrogel in the presence and absence of glutathione (GSH). 86

Figure 5.19. Release of 150 kDa and 20 kDa FITC-label dextran from hydrogels in DTT and PBS solutions. 87

Figure 5.20. The prelease profile of FITC-labeled BSA from hydrogels in DTT and PBS solutions. 88

Figure 5.21. (a) Cell viability of L929 fibroblasts upon treatment with varying amounts of HGs and with the degradation product of the HG (HG-d). Fluorescence microscopy images of the live/dead cell viability assay upon treatment with the (b) HG and (c) with the degradation product of hydrogel (scale bar in images: 50 μm). 89

Figure 6.1. Schematic illustration of the fabrication of drug-loaded targeted nanogel. 93

Figure 6.2. (a) Synthetic pathway and (b) ^{1}H NMR spectrum of the masked maleimide-disulfide-containing monomer. 101

Figure 6.3. ^{13}C NMR spectrum of the masked maleimide-disulfide-containing monomer. 101

Figure 6.4. FTIR spectra of masked maleimide-disulfide-containing monomer. 102

Figure 6.5. ^{1}H NMR spectrum of the redox-responsive polymer. 103

Figure 6.6. SEC chromatographs of the redox-responsive copolymer. 103

Figure 6.7. (a) Synthesis, and (b) ^{1}H NMR of the copolymer. 104

Figure 6.8. ^{1}H NMR spectrum of the polymer after and before treated with 2-mercaptoethanol. 105

Figure 6.9. (a) Change in % transmittance of copolymer solution with temperature change, (b) hydrodynamic size as determined by DLS analysis of

copolymer solution at 25 and 60 °C, (c) TEM image, and (d) DLS analysis of NG. 106

Figure 6.10. UV-vis spectra of Ellman's reagent solution incubated with nanogel. 107

Figure 6.11. (a) Schematic representation of degradation and visual images of redox-responsive degradation of hydrophobic dye NR-containing nanogels under UV light. Fluorescence intensity of NR-containing nanogel solutions incubated in (b) PBS and (c) 10 mM GSH solution for five days. Stability of nanogels after 4 hours in (d) PBS and (e) GSH solution (10 mM). 108

Figure 6.12. (a) DTX release in a reductive and non-reductive environment for 24 hours at 37 °C, (b) Cell viabilities of MDA-MB-231 tumor cells treated with the DTX, cRGDfC-NG-DTX, cRGDfC-NG-DTX+GSH, and NG-DTX..... 110

Figure 6.13. (a) NR-internalization of NG, RGD-NG, and RGD+RGD-NG into MDA-MB-231 cells after six hours. NR provides a red fluorescent signal, whereas the cell nuclei are blue due to DAPI staining (Scale bar 50 μm). (b) Overlapping histograms of the control, NG, and cRGDfC-NG treatment. 111

Figure 7.1. Schematic illustration of the formation and degradation of the pH-sensitive micelle. 115

Figure 7.2. (a) Synthetic pathway, (b) ^{1}H NMR spectrum, and (c) ^{13}C NMR spectrum of 5-fluorouracil monomer. 122

Figure 7.3. ^{1}H NMR spectrum of macroinitiator 123

Figure 7.4. SEC chromatographs of the macroinitiator. 124

Figure 7.5. ^{1}H NMR spectrum of diblock copolymer. 124

Figure 7.6. SEC chromatographs of the diblock copolymer. 125

Figure 7.7. ^{1}H NMR spectrum of NHS-activated diblock copolymer. 126

Figure 7.8. ^{1}H NMR spectrum of cRGDfK diblock copolymer. 126

Figure 7.9. (a) CMC, (b) PDI, and (c) Z-ave valuse of polymer solutions at various concentrations. 128

Figure 7.10. DLS measurement of micellar structures at CMC. 129

Figure 7.11. (a) Cell viability results of Drug, micelle and RGD combinations and (b) internalization experiment results of NR-loaded RGD-bearing and non-bearing micelles. 130

Figure 7.12. (a) Z-average size of micelles in pH 7.4 and (c) in pH 5.5. The release of (b) 5-fluorouracil and (c) docetaxel in pH 5.5 and 7.4. 131

Figure 7.13. (a) Cell viability results of Drug, micelle and RGD combinations and (b) internalization experiment results of NR-loaded RGD-bearing and non-bearing micelles. 133

Figure A.1. LC-MS characterization of the solution of the reaction between maleimide-disulfide terminated PEG with (a) the stoichiometric equivalent of 2-mercaptoethanol and (b) four equivalent of 2-mercaptoethanol 186

Figure A.2. LC-MS characterization of the solution of the reaction between copolymer with (a) the stoichiometric equivalent of 2-mercaptoethanol and (b) four equivalent of 2-mercaptoethanol. 187

Figure B.1. Permission for Figure 1.2 from Ref [21]. 188

Figure B.2. Permission for Figure 1.3 from Ref [28]. 189

Figure B.3. Permission for Figure 1.4 from Ref [49]. 190

Figure B.4. Permission for Figure 1.5 from Ref [57]. 191

Figure B.5. Permission for Figure 1.6 from Ref [58]. 191

Figure B.6. Permission for Figure 1.7 from Ref [75]. 192

Figure B.7. Permission for Figure 1.8 from Ref [77]. 193

Figure B.8. Permission for Figure 1.9 from Ref [79]. 193

Figure B.9. Permission for Figure 1.10 from Ref [84]. 194

Figure B.10. Permission for Figure 1.12 from Ref [99]. 194

Figure B.11. Permission for Figure 1.13 from Ref [103]. 195

Figure B.12. Permission for Figure 1.14 from Ref [112]. 195

Figure B.13. Permission for Figure 1.15 from Ref [119]. 196

Figure B.14. Permission for Figure 1.16 from Ref [123]. 196

Figure B.15. Permission for Chapter 3 from Ref [129]. 197

Figure B.16. Permission for Chapter 4 from Ref [184]. 197

Figure B.17. Permission for Chapter 5 from Ref [239]. 198

LIST OF TABLES

Table 3.1. Minimum inhibitory concentrations of ampicillin and cefepime for different bacteria strains 40

LIST OF ACRONYMS/ABBREVIATIONS

3D	Three dimensional
5FMA	5-Fluorouracil-containing monomer
AIBN	Azobisisobutyronitrile
AMP	Ampicillin
CFP	Cefepime
DMAC	Dimethylacetamide
DMEM	Dulbecco's modified eagle medium
DMF	Dimethylformamide
DMSO	Dimethyl sulfoxide
DTT	1,4-Dithiothreitol
EDC	1-Ethyl-3-(3-dimethylaminopropyl)carbodiimide
eNPs	Expansile nanoparticles
FMDSMA	Masked maleimide-disulfide-containing monomer
FTIR	Fourier transform infrared (FTIR)
GO	Graphene oxide
HEPES	Hydroxyethyl-piperazineethane-sulfonic acid buffer
HG	Hydrogel
PNIPAM	Poly(*N*-isopropylacrylamide)
NG	Nanogel
NHS	*N*-Hydroxysuccinimide
NIR	Near-infrared
NIPAM	*N*-isopropylacrylamide
NMR	Nuclear magnetic resonance
NR	Nile Red
LCST	Lower critical solution temperature
LED	Light-emitting diode
FuMA	Furfuryl methacrylate
PAA	Poly(acrylic acid)
PEG	Poly(ethylene glycol)

PEGMEMA	Poly(ethylene glycol) methylether methacrylate
PEGDA	Poly(ethylene glycol) diacrylate
PEGDMA	Poly(ethylene glycol) dimethacrylate
PEO	Poly(ethylene oxide)
PCL	Poly(ε-caprolactone)
PDS	Pyridyl disulfide
RAFT	Reversible addition-fragmentation chain transfer
RPMI	Roswell Park Memorial Institute
rGO	Reduced-graphene oxide
SEC	Size-exclusion chromatography
SEM	Scanning electron microscopy
THF	Tetrahydofuran
XPS	X-ray photoelectron spectroscopy

1. INTRODUCTION

1.1. Smart Polymeric Materials for Drug Delivery

Polymeric materials have been used widely in the field of biomedical science due to their exceptional physical and chemical properties and functional attributes for different applications [1-6]. Polymeric materials used for biomedical applications should meet certain basic criteria, such as biodegradability and biocompatibility, apart from the specific characteristics required for the specific purpose. These conditions are essential in biomedical applications because polymeric materials should have sustained stability and not cause systematic toxicity in the biological environment. Additionally, the functionality of polymeric materials should be designed so that polymeric materials do not interfere with biochemical reactions.

One of the most studied applications of polymeric materials is drug delivery applications. Conventional drug treatments have been used for centuries to treat diseases such as cancer and bacterial infections. Unfortunately, there are many cases where conventional drugs are ineffective due to their low solubility, low bioavailability, nonspecific distribution, rapid clearance, toxicities to healthy tissues, and fluctuation in plasma drug levels [7]. The required effective drug concentration in the disease site can not be achieved because only a few percent of administered drugs reach that particular site, while the rest cause toxicity and side effects. To circumvent this issue, smart polymeric materials, such as hydrogels, nanofibers, nanogels, and micelles, have been used for selective drug delivery, reaching high local drug concentrations on the disease side with minimum impact on other body parts. The effectiveness of such drug delivery systems can be further increased by exploiting the exogenous and endogenous stimuli at the site of delivery. This thesis will focus on the evaluation of stimuli-responsive drug delivery platforms. Figure 1.1 shows novel redox-responsive hydrogels, near-infrared light-responsive nanofibers, pH-responsive nanofibers, redox-responsive nanogels, and pH-responsive micelles are developed and evaluated to address a specific type of cancer and microbial infections.

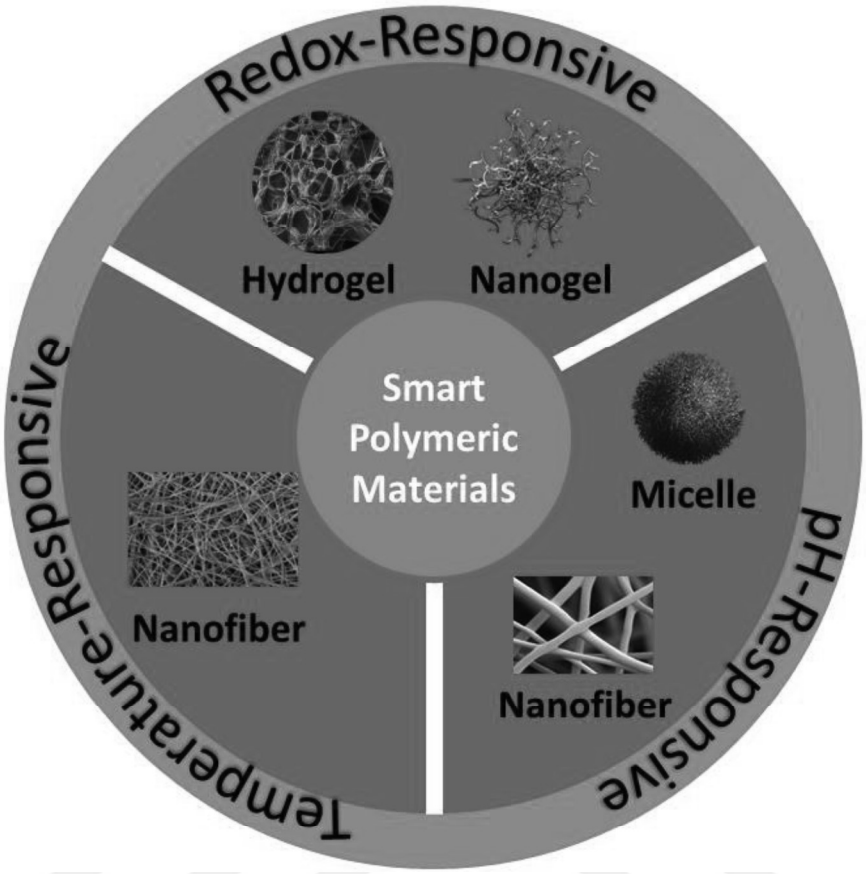

Figure 1.1. Polymeric materials with different stimuli-responsiveness used in this thesis.

1.2. Stimuli-Responsive Polymeric Materials

For a variety of purposes, synthetic polymeric materials with stimuli-responsive properties, such as responsive biointerfaces that are functionally similar to natural surfaces [8]: controlled drug-delivery and release systems [9-11]. Control over the drug release mechanism from polymeric materials is essential for effective drug delivery. Manipulating these mechanisms can be achieved by changing the chemical or physical properties in a controlled manner. Stimuli-responsive polymers change their chemical or physical structures as a response to an endogenous such as redox [12], pH [13], enzyme [14], ionic microenvironment [15], or exogenous stimuli such as temperature [16], photo/light [17], magnetic [18], ultrasound [19], electrical [20] as illustrated in Figure 1.2 [21].

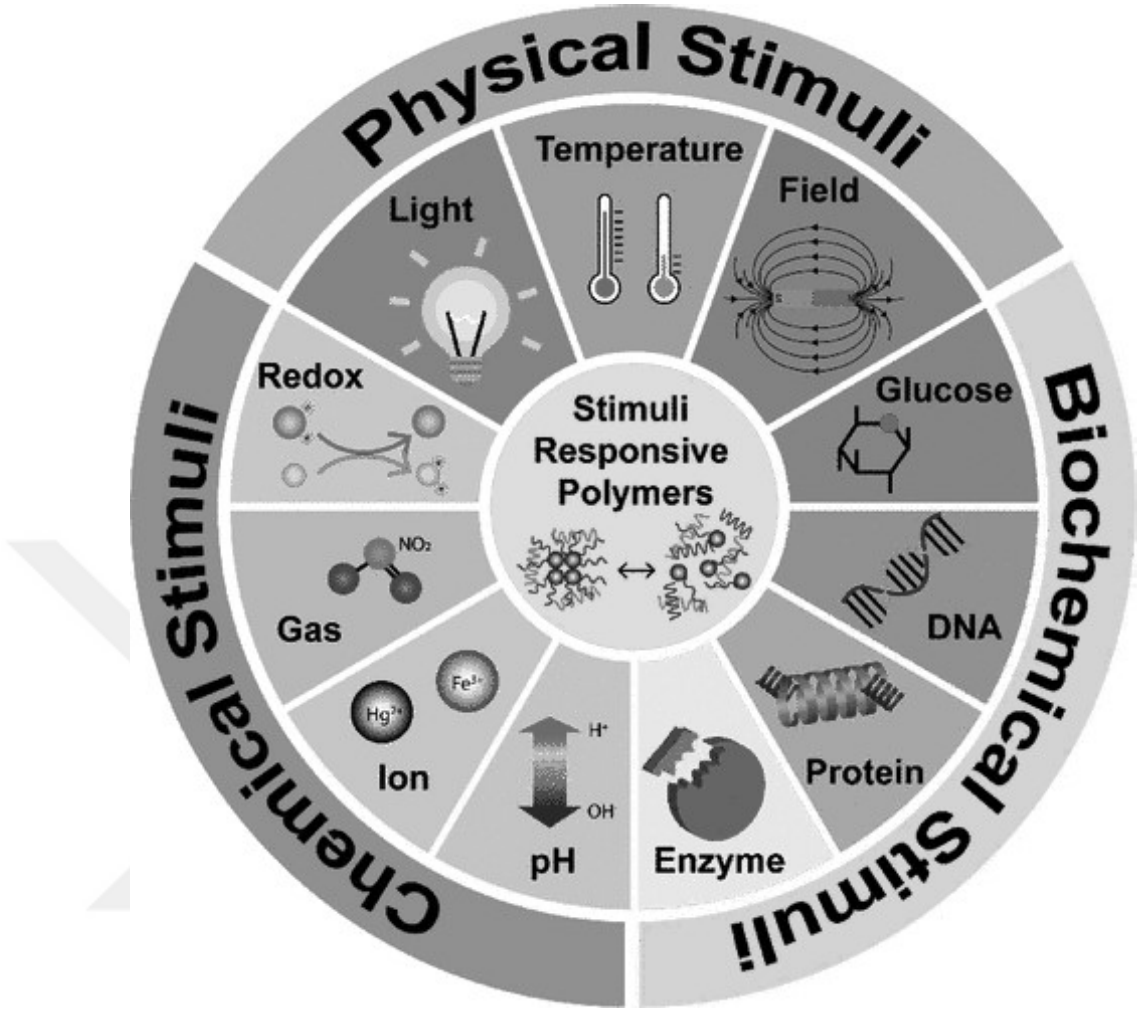

Figure 1.2. An overview of biochemical, physical, and chemical stimuli used for stimuli-responsive polymers [21].

The intrinsic characteristics of cancer tissues, such as different levels of glutathione (GSH) concentration, an acidic environment, and specific types of enzymes, are known as endogenous stimuli. This type of stimulus does not require any external action to trigger the responsive materials. However, the control over materials response is relatively limited because stimuli rely on biological activities [22]. On the other hand, exogenous stimuli require physical stimuli applied externally to the target site. Compared to endogenous stimuli, the response of the material can be controlled at desired time point using exogenous stimuli. However, this method requires constant care of an operator while endogenous stimuli work by themselves.

1.2.1. Drug Delivery with Hydrogels

Hydrogels, as three-dimensional (3D), hydrophilic, polymeric networks, can absorb large amounts of water [23]. Because of chemical or physical crosslinks, 3D hydrogel networks made of homopolymers or copolymers are insoluble in water. Hydrogels play a critical role in the field of controlled drug delivery, tissue engineering, sensors, and implant materials, as illustrated in Figure 1.3 [24-28]. For the last decades, hydrogels have attracted a lot of attention due to facile fabrication, low cost, and ease of interaction with their surrounding biological environment. Properties such as 3D structure, large surface area/volume ratio, porosity, biocompatibility, mechanical strength, and degradability make hydrogels suitable for delivering bioactive molecules. To achieve prolonged local drug delivery, ideal scaffolds should exhibit structural stability, bio-similar characteristics, and an appropriate degradation profile.

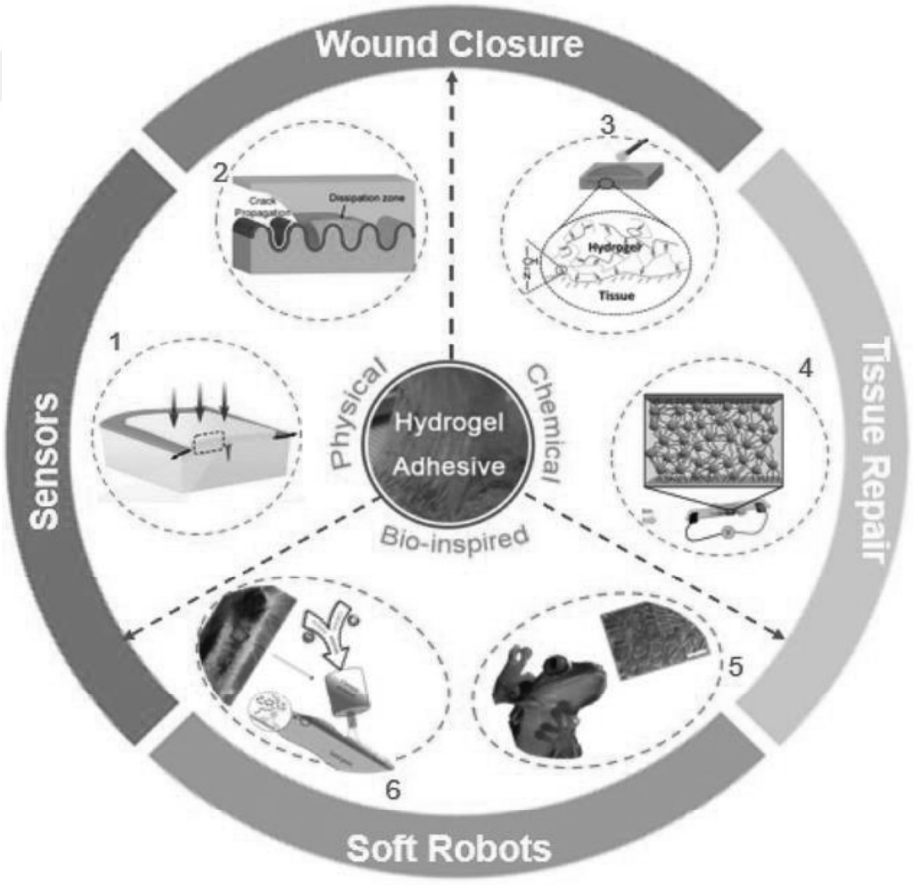

Figure 1.3. Application of hydrogels in biomedical science [28].

Hydrogels can be divided into two categories depending on their crosslinking strategies: physically and chemically crosslinked hydrogels. Chemically crosslinked hydrogels are composed of chemical bonds between polymer chains, whereas physically crosslinked hydrogels are formed by physical interactions that keep the hydrophilic polymer chains together. Physically crosslinked hydrogels are utilized using a transient junction point, which is formed by physical interactions such as hydrogen bonding [29], ionic interactions [30,31], physical entanglement [32], and hydrophobic interactions [33]. Chemically crosslinked hydrogels can be fabricated using chemical methods such as photo- and thermal-initiated polymerization and crosslinking polymers using "click" reactions. The wide use of hydrogels requires the development of new approaches to these materials. One of the most common methods for synthesizing hydrogels is free radical chain polymerization of hydrophilic monomers containing double bonds in the presence of a small amount of bifunctional monomer [34]. The most commonly used hydrophilic monomers in the fabrication of hydrogels are hydroxy ethyl methacrylate [35], *N*-isopropylacrylamide [36], acrylic/methacrylic acid [37], and poly(ethylene glycol) methacrylate [38]. These monomers were widely utilized with a co-monomer and a bifunctional crosslinker to obtain a crosslinked hydrophilic polymeric network. In recent years, with the beginning of 'click' chemistry, the fabrication and functionalization of hydrogels have undergone remarkable progress [39-41]. In the last decade, the copper-catalyzed Huisgen-type azide-alkyne cycloaddition was widely employed for hydrogels' facile and effective fabrication [42,43]. Recently, the focus has turned to the use of metal-free conjugation-based strategies. The strain-promoted azide-alkyne cycloaddition [44], nucleophilic thiol–ene [45], radical thiol–ene [46], and the Diels–Alder reactions [47] are the most frequently employed metal-free reactions that have been used in the fabrication of the hydrogels.

Drug delivery from hydrogels became a vital field to overcome the drawbacks of conventional drug delivery. 3D structures such as hydrogels can protect the drugs from harsh conditions of the biological environment, such as low pH in the stomach and the presence of enzymes. For instance, the concentration of drugs administered orally significantly decreases before reaching the bloodstream [48]. Hydrogels can also host poorly soluble drugs, which can not be administered in high concentrations with conventional drug therapy. Another problem of traditional drug therapy is that frequent drug administration can be

overcome by controlled drug delivery from hydrogel via sustained release at predetermined rates and periods. Drug delivery from hydrogels can also be controlled by tailoring the chemical and physical structure of the 3D network in response to endogenous or exogenous stimuli such as temperature, pH, light, and redox.

A "sensor" like the property of hydrogel makes them called "intelligent" or "smart" hydrogel. These materials can be produced by using dynamic covalent linkages sensitive to certain stimuli. For Sanyal and coworkers, redox-responsive crosslinker to crosslink furan-bearing PEG-based polymer, as illustrated in Figure 1.4 [49]. The hydrogel was used for protein encapsulation and release in a reductive environment for controlled drug delivery. The degradation of hydrogels was monitored in the reductive and non-reductive environment using a rheometer, and the effect of disulfide bond cleavage on protein release was investigated.



Figure 1.4. Schematic representation of degradation of and protein release from redox-responsive hydrogels [49].

Alternatively, stimuli-responsive polymers such as poly(N-isopropylacrylamide) (PNIPAM) can be directly used to obtain control over the physical properties of polymeric materials. PNIPAM is a thermoresponsive polymer that switches from swollen to collapsed at relatively high temperatures [50]. For example, Lu and coworkers developed a hydrogel system using NIPAM and a disulfide-containing crosslinker [51]. Fabricated hydrogels were loaded with the antibacterial drug levofloxacin as a model drug. Due to the thermosensitive PNIPAM and redox-responsive disulfide bonds, the hydrogel system became dual-responsive. Drug release was analyzed in a reductive environment and above the lower

critical solution temperature (LCST) of PNIPAM. Selective release of loaded-drug was observed in both cases.

Another way to obtain stimuli-responsive hydrogels is to use extraneous responsive materials such as light-absorbing graphene oxide or gold nanoparticles [52,53]. In this way, non-responsive polymeric hydrogels can be stimulated with exogenous or endogenous stimuli. Photothermally active materials can absorb light with specific wavelengths and convert the light energy to heat. This property has been used in hydrogel systems to trigger drug release [54-56]. For example, Sanyal and coworkers fabricate a photothermally active cryogel system to deliver antimicrobial peptides [57]. In this study, cryogels were prepared via photopolymerization of furfuryl methacrylate (Fuma), poly(ethylene glycol) methyl ether methacrylate (PEGMEMA), and poly(ethylene glycol) dimethacrylate (PEGDMA). Cryogels were loaded with reduced-graphene oxide (rGO) and functionalized with maleimide-containing therapeutic peptides. Figure 1.5 demonstrates the thermoresponsive Retro Diels-Alder reaction was used to trigger peptide release under Near-infrared (NIR) light which absorbed and converted to heat by rGO.

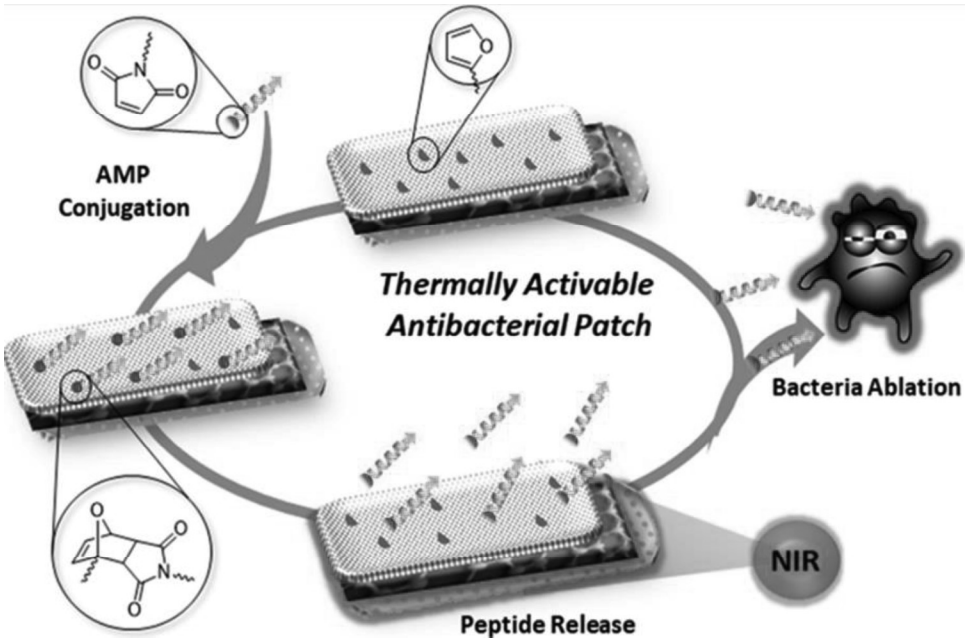

Figure 1.5. Schematic representation of photothermally triggered antibacterial peptide release from cryogel patches [57].

1.2.2. Drug Delivery with Stimuli-Responsive Nanofibers

In the last few decades, nanofibers have become a highly preferred polymeric material used in various biomedical applications, as illustrated in Figure 1.6 [58]. The nanofibrous substances provide a material with a distinctive nanostructure and a large surface area. Moreover, using suitable polymers, these nanofiber mats can be given the desired physical and chemical properties such as hydrophilicity, degradability, and functionalizability. Although there are other ways to fabricate polymeric nanofibers, the electrospinning method is still the most common approach [59-61]. The electrospinning method is widely used as a result of the straightforward and inexpensive instrumentation needed for it. Additionally, the method can be scaled up to fabricate nanofibrous mats on an industrial level while still being suitable for small-scale fiber preparation in a research laboratory [62-64]. Various synthetic and natural polymers can be used as precursors in nanofiber production for biomedical applications. The type of polymer can be determined by the respective purposes, which include tissue engineering [65-67], biosensing [68-70], diagnostics, and drug delivery [71,72]. For the abovementioned bioapplications, hydrophilic polymers were preferred since the interaction between the surface and biological environment is essential. However, protecting the fibrous structure of hydrophilic polymers in an aqueous environment is challenging due to solubility of these polymers. Over the past few years, stability through chemical and physical cross-linking has become a viable alternative to avoid the problems brought on by their dissolution.

The most common method of chemical crosslinking of hydrophilic polymers in the nanofibers is to use functional groups such as carboxylic acids, hydroxyls, amines, aldehydes, and thiols. One of the most common chemicals crosslinking for nanofibers from blends of natural or synthetic polymers containing hydroxyl or amine for tissue engineering applications is to use of glutaraldehyde vapor. For instance, Rabolt and coworkers fabricated crosslinked gelatin nanofibers using different crosslinking methods, including vapor-phase glutaraldehyde. Alternative to possibly toxic glutaraldehyde, aqueous phase genipin and glyceraldehyde were also used for crosslinking, and cells grown on each of these nanofibers were studied. Compared to the other two methods, nanofibers crosslinked with glyceraldehyde showed better cell proliferation [73].

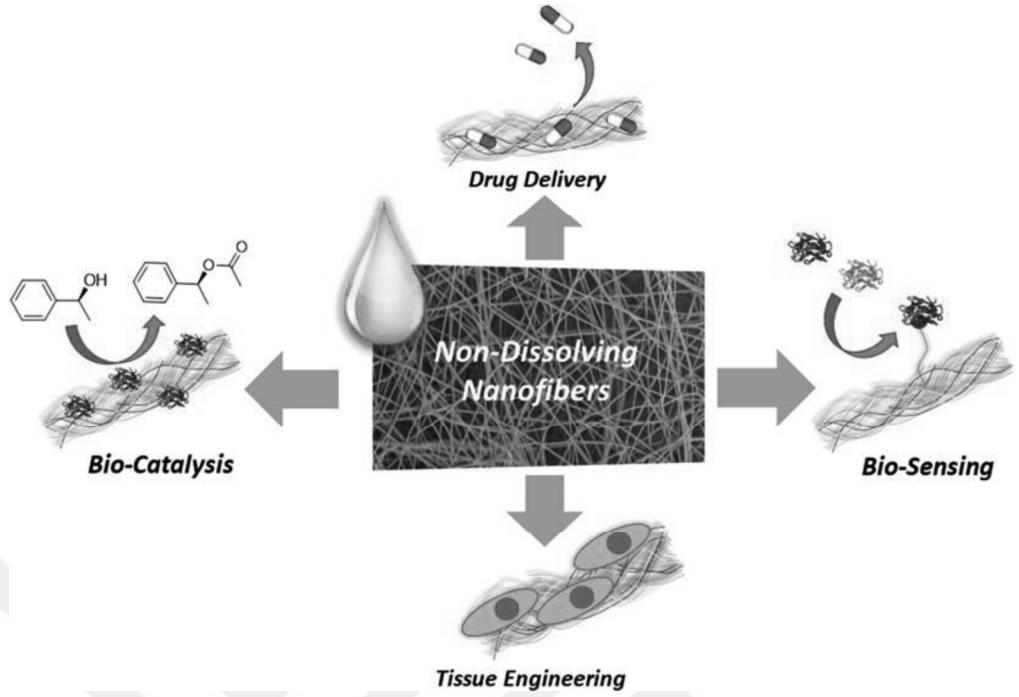

Figure 1.6. Applications of stable hydrophilic nanofibers in the biomedical field [58].

Poly(acrylic acid) (PAA) is another common hydrophilic used in the synthesis of nanofibers due to its biocompatibility and functional groups. Typical crosslinking of PAA requires thermal treatment in the presence of multiple alcohol-bearing crosslinkers through heat-induced intermolecular esterification. For instance, Wnek and coworkers crosslinked PAA nanofibers using ethylene glycol in a vacuum oven at 130 °C [74]. Crosslinked PAA nanofibers showed swelling properties after immersing in water, as shown in Figure 1.7. In another study by Wnek and coworkers, silver nanoparticles with antimicrobial activity were loaded into the PAA nanofibers crosslinked with the same method above. It was demonstrated that the silver nanoparticle-loaded nanofiber patches have the potential to be used as an antimicrobial agent in infectious diseases due to their various inhibitory activities against bacterial and fungal strains [75].

Ester or amide-mediated crosslinking is another crosslinking strategy technique with several examples in the literature. For instance, Deng, Yang and coworkers developed a synthetic method to crosslink gelatin nanofibers using 1-Ethyl-3-(3-dimethyl aminopropyl)carbodiimide (EDC) and *N*-Hydroxysuccinimide (NHS). In the study, the degree of crosslinking was found to be proportional to EDC concentration so that the

mechanical properties of nanofibers can be controlled [76]. In another study, Lelkes and coworkers fabricated crosslinked nanofibers from polyaniline and gelatin through post-electrospinning crosslinking using EDC coupling. An increase in the extent of crosslinking was observed with longer treatment durations. Figure 1.8 shows the biocompatibility of obtained nanofibers that were investigated on H9c2 rat cardiac myoblasts for tissue engineering applications [77].

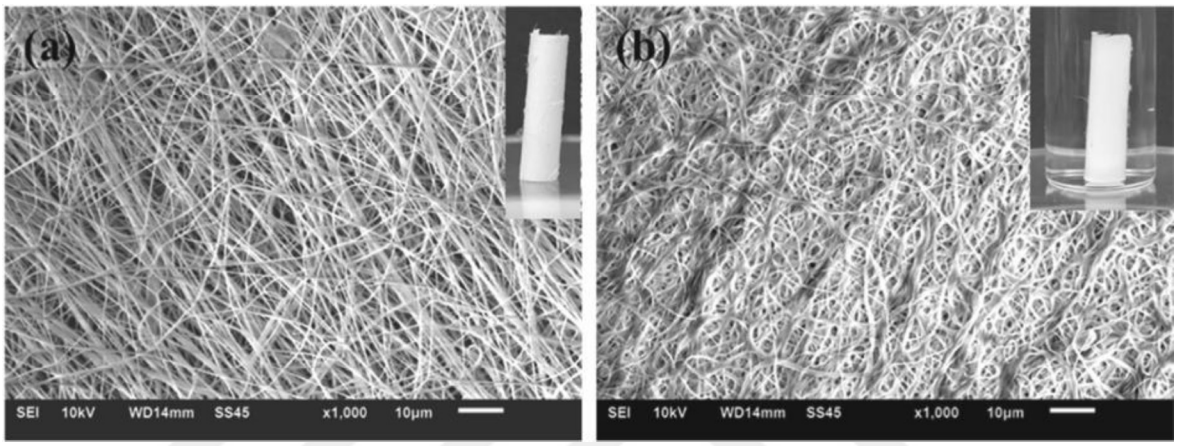

Figure 1.7. SEM images of PAA nanofibers (a) before and (b) after immersing in water [75].

In the last few decades, thiol-mediated crosslinking strategies have become popular due to highly efficient reactions such as nucleophilic addition and substitution reactions. Powerful thiol-mediated "click" reactions such as nucleophilic Michael-type addition and radical thiol-ene have been commonly used in the functionalization of polymeric materials. Due to their efficiency and orthogonality in mild conditions, thiol-bearing polymers have been employed for nanofiber crosslinking. Rafailovich and coworkers fabricated electrospun nanofibers from a thiolated hyaluronic acid and poly(ethylene oxide). These nanofibers were then crosslinked by the addition of PEGDA through a thiol-ene reaction. Besides crosslinking, free thiol moieties were also oxidized to disulfide bonds [78]. In another example, Sanyal, Hoogenboom, and coworkers used a synthetic polymer and crosslinked them using a UV-mediated thiol-ene reaction [79]. In the study, an alkene-bearing polymer, namely poly(2-ethyl-2-oxazoline-co-2-(but-3-enyl)-2-oxazoline), was used for electrospinning and crosslinked with tetra-thiol-based crosslinker through thiol-ene reaction

as shown in Figure 1.9. The obtained nanofiber mat was further functionalized with thiol and maleimide-containing molecules using a nucleophilic thiol-ene reaction.

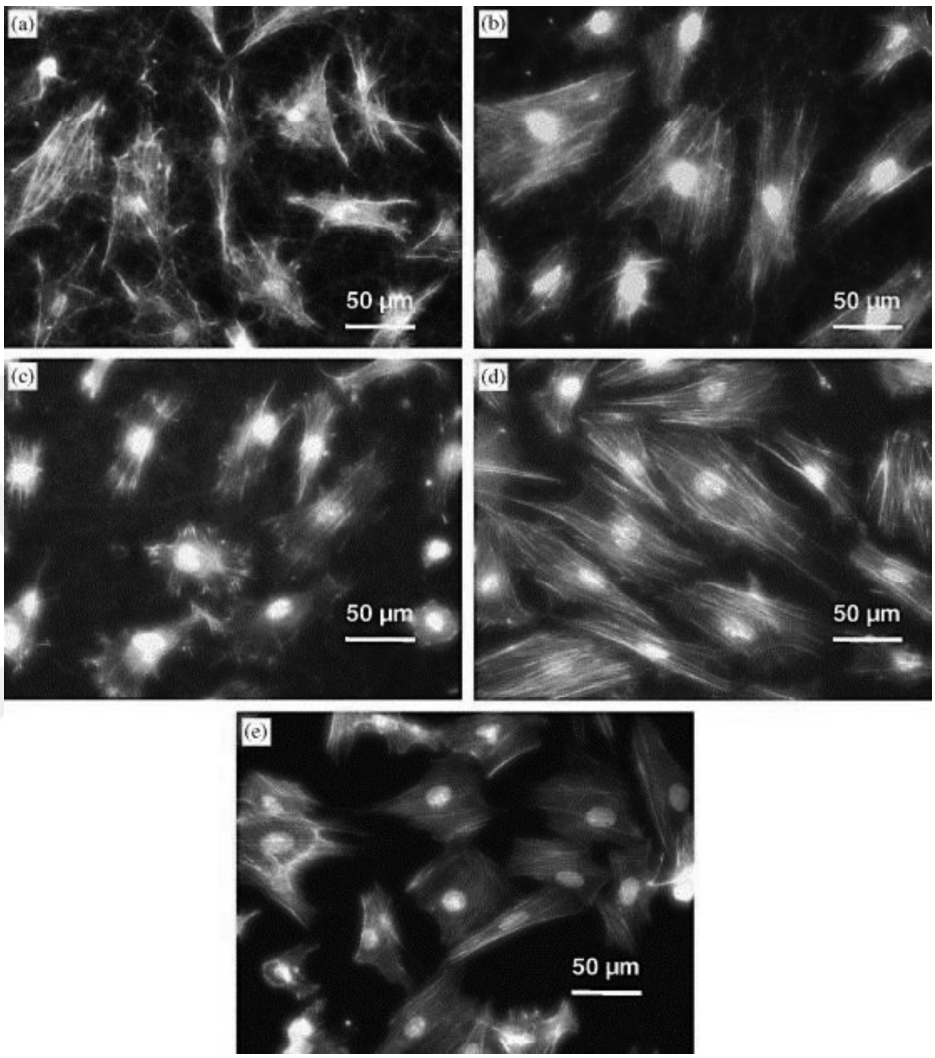

Figure 1.8. Morphology comparison of H9c2 myoblast cells at 20 h of post-seeding on (a) gelatin only, (b) 15:85 polyaniline-gelatin, (c) 30:70 polyaniline-gelatin, (d) 45:55 polyaniline-gelatin fibers, (e) glass matrices [77].

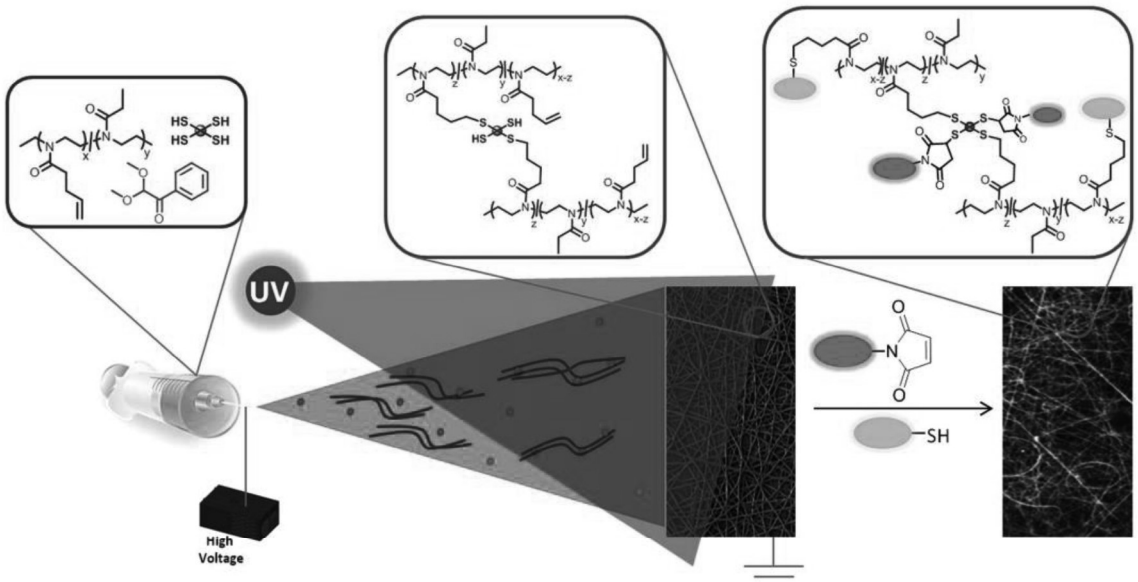

Figure 1.9. Schematic diagram of the production of PAOx-based crosslinked nanofibers employing in-place situ UV-crosslinking during electrospinning and their the multifunctionalization [79].

It is well known that the physical or chemical structure nanofibrous network can be strongly governed by different stimuli. The submicrometer diameter and high surface-to-volume ratio of nanofibers could lead the polymers to undergo a fast physical or chemical change and cause to trigger their cargo under certain stimuli. In the last decades, different endogenous and exogenous stimuli have been used in nanofiber systems, such as pH [80], temperature [81], magnetic field [18], photo/optical [82], and redox [83]. pH-sensitivity is one of the most studied stimuli for drug delivery application due to intracellular pH differences between cancer and healthy cells. pH sensitivity can be provided by using carboxylic acid or amine groups containing polymers, as a change in pH results in protonation or deprotonation, leading to changes in hydrophilicity. To promote drug release selectively at low pH, polymers made of acid-labile linkages (such as acetal or hydrazone groups) can be used [80]. For example, Li and coworkers fabricated a pH-sensitive nanofiber mat containing *ortho*ester groups which are used for drug delivery in slightly acidic conditions. Figure 1.10 shows that nanofibers were stable at neutral pH but degraded through acid-sensitive bonds at lower pH, which triggers the entrapped drug release [84].

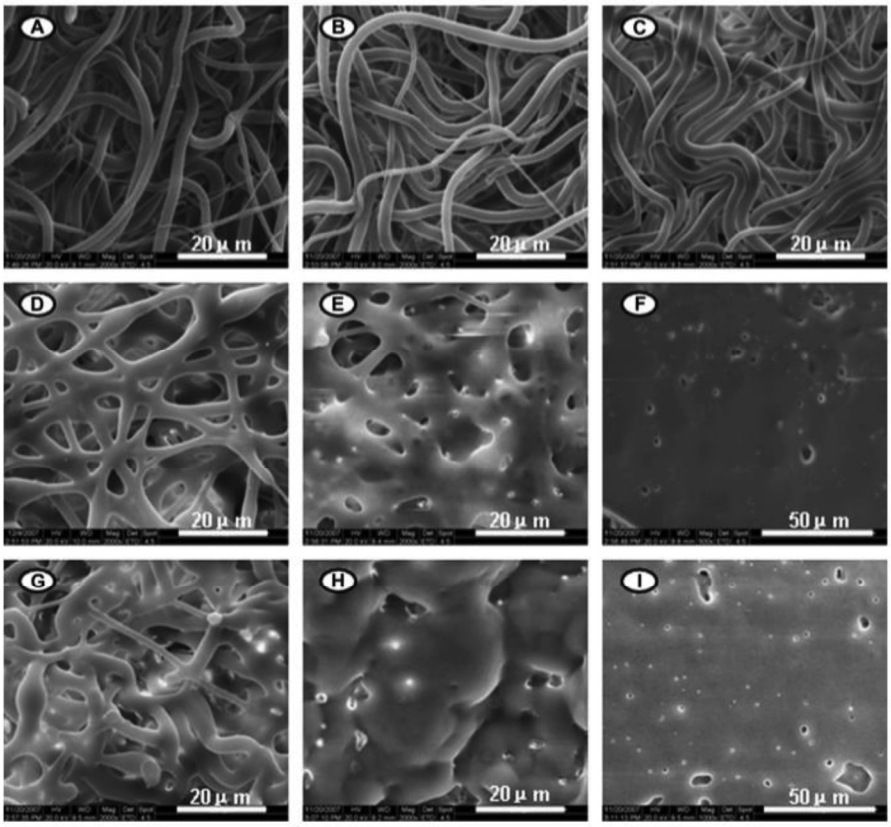

Figure 1.10. SEM images of PLA fiber mats loaded with paracetamol after 24 hours at 37 °C in pH 7.4 (a), 5.6 (b), and 4.0 (c) buffer solutions, $PLAOE_D$ mats in pH 7.4 (d), 5.6 (e), and 4.0 (f) buffer solutions, and $PLAOE_P$ mats in pH 7.4 (g), 5.6 (h), and 4.0 (i) buffer solutions [84].

The possibility of using thermoresponsive polymers in drug delivery systems has attracted much attention [85]. Poly(N-isopropyl acrylamide) is one of the most common thermo-responsive polymers with LCST between 31-35 °C. PNIPAM easily dissolves in aqueous media below the LCST, while it is insoluble above LCST due to the change in hydrophilicity. Alternative to using thermoresponsive polymers, drug delivery from nanofibers can be controlled by simply increasing the temperature of non-thermoresponsive polymers. The diffusion of drug molecules inside the nanofiber network can be increased by increasing the temperature of the mat. For example, Irani and coworkers prepared gold nanorods/graphene oxide loaded-core-shell nanofibers to deliver paclitaxel [86]. In the study, the core-shell nanofiber is fabricated from poly(tetramethylene ether) glycol based-polyurethane (core)/chitosan (shell). Gold nanorod/graphene oxide-containing nanofibers

were heated to around 50 °C upon exposure to NIR light, and photothermally triggered drug release was observed.

1.2.3. Drug Delivery with Nanogels

While many different polymeric nanoparticles have been studied to date, interest in nanogel is growing. There are three main routes to fabricate nanogels: polymerization or crosslinking in the nanoemulsion and crosslinking of polymers in their nanoaggregate forms, as shown in Figure 1.11. Polymeric nanogels have been widely chosen as a drug delivery platform over other nano-constructs because of their distinctive characteristics, such as variations in the type of polymers that can be used to form nanogels[87], tunable particle size[88], increased drug loading capacity[89], surface functional groups[90], and stimuli-responsive design[13]. Polymer hydrophilicity improves particle biocompatibility, allowing them to transport cargo safely to desired locations. Flexible polymer chains and a porous structure result in a sponge-like material that can hold large amounts of chemotherapy drugs. Crosslinked networks prevent dissolution while maintaining the integrity of nanogels during swelling or excessive drug loading, and they also prevent unwanted cargo leakage. On the other hand, the multifunctionality of nanogels opens up many possibilities for modifying the surface of particles with various agents. Although physical drug loading is preferred, chemical loading is possible due to its multifunctionality. Chemotherapy's disadvantages, such as non-specificity and toxicity to healthy tissue, can be overcome by immobilizing cancer cells targeting ligands onto a nanogel surface to improve the accumulation in tumor tissue. Another benefit is that specific stimuli can change the chemical and physical form of the delivery system. Stimuli-responsive chemistries have opened up new possibilities in the architecture, formulation, and utilization of nanogels. Unique local circumstances, biological triggers, and external stimuli such as a change in pH, temperature, redox potential, and light can all be used to control the drug release profile of a nanogel system[91]. These triggers, which occur when the chemical connections between the drug and nanogels are broken or when the nanogels expand or contract, can lead to concentrated and cumulative drug release. Another characteristic of nanogels is that they are described as soft, sponge-like particles that change in size and shape in response to external forces[92]. In contrast to hard nanoparticles that maintain their size and structure

during circulation, such as silica, gold, magnetic, and PLLA nanoparticles, nanogels can be squeezed to diffuse past extremely dense biological barriers to reach desired places [93,94]. Furthermore, it has been demonstrated that more soft nanoparticles remained in circulation due to their resistance to phagocytosis in comparison to their hard nanoparticle counterparts, meaning that more particles can reach the targeted region [95,96]. As a result, these structural modifications can be performed to achieve the optimal drug delivery system, which must have efficient targeting to accumulate in the targeted site, a selective drug release to lessen side effects, and a good clearance rate from the body to prevent further toxicity.

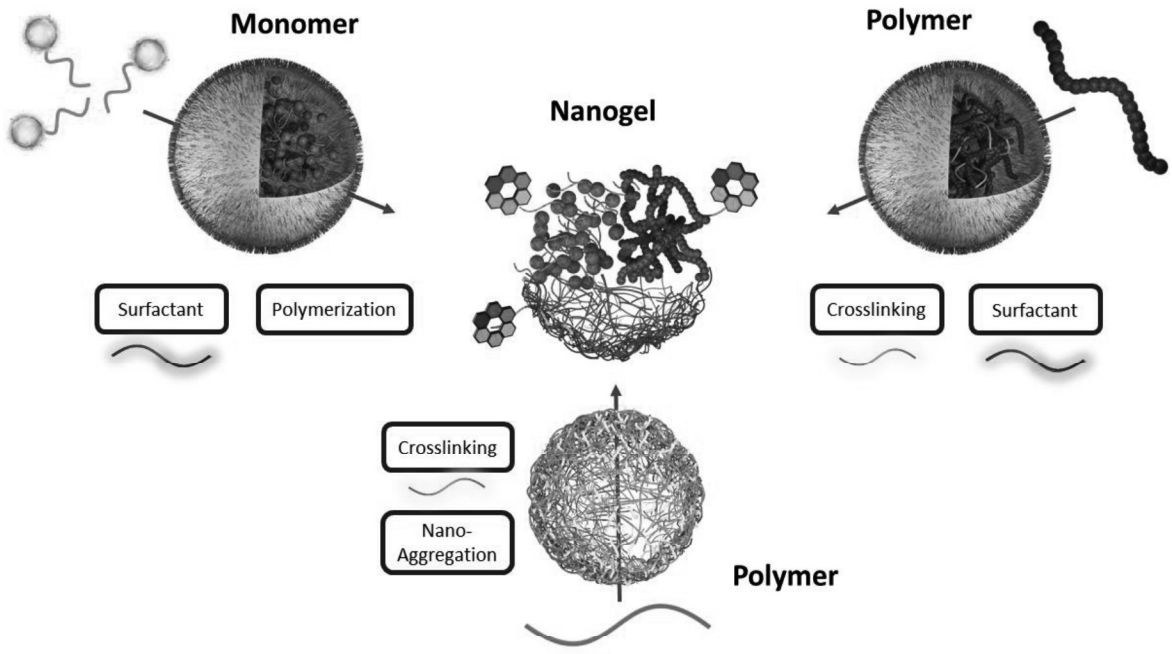

Figure 1.11. Different approaches in the synthesis of polymeric nanogels.

Nanogels are crosslinked soft polymeric nanoparticles that are water dispersible but not soluble. Since they are constructed of stretchable, extensible hydrophilic polymer chains, particles can absorb a lot of water when they come into contact with an aqueous environment. The fabrication of nanogels has involved using various polymers, ranging from natural polymers like hyaluronic acid, gelation chitosan, cellulose, and alginate to synthetic polymers like polyethylene glycol, poly(acrylic acid), poly(lactic acid), etc. [97]. The production of nanogels has primarily relied on the polymerization of monomers and the crosslinking of pre-formed polymers. The first method is inverse emulsion polymerization,

which necessitates using nanosized emulsions that determine the shape and size of nanogels. By utilizing initiators and crosslinkers, the monomers in these emulsions are polymerized to form nanogels directly. Stable nanogel in an aqueous media can be produced after removing both the solvent and the surfactant. For example, Deen and coworkers prepared nanogel from *N*-acryloyl-*N*'-methyl piperazine and methyl methacrylate using oil in water-type microemulsion polymerization[98]. In the study, ethylene glycol dimethacrylate was used as a crosslinker. Due to the pH-responsive polymer, the swelling profile of nanogels exchanged between swollen and deswollen states. Because of their swelling property as a function of pH, they could be good candidates for targeted drug delivery systems. In another study, Thayumanavan, Hardy, and coworkers prepared redox-responsive nanogels from cystine diacrylamide and hydroxyethyl acrylamide using inverse emulsion polymerization for drug delivery applications [99]. As illustrated in Figure 1.12, an apoptotic protein, Caspase-3 was also loaded into the emulsions before polymerization. Redox-responsive nanogels demonstrated better cytotoxicity against HeLa cells compared to redox-insensitive control nanogels.

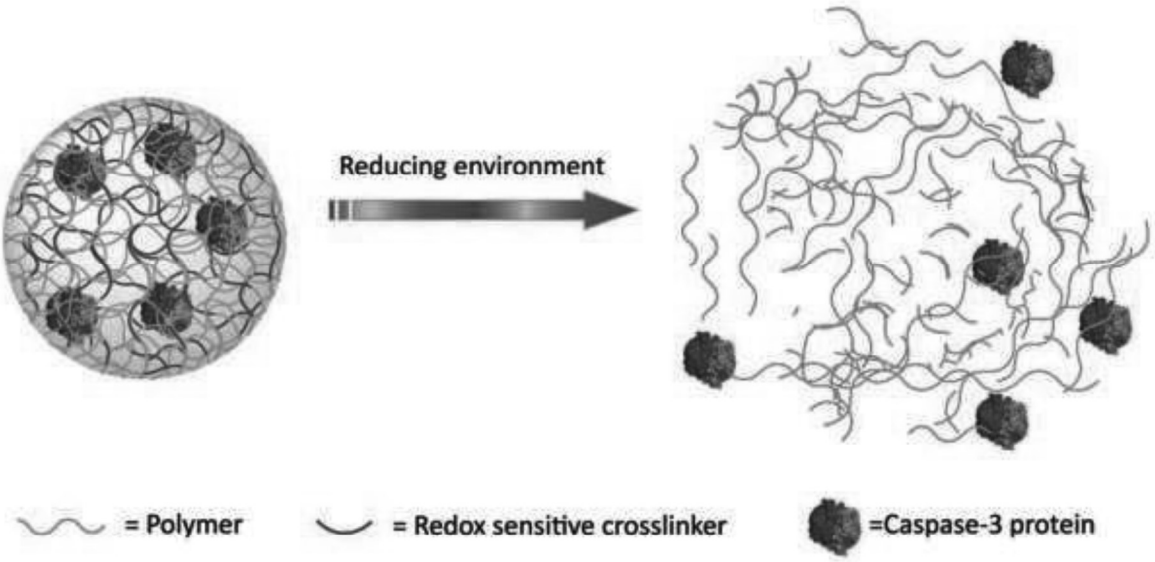

Figure 1.12. Schematic illustration of redox-sensitive nanogels [99].

Although relatively toxic initiators and emulsifiers must be introduced to the system, this method does not require a pre-formed polymer or any extra crosslinking techniques. The

second method relies on the crosslinking of pre-formed polymers in their nanoscale forms. The aggregation process and the nano-emulsion approach have been utilized frequently to produce these nano-size forms. By using physical interactions, including hydrophobicity and electrostatic interactions, polymers self-assemble into nanoaggregates. By crosslinking these polymeric nanoaggregates, nanogels can be formed. By employing this method, Thayumanavan and colleagues have made fundamental progress in the creation of redox-responsive nanogels using copolymers that include pyridyl disulfide [100-102]. In one of their studies, RAFT polymerization was used to randomly copolymerize pyridyl disulfide (PDS) methacrylate and PEGMA, as shown in Figure 1.13a [103]. These PEGMA-based polymers have a low LCST and produce nanoaggregates at higher temperatures than their LCST. Figure 1.13b demonstrates the 1,4-Dithiothreitol (DTT) addition to the solution to trigger crosslinking after the synthesis of nanoaggregates, resulting in nanogels. When the nanogels are formed, hydrophobic compounds like pharmaceuticals can be encapsulated *in situ.* These molecules can then be released when the nanogels are exposed to biological reducing agents like GSH. The easy manufacture of the drug-encapsulated delivery system, where crosslinking can be broken under biological conditions observed in malignant tissues and cells, makes this nano-drug delivery method a potential platform for tackling problems associated with diseases like cancer.

The nano-emulsion approach involves adding polymers to pre-formed nanosized emulsions, allowing for fine-tuning these polymer clusters' size by emulsion size. Once these clusters have developed, crosslinkers can be added to create nanogels. For example, Podgorna and coworkers prepared gadolinium alginate nanogels using reverse microemulsions and physical crosslinking. In the study, alginate and gadolinium(III) chloride hexahydrate was added separately to the microemulsions generated by oil in water microemulsion. Emulsions were then mixed to obtain nanogels with a diameter of around 100 nm. Nanogels were further used for magnetic resonance imaging (MRI) and drug delivery applications[104].

Depending on the functional groups on polymer chains, different crosslinking techniques are used with different types of polymers. Chemical crosslinking and physical crosslinking are the two categories of crosslinking methods. In chemical crosslinking,

polymers and crosslinkers form a new covalent bond. For example, Nguyen and coworkers used poly(styrene-alt-maleic anhydride) copolymers which are functionalized with furfuryl amine and hydrazine. This copolymer was crosslinked using dithiobismaleimidoethane molecules as crosslinker through the Diels-Alder reaction [105]. Contrarily, physical crosslinking necessitates physical interactions such as hydrogen bonds, electrostatic interactions, hydrophobic or host-quest interactions, chain entanglements, etc. For example, Keul, Möller, and coworkers used poly(ethylene imine) functionalized with C-10 alkyl chains and azetidinium groups, yielding an amphiphilic polymer. Nanogels composed of this polymer has high colloidal stability due to hydrophobic interactions between alkyl chains and ionic interactions between azetidinium groups [105]. Physical crosslinking produces more loosely bonded structures, whereas chemical crosslinking produces considerably more stable links. The essential motivation underlying all of those various nanogel designs and syntheses is to create incredibly precise structures that can be directed to the correct spot with the desired concentration at a predetermined time.

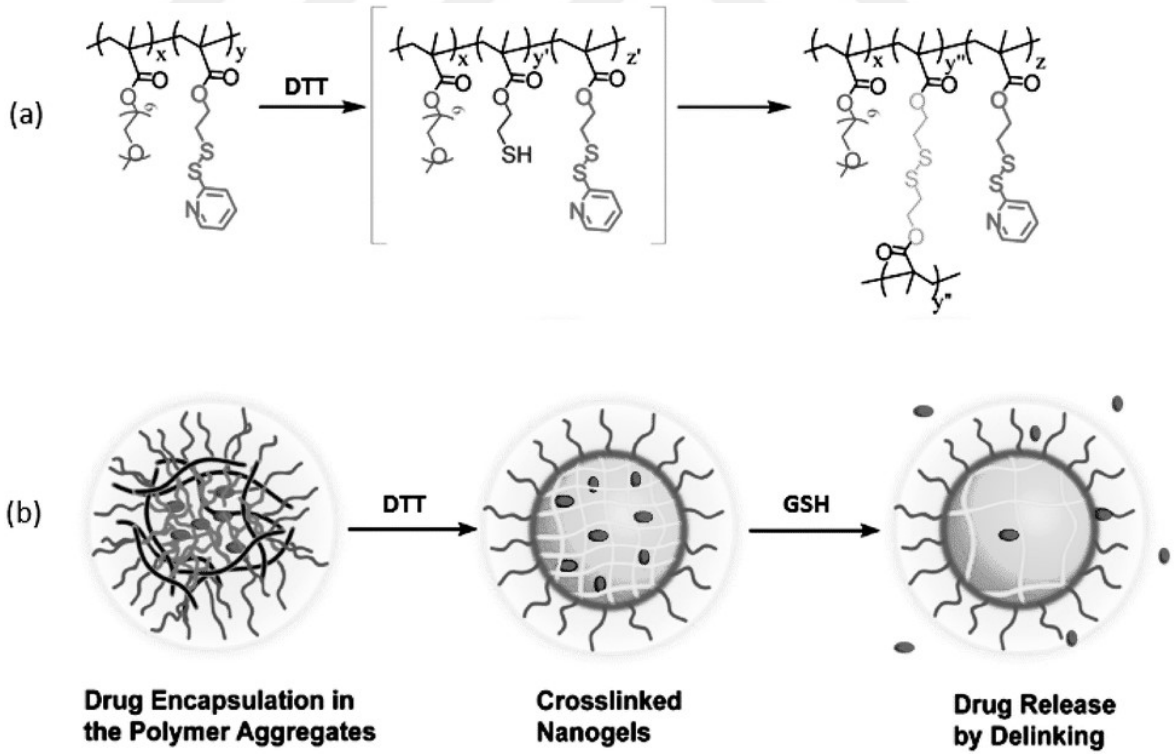

Figure 1.13. (a) Synthetic technique, and (b) crosslinking method of PDS-bearing polymers to produce a redox-responsive nanogel-based drug delivery system [103].

1.2.4. Drug Delivery using Micellar Nanoparticles

As an interdisciplinary science, nanotechnology allows the combining of biologically active chemicals on a single platform, ranging from relatively small molecules like diagnostic and therapeutic medicines to bigger molecules like targeting groups. NPs may facilitate transport across membranes, increase the stability and solubility of encapsulated cargos, and lengthen circulation periods to boost effectiveness [106,107]. Although it may appear unimportant, nanoparticle size is crucial for medication administration and imaging because poorly aligned cancer cells have an enhanced permeability and retention effect (EPR) that causes nanosized particles to accumulate in tumor tissue rather than healthy tissues. A wide range of tunings, including multifunctionality, size, elasticity, and stimulus reactivity, are provided for nanosized polymeric particles such as micelles [108] and nanogels [109]. Additionally, biocompatibility polymeric nanoparticles can easily elude the immune system and preserve their "stealth" to continue functioning in drug delivery [110]. For these reasons, NP investigation has been widely conducted, producing encouraging *in vitro* and small animal model outcomes [111].

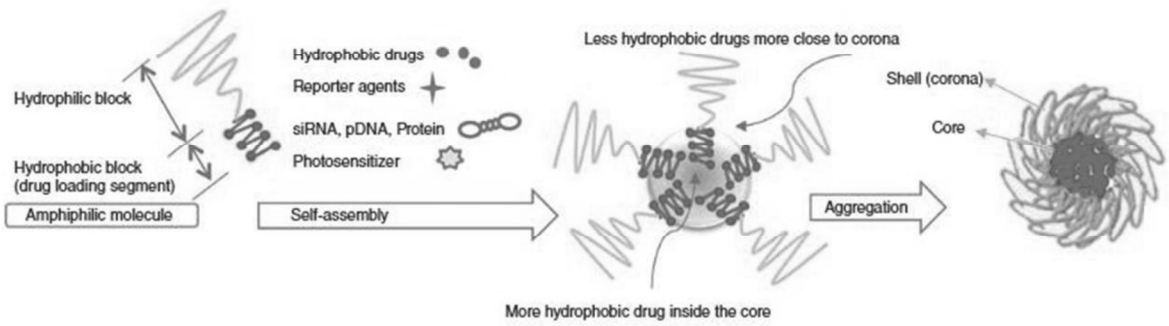

Figure 1.14. Formation of micellar structures and loading of functional agents [112].

Micellar delivery systems are a rapidly expanding and fascinating area of drug delivery research. The pharmaceutical industry is researching micellar structures for cancer drug solubilization, stability, and distribution. Polymeric micelles have properties that make them especially suitable for use in medication delivery, such as small size, custom nanoscopic architecture, stability, and ease of choice of polymer for compatibility with drug [113]. The

inner core and outer shell are the two distinct functional components that make up polymeric micelles, as illustrated in Figure 1.14 [112]. The inner core is in charge of drug loading capacity, stability, and release behavior, whereas the outer shell regulates *in vivo* pharmacokinetic behavior. The micellar structure must be large for extravasation from normal vessel walls and renal clearance and small enough for extravasation from tumor blood vessels so that micellar structure can accumulate in the tumor tissue, called passive targeting [114]. Micellar structures can also be decorated with biologically active molecules that interact with the receptors overexpressed in cancer cells, called active targeting. This method can change the drug internalization mechanism and subcellular positioning, reducing the P-glycoprotein (P-gp) efflux effect and, as a result, easing the release of entrapped molecules [115,116]. For example, HER2 targeting trastuzumab ligand has been used to decorate the PEGylated liposome formulation for gastric and breast cancers [117,118]. Sanyal and coworkers developed a dendron-polymer conjugate modified with trastuzumab to deliver docetaxel for breast cancer. As illustrated in Figure 1.15, dendron-polymer conjugates are composed of a linear PEG as the hydrophilic part and the generation four dendrons as the hydrophobic part. The hydrophilic end of conjugated is modified with NHS so that the outer shell of the micellar structure can be functionalized with trastuzumab. While internalization experiments showed an increased absorption of antibody-conjugated micelles by cells, cytotoxicity experiments showed improved toxicity for targeted micelles compared to non-targeted micelles [119].

Another highly common targeting ligand is the cyclic peptide c(RGDfK-) which is known for its selective binding to integrin receptors overexpressed on the endothelial cell surfaces of tumor vasculatures [120,121]. For example, Zhang, Gan, and coworkers designed a micellar structure made of PEO and PCL for the delivery of doxorubicin (DOX) for bladder cancer. In the study hydrophilic end of the copolymer was modified with the cyclic c(RGDfK) peptide and the fluorescence molecules for targeting and imaging purposes. In the study, it has been shown that c(RGDfK) modified micelles strongly interact with the bladder cancer cells (T-24 cells), and also DOX-loaded micelles inhibit the T-24 cell growth [122]. Sanyal and coworkers designed a core-crosslinked micelle system for targeted drug delivery [123]. Micelles were composed of hydrophobic polyester dendrons containing peripheral alkene groups and a hydrophilic copolymer of PEG-based monomer and NHS-

bearing monomer. Hydrophobic dendrons and hydrophilic dendrons were conjugated through azide-alkyne Huisgen cycloaddition. The polymer was then functionalized with c(RGDfK) peptide using NHS groups on the hydrophilic part of the copolymer. As illustrated in Figure 1.16, to obtain a stable micellar structure, the core of the micelles was crosslinked using a thiol-ene reaction in the presence of a tetra-arm thiol molecule under UV light. Results showed that although the release rate is slower, the core crosslinked micelle is more stable. Internalization experiments proved that targeted micelles are more easily internalized. Furthermore, *in vitro* cytotoxicity assay demonstrated that targeted micelles show higher toxicity than the nontargeted counterpart.

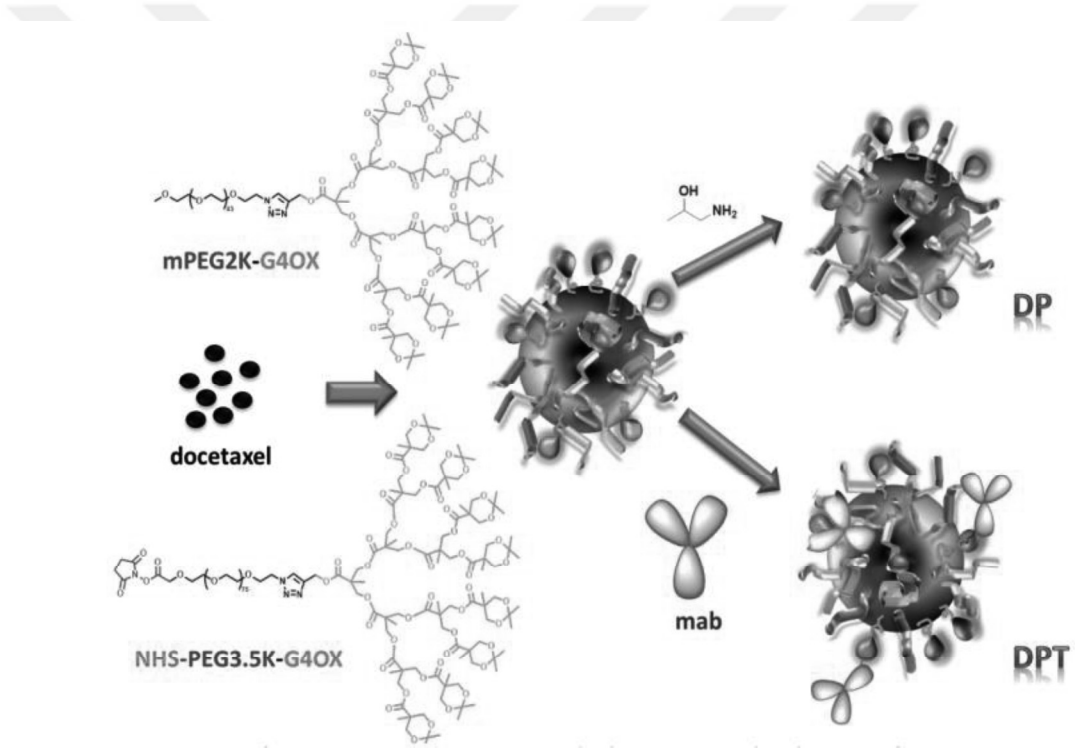

Figure 1.15. Schematic representation of targeted and non-targeted docetaxel-loaded micelles [119].

Although the physical loading of chemotherapeutic agents into micelle is prevalent, there are few examples of covalently bonding drugs. There are two main pathways to immobilize the drug molecules on the micellar structures chemically. One of the methods is to post-polymerization modification of polymers with drug molecules [124,125]. For example, Vetvicka and coworkers synthesized poly(ethylene oxide)-block-poly(allyl

glycidyl ether) polymer and modified the hydrophobic block with DOX through cleavable hydrazone bonds [126]. The second method is to use a drug monomer to make a hydrophobic block of the copolymer of micelles. One of the advantages of using drug monomers is to be able to attach multiple drug molecules to a single polymer chain so that drug loading can be increased as desired. The other advantage is to attach drug molecules to the polymer's backbone with a degradable chemical bond so that selective drug release can be achieved [127]. For example, Sarma, Shunmugam, and coworkers used norbornene-derived doxorubicin and poly(ethylene glycol) to get block copolymer for micellar structure [128]. Release studies showed that there was almost no release at neutral pH for 24 hours. However, an accelerated release was observed at lower pH solutions.

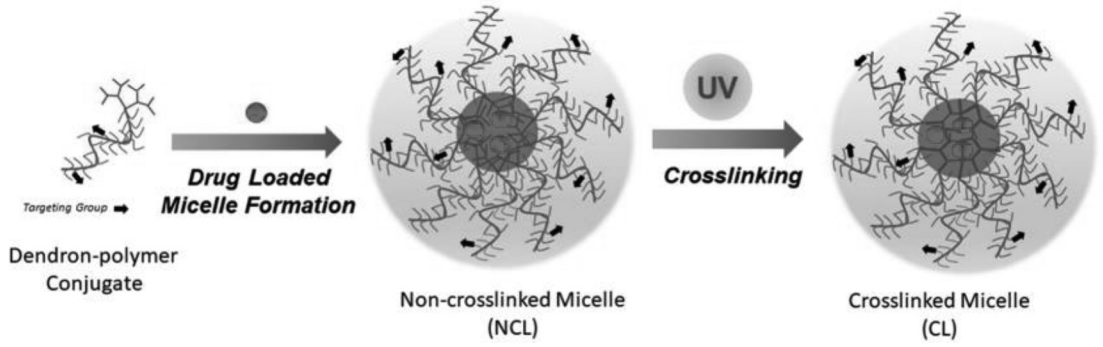

Figure 1.16. Schematic illustration of the synthesis of core-crosslinked targeted docetaxel-loaded micelles [123].

2. RESEARCH OVERVIEW

The goal of this thesis is to design and create a variety of stimuli-responsive polymeric materials for drug delivery. This goal was achieved by creating four types of polymeric materials: nanofibers, hydrogels, nanogels, and micelles.

The first two chapters discuss stimuli-responsive nanofibers for applications in drug delivery. Reduced graphene oxide (rGO)-embedded nanofibers were fabricated for the photo-thermally triggered delivery of antibiotics. Due to its high surface area and effective light-to-heat conversion, rGO is a unique material that can be used for photothermal applications. In this part, rGO-embedded poly(acrylic acid) nanofiber was fabricated and evaluated for the on-demand delivery of ampicillin and cefepime. The second chapter explores pH-responsive nanofibers for the delivery of doxorubicin and docetaxel. Highly acid-sensitive nanofiber mats with a high surface area to volume ratio were designed to treat cancer reoccurrence. The presence of cancerous cells will change the local pH and thus trigger drug release to eradicate them. In the following chapter, fast-forming dissolvable redox-responsive hydrogels were fabricated to deliver therapeutic proteins. In this chapter, two different polymers were synthesized, which upon mixing, rapidly reacted with each other to yield hydrogels. On-demand dissolution of hydrogels and release of entrapped cargo were achieved through redox-responsive degradation. In the fourth chapter, biodegradable redox-responsive nanogels were designed to deliver the anticancer drug docetaxel. The cellular internalization of nanogels with active and passive targeting abilities was investigated. The cytotoxicity of redox-responsive nanogel loaded with docetaxel was analyzed in the reductive and non-reductive intracellular environment. In the last chapter, pH-responsive and targeted micelles for the delivery of chemotherapeutic agents were fabricated. Micelles were prepared using a diblock copolymer, where the first block was composed of poly(ethylene glycol)-based side chains, and the second block was composed of 5-fluorouracil-containing side chains. In the next step, micelles were modified with a targeting group and loaded with a second drug, docetaxel. Internalization and cytotoxicity experiments of pH-responsive and targeted micelles were investigated. In conclusion, this

dissertation describes the design and synthesis of various stimuli-responsive polymeric materials, which could address some of the challenges in drug delivery.

3. REDUCED GRAPHENE-OXIDE-CONTAINNING POLY(ACRYLIC ACID) NANOFIBER: A PHOTOTHERMALLY CONTROLLED ANTIBIOTIC DELIVERY PLATFORM

Adapted with permission from {Altinbasak, I., R. Jijie, A. Barras, B. Golba, R. Sanyal, J. Bouckaert, D. Drider, R. Bilyy, T. Dumych, S. Paryzhak, V. Vovk, R. Boukherroub, A. Sanyal, and S. Szunerits, "Reduced Graphene-Oxide-Embedded Polymeric Nanofiber Mats: An 'On-Demand' Photothermally Triggered Antibiotic Release Platform.", ACS Applied Materials and Interfaces, Vol. 10, pp. 41098–41106, 2018.} Copyright {2018} American Chemical Society [129].

3.1. Introduction

One of the challenges frequently encountered in traditional methods of drug delivery relates to poor control over the proper dosage of the therapeutic agent [130-132]. Maintaining the drug concentration within a particular therapeutic window and below toxic concentrations is challenging, and a lack of efficient treatment can lead to severe side effects, along with the development of drug resistance in cells and pathogens. These problems have fostered the development of different approaches that enable the controlled release of a precisely defined amount of drug but allow the release of the therapeutic dose on demand upon the application of an external trigger rather than passively driven diffusion processes. In the last decade, several delivery systems have been fabricated to deliver a drug locally by controlling release kinetics through the utilization of various types of stimuli, either external or intrinsic to the disease site [133,134]. The capability to tune the physicochemical properties of polymeric nanostructures, as well as other advantages such as their stability *in vitro* and *in vivo* conditions and good biocompatibility, has laid the foundation for the emergence of a large number of polymeric nanosystems for controlled drug release [135-138].

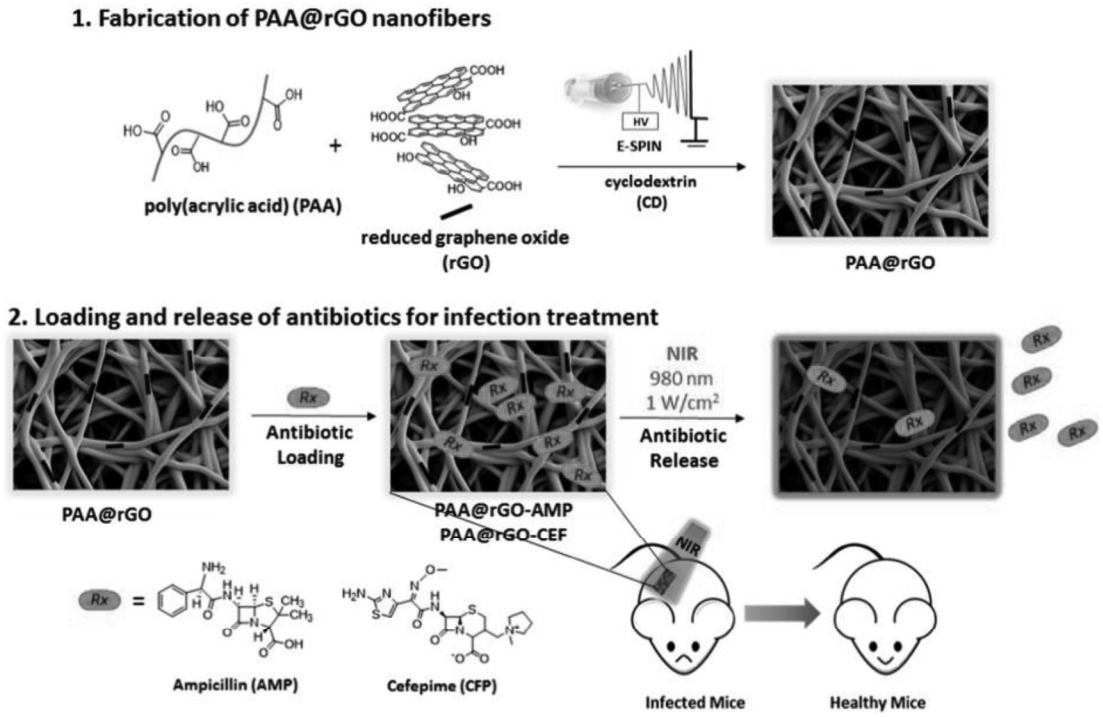

Figure 3.1. Illustration of the fabrication of antibiotic-loaded PAA@rGO nanofibers: (1) electrospinning of rGO-loaded PAA nanofiber mats followed by (2) loading with different antibiotics and photothermal-triggered antibiotic release.

Over the past decades, there has been considerable evidence of the benefits of polymeric materials as antibiotic delivery platforms [139-141]. Polymeric materials have been shown to solve problems related to the solubility of hydrophobic antibiotics, as well as provide a protective coating against environmental degradation and deactivation through the body's clearing mechanisms. The structures proposed range from discrete soluble polymers conjugated with antibiotics [142] to materials where polymers are chemically or physically assembled in the form of hydrogels [143-146], micelles [147], nanogels [148], nanoparticles [149], and nanofibers [150]. Polymeric nanoparticles are well suited for addressing bacterial infections inside the body as the nanometric size of antibiotic-loaded nanoparticles enables efficient penetration through the mucus layer around bacteria biofilms, thus increasing the local concentration of antibiotics in the biofilm. On the other hand, antibiotic-loaded bandages, foams, and dressings are preferential for external applications such as the management of chronic wounds [151,152]. In this regard, antibiotic-loaded nonwoven fibrous materials obtained using polymeric nanofibers could be ideal candidates for wound

infection treatment, as they can be directly fabricated in the form of ready-to-apply materials. One of the most commonly encountered challenges in wound healing is infection. Next to iodine- or silver-ion-containing dressing, antibiotic ointments are regularly used to prevent wound infection [153]. In the case of antibiotic ointments, discomfort caused to the patient, along with the chances of developing resistance to antibiotics and contact dermatitis, have put their efficiency into question [154].

One attractive alternative as a wound-healing material and a protective scaffold after surgical procedures, favoring site-specific therapy by increasing the local antibiotic concentration, might be using antibacterial-loaded nanofiber mats. These polymeric scaffolds are engineered via a polymer-processing technique called electrospinning, which allows the usage of a variety of polymers with different chemical compositions and morphologies [155-157]. This enables selecting the most appropriate material for the intended application and tailoring drug release profiles [158]. Hadjiargyrou and co-workers demonstrated the incorporation of hydrophilic antibiotics (mefoxin and cefoxitin) and their release in a sustained manner from poly(lactide-co-glycolide) nanofiber-based scaffolds obtained using electrospinning without compromising their bioactivity and structure [159]. A passive diffusion release of about 70% of loaded cefoxitin was observed in the first hour, and the rest of the loaded antibiotic was released over one week. Although the antibiotic that was released from these nanofibers was effective in inhibiting *Staphylococcus aureus* growth (>90%), burst release is an undesirable feature. To achieve an antibiotic release at a constant rate over a prolonged time period, stimuli-responsive nanofibers have been designed, mainly using pHbased triggers [160,161]. For example, ciprofloxacin-loaded pH-responsive electrospun nanofibers fabricated from a copolymer of vinyl benzoic acid and vinyl benzyl-trimethylammonium chloride, as reported by Uyar and co-workers, undergo enhanced drug release at pH 5.8. Although external modulation of pH is nontrivial, modulation of temperature is unique, as it can be considered either internal stimuli, as some infections are naturally at elevated temperature or external through the application or generation of heat in the nanostructure. In the case of polymers, a temperature change can result in rapid swelling of its structures, leading to high volume alterations and thus inducing enhanced drug release. Some photothermal active nanofibers formed through the incorporation of gold nanostructures [162-164], carbon nanotubes [165,166], carbon

nanoparticles [167], or, more recently Cu_2S [168] have been described. Recently, we have shown interest in reduced graphene oxide (rGO)-loaded hydrogels for photothermal-initiated insulin release [55].

Interestingly, although reports of graphene oxide (GO) and rGO-containing nanofibers have emerged in recent years [169-172], only one report used the photothermal properties of the resulting nanocomposite [173] and showed photothermal eradication of captured cancer cells. The photothermally triggered release of antibiotics from rGO-containing nanofibers and its use for the treatment of infections has not been explored until now. Herein, we disclose rGO-containing poly(acrylic acid) (PAA) based nanofiber mats (PAA@rGO) for the loading of different antibiotics due to their swelling and noncovalent interaction with rGO, as well as demonstrate controlled and on-demand release promoted by near-infrared photothermal heating as illustrated in Figure 3.1. To allow facile diffusion of antibiotics under an aqueous environment into nanostructures, we opted for the formation of rGO-loaded hydrophilic nanofibers by electrospinning PAA in the presence of cyclodextrin as a cross-linker. These nanofiber mats showed controlled photothermal heating ability, with the temperature reaching 67 ± 2 °C using a light source of 980 nm and 1 W cm^{-1} power density. The PAA@rGO nanomats achieved high loading capability for ampicillin (AMP) and cefepime (CFP) with minimal passive antibiotic release. Ampicillin, part of the aminopenicillin family, was chosen for its favorable structure (aromatic ring together with the presence of amine and acid functional groups), enabling ampicillin to interact with rGO through electrostatic and π-stacking interactions. The same is true for cefepime (CFP), an antibiotic belonging to the class of cephalosporin commonly applied for the treatment of bacterial conditions such as pneumonia, kidney, urinal, as well as skin infections. This antibiotic works by simply stopping the growth of bacteria [174]. Enhanced drug release was achieved under irradiation of the antibiotic-loaded PAA@rGO nanofiber mats with near-infrared light at 980 nm, where the antibiotic release rate can be tuned upon using different power densities. In vitro antibacterial assay demonstrates clearly that the released antibiotics did not lose their biological activity to inhibit growth of pathogens. The nanofiber platform could be reloaded with antibiotic and release was achieved in a controlled fashion, thus demonstrating recyclability of the platform. Furthermore, through in vivo studies on *S.*

aureus infected Balb/c mice, the antibiotic-loaded PAA@rGO nanofiber mats demonstrated excellent wound healing capability, making them viable candidates for clinical applications.

3.2. Experimental

3.2.1. Materials

Poly(acrylic acid) (PAA, Mn = 450 000 g mol^{-1}), hydrazine, β-cyclodextrin, phosphate-buffered saline (PBS, pH 7.4), and cefepime were purchased from Sigma-Aldrich. Ampicillin (AMP) was obtained from Fisher BioReagents (BP1760-25). Graphene oxide (GO) in powder form was purchased from Graphenea (Spain).

3.2.2. Methods

Scanning Electron Microscopy (SEM) images were obtained using an electron microscope ULTRA 55 (Zeiss, France) equipped with a thermal field emission emitter and three different detectors (EsB detector with filter grid, high-efficiency In-lens SE detector, and Everhart-Thornley Secondary Electron Detector). A Horiba Jobin Yvon LabRam high-resolution micro-Raman system combined with a 473-nm (1 mW) laser diode as an excitation source was used for Micro-Raman spectroscopy measurements. Visible light was focused by a 100× objective. Using a backscattering configuration, the scattered light was collected by the same objective, dispersed by an 1800 mm focal length monochromator, and detected using a CCD camera. A Thermo Scientific Nicolet 380 FT-IR spectrophotometer was used for obtaining Fourier transform infrared spectrum. Kratos Analytical Axis Ultra X-ray photoelectron spectrometer (XPS/ESCA) with an Al Kα-monochromatic source of 1486.71 eV was used for recording XPS spectra.

All irradiations were performed in standard 96- well plates. For photothermal experiments, a 980 nm-continuous wave laser (Gbox S-3 model, Fournier Medical Solution) was used at laser power densities between 0.5 and 2 W cm^{-2}. This laser was injected into a

400 μm-core fiber and placed at 6 cm from the bottom of the wells. The output was non-collimated and the resulting beam divergence allows uniform illumination of four wells. The temperature changes on the surface of the nanofiber mats were captured by an infrared camera (Thermovision A40) and processed with the ThermaCam Researcher Pro 2.9 software.

The concentration of ampicillin and cefepime loaded PAA@rGO was determined by an HPLC system (Shimadzu, Tokyo, Japan) equipped with a 5 μm C4 QS Uptisphere® 300 Å, 250 mm × 4.6 mm column (Interchim, Montluçon, France) heated to 40 °C. The mobile phase consisted of a mixture of eluent A (trifluoroacetic acid 0.1% in water) and eluent B (trifluoroacetic acid 0.1 % in acetonitrile) at a flow rate of 1 mL/min. The samples were injected at a volume of 40 μL and the detection at a wavelength of 227 nm.

The Gram-negative *E. coli* K12 were grown at 37 °C with shaking in Luria Bertani (LB) broth overnight. Upon 100-fold dilution, incubation was prolonged until the OD_{600} had reached 0.3-0.5. *S. epidermidis*, a clinical strain obtained from the Central Hospital of Roubaix (France), and S. aureus (ATCC® 25923) were grown in brain heart infusion (BHI) medium at 37°C overnight without agitation.

Following the release of ampicillin and cefepime, bacteria survival was measured by determining the titer of viable bacteria's ability to grow. A 10-fold dilution series of the bacterial solutions in phosphate buffer saline were spotted in 10 μL aliquots on an LB-agar medium. Visual counting of the number of colonies upon overnight incubation at 37 ºC allowed reading out the initial and final concentrations of the bacteria strains in cfu mL^{-1}.

Studies involving animals, including housing and care, method of euthanasia, and experimental protocols, were conducted in accordance with the local animal ethical committee in the animal house (Permission 20170918/8) of Danylo Halytsky Lviv National Medical University, under the supervision of Prof. R. Bilyy. S-5 Six to 8-week-old male Balb/c mice were used for this investigation. The mice were housed in cages covered with air filters in a temperature-controlled room with a 12 h light and 12 h dark schedule and kept on a standard diet with drinking water available *ad libitum*. All animal experiments were

performed in accordance with institutional ethical guidelines. For the bacterial surface infection, mouse fur on the back was removed using MedaSept medical depilation cream. The superficially damaged skin infection model was performed as described previously [175] with some modifications. After removing the fur, plaster was applied to the mouse skin (1 cm^2) 15 times to remove the superficial epidermis. The skin became visibly damaged and characterized by reddening and glistening but no regular bleeding. Then ten μL of S. aureus bacterial cells (4×107 cfu mL^{-1}) were applied to the skin was allowed to dry for 10 min. Superficial skin infection was established after 24 h, and PAA or cefepime-loaded PAA@rGO nanofiber mats were applied to the skin of anesthetized mice. Untreated mice were used as control. The mat was illuminated for 10 min with a Near-Infrared light-emitting diode (LED) array (6×6 mm^2 in size, 8 W, 2A, 940 nm), previously shown to be a safe condition for animals [175]. The temperature was monitored by an infrared camera (Thermovision A40). Mice were photographed with an S-6 Nikon camera, equipped with a Micro-Nikkor objective, from a fixed position and with a reference ruler present in each picture. Photos were processed with ImageJ software to detect erythema, and its area before and 24 h after treatment with a patch was evaluated. After 24 h, the mice were sacrificed, and the skin was removed, photographed, and fixed with 4% neutral buffered formalin solution and embedded in paraffin according to the standard laboratory protocol. The sliced tissues were stained by hematoxylin and eosin (H&E) (Sigma-Aldrich) or Gram stain (Remel, Lenexa, KS) using routine laboratory procedures. Gram staining was performed by applying crystal violet to the tissue sections for 5 min at room temperature, and slides were rinsed to remove excess crystal violet. Gram iodine mordant was applied for 2 min to the tissue sections and washed in tap water. To remove any non-specific crystal violet staining, a Gram decolorizer solvent was applied to the slides for 30 s, then quickly rinsed under running tap water until the water ran clear. The sections were then stained with Gram Safranin for 1 min and 40 s, followed by dehydration through a series of alcohol (95–100 %) to xylene and then coverslipped.

3.2.3. Fabrication of rGO-Loaded PAA Nanofiber (PAA@rGO)

GO precursor was chemically reduced to reduced graphene oxide (rGO) using hydrazine according to a procedure previously reported by us [176,177]. Briefly, GO

aqueous suspension (5 mL, 0.5 mg mL^{-1}) was treated with hydrazine (0.50 mL, 32.1 mM) at 100 °C for 24 h. After this time, the reduced GO gradually precipitates. Filtration through a poly(vinylidene difluoride) membrane (0.45 μm pore size) is used to collect the product. The obtained residue is washed with copious amounts of water (5 × 20 mL) and methanol (5 × 20 mL). Finally, the product is dried in an oven for 18 h at 100 °C. Thereafter, PAA (100 mg) and βcyclodextrin (20 mg) were added to rGO aqueous suspension (1.2 mL, 2.5 mg mL^{-1}), and the resulting mixture was stirred for 24 h at room temperature. This corresponds to rGO (2.4 wt %), PAA (81.4 wt %), and β-cyclodextrin (16.2 wt %). A clear polymer solution of PAA, β-cyclodextrin, and rGO was electrospun using a 1 mL syringe fitted with a 14-gauge blunt needle at the rate of 0.005 mL min^{-1} with 15 kV. The distance was kept at 15 cm during the electrospinning process. The resulting electrospun fibers were cross-linked under vacuum at 140 °C for 30 min.

3.2.4. Loading of Antibiotics onto Nanofibers

Antibiotic loading into the nanofibers was achieved by immersing the nanofiber mat (4 mg) into the aqueous solution of ampicillin (80−400 μg mL^{-1}) or cefepime (80−400 μg mL^{-1}) and shaking (150 rpm) at four °C for 72 h. The concentration of ampicillin and cefepime loaded into the nanofibers was determined from the absorption intensity of the AMP and cefepime remaining in the solution using a high-performance liquid chromatogram (HPLC). Ampicillin and cefepime calibration curves were obtained using a series of antibiotic-containing solutions (1−100 μg mL^{-1}) and are shown in Figure 3.2a and Figure 3.2b.

3.2.5. Photothermal-Triggered Antibiotics Release

The antibiotic release was assessed in phosphate-buffered saline (PBS) (1 mL, pH 7.4) through direct irradiation of the nanofibers using a continuous wave laser at 980 nm at varying power densities (1−2 W cm^{-2}) for several minutes. The amount of antibiotics released was determined from HPLC results of the solution collected after irradiation using previously established calibration curves shown in Figure 3.2. Control experiments were

carried out in an environmentally controlled cabin at 37 °C, and the samples were gently shaken during incubation.

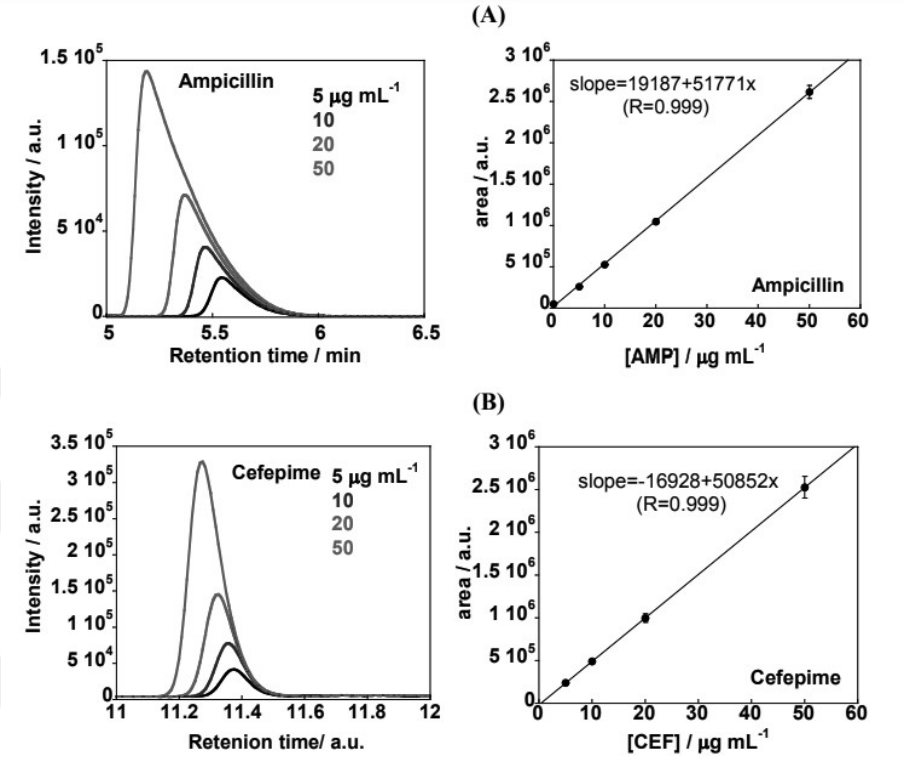

Figure 3.2. (a) HPLC plot of AMP (5, 10, 20 and 50 µg mL-1) in PBS (0.1 M, pH 7.4) together with AMP calibration curve; (b) HPLC plot of CFP (5, 10, 20 and 50 µg mL-1) in PBS (0.1 M, pH 7.4) together with CFP calibration curve.

3.2.6. Wound Healing and Histology

6−8-Week-old male Balb/c mice were selected for the experiment. The infection model with superficial skin damage was used. After removing the fur, plaster was applied to the mouse skin (1 cm^2) several times to remove the superficial epidermis. The skin damage was visible and characterized by reddening and glistening but no regular bleeding. Then, ten µL of *S. aureus* bacterial cells (4 × 107 cfu mL^{-1}) were applied to the skin and allowed to dry for 10 min. Superficial skin infection was established after 24 h, and PAA- or cefepime-loaded PAA@rGO nanofiber mats were applied to the skin of the anesthetized mice.

Untreated mice were used as control. The mat was irradiated for 10 min with a near-infrared light-emitting diode (LED) array (6 × 6 mm^2 in size, 8 W, 2A, 940 nm), previously shown to be a safe condition for animals. The temperature was monitored by an infrared camera (Thermovision A40). Mice were photographed, and images were processed with ImageJ software to detect erythema, and its area before and after a 24 h treatment was evaluated. After 24 h, the mice were sacrificed, and the skin was removed and subjected to histological analysis.

3.3. Results and Discussion

3.3.1. Fabrication and Characterization of rGO-Containing Nanofibers

First, PAA nanofibrous mat containing rGO was fabricated through electrospinning of a mixture of rGO (2.4 wt %), PAA (81.4 wt %), and β-cyclodextrin (16.2 wt %) as a cross-linker. A stand-alone nanofiber mat is fabricated upon electrospinning, as shown in Figure 3.3a. Figure 3.3b shows the Raman spectra of PAA and PAA@rGO that were recorded to confirm the incorporation of rGO into the nanofibers. Raman analysis revealed the presence of the expected bands at ≈1350 cm^{-1} (D-band) and ≈1580 cm^{-1} (G-band) due to the defects and disorders and the graphitized structure of rGO, respectively. The ID/IG intensity ratio was found to be 0.93 for rGO. The PAA fibers did show a Raman band at 1728 cm^{-1} assigned to C=O functional groups, whereas the bands at 1235 and 1285 cm^{-1} are ascribed to $-CH_2-$ bonds [178]. In the case of PAA@rGO, the bands of rGO are identifiable in the Raman spectrum. Additionally, Fourier transforms infrared (FTIR) and X-ray photoelectron spectroscopy (XPS) spectra of PAA@rGO were obtained, where the FTIR analysis did not provide any information about rGO incorporation due to its low amount, as can be seen in Figure 3.4a, but Figure 3.4b shows that the XPS spectra (C 1s scan) which prove the presence of delocalized π-electrons.

To ensure long-term stability in the aqueous media of the hydrophilic PAA@rGO nanofibers, the fibers were cross-linked to prevent their dissolution. As reported earlier, β-

cyclodextrin, a molecule containing multiple hydroxyl groups, can be efficiently used to cross-link the PAA polymer upon heat treatment under vacuum for 30 min [179]. The morphology of the resulting cross-linked PAA@rGO nanofibers was probed using scanning electron microscopy (SEM). Figure 3.3c shows the formation of dense mats of interwoven nanofibers 400 ± 150 nm in diameter. Furthermore, as can be seen in Figure 3.5, the integration of rGO did not alter the morphology of the nanofibers. The stability of the cross-linked PAA@rGO nanofibers was confirmed by treating them in water for 60 hours at 37 °C. SEM analysis in Figure 3.3d shows that the nanofibers keep their morphology, and no degradation of fibrous networks is observed.

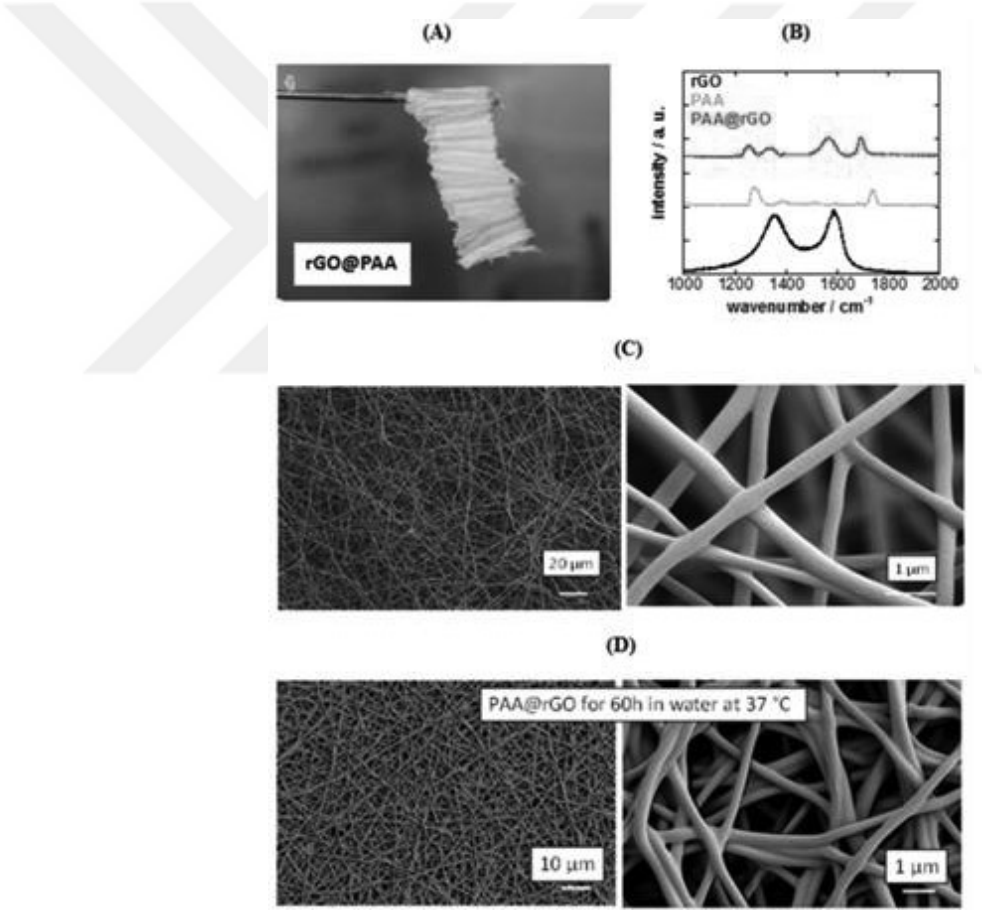

Figure 3.3. Characterization of rGO-loaded PAA nanofiber mats formed by electrospinning: (a) photograph of electrospun PAA@rGO; (b) Raman spectra of rGO (black), PAA (gray), and PAA@GO (red); (c) scanning electron microscopy (SEM) images of nanofiber mats; and (d) stability of β-cyclodextrin cross-linked PAA@rGO nanofibers in water at 37 °C for 60 h.

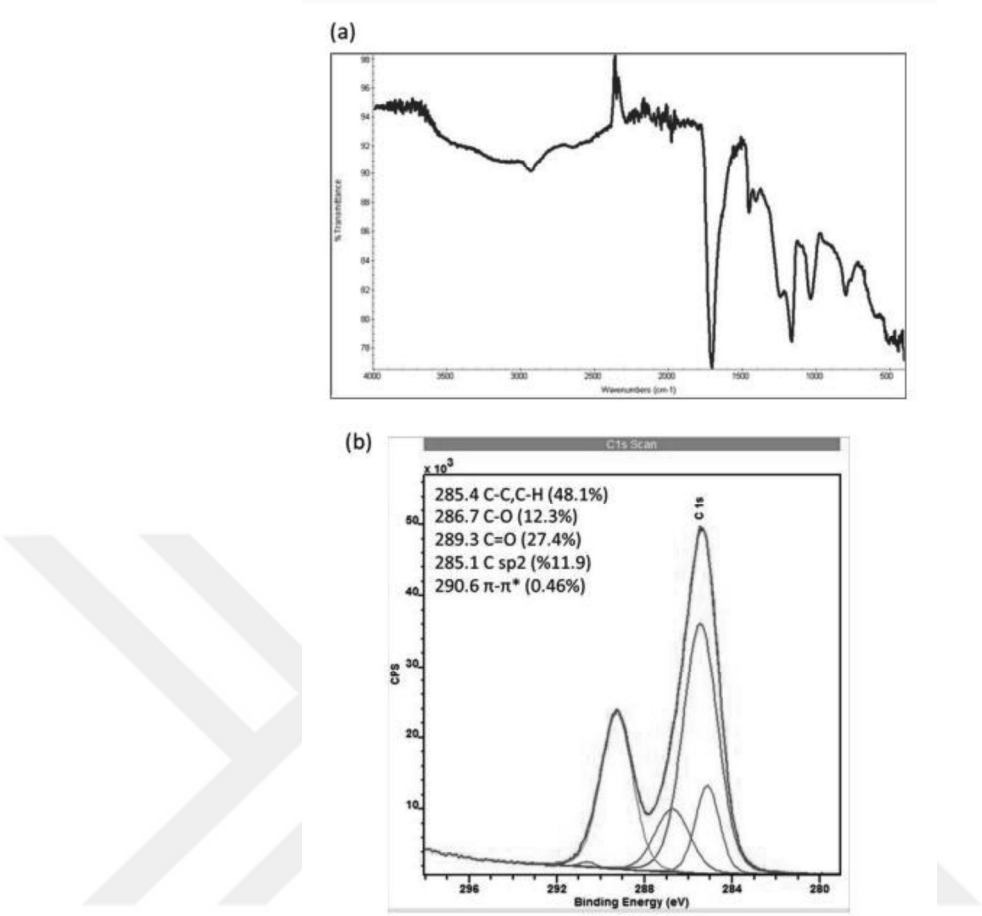

Figure 3.4 (a) FTIR and (b) XPS (C1s Scan) spectra of PAA@rGO nanofibers.

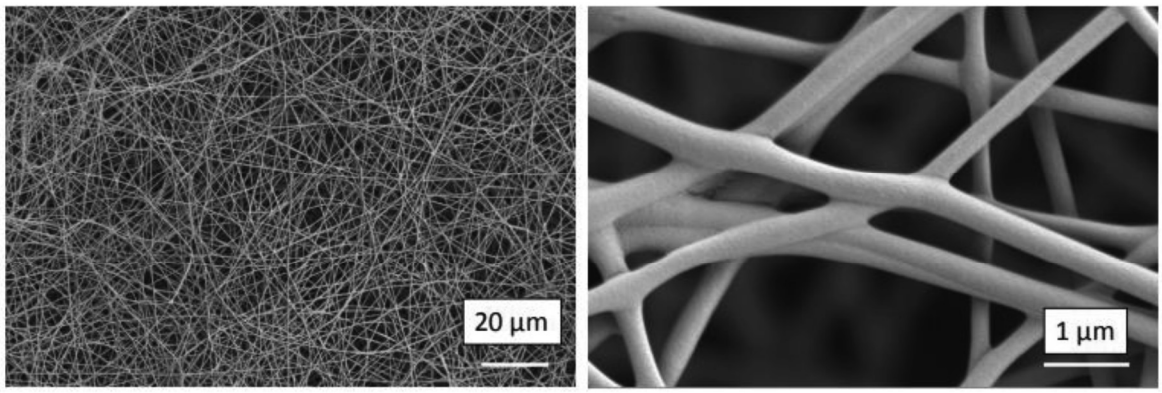

Figure 3.5. SEM images of fabricated rGO@PAA nanofiber mats at different scales.

Figures 3.6a and b demonstrate the thermal behavior of nanofiber mats under NIR lights. Whereas PAA displayed only negligible photothermal heating, direct irradiation of PAA@rGO (4 mg immersed in 1 mL PBS) with a continuous wave laser at 980 nm (1 W cm^{-2}) for 5 min resulted in a surface temperature of about 67 ± 2 °C. Even decreasing the laser power density to 0.5 W cm^{-2} showed a rapid increase in the surface temperature of PAA@rGO nanofibers, reaching saturation at approximately 51 ± 2 °C within 5 min in a wet environment. No melting of nanofibers occurred under the used conditions, thus preserving the structural integrity of the fibrous mats. Thus, with modulation of laser power density, these nanofiber mats exhibited controlled photothermal heating ability within a temperature range from 20 to 67 ± 2 °C.

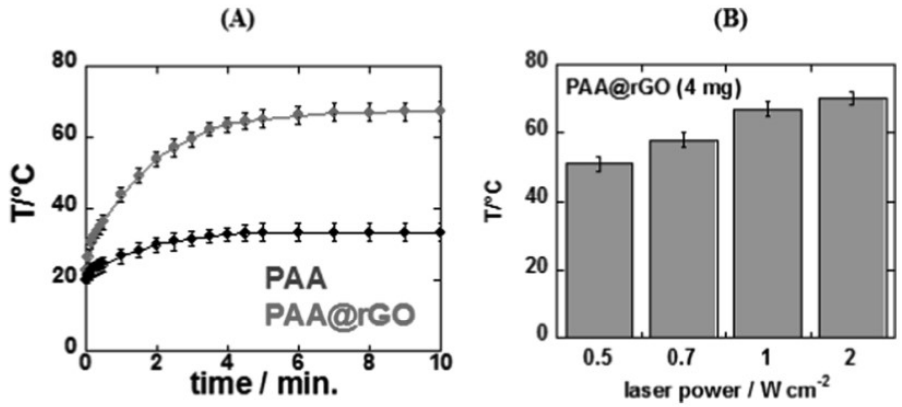

Figure 3.6. Photothermal properties of cross-linked PAA@rGO: (a) photothermal heating curves of PAA (gray) and PAA@rGO (red) nanofiber patches (4 mg) immersed in PBS (0.1 M, pH 7.4) and irradiated at 980 nm (1 W cm^{-2}) for 10 min and (b) temperature profile of PAA@rGO nanofiber mats upon 10 min irradiation at varying power densities.

3.3.2. Loading and Release of Antibiotics into Nanofibers

Integration of antibiotics into the cross-linked PAA@rGO nanofiber mats was achieved by simply immersing the nanofibers into the aqueous solution of ampicillin or cefepime in water at 4 °C for 72 h. Both antibiotics contain aromatic structures together with amino and carboxylic acid functional groups, thus promoting their interaction with rGO through π–π stacking and/or electrostatic interactions. The loading capacity of PAA@rGO

nanofibers for AMP and cefepime was determined from the amount of the antibiotic in the solution before and after loading using HPLC. The loading capacity of PAA@rGO for ampicillin and cefepime is comparable, as seen in Figure 3.7a. Using the solution concentration of 400 μg mL^{-1} of the antibiotics resulted in the loading of about 85 ± 3 μg mL^{-1} (21%) and 89 ± 3 μg mL^{-1} (22%) for ampicillin and cefepime, respectively. Ampicillin has pKa ≈ 4−5 (COOH) and pKa ≈ 9 (NH_2), making it zwitterionic at physiological pH. A fair amount of the amine groups are positively ionized at physiological pH, and this promotes their interaction with the PAA@rGO nanofiber mats (pKa ≈ 4.5) [180]. The quaternary ammonium group of the *N*-methyl pyrrolidine groups in cefepime makes the drug positively charged and results in interaction with the ionized carboxylic acid groups in PAA and negatively charged rGO that has a ζ-potential of −50 ± 2 mV. Due to their hydrophilic nature, it can be expected that the nanofibers swell in aqueous media and thus load the antibiotics efficiently. Remarkably, the passive release from the antibiotic-loaded PAA@rGO nanofibers, PAA@rGO−AMP, and PAA@rGO−CFP was negligible. For the first five h, the amount of antibiotic release was below the detection limit of the HPLC analysis. After 24 h incubation in PBS (0.1 M, pH 7.4), about 0.8 ± 0.1% was released via passive diffusion (Figure 3.7b).

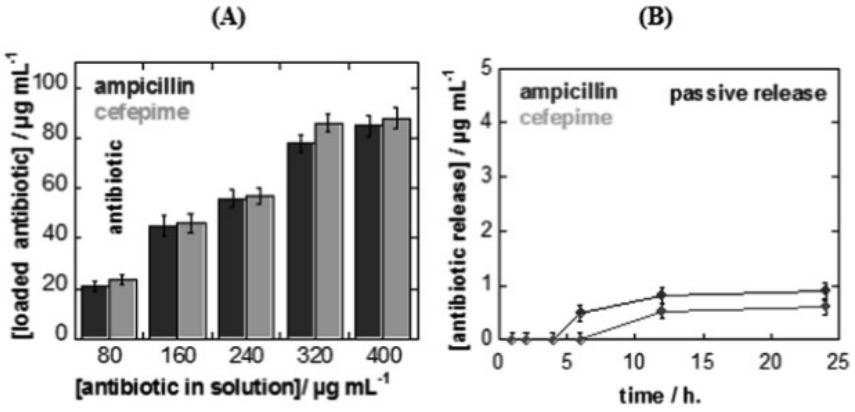

Figure 3.7. (a) Loading capacity of PAA@rGO nanofiber mats (4 mg) with ampicillin and cefepime upon incubation for 24 h into PBS (0.1 M, pH 7.4) under shaking at different drug concentrations. (b) Passive release from antibiotic-loaded cross-linked PAA@rGO nanofibers when immersed in 0.1 M PBS (pH 7.4) for 24 h at 37 °C.

Encouraged by the excellent stability of the PAA@rGO to retain the loaded antibiotics, we explored the photothermal properties of the PAA@rGO nanofiber mat to trigger the drug release. Figure 3.8a shows the release profiles for ampicillin as well as cefepime upon irradiating PAA@rGO nanofibers loaded with ampicillin (25 μg mL^{-1}) and cefepime (25 μg mL^{-1}) with NIR light. Using a laser power density of 2 W cm^{-2} results in an almost complete release of ampicillin (24 μg mL^{-1}; ≈96% of loaded ampicillin) with a release rate of 3.2 μg mL^{-1} min^{-1}, which can be lowered to 0.5 μg mL^{-1} min^{-1} using a photo trigger of 1 W cm^{-2}. The released ampicillin concentrations are much larger than the minimum inhibitory concentration (MIC) value of ampicillin for Gram-negative *Escherichia coli* K12 as shown in Table 3.1. Ampicillin shows no activity for *S. aureus* and *Staphylococcus epidermidis*.

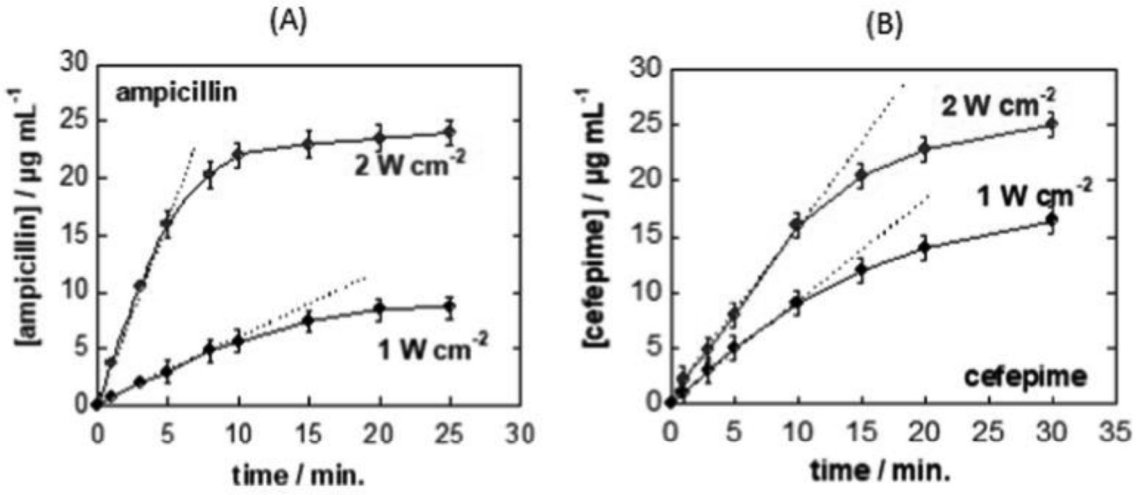

Figure 3.8. Photothermal-triggered antibiotics' release for PAA@rGO nanofibers: (a) release profile of ampicillin from a PAA@rGO nanofiber loaded with ampicillin (25 μg mL^{-1}) when activated at 980 nm at 2 and 1 W cm^{-2} and (b) release profile of cefepime from PAA@rGO nanofibers loaded with cefepime (25 μg mL^{-1}) when activated at 980 nm at 2 and 1 W cm^{-2}.

In the case of cefepime-loaded nanofiber mats, photothermal activation of the fibers with 2 W cm^{-2} leads to a complete release of the entrapped antibiotic (25 μg mL^{-1}) in a time frame of ≈25 min, with a release rate of 1.36 μg mL^{-1} min^{-1} for cefepime for the first 10 min. The release rate can be tuned upon using a lower power density: using a laser power of

1 W cm^{-2}, the release rate of cefepime decreased to 0.91 μg mL^{-1} min^{-1}. Importantly, no burst release was observed in any of these examples, and the maximal amount released is about twice the minimum inhibition concentration (MIC_{50}) value for cefepime for *S. epidermidis* and several times larger than the MIC value for cefepime for *E. coli* K12 and *S. aureus* ATCC 25923 as indicated in Table 3.1.

Table 3.1. Minimum inhibitory concentrations of ampicillin and cefepime for different bacteria strains.

Antibiotic	MIC_{50}/ μg mL^{-1} (E. coli K12)	MIC_{50}/ μg mL^{-1} (S. aureus ATCC 25923)	MIC_{50}/ μg mL^{-1} (S. epidermis)
ampicillin	4.9 ± 0.5		
cefepime	1.1 ± 0.3	4.1 ± 0.8	10 ± 1.8

3.3.3. Antibacterial Activity Under Passive and Active Release

Although ampicillin has sufficient stability in the dry state, it is only short-lived in a solution. Following photothermal-triggered ampicillin release, their antibiotic efficiency was assessed by determining the titer of viable bacteria able to grow. Figure 3.9a depicts the change in OD_{600} values upon *E. coli* K12 incubation with different ampicillin-released samples at 1 W cm^{-2}. In agreement with the photothermal release profile in the Figure 3.8b, about 2.5 μg mL^{-1} of ampicillin was released in the first minute, below the MIC_{50} value, whereas 6.8 μg mL^{-1} ampicillin (above the MIC_{50} value) was released after three min, resulting in the inhibition of *E. coli* growth. This underlines the fact that the photothermal-triggered ampicillin release does not affect the biological activity of the antibiotic.

Whereas ampicillin is only effective toward Gram-negative *E. coli* K12, cefepime is active for Gram-negative and Gram-positive strains, with a higher MIC for the *S. epidermidis* strain. *S. epidermidis* is known to be one of the most frequently encountered skin-colonizing bacteria and the predominant cause of nosocomial and community-associated skin infections. As expected, cefepime doses proved to be active against *S. epidermidis*. Cefepime released from cefepime-loaded nanofibers shows a release-dependent killing effect on *S. epidermidis* in accordance with the release profile determined

in Figure 3.8b. Figure 3.9c displays the SEM images of *S. epidermidis* treated with photothermally released cefepime. Whereas the amount of cefepime is below the MIC value after 5 min and does not affect in any way the *S. epidermidis* growth, the pathogen is completely destroyed above the MIC value (corresponding to times >10 min). This indicates that the developed approach can be easily adapted for any desired antibiotic to eliminate a particular bacterial strain. In addition to the sustained antibiotic release, an essential feature of any drug-release system is its reusability. Reloading of PAA@rGO with ampicillin or cefepime and photothermally induced release could be attained with similar efficiency over several cycles (Figure 3.10). Apart from just the possibility of reuse, the multiple loadings and release of antibiotics also demonstrate that the extent of upload and release is highly reproducible for these nanofibrous mats.

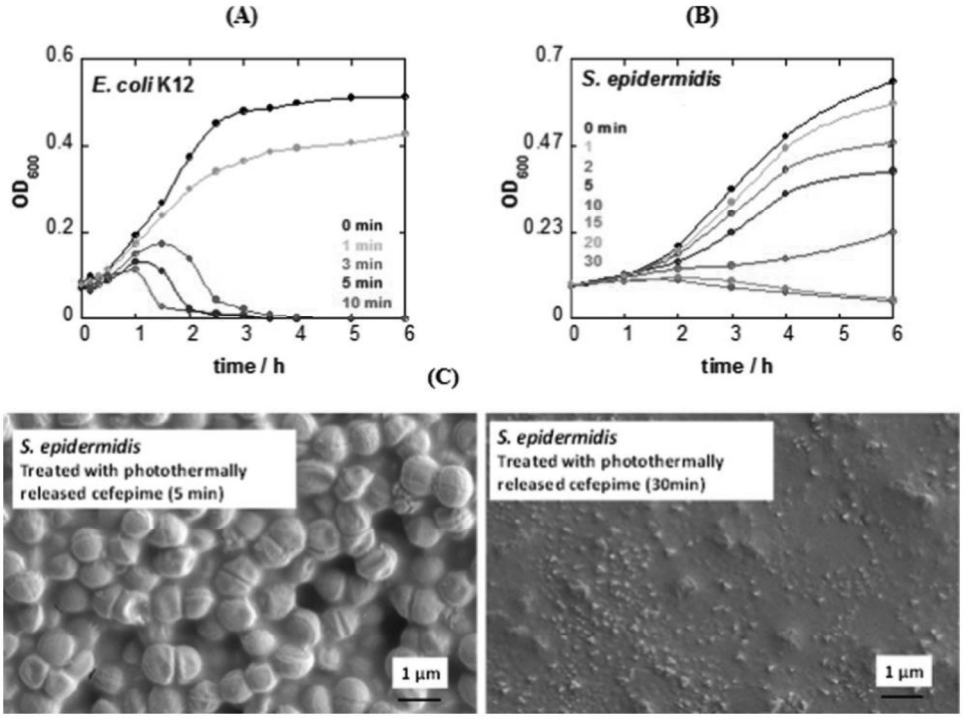

Figure 3.9. (a) Planktonic growth of *E. coli* K12 (1 × 108 cfu mL^{-1}) treated with ampicillin released photothermally from nanofiber mats at different time intervals. (b) Planktonic growth of *S. epidermis* treated with cefepime released photothermally from nanofiber mats at different time intervals. (c) SEM images of *S. epidermidis* treated with cefepime photothermally released from PAA@rGO nanofiber mats for 5 and 30 min.

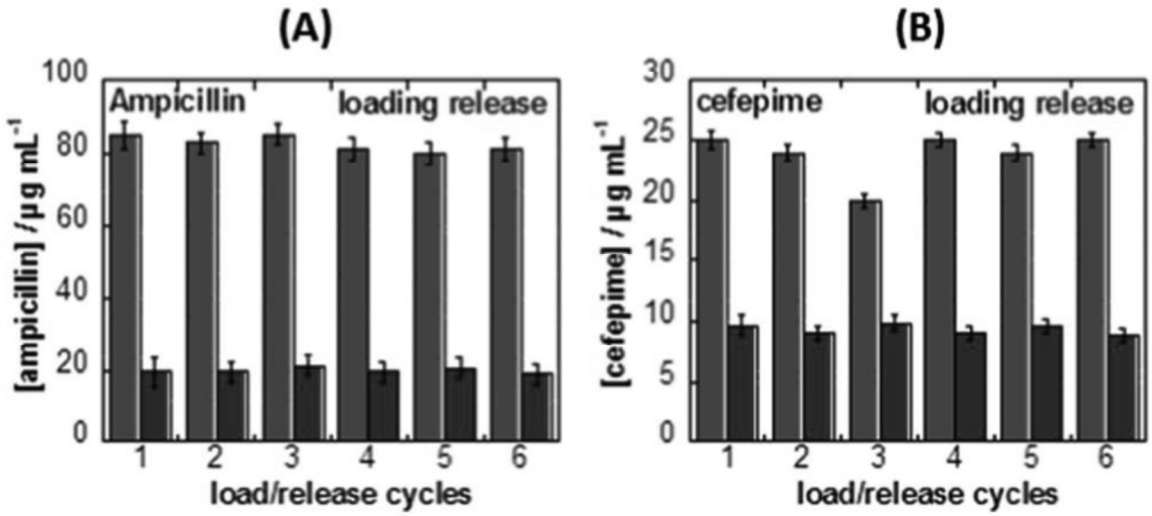

Figure 3.10. (a) Loading of ampicillin (85 μg mL^{-1}) and the amount of photothermally released ampicillin after 10 min laser irradiation (1 W cm^{-1}). (b) Loading of cefepime (25 μg mL^{-1}) and release of cefepime when activated at 980 nm at 2 W cm^{-2}.

3.3.4. Infectious Wound-Healing Studies Using rGO Nanofibers

There are different experimental models of skin infections that are caused by *S. aureus* [181,182]. In our research, the bacteria were directly applied to the previously damaged skin. The tape-stripping approach, one of the most common models for the generation of superficial skin infection in mice [183], was used here as it establishes superficial infections in the epidermis and the upper layer of the dermis. We monitored the skin infection progress in three animal groups: those treated with skin application of cefepime-loaded either PAA (PAA-CFP) or PAA@rGO (PAA@rGO-CFP) nanofiber mats and untreated mice (controls). The treatment in all groups started 24 h following the infection induction. Figure 3.11 displays images of the noninfected- and infected-wound groups untreated and treated with antibiotic-loaded nanofiber mats 48 h after infection initiation. The dressing (white arrows) was applied tightly to the wound area. The untreated areas and those treated with cefepime-loaded PAA nanofiber mats (PAA-CFP) and light-activated for 10 min to release the antibiotics revealed inflammation and areas with abundant edema, erythema, and bacterial infiltration/pus. Blood vascularization and bacterial infiltration are also detected in the untreated groups and cefepime-loaded PAA fiber mats without embedded rGO as shown in

Figure 3.11b. This is in contrast to cefepime-loaded PAA@rGO mats, wherein the photothermal treatment prevented the bacteria from spreading, as shown in Figure 3.11a). Infected layers after 10 min illumination with a LED array through the antibiotic-loaded PAA@rGO nanofiber mats (PAA@rGO-CFP) show signs of resolution of inflammation and reduced blood vascularization and bacterial infiltration. No damage to the skin was observed with LED illumination of the PAA@rGO nanofiber patch during the in vivo experiments, as the skin surface temperature was kept maximal at 52 °C. This is opposed to skin heating up to 67 °C when tissue damage could be observed in meat samples, as shown in Figure 3.12.

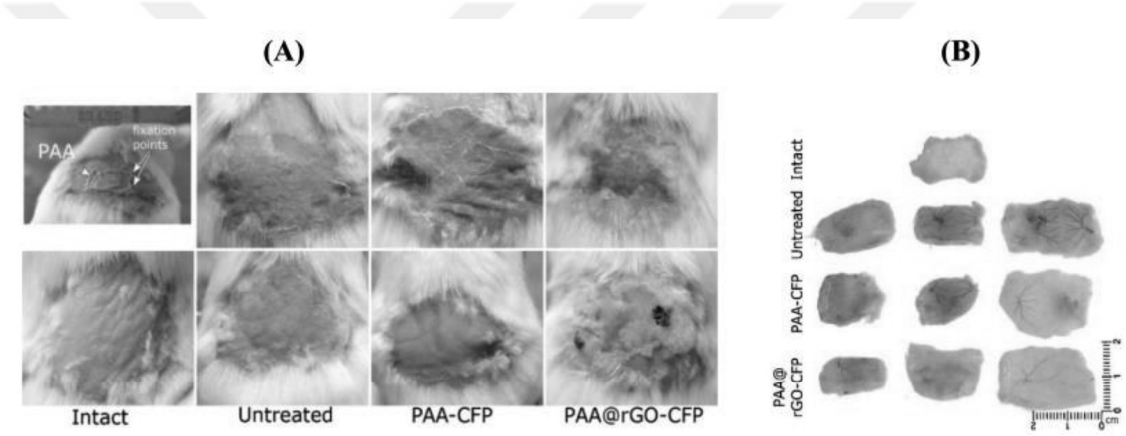

Figure 3.11. (a) Photographs of wound scars 24 h after treatment (940 nm, LED array) for 10 min with cefepime-loaded nanofibers mats. Negative control-intact skin; positive control-infected untreated skin. Insert at the top left demonstrates the setup for animal treatment. (b) Photographs of intact mouse skin and three representative skin samples after 48 h of infection under different treatment conditions.

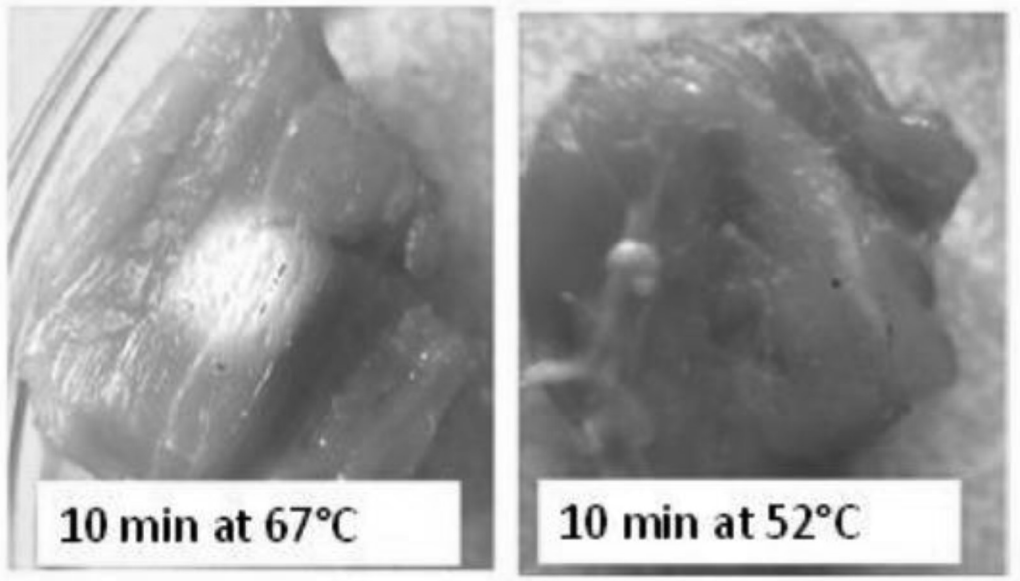

Figure 3.12. Controlled heating of meat with PAA@rGO with NIR LED: Heating up to 67°C for 10 min causes meat to burn, but heating skin to 52°C shows no visible tissue damage.

The histological section of a representative skin specimen (harvested at day 2 postinfection) after Gram staining in Figure 3.13 showed that *S. aureus* was superficially localized in the epidermis and penetrated the dermis layers of untreated and PAA-CFP skin samples. In addition, the leukocytic infiltration was abundant in the deep layer of hypodermis, indicating abundant bacterial presence. However, the infected wound irradiated through the antibiotic-loaded PAA@rGO patch for 10 min indicated active wound healing without marks of inflammation and bacterial foci. The epidermis revealed signs of active regeneration. Thus, it could be concluded that the topical application of PAA@rGO-CFP mats for photothermal therapy exhibited the best wound-healing capability among those tested.

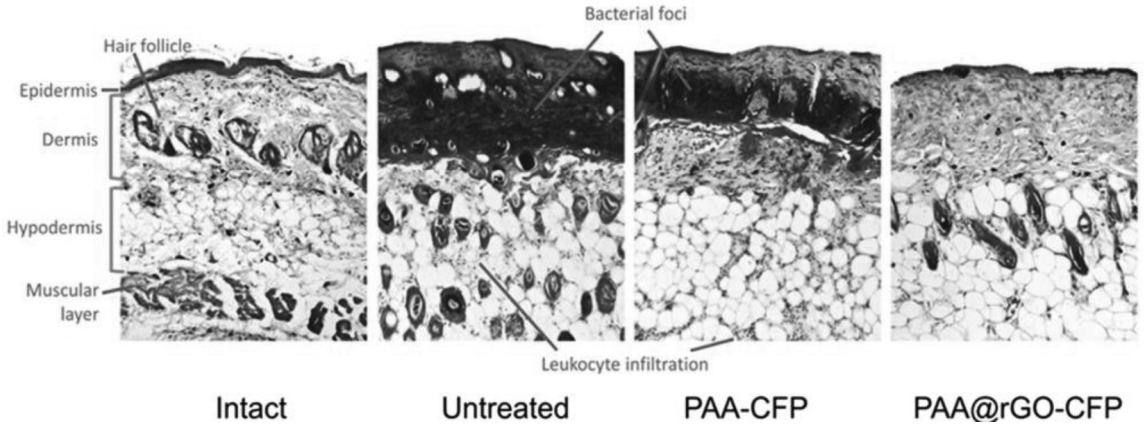

Figure 3.13. Histological examination of skin wound healing 48 h after the infection. Sections of skin tissues with Gram staining. Intact mouse skin; untreated skin (after infection); and photothermally treated infected skin part of the wound (PAA-CFP and PAA@rGO-CFP).

3.4. Conclusion

In summary, a novel nanofiber-based platform for the “on-demand” release of antibiotics is fabricated using rGO-containing polymeric nanofibers. The rGO-embedded hydrophilic nanofibers obtained using solution electrospinning are loaded with two different antibiotics: ampicillin and cefepime. Although the minor release of antibiotics is observed under physiological conditions, exposure to NIR irradiation leads to release amounts sufficient to kill Gram-positive and Gram-negative bacteria alike. A clear correlation between the NIR-triggered antibiotic release and bactericidal activity is observed. It can be anticipated that the facile fabrication and modular nature of the construct reported here provide a platform that can be adapted for the on-demand delivery of various drugs for combating different diseases. Although only two specific antibiotics were chosen in this study, the platform is amenable to loading other antibiotics, solo or in combination, to combat a plethora of bacterial infections.

4. pH-SENSITIVE POLYMERIC NANOFIBER FOR LOCAL CANCER TREATMENT

Adapted with permission from {Altinbasak, I., S. Kocak, A.H. Colby, Y. Alp, R. Sanyal, M.W. Grinstaff, and A. Sanyal, "pH-Responsive Nanofiber Buttresses As Local Drug Delivery Devices.", Biomaterials Science, 2022.} Copyright {2022} Royal Society of Chemistry [184].

4.1. Introduction

Polymeric materials that undergo a transformation of their chemical, physical, and/or mechanical properties in response to environmental changes are of significant interest in myriad biomedical applications [185-189]. Light [190-192], temperature [193], pH [194], magnetism [195] or exposure to a specific biological molecule are examples of relevant stimuli [196,197]. Of these, pH is one of the most studied as differences in pH between neighboring tissues (e.g., stomach vs. intestine), within the extracellular matrix of tumors (pH 6.5), and within the intracellular compartments of cells (pH 5) allow for the accurate triggering of systems based on physiological location [198-201]. Common form factors for such stimuli-responsive polymer materials include micro- and nano-particles [202,203], hydrogels [204,205], surfaces and coatings [206], and nanofibers [207]. Electrospun nanofibers are particularly advantageous in drug delivery applications due to their high surface area to volume ratio, their capacity for both high as well as efficient drug-loading, their functionalizable surface chemistry, and their ease of *in situ* placement at a target site during surgical producedures [208-211]. Furthermore, electrospinning is a robust and scalable industrial process, enabling ready access to large-scale production of such materials for clinical applications [212,213].

Stimuli-responsive nanofibers, and their corresponding macroscopic polymer buttresses, have been designed to leverage changes in temperature [214] or pH [215], the

application of light [216] or ultrasound [217], and even increases in oxidative stress [218] to trigger drug release. In general, stimuli such as light, ultrasound, and temperature are pragmatic only for on-demand drug release over relatively short periods and are restricted to tissue locations accessible to these externally applied stimuli [219,220]. On the other hand, endogenous stimuli, such as changes in local redox or pH, may occur over longer periods, allowing the ability to control drug release over extended periods [221,222]. For example, Li and coworkers reported pH-responsive nanofibers composed of triblock copolymers comprised of poly(dl-lactide) as outer blocks and an acetal-linked poly(ethylene glycol) central block [223]. The fiber morphology of this system gradually changes after incubation in pH 7.4, 5.6, and 4.0 buffer solutions, with eventual loss of the fiber structure. Entrapped paracetamol (logP = 0.46) releases from the nanofibers over 120 hours in a pH-dependent manner, with the fastest release occurring in a pH 4 buffer. However, a limitation of this system is significant passive release regardless of pH leading to rapid emptying of the delivery vehicle within a matter of days.

As an alternative to a hydrolytic polymer backbone which undergoes degradation to release its drug payload, we employ a polymer with a non-hydrolyzable methacrylate backbone with acid-labile side chains that undergo cleavage under mildly acidic conditions, thereby resulting in an overall change in the polymer composition from hydrophobic to hydrophilic. Due to the presence of the methacrylate backbone, the fibers can maintain their structure, rather than degrading/dissolving into solution, while swelling and increasing in diameter. The 2,4,6-trimethoxybenzaldehyde moiety, reported by Fréchet [224] and Grinstaff [225,226], is one example of an acid-labile protecting group that is, itself, hydrophobic in nature and, upon cleavage, can afford two hydrophilic hydroxyls. For example, Fréchet-type amphiphilic dendrons terminated with 2,4,6-trimethoxybenzaldehyde acetal groups assemble into micelles and encapsulate doxorubicin[224]. Hydrolysis of the acetal group at pH 6 causes the release of doxorubicin and disruption of the micelle. Grinstaff *et al*. describe an acrylate-based diol monomer protected with a 2,4,6-trimethoxybenzaldehyde moiety for preparing polymeric nanoparticles via a mini-emulsion polymerization technique. In their initial state, the 100 nm particles are hydrophobic, but when exposed to a mildly acidic environment of pH 5-6, they swell in diameter to 1,000 nm; as a result of this swelling behavior, they are termed “expansile nanoparticles” (eNPs) [226]. Drug-loaded eNPs are readily taken up by multiple cancer cells [227-230] and localize with

high specificity to mesothelioma, ovarian and pancreatic tumors following intraperitoneal injection [231,232]. Improved outcomes have been shown in xenograft murine models of pancreatic [225], breast cancer [228], mesothelioma [233], and ovarian cancer [234].

Herein, we repurposed this eNP polymer to create drug-loaded nanofibers that can be formed into surgical buttresses to enable site-specific, pH-controlled drug release, as illustrated in Figure 4.1. We report the free radical polymerization of a 2,4,6-trimethoxybenzaldehyde-containing methacrylate monomer and the subsequent fabrication of electrospun buttresses using this polymer. Both hydrophilic (doxorubicin) and hydrophobic (docetaxel) drugs are loaded into the nanofibers as characterized by scanning electron microscopy (SEM) and confocal microscopy. The nanofibers retain their shape but increase in size while swelling in a mildly acidic buffer solution. Docetaxel and doxorubicin release from the nanofiber buttresses is negligible at neutral pH and occurs more rapidly in a mildly acidic buffer solution. The released drug is still active and cytotoxic to lung (NCI-H460, A549) and breast cancer (MDA-MB-231) cells.

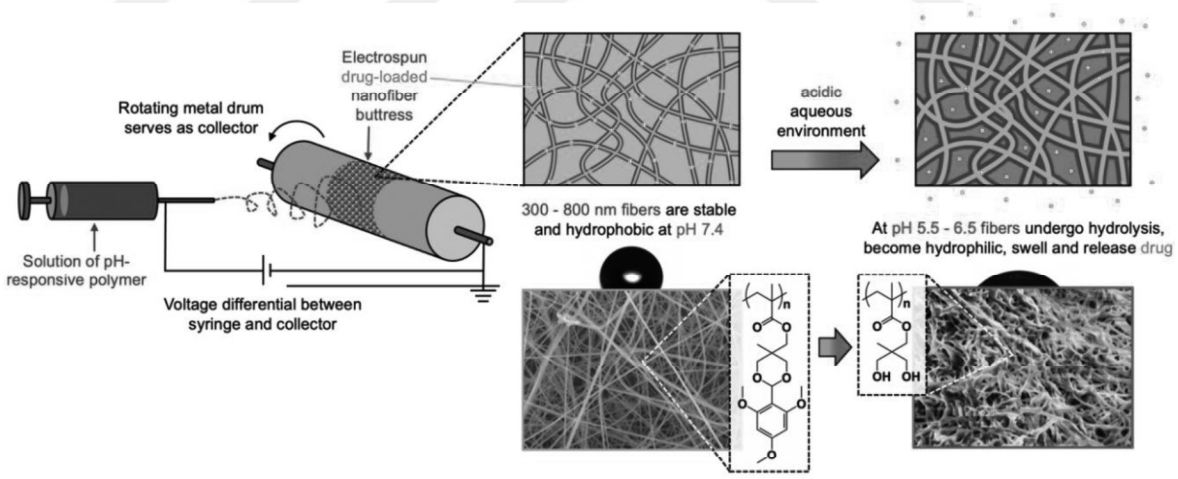

Figure 4.1. Illustration of pH-dependent drug release from pH-responsive electrospun nanofibers.

4.2. Experimental

4.2.1. Materials

2,4,6-Trimethoxybenzaldehyde was purchased from Acros Organics. 1,1,1-Tris(hydroxymethyl)ethane was purchased from Alfa Aesar. Methacryloyl chloride was purchased from Sigma Aldrich. The organic solvents dichloromethane, hexane, dimethylformamide, and methanol were analytical grade and purchased from Sigma Aldrich. Doxorubicin hydrochloride and fluorescein amine isomer I were purchased from Sigma Aldrich. These chemicals were used without further purification. MDA-MB-231, A549, and NCI-H460 cell lines were purchased from ATCC (LGC Standards, Germany) and grown according to the culture method requirements of the manufacturer. Cells were incubated at 37 °C in a humidified atmosphere of 5% CO_2. Cytotoxicity experiments were performed with a plate reader (Multiscan FC, Thermo Scientific, USA) and Cell Counting Kit8 (CCK-8, Fluka) obtained from Sigma-Aldrich. 5-methyl-2-(2,4,6-trimethoxyphenyl)-[1,3]-5-dioxanylmethyl methacrylate was prepared according to previously reported literature [226,235].

4.2.2. Synthesis of Polymer

Synthesis of homopolymer has been reported by Grinstaff and coworkers previously.56 Briefly, 5-methyl-2-(2,4,6-trimethoxyphenyl)-[1,3]-5-dioxanylmethyl methacrylate (0.55 g, 1.5 mmol, 150 equiv.), AIBN (0.16 mg, 0.001 mmol, 0.1 equiv.) and the solvent dimethylacetamide (0.41 mL) were added to a round bottom flask. The solution was purged with N_2 gas for 60 minutes. After 30 minutes, the solution was put in an oil bath at 80 °C for two hours. To purify the highly-dense polymer solution, the resulting mixture was diluted with 10 mL of dichloromethane and precipitated in cold ether. Polymers with 120 and 320 kDa (Mn) were characterized by size exclusion chromatography using Shimadzu PSS-SDV (length/ID 8 x 300 nm, 10 μm particle size) calibrated with polymethylmethacrylate standards using a refractive index detector.

4.2.3. Fabrication and Characterization of Drug-Loaded Nanofibers

For a typical experiment, a polymer solution of 17 wt% and drug (docetaxel or doxorubicin) 1 wt%, and fluorescein amine 1 w% in 1:1 (v/v) DMF:THF solvent mixture was prepared, and the solution was stirred for 24 h at room temperature. Transparent polymer/drug solution was electrospun using a syringe pump (KD Scientific 101) at a constant flow rate (0.005 mL/min) with a 1 mL syringe fitted with a 14-gauge needle with 15 kV. The tip-to-collector distance was maintained at 15 cm during the electrospinning process. Fibers were collected on a rotating aluminum drum for further use. To calculate the drug loading efficiency, the nanofiber buttress was dissolved in dichloromethane, and the solution was precipitated in methanol, and the aliquot was analyzed via liquid chromatography-mass spectrometry (LC-MS) using an LC-MS-2020-Mass Spectrometer System (Shimadzu, Japan). To calculate the fluorescein amine loading efficiency, the aliquot was analyzed via UV-Vis spectrophotometry using a Cary Varian UV−Vis spectrometer (Santa Clara, CA). Surface morphology was analyzed with scanning electron microscopy using a JEOL NeoScope JCM-5000. The distribution of doxorubicin in the nanofiber buttress was evaluated using a confocal laser scanning microscope (Leica TCS SP5). The static contact angle of a water droplet on electrospun nanofiber buttresses were measured under open-air conditions. Approximately 25 μL of deionized water was dropped on the surface, and images were taken via an integrated digital camera. The software of the camera provides contact angle measurements once the liquid is dispensed. Freshly prepared nanofiber buttresses incubated in water and buffer solutions with different incubation times were used to measure contact angles after they were washed with distilled water to remove residual salt remaining from the buffer solutions used for incubation. Mechanical testing of the drug-loaded buttresses was performed using an Instron 5944 Microtester with 1 cm x 10 cm shaped rectangles secured at each end with binder clips and a nominal strain rate of 1 mm/s.

4.2.4. Hydrolysis of Nanofibers

Hydrolysis studies were performed in phosphate-buffered saline (PBS) (1 mL, pH 7.4), phosphate buffer (1 mL, pH 6.5), or acetate buffer (1 mL pH 5.5) in an environmentally

controlled thermal shaker at 37 °C with samples shaking at 100 rpm. The amount of 2,4,6-trimethoxybenzaldehyde protecting group released at each time point was quantified via LC-MS.

4.2.5. Drug and Fluorescein-Amine Release from Nanofibers

Studies were performed in PBS (1 mL, pH 7.4), phosphate buffer (1 mL, pH 6.5), or acetate buffer (1 mL pH 5.5) in an environmentally controlled thermal shaker at 37 °C with samples shaking at 100 rpm. Additionally, drug release studies were also performed in two different cell culture media (RPMI-HEPES) at pH 7.4 and pH 6.5. The amount of drug released into the solutions at each time point was monitored via LC-MSMS (Shimadzu triple quadrupole 8040) and the amount of fluorescein amine released in the solution was monitored via UV-vis spectrophotometer.

4.2.6. Cytotoxicity Assay

Cytotoxicity of the drug-loaded buttresses was evaluated using a CCK-8 viability assay on MDA-MB-231, A549, and NCI-H460 cells. Cells were seeded into 96-well plates (6,000, 7,000, and 10,000 cells/well, respectively) in quadruplicate and incubated at 37 °C overnight to allow for complete adherence. For free drug treatments, the doxorubicin stock solution was prepared as 10^{-3} M (with 2.5% dimethyl sulfoxide (DMSO)) to ensure the complete dissolution of free doxorubicin. Serial dilutions were made from stock solution (10^{-3} M) using cell media, and the final DMSO concentration in each well was kept below 0.5% (v/v). Nanofibers with doxorubicin (1 mg/mL) and empty nanofibers for control (1 mg/mL) were incubated in media (pH 6.5 and pH 7.4) at 37 °C for five days. For aliquots from drug-loaded nanofibers, one to five dilutions were made with fresh media before adding the solution to cells. For aliquots from control nanofibers, one to ten serial dilution was made with fresh media before addition to the cells. After 48 h, CCK-8 solution (0.1%) was added to each well. After two hours of incubation, the absorbance values were measured with a plate reader (Multiscan FC, Thermo Scientific, USA) at 450 nm. The cell viability of treated cells was determined according to the percentage of control cells (cell media only). Results were calculated using GraphPad prism software using a nonlinear regression mode.

4.3. Results and Discussion

4.3.1. Synthesis of pH-Responsive Polymer

To manufacture a pH-responsive polymer buttress drug delivery system, we first synthesized an acid-labile methacrylate monomer for subsequent polymerization and buttress fabrication. Specifically, 5-methyl-2-(2,4,6-trimethoxyphenyl)-[1,3]-5-dioxanylmethyl methacrylate, an acetal-containing pH-sensitive hydrophobic monomer obtained using 2,4,6-trimethoxybenzaldehyde as a building block was prepared. According to a previously reported protocol[226], we reacted 2,4,6-trimethoxybenzaldehyde with 1,1,1-tris(hydroxymethyl)ethane to obtain acetal-containing alcohol, which was coupled to methacryloyl chloride to yield the monomer in high yield and purity. Using this monomer, we performed a conventional free radical polymerization to obtain the polymers in good yield (90%) and high molecular weight. Specifically, the monomer was polymerized in the presence of varying amounts of AIBN at 80 °C for two hours in dimethylacetamide to afford polymers with weight average molecular weight of approximately 120 kDa and 320 kDa, with dispersity of 2.5 and 2.2, respectively, as determined using size exclusion chromatography as shown in Figure 4.2. Figure 4.3 shows the chemical composition of the polymer that was confirmed using ^{1}H NMR spectroscopy.

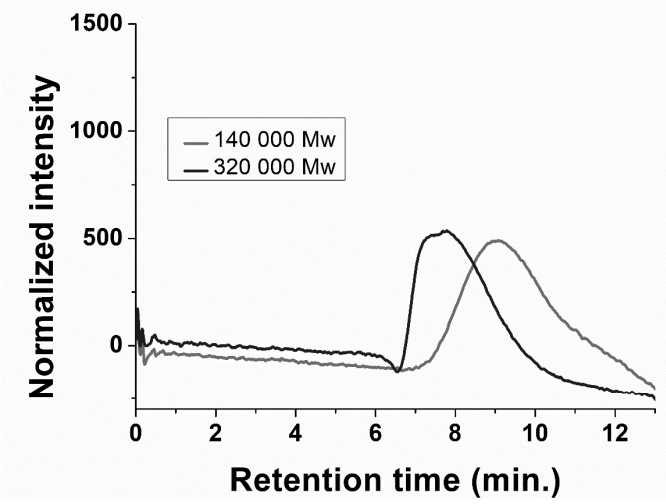

Figure 4.2. SEC traces of polymers (eluent: DMAC).

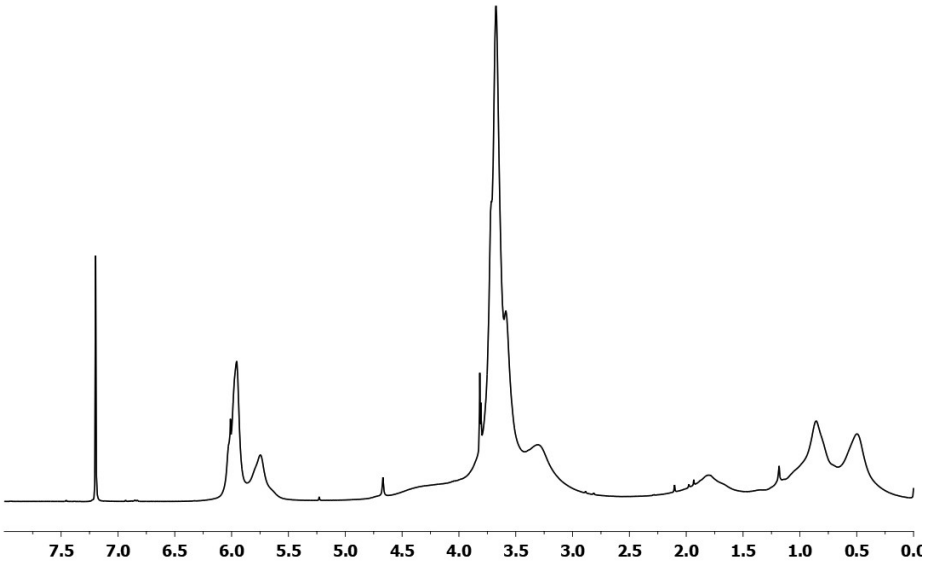

Figure 4.3. ^{1}H NMR spectrum of polymer.

4.3.2. Fabrication of Drug-Loaded pH-Responsive Nanofibers

We fabricated nanofibers and corresponding buttresses using electrospinning. We targeted two different nanofiber diameters to determine whether smaller-diameter nanofibers would release the drug more rapidly due to an increase in the surface area to volume ratio. Using polymers of 120 kDa and 320 kDa, we obtained nanofibers with significantly different ($p< 0.0001$) diameters of 350 ± 64 and 800 ± 125 nm, respectively. We used a DMF/THF (1:1) solvent mixture with a flow rate of 0.005 mL/min and a 15 kV voltage potential between collector-needle at 15 cm to obtain bead-free, uniform nanofibers as shown in Figures 4.4a,b,c, and d). Compounds (e.g., doxorubicin, docetaxel, or fluorescein amine) were loaded into the fibers by dissolving them in the DMF/THF solvent prior to electrospinning. The spatial distribution of doxorubicin was assessed via confocal laser microscopy, as shown in Figure 4.4e, and found to be relatively homogeneous (Figure 1e). The loading efficiency of drugs within nanofibers was calculated by dissolving the fibers in a minimal amount of CH_2Cl_2, followed by removal of the polymer by precipitation in CH_3OH and centrifugation. The loading efficiencies of doxorubicin, docetaxel, and fluorescein amine were found to be 71%, and 64%, respectively, as quantified by LC-MS. The loading efficiency of fluorescein amine was determined as 27% using UV-vis spectroscopy.

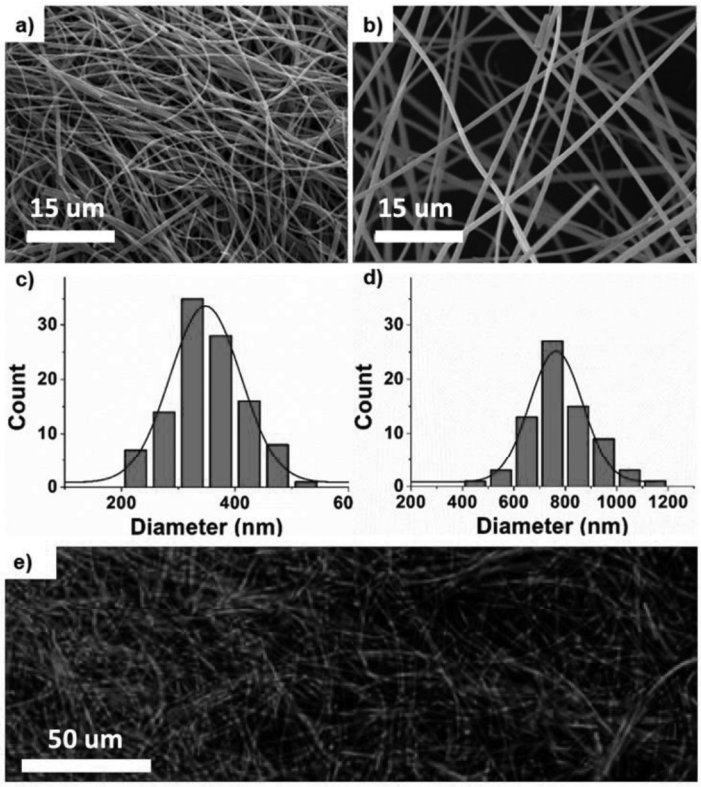

Figure 4.4. SEM images of (a) 350 nm and (b) 800 nm nanofibers with their size distribution histograms, (c) and (d), respectively. Representative confocal image (e) of doxorubicin-loaded nanofibers.

4.3.3. pH-Responsiveness of Nanofibers

To characterize the response of the nanofiber buttresses to pH changes, we measured their surface contact angle. Since acetal bonds are susceptible to low pH, they hydrolyze with the release of the hydrophobic trimethoxybenzaldehyde groups with the formation of hydrophilic diols along the polymer backbone, as illustrated in Figure 4.5a. Figure 4.5b showed that the contact angle of deionized water on a dry nanofiber buttress was approximately 140°, indicating the strongly hydrophobic nature of these materials. Figure 4.5d proved that incubating the nanofiber in water or PBS (pH 7.4) for up to 2 days did not result in major changes in contact angle. In contrast, when the nanofiber buttresses were immersed in an acidic buffer (pH 5.5), we observed a substantial decrease in the contact angle to 107° after 3 hours, with a further reduction to 60º after six hours, as shown in Figure 4.5c. Figure 4.5e showed that over the next three days, the rate of change in contact angle

did not decrease further, suggesting that most of the surface had already transformed from a hydrophobic to a hydrophilic state.

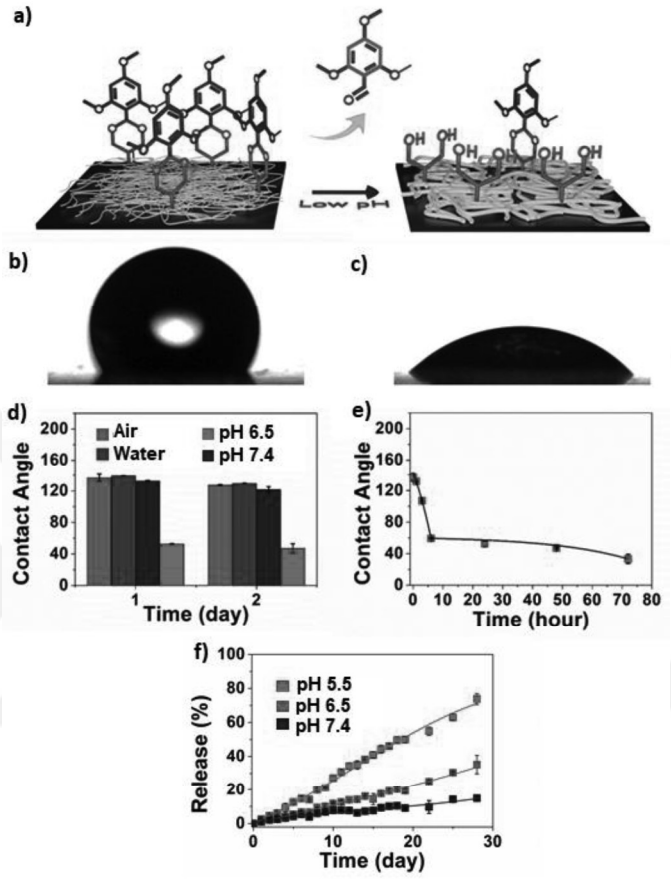

Figure 4.5. (a) Schematic of pH-labile polymer cleavage and fiber swelling. Image of the water droplet on a nanofiber buttress incubated in (b) PBS or (c) in pH 5.5 buffer. (d) Contact angle measurements of nanofiber buttresses incubated in different conditions. (e) Change in contact angle of nanofiber buttresses in the acidic buffer. (f) Release kinetics of trimethoxybenzaldehyde during incubation under different pH conditions (N=3).

To further characterize this transformation and corroborate the contact angle findings, we measured the release kinetics of the trimethoxybenzaldehyde protecting group from the nanofiber buttress as a function of pH and time. As quantified by LC-MS, the release of trimethoxybenzaldehyde from the nanofiber buttress at pH 7.4 was minimal, with only 15% release after 28 days. In contrast, nearly 75% of the trimethoxybenzaldehyde was released at pH 5.5 over the same timeframe. To mimic the pH environment of tumor tissue, we

repeated the study at a mildly acidic condition of pH 6.5. Figure 4.5f demonstrated that the release of trimethoxybenzaldehyde was more than 2-fold greater at pH 6.5 compared to the release at neutral pH but slower than at pH 5.5.

The increase in hydrophilicity of the polymer fibers was expected to result in swelling, manifested as an increase in average fiber diameter over time. Therefore, we used SEM to monitor the size of nanofibers incubated under various pH conditions. Nanofiber buttresses incubated in PBS for four weeks at 37 °C showed no significant change in fiber morphology or diameter, as seen in Figures 4.6a,b, and c. In contrast, nanofiber buttresses incubated in pH 5.5 aqueous buffer over the same timeframe showed a three-fold increase in fiber diameter, as seen in Figure 4.6d. Interestingly, by four weeks, the fibers began to lose their distinct shape and coalesce into somewhat larger, amorphous structures. This difference in morphology and increase in nanofiber diameter is consistent with hydrolysis and swelling of the polymer observed in other applications, such as with nanoparticles of the same material [236].

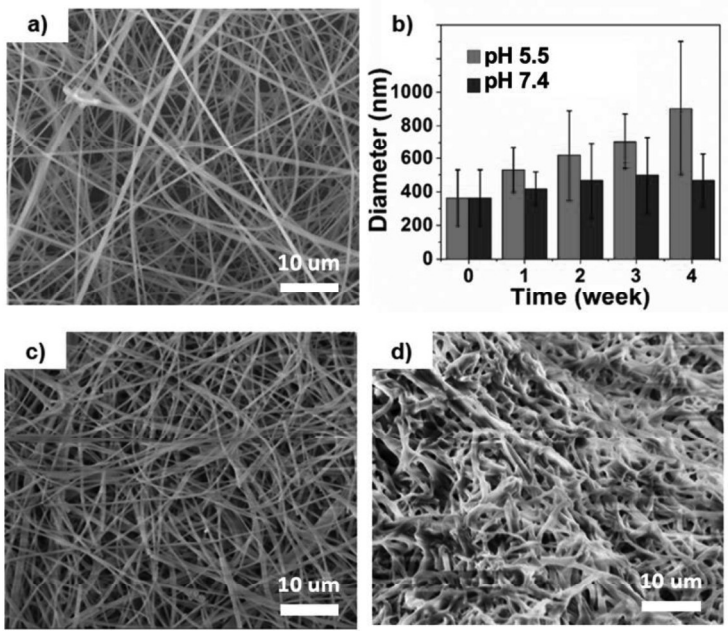

Figure 4.6.(a) SEM image of nanofibers prior to incubation in aqueous solution. (b) Change in fiber diameter as a function of time and buffer pH (N=3). (c) SEM image of nanofibers after incubation for four weeks in pH 7.4 PBS and (d) after four weeks in pH 5.5 aqueous buffer.

4.3.4. Effect of Fiber Diameter on Release Rate of an Encapsulated Cargo

To evaluate the impact of fiber diameter on the release rate of an encapsulated small molecule cargo, we loaded the nanofibers with fluorescein amine. Fluorescein amine-loaded nanofiber buttresses with average diameters of 350 nm and 800 nm were immersed in pH 5.5 aqueous buffer and incubated in a thermal shaker at 100 rpms at 37 °C for nine days. Aliquots of release medium were taken daily and analyzed via UV-vis spectroscopy. As shown in Figure 4.7, fiber diameter significantly impacted the release rate of fluorescein amine, with 100% release from the 350 nm diameter fibers occurring within five days compared to only 30% release from the 800 nm diameter fibers over the same period. The 800 nm diameter fibers took entirely nine days to release 100% of their cargo. This nearly two-fold difference in release rate is likely due to the increased surface area to volume ratio of the 350 nm fibers compared to the 800 nm fibers, which leads to faster hydrolysis of the pH-responsive polymer and the ensuing release of cargo.

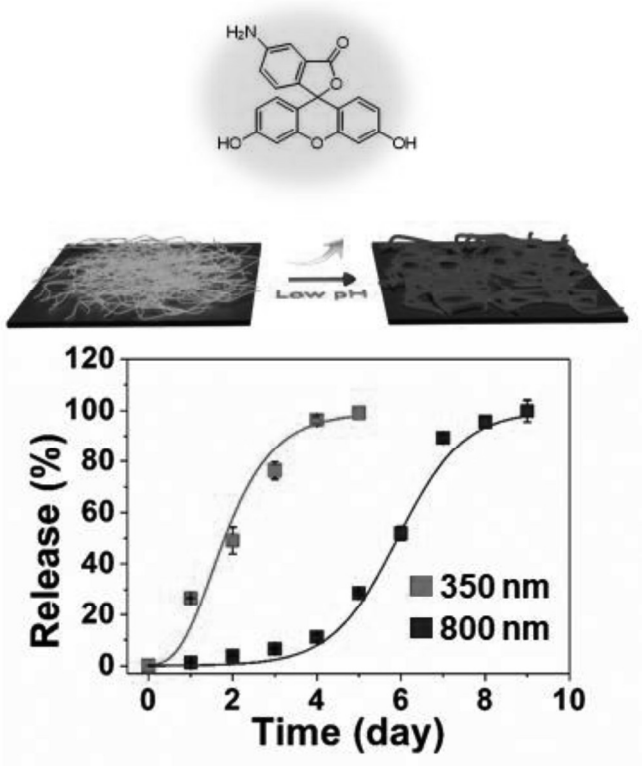

Figure 4.7. The release of fluorescein amine from nanofiber buttresses as a function of fiber diameter and time while incubated in pH 5.5 aqueous buffer (N=3).

4.3.5. pH-Responsive Drug Release from the Nanofibers

Due to the faster response time (i.e., the shorter lag between pH change and induction of significant drug release) of the smaller, 350 nm diameter fiber system, we chose to use these in subsequent studies evaluating the encapsulation and release of chemotherapeutic agents to shorten the experimental duration of these studies and, therein, reduce potential confounding factors. We characterized the release of both a hydrophilic drug (doxorubicin; log p = 1.3) and a hydrophobic drug (docetaxel; log p = 2.4) from the nanofiber buttresses incubated in both aqueous buffer solutions (pH 5.5 and 7.4) as well as cell culture media (RPMI-HEPES) adjusted to pH 7.4 and 6.5. As shown in Figure 4.8a, docetaxel did not release from the buttresses at pH 7.4 over 18 days. In contrast, the measurable release of docetaxel began after seven days of incubation at pH 5.5, with 100% release by day 18. Similar trends were observed with doxorubicin; however, the time scale of release was substantially shorter. As shown in Figure 4.8b, doxorubicin did not release from the buttresses at neutral pH. However, at pH 5.5, doxorubicin release began within 24 hours of incubation and reached 100% within six days. The faster doxorubicin release rate compared to docetaxel is expected based on its significantly more hydrophilic nature than docetaxel, which leads to a greater affinity for the surrounding aqueous environment.

Given the negligible release of docetaxel at pH 7.4 over eighteen days, we performed a comprehensive study in which doxorubicin release was monitored for four months under the same conditions as the previous study. Notably, the nanofibers retained the doxorubicin cargo without appreciable “leakage” (i.e., unintended release at neutral pH) for the four-month study. Furthermore, extraction and quantification of the payload after four months demonstrated that the docetaxel payload was preserved within the fibers without degradation, as seen in Figure 4.9.

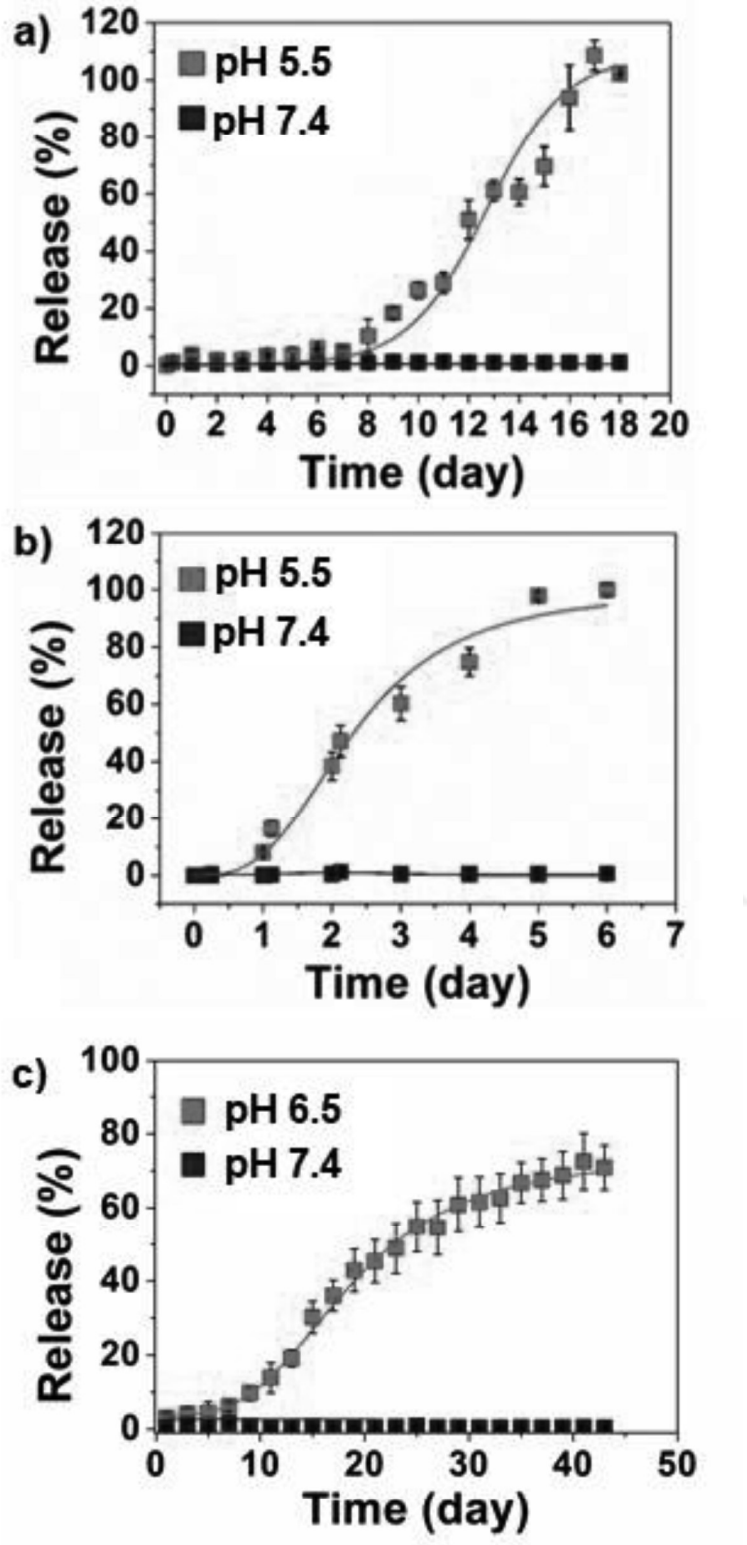

Figure 4.8. Release of (a) docetaxel and (b) doxorubicin from nanofiber buttresses as a function of time and pH in an aqueous buffer. (c) Doxorubicin release in RMPI-HEPES media (all data N=3).

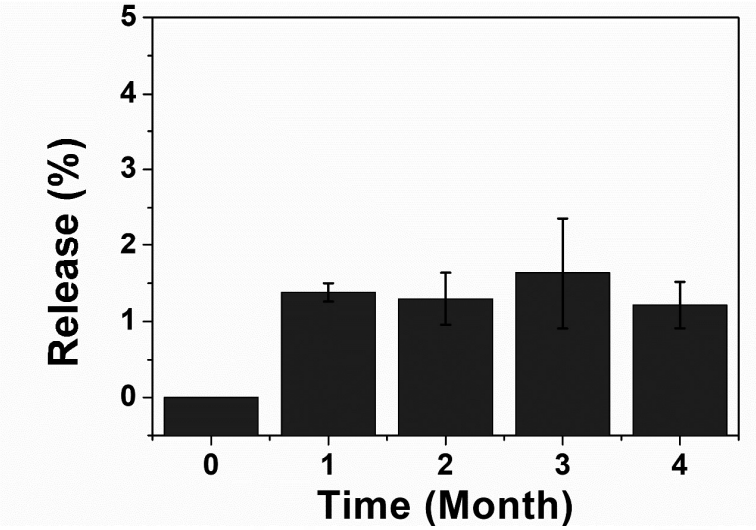

Figure 4.9. Long-term release of doxorubicin from nanofibers incubated at pH 7.4.

Similarly, based on the rapid release of doxorubicin observed at pH 5.5, we chose to evaluate its release rate at pH 6.5. This slightly higher, yet still mildly acidic, pH is physiologically relevant as it is a hallmark of the tumoral microenvironment [237,238], and a device implanted against the tumor bed may be expected to be exposed to these conditions. Compared to pH 5.5, doxorubicin release at pH 6.5 was slower, reaching approximately 13% after two weeks. As before, no significant release was observed in pH 7.4, as seen in Figure 4.10.

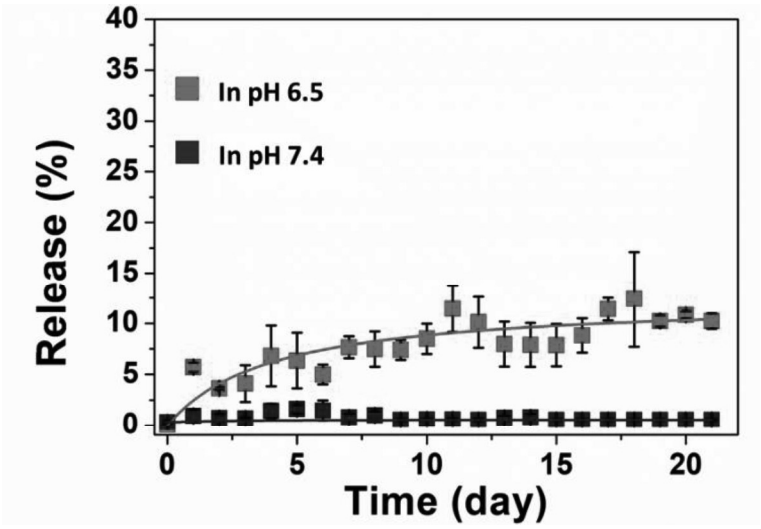

Figure 4.10. Doxorubicin release from nanofibers at pH 6.5 phosphate buffer.

Lastly, in order to more accurately model physiological drug release conditions, we repeated the doxorubicin release studies in cell media (RPMI-HEPES), as opposed to simple aqueous buffers, adjusted to pH 6.5 and pH 7.4. Figure 4.8c shows that the release profile of doxorubicin from nanofibers in cell culture was, again, pH-dependent. Sustained release of doxorubicin occurred at pH 6.5, with 70% of the payload being released by day forty-five. The negligible release occurred at pH 7.4 (2% over the same period). Notably, the release was significantly faster in media than in a simple aqueous buffer (~25% v. ~13% release over two weeks, respectively; Figure 4.8c and Figure 4.10). This is likely the result of the presence of protein in the media, which leads to faster wetting of the fibers and, hence, hydrolysis, as well as increasing the affinity of the drug for the sink.

4.3.6. Cell Viability Studies

First, we assessed the cytotoxicity of unloaded nanofiber buttresses by immersing them in DMEM cell culture media at pH 7.4 and pH 6.5 for five days. This media was then serially diluted 10-, 100- or 1000-fold with fresh media, and MDA-MB-231 breast cancer cells were incubated in these dilutions for two days. No cytotoxicity was observed for the unloaded buttresses, as seen in Figure 4.11a.

We then repeated this study with doxorubicin-loaded buttresses. Supernatant from buttresses incubated at pH 7.4, as expected, showed no cytotoxicity; while, in contrast, the supernatant from buttresses incubated at pH 6.5 significantly reduced cell viability in three different human cancer cell lines, including breast cancer (MDA-MB-231) and lung cancer (NCI-H460 and A549;) as shown in Figure 4.11b. We used LC-MS to quantify doxorubicin release from the buttresses and, hence, present in the treatment of these cells. The final concentration of doxorubicin in the cell culture media was found to be 0.2 μM. The resultant ~20% to 40% reduction in cell viability is consistent with the EC_{50} values for two-day treatments of doxorubicin alone (i.e., a free drug not loaded into a buttress) in MDA-MB-231, NCI-H460, and A549 cell lines (i.e., 0.31 μM, 0.17 μM, and 0.44 μM, respectively) as shown in Figure 4.11c. These results demonstrate that doxorubicin maintains its anticancer activity even after release from the buttress and, furthermore, that it is active against a variety of different cancer types.

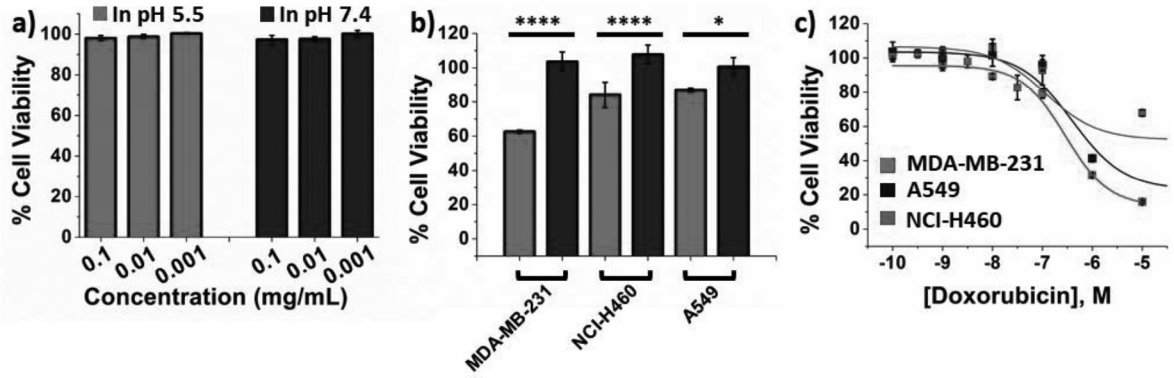

Figure 4.11.(a) Cytotoxicity of supernatant from unloaded nanofibers incubated at pH 6.5 or 7.4 diluted and incubated with MDA-MB-231 cells. (b) Cytotoxicity of supernatant from doxorubicin-loaded nanofibers incubated at pH 6.5 or 7.4 diluted and incubated with MDA-MB-231, A549, and NCI-H460 cells. (c) Cytotoxicity of free doxorubicin on MDA-MB-231, A549, and NCI-H460 cells (all data N≥3).

4.3.7. Feasibility Testing for Use as a Surgical Buttress.

To determine the feasibility of using these pH-responsive nanofiber buttresses as a reinforcing material in tumor resection surgery, we evaluated their mechanical properties using an Instron Microtester. The Young's Modulus, a measure of the tensile strength of a material, of the nanofiber buttresses was found to be 6.3 ± 1.4 MPa. For comparison, the Young's Modulus of Seamguard, a commercially available (non-drug loaded) surgical buttress used in lung and gastric resection surgeries, was measured to be 36.1 ± 4.0 MPa. While the nanofiber buttress is weaker than this particular example of a commercial buttress, it can nonetheless function as a reinforcing material in surgical resections. To demonstrate this functionality, we performed a mock wedge resection on a porcine lung using a surgical cutting stapler to which two pieces of pH-responsive buttress were secured, as seen in Figure 4.12. After resection, the lung was inflated to 18 mm Hg (25 mm H_2O), which is the standard pressure to which lungs are tested following surgical resection procedures to ensure no air leaks are present prior to the conclusion of surgery. The inflated lung was submerged in water, and no bubbles evolved from the resection margin indicating a patent seal.

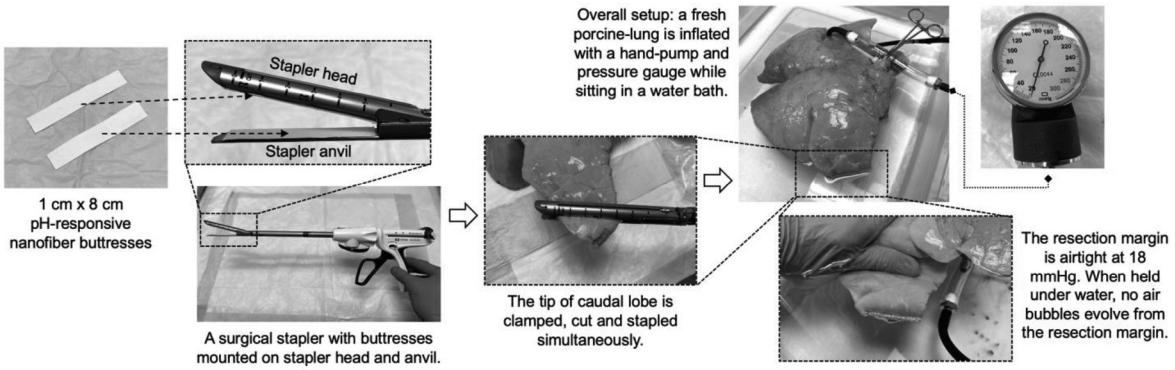

Figure 4.12. Demonstration of the feasibility of using pH-responsive nanofiber buttresses as reinforcements for surgical resection margins.

4.4. Conclusion

We describe a new pH-responsive nanofiber buttress that transforms from a hydrophobic to a hydrophilic state in the presence of mildly acidic aqueous conditions. The base polymer of the buttress contains hydrophobic acetal side chains, which are acid labile and, upon acid-induced cleavage, reveal two hydroxyl groups on the side chain of the polymer repeat unit. This polymer is readily electrospun to afford flexible, non-woven polymer buttresses with a cloth-like character. Contact angle measurements confirm the fibers' wettability change, and SEM reveals an increase in fiber diameter when the buttresses are incubated under pH 5.5 or 6.5 conditions. In contrast, no changes are observed at pH 7.4. As electrospinning is a versatile process, drug-loaded buttresses can be fabricated in a single synthetic step. While minor passive drug release occurs at pH 7.4, a mildly acidic pH of 5.5 - 6.5 triggers increased drug release in a pH-dependent manner. Drug-loaded buttresses are cytotoxic to multiple human cancer cell lines. Using these in standard lung tumor resection surgeries is feasible to reinforce the resection margin and deliver drugs locally. Future studies may explore the *in vivo* efficacy of such systems as drug delivery devices for treating diseases where a change of pH is integral to the pathology of the disease, such as cancer or some inflammatory diseases.

5. REDOX-SENSITIVE HYDROGELS FOR ON-DEMAND PROTEIN DELIVERY

Adapted with permission from {Altinbasak, I., S. Kocak, R. Sanyal, and A. Sanyal, "Fast-Forming Dissolvable Redox-Responsive Hydrogels: Exploiting The Orthogonality Of Thiol–Maleimide And Thiol–Disulfide Exchange Chemistry.", Biomacromolecules, Vol. 23, pp. 3525–3534, 2022.} Copyright {2022} American Chemical Society [239].

5.1. Introduction

An ever-increasing utilization of hydrogels as an attractive platform for biomedical applications such as wound healing [240-242], combating burn incidences [243,244], and local delivery of therapeutic agents ranging from small molecules to biological macromolecules such as proteins and antibodies [245,246] has been noticeable in recent years. The choice of polymeric materials and the connectivity between the polymer chains tuned through the architecture of macromolecular building blocks or interchain crosslinking junctions enable the modulation of a wide range of properties in these materials. The HG matrix can provide one or more desirable attributes, such as eliciting therapeutic agents in a localized manner at the site of disease, protecting the therapeutic agent against long-term degradation, acting as a depot for slow release, and thus eliminating frequent drug administration. The material can also act as a sponge for soaking up exudes from the wound or the site of infection. While bandages bring desirable attributes to take care of the wound/disease site, one of the issues that compromises patient comfort is the removal of bandages during routine clean-up and replacement with a new bandage [247,248]. In light of this, development of hydrogel based dissolving bandages have been investigated in recent years [249]. To address this issue, the installation of crosslinking junctions that can be ruptured on-demand through the application of specific stimuli such as light [250] or reducing agents [251,252] has been evaluated as a viable pragmatic approach. In recent years, hydrogels have also played a vital role in developing injectable formulations. While

the HG matrix provides a suitable environment for the therapeutic agent, localized release at the disease site circumvents several problems conventional oral or intravenous administration encounters [253,254].

HG-based materials that can be obtained through rapid gelation to afford robust crosslinked materials offer several advantages and thus would render them pragmatic for adaptation for real-life applications. In this regard, various “click” reactions have been adapted to engineer fast-forming HGs. For example, strain-promoted azide-alkyne cycloaddition [255], Diels-Alder reaction [256], and oxime click chemistry [257] have been used to fabricate injectable hydrogel systems. Among various efficient chemical transformations that are available to this end, the thiol-maleimide Michael addition reaction has been extensively investigated, in particular, due to its rapid gelation kinetics under mild and reagent-free conditions [258-262]. The reaction usually proceeds in the aqueous environment without any additional reagents and catalysts. This linkage's relatively high degree of stability in the biological milieu provides reasons for its widespread utilization. The thiol-maleimide linkage is considerably robust in nature and only upon exposure to excess competitive thiol, undergoes a relatively slow degradation [251]. In this regard, the disulfide bond is unique for its rapid cleavage upon exposure to moderate amounts of thiol. This attribute has been widely exploited in the fabrication of stimuli-responsive polymeric materials [262-266]. The advantage of the approach outlined here is that the complementary reactive groups are used to allow the formation of a disulfide-containing near-well-defined network structure. During gelation, there is no small-molecule byproduct formation; thus, gels can be used as prepared. It can be envisioned that the design of a system that embodies the rapid conjugation kinetics of the thiol−maleimide chemistry and the efficient bond scission of disulfides upon exposure to reducing conditions bear the potential to afford fast-forming crosslinked HGs with on-demand fast dissolution.

In this study, we report the fabrication of a new class of fast-forming redox-responsive HG systems. In particular, HGs were synthesized using the Michael-type conjugation reaction between thiol-terminated tetra-arm poly(ethylene glycol) (PEG) and disulfide-containing maleimide-terminated PEG polymers, as illustrated in Figure 5.1. The thus-obtained HGs were evaluated as platforms for the sustained release of large macromolecules

and proteins. The release of fluorescent dye-labeled dextran polymers and bovine serum albumin (BSA) was assessed for stimuli-responsive triggered release.

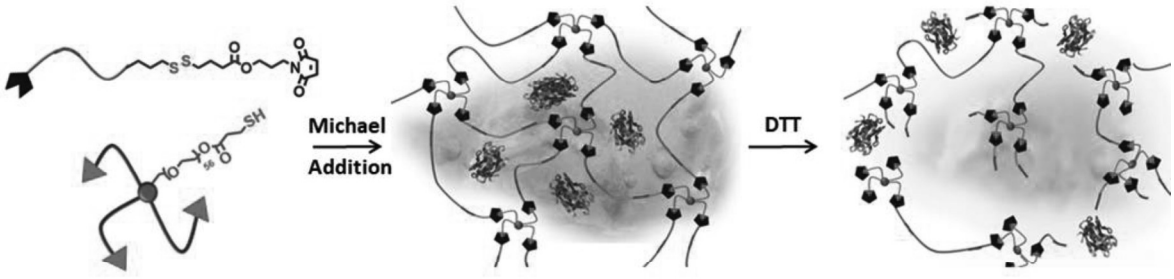

Figure 5.1. Schematic illustration of fabrication and protein encapsulation and release from fast-forming dissolvable hydrogels.

5.2. Experimental

5.2.1. Materials

Triethylamine and diethyl ether were purchased from Merck. 1,4-Dithio-dl-threitol (DTT) (98%) and trifluoroacetic acid were purchased from Alfa Aesar. 4-(Dimethylamino)pyridine (DMAP, >99%), 4,4′-dithiodibutyric acid (95%), 3-mercaptopropionic acid, *N*,*N*′-dicyclohexylcarbodiimide (DCC), PEG (4 kDa), toluene, fluorescein isothiocyanate–dextran (FITC-dextran, 20, 150 kDa), albumin–FITC conjugate (FITC–BSA), and *p*-toluenesulfonic acid monohydrate (99%) were purchased from Sigma-Aldrich. Four-arm PEG (10 kDa) was purchased from Creative PEGWorks. The thiol-terminated four-arm PEG [267] and the furan-maleimide adduct containing alcohol [268] were obtained using literature procedures.

5.2.2. Methods

Ultra-pure water was obtained via MilliQ Water Purification System (Merck Millipore, USA). FTIR spectroscopy measurements were done on a Thermo Scientific

Nicolet 380 FTIR spectrometer. NMR analysis was carried out using a 400 MHz Bruker spectrometer. The size of the polymers were monitored using a gel permeation chromatography using a PSS-SDV (gram linear, length/ID 8 × 300 mm, ten μm particle size) column calibrated with poly(methyl methacrylate) standards (1−175 kDa) using a refractive index detector. Dimethylacetamide with 0.05% lithium bromide was used as an eluent at a flow rate of 1.0 mL/min at 30 °C. The surface morphology of hydrogels was examined using scanning electron microscopy (SEM) (JEOL NeoScope JCM-500, with an accelerating voltage of 10 kV). The mechanical properties of hydrogels were analyzed using a rheometer (Anton PAAR MCR 302). UV-vis spectrophotometer measurements were carried out using Thermo Scientific Nanodrop 2000 spectrophotometer and a Varian Cary Eclipse, Agilent, USA). Side products of reactions were analyzed by LC-MS analysis using an LC-MS-2020-spectroscopy (Shimadzu, Japan) equipped with a C-18, five μm, 150 × 4.6 mm column.

5.2.3. Cell lines

L929 mouse fibroblast cell line was purchased from ATCC (LGC Standards, Germany) and grown according to the culture methods requirements of the manufacturer. Cells were kept in the logarithmic phase of cell growth for the duration of experiments and incubated in a humidified atmosphere of 5% CO2 at 37 °C. Cytotoxicity experiments were done with a plate reader (Multiscan FC, Thermo Scientific, USA), and Cell Counting Kit8 (CCK-8, Fluka) was obtained from Sigma-Aldrich.

5.2.4. Synthesis of Masked Maleimide Disulfide Acid

4,4′-Dithiodibutyric acid (2.16 g, 0.010 mol), furan-protected maleimide-containing alcohol (1.00 g, 0.004 mol), and DMAP (0.350 g, 0.003 mol) were added to a round-bottom flask and dissolved in anhydrous dichloromethane (40 mL). DCC (2.00 g, 0.009 mol) was dissolved in dichloromethane (20 mL) in another flask. The content of the second flask was slowly added to the ice-cold mixture in the first flask. The combined reaction mixture was stirred at room temperature for 24 h. To the reaction mixture was added dichloromethane (25 mL), and then the precipitated dicyclohexylurea was removed by filtration, followed by washing of the organic phase with a saturated $NaHCO_3$ solution. Anhydrous Na_2SO_4 was

used to dry the organic layer and was concentrated under low pressure. Purification using column chromatography on SiO_2 using CH_2Cl_2 and EtOAc (1:1) as eluents yielded the pure product (1.90 g, 80%). ^{1}H NMR ($CDCl_3$, δ, ppm), 6.50 (s, 2H, CH═CH), 5.26 (s, 2H, CH bridge protons), 4.02 (t, 2H, OCH_2CH_2), 3.57 (t, 2H, NCH_2CH_2), 2.85 (s, 2H bridgehead protons), 2.72 (t, 4H, SCH_2CH_2), 2.47 (t, 4H, $COCH_2CH_2$), 2.03 (m, 4H, $SCH_2CH_2CH_2$), 1.94 (m, 2H, $NCH_2CH_2CH_2$).

5.2.5. Synthesis of Maleimide Disulfide-Terminated PEG Polymer

Masked maleimide disulfide acid (0.25 g, 0.500 mmol), PEG (4 kDa, 0.56 g, 0.140 mmol), and DMAP (0.01 g, 0.080 mmol) were added to a round-bottom flask and dissolved in dichloromethane (0.35 mL). DCC (0.12 g, 0.550 mmol) was added to another round-bottom flask and dissolved in dichloromethane (0.20 mL). The first solution was cooled down, and the second solution was added to the ice-cold mixture slowly, and the reaction was stirred at room temperature for 24 h. Dichloromethane (5 mL) was added to the reaction mixture, the precipitated dicyclohexylurea was removed by filtration, and the concentrated solution was precipitated in ether. ^{1}H NMR ($CDCl_3$, δ, ppm), 6.50 (s, 4H, CH═CH), 5.26 (s, 4H, CH bridgehead protons), 4.25 (t, 4H, OCH_2CH_2O), 4.02 (t, 4H, OCH_2CH_2), 3.40–3.80 (broad s, 360 H), 2.85 (s, 4H bridge protons), 2.72 (t, 8H, SCH_2CH_2), 2.47 (t, 8H, $COCH_2CH_2$), 2.03 (m, 8H, $SCH_2CH_2CH_2$), 1.94 (m, 4H, $NCH_2CH_2CH_2$). The furan protection was removed by dissolving the above compound (0.65 g) in toluene (20 mL). The solution was refluxed for ten h. The concentrated solution was purified by precipitation with diethyl ether to yield the PEG-based bis-maleimide crosslinker (92% yield). ^{1}H NMR ($CDCl_3$, δ, ppm), 6.70 (s, 4H, CH═CH), 4.25 (t, 4H, OCH_2CH_2O), 4.02 (t, 4H, OCH_2CH_2), 3.40–3.80 (broad s, 360 H), 2.72 (t, 8H, SCH_2CH_2), 2.47 (t, 8H, $COCH_2CH_2$), 2.03 (m, 8H, $SCH_2CH_2CH_2$), 1.94 (m, 4H, $NCH_2CH_2CH_2$).

5.2.6. Selectivity in Thiol–Maleimide and Thiol–Disulfide Exchange Reactions

For a 1:1 M ratio of the maleimide/thiol reaction, maleimide disulfide-terminated PEG polymer (10 mg) and 2-mercaptoethanol (0.30 mg) were dissolved in phosphate-buffered saline (PBS) (1× 100 μL) and stirred at 200 rpm for 30 min at 37 °C. The reaction solution

was then freeze-dried and redissolved in CH_2Cl_2. The solution was precipitated in 1.5 mL of diethyl ether and centrifuged at 17,000 rpm for 5 min to remove the polymeric component. The supernatant was passed through a short silica gel plug using methanol as eluent. The solution was then evaporated, and redissolved in acetonitrile (1 mL), and analyzed by liquid chromatography-mass spectrometry (LC-MS). The same procedure was also applied for the reaction where a maleimide/thiol ratio of 1:4 was utilized.

5.2.7. Preparation and Characterization of the HGs

HGs were prepared by rapidly mixing the two polymer solutions. Briefly, maleimide disulfide-terminated telechelic PEG polymer (10 mg) and thiol-terminated four-arm PEG polymer (10 mg) were separately dissolved in 50 μL of PBS solutions. Solutions were sonicated for one min, and then one solution was added to the other. The HG was formed upon mixing the two polymer solutions. To ensure high interchain coupling, the mixture was incubated at 37 °C for 30 min. For the loading of FITC-labeled protein and dextran polymers, the maleimide-containing HG precursor was dissolved in the FITC-labeled macromolecule or protein-containing PBS solution, and HGs were prepared with the process described above. Dye-labeled polymers and proteins were encapsulated in a quantitative manner. Lyophilized HG disks (ca. 80 mg) were dipped in deionized water at 37 °C. The HG samples were periodically weighed after removing adherent water from their surface using tissue paper. The water uptake was recorded until no additional increase in weight was observable. Swelling ratio percentages were calculated using $(M_s - M_{dry})/M_{dry} \times 100$, where M_{dry} and M_s refer to the weight of dry and swollen HGs, respectively. The linear viscoelastic limit regime (LVR) and degradation profiles of HGs were recorded using an Anton Paar MCR 302 rheometer. A 15 mm diameter plate was utilized for the tests. The LVR of HGs was determined using the strain sweep test. Nonlinear strain regions indicated a breakdown in HGs and were regimes that were out of the LVR range. The frequency sweep test allows us to ascertain the lower frequency limit where gel-like behavior can be observed. The frequency sweep test with a suitable strain value enabled the determination of the frequency range for doing time sweep tests. A time sweep test with a strain of 1% and an angular frequency of 10 rad/s was employed to follow the degradation process. A time sweep test was performed with a swollen HG between preheated rheometer plates and DTT or

glutathione solution around the HG. To minimize any effect of solvent loss due to vaporization, a closed chamber was used for degradation experiments.

5.2.8. Degradation of the HG and FITC-Labeled Protein and Dextran Release

Two pieces of the disk-shaped HG were kept at 37 °C in a thermal shaker (200 rpm) in 1 mL of PBS solution and 200 mM DTT containing 1 mL of PBS solution. The degradation process of bulk HGs for 10 min was recorded using a digital camera. FITC–BSA and FITC-dextran (150 and 20 kDa) were encapsulated in HGs as described above. After gelation, HG disks (1 cm diameter, 2 mm thick) were placed in an Eppendorf tube with 1 mL of PBS and DTT (10 mM DTT in PBS). The amount of biomolecule and dextran polymer released in the supernatant was obtained using a UV–vis spectrophotometer.

5.2.9. Cytotoxicity Experiments

Cytotoxicity of the HGs was investigated via a CCK-8 viability assay on L929 mouse fibroblast cells. Cells (6000 cells/well) were seeded on a 96-well plate in quadruplicate with 100 μL of the culture medium and incubated at 37 °C overnight to grow and adhere completely. Cells were treated with gels (1.0, 0.5, and 0.1 mg) for 48 h. After the incubation time, gels were removed, and cells were treated with a 10% CCK-8 solution for 3 h, and the absorbance values at 450 nm were measured using a microplate reader. Viability results were obtained on GraphPad prism software in the nonlinear regression mode.

5.2.10. Live/Dead Cell Viability Assay

L929 cells were seeded in a 12-well plate (200,000 cells/well) with Dulbecco's modified Eagle's medium (low) and incubated at 37 °C overnight to grow and adhere. After the incubation process, the medium was removed, and cells were treated with varying amounts of the HGs for 24 h. Thereafter, HGs were removed, and cells were rinsed twice with PBS. Finally, cells were stained according to the protocol of the live/dead assay kit (Sigma, 04511-1KT-F). The cells were stained with PBS solution containing 10 μL of calcein-AM and then with five μL of propidium iodide (PI) for 30 min at 37 °C. After

removing the solution and washing it with PBS, the cells were imaged using a fluorescence microscope (Zeiss Observer A1 equipped with AxioCam MRc5) and AxioVision software. The live cells exhibited green fluorescence due to calcein-AM, and dead cells showed red fluorescence due to PI.

5.3. Results and Discussion

5.3.1. Synthesis and Characterization of Maleimide Disulfide-Terminated Telechelic PEG Polymer

The telechelic PEG-based polymeric component containing maleimide functional groups linked through a disulfide linker was derived from a readily available furan-protected maleimide-containing alcohol, as seen in Figure 5.2. To yield the desired chain-end functionality, the furan-protected maleimide-containing alcohol fragment was linked to 4,4′-dithiodibutyric acid through esterification. The composition and purity of the synthesized molecule were confirmed using ^{1}H NMR spectroscopy in Figure 5.3a and ^{13}C NMR spectroscopy in Figure 5.3b, Fourier transform infrared (FTIR) spectroscopy in Figure 5.4, and LC−MS analysis in Figure 5.5. The FTIR spectrum exhibited the expected carboxylic acid and carbonyl bands at around 3200 and at 1699 cm^{-1}, respectively. The ^{1}H NMR spectrum exhibited the presence of proton resonances at 6.50 and 5.26 ppm belonging to protons on the bicyclic moiety and at 2.72 ppm belonging to protons adjacent to the disulfide unit, confirming the structure. In the ^{13}C NMR spectrum, the resonances at 176.3 and 172.9 ppm belonging to imide and ester carbonyls and at 178.0 ppm belonging to carbon on the carboxylic acid were evident. The esterification reaction was used for coupling this fragment with a linear PEG polymer to yield the masked maleimide disulfide-terminated telechelic PEG polymer as an HG precursor, as seen in Figure 5.2. The composition and purity of the functionalized linear PEG polymer were confirmed using ^{1}H NMR spectroscopy in Figure 5.6 and ^{13}C NMR spectroscopy in Figure 5.7. The proton resonances at 6.50 and 4.25 ppm belonging to the vinylic protons on the bicyclic structure and ester protons next to the

hydroxyl unit of the precursor PEG, respectively, indicated successful chain-end modification

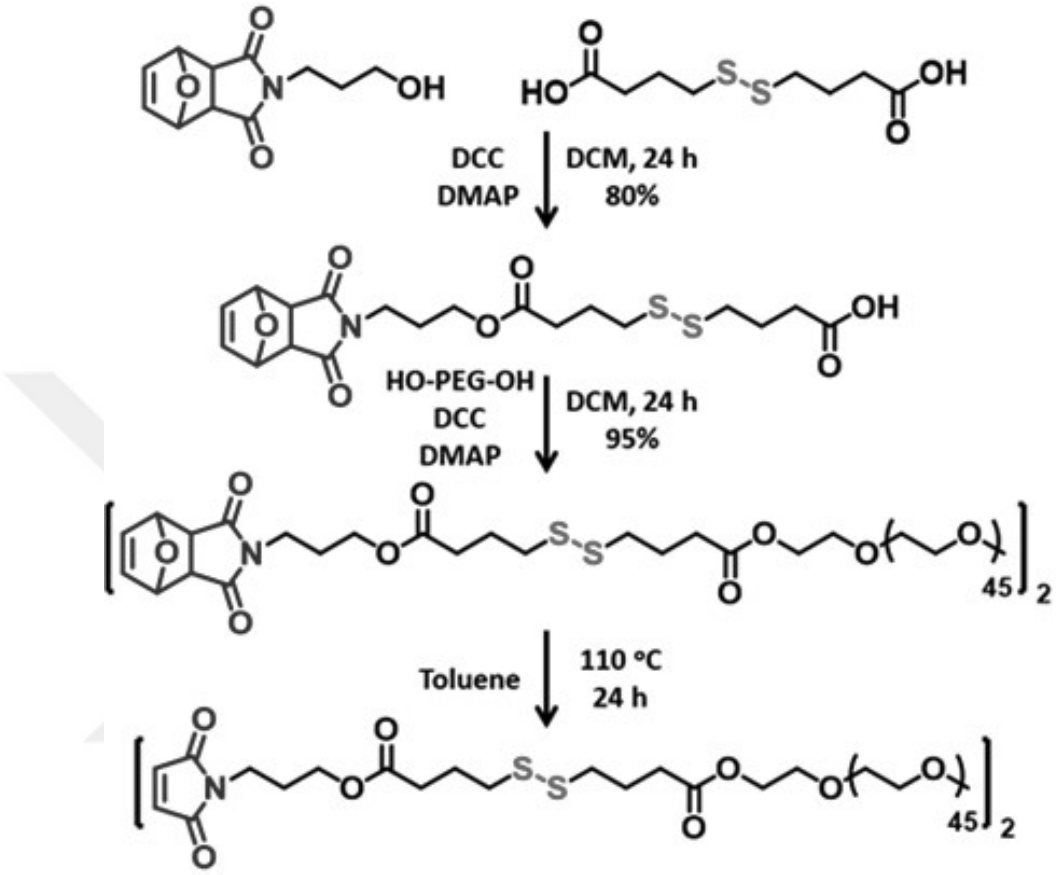

Figure 5.2. Synthesis of disulfide-containing PEG bis-maleimide precursor.

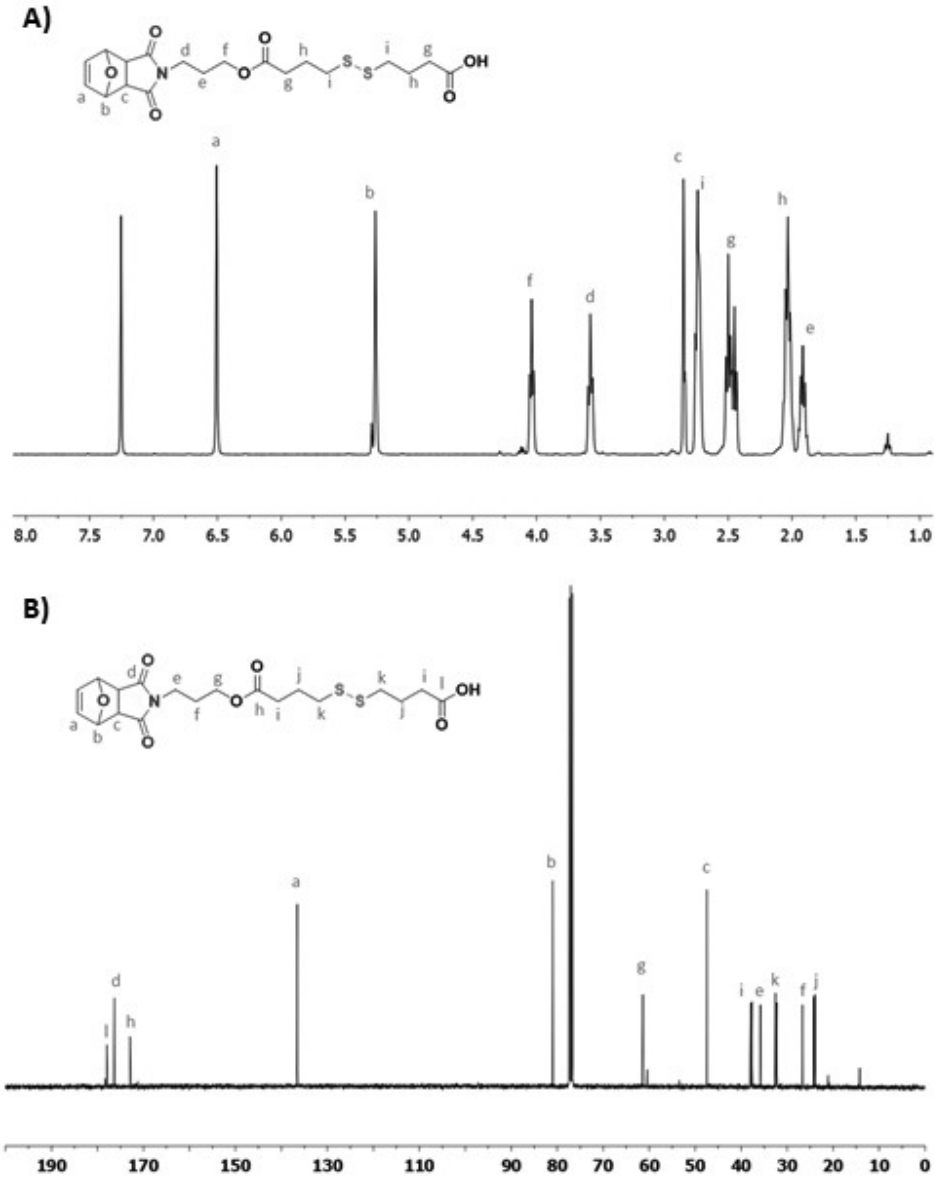

Figure 5.3.(a) ^{1}H NMR and (b) ^{13}C NMR spectra of the masked maleimide-disulfide acid.

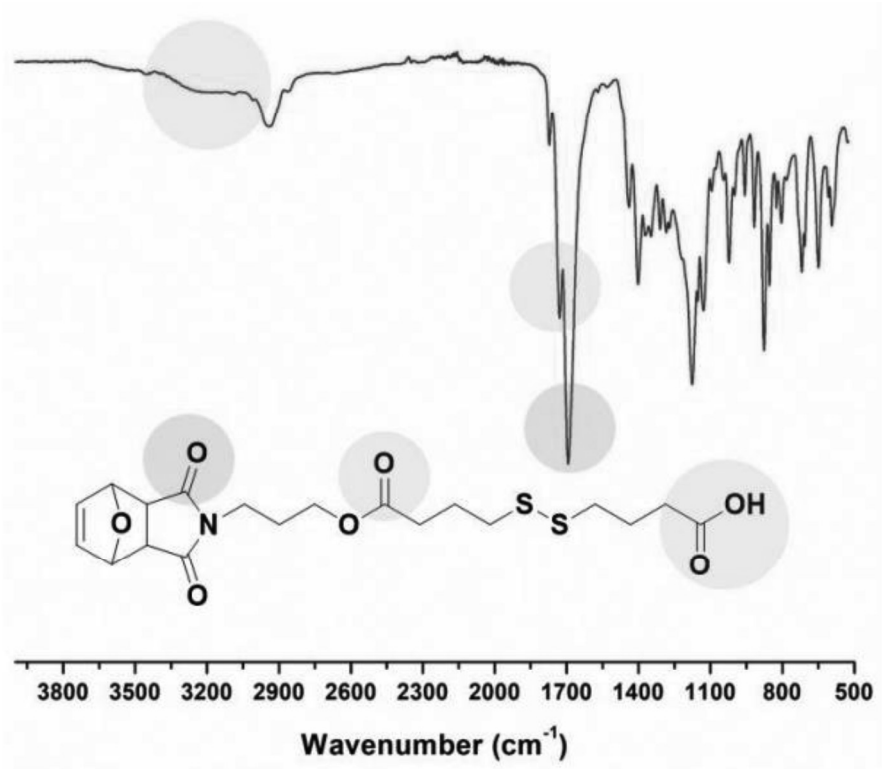

Figure 5.4. FTIR spectrum of masked maleimide-disulfide acid.

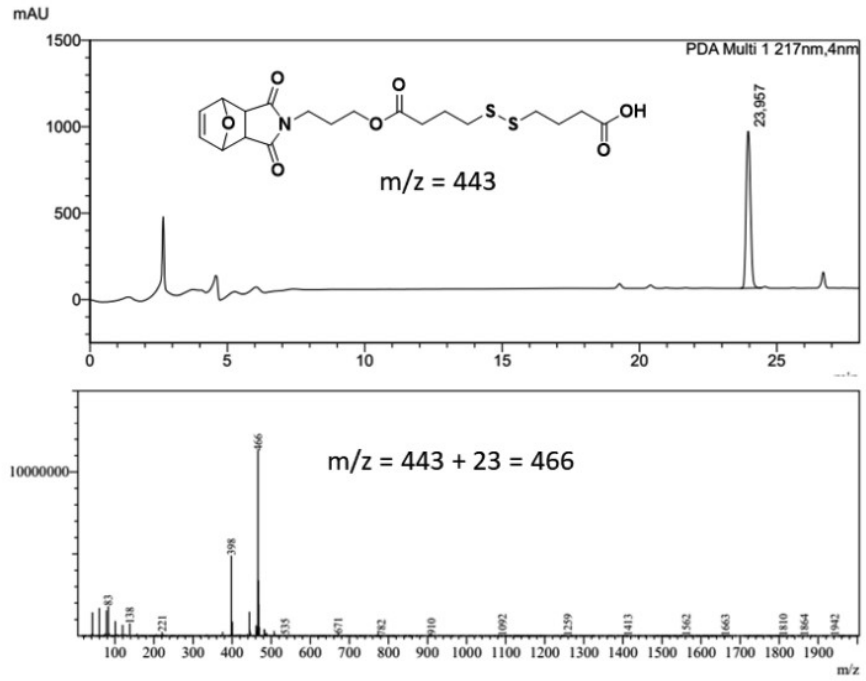

Figure 5.5. LC-MS characterization of the masked maleimide-disulfide acid.

Removal of the furan protection group to obtain the thiol-reactive maleimide form was accomplished via the retro Diels–Alder reaction by refluxing in anhydrous toluene. The composition and purity of this HG precursor were also confirmed using ^{1}H and ^{13}C NMR spectroscopy in Figures 8a and b. The presence of a proton resonance at 6.70 ppm belonging to the vinylic protons on the maleimide ring and other expected proton resonances confirmed the structure. The carbon resonance at 134.2 ppm belonging to the vinylic carbon on the maleimide ring and at 170.6 ppm belonging to the carbonyl group on the maleimide ring also confirmed the presence of this reactive group. The successful synthesis of the maleimide disulfide-terminated telechelic PEG polymer was also confirmed using FTIR in Figure 5.9. After synthesizing masked maleimide disulfide-terminated PEG, new carbonyl peaks of ester bonds and imide groups appeared at 1731 and 1699 cm^{-1}, respectively. After the retro-Diels–Alder reaction, carbonyl peaks of imide groups shifted to 1704 cm^{-1}, and a new peak appeared at 696 cm^{-1}, corresponding to the C–H vibration of the maleimide moiety [269].

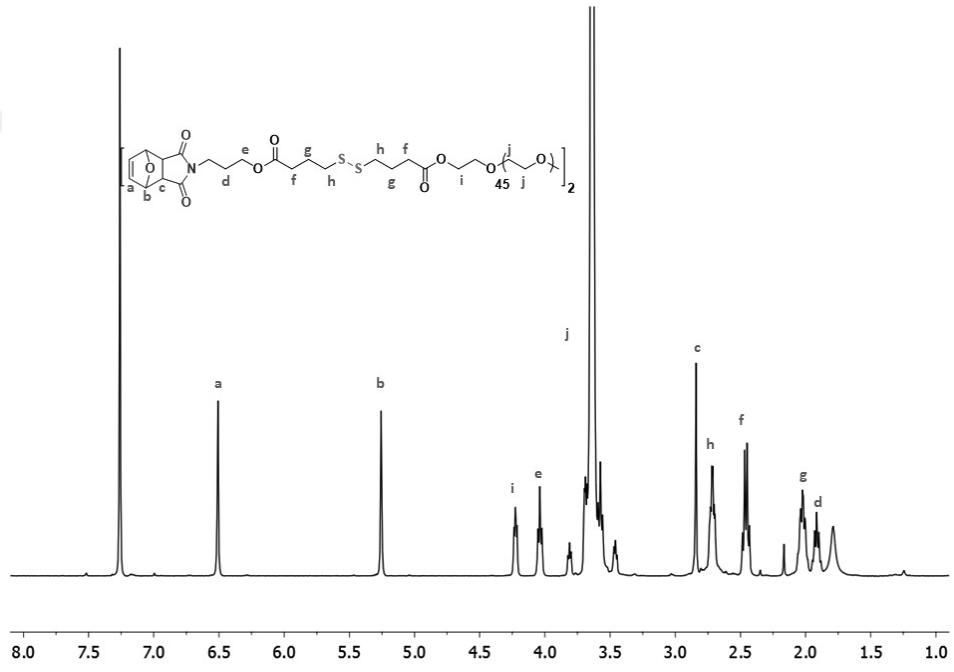

Figure 5.6. ^{1}H NMR spectrum of disulfide- and furan-protected bis-maleimide containing PEG polymer.

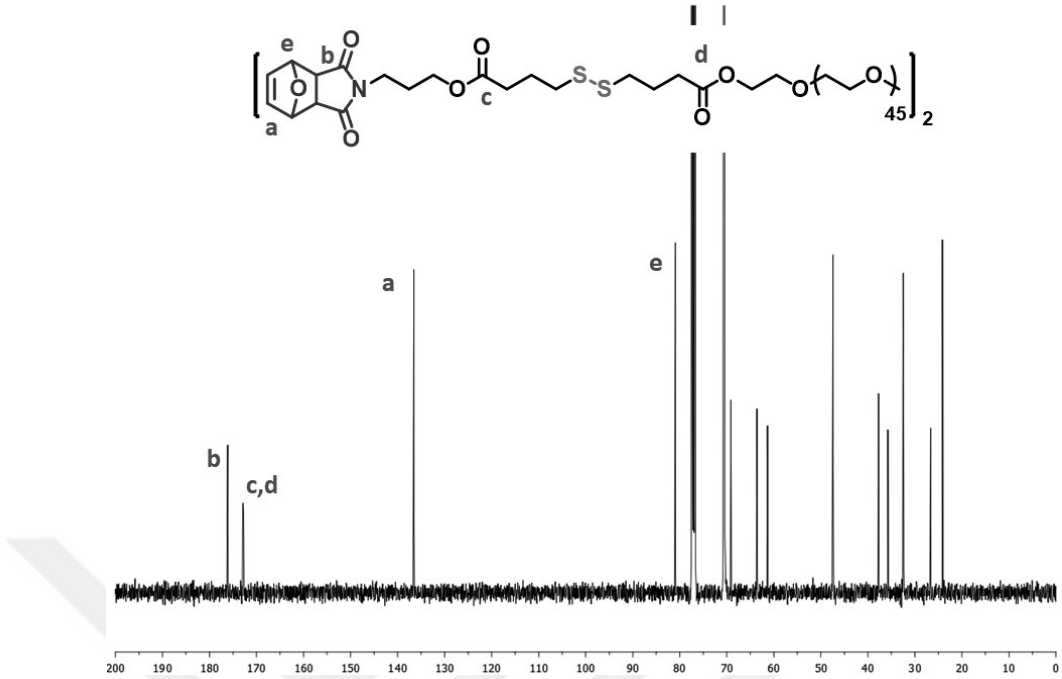

Figure 5.7. ^{13}C NMR spectrum of disulfide containing PEG furan-protected bis-maleimide polymer.

5.3.2. Orthogonality of the Thiol–Maleimide, and Thiol–Disulfide Exchange Chemistry

At this point, it was important to confirm that the hydrogel precursors that contain two different thiol-reactive bonds: the maleimide and the disulfide groups, will have a much higher propensity to undergo the thiol-maleimide conjugate addition compared to the thiol-disulfide exchange reaction. Selectivity of thiol addition was investigated by treatment of the disulfide-containing maleimide-terminated polymer with the stoichiometric equivalent of 2-mercaptoethanol. Figure 5.10a shows the ^{1}H NMR analysis of obtained polymer, which revealed that the proton resonance at 6.7 ppm belonging to the vinylic proton on the maleimide ring had disappeared entirely. In contrast, new proton resonance from the 2-mercaptoethanol fragment appears. The ^{13}C NMR analysis of Figure 5.10b demonstrated that vinylic carbon resonance at 134.2 had vanished entirely. The resonance of carbonyls on the maleimide ring had also shifted to 174.5 and 177.5 as two different peaks due to thiol-maleimide conjugation. As expected, there was minimal change in the size exclusion chromatograph of the bis-maleimide-containing polymer after this treatment, as seen in

Figure 5.11. Furthermore, the solution of the reaction of the maleimide disulfide-terminated PEG with the stoichiometric equivalent of 2-mercaptoethanol was also analyzed using LC-MS, and no side product due to disulfide cleavage was observed, as seen in Figure A.1a. On the other hand, using an excess (4 equiv) of 2-mercaptoethanol led to the formation of products from disulfide bond cleavage, as seen in Figure A.1b. Hence, it was inferred that for these constructs, the thiol groups preferentially undergo Michael addition reaction with electron-deficient conjugated alkenes compared to thiol-disulfide exchange reactions with disulfide linkages.

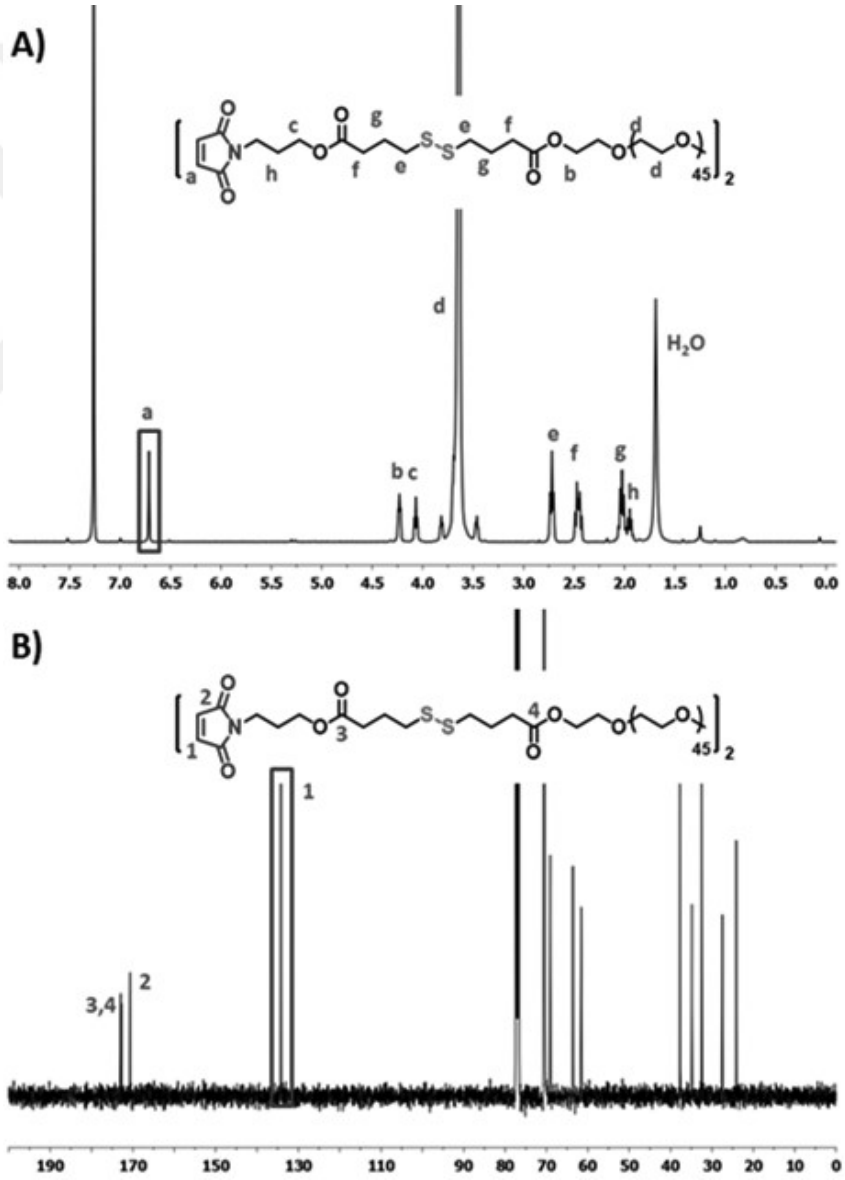

Figure 5.8. (a) ^{1}H and (b) ^{13}C NMR spectrum of disulfide containing PEG bis-maleimide.

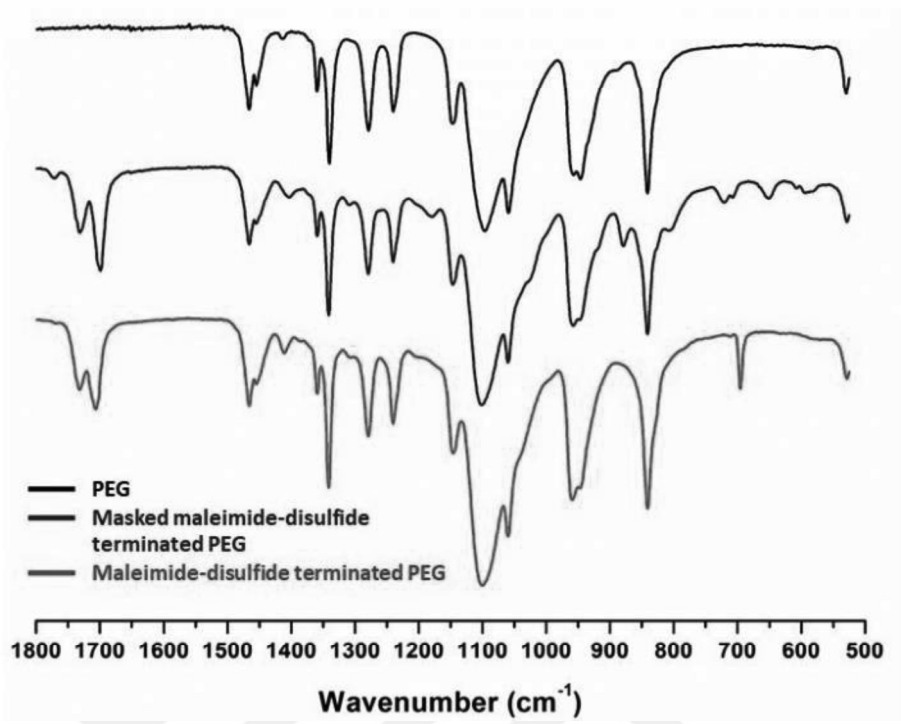

Figure 5.9. FTIR spectra of PEG, masked maleimide-disulfide terminated PEG, and maleimide-disulfide terminated PEG.

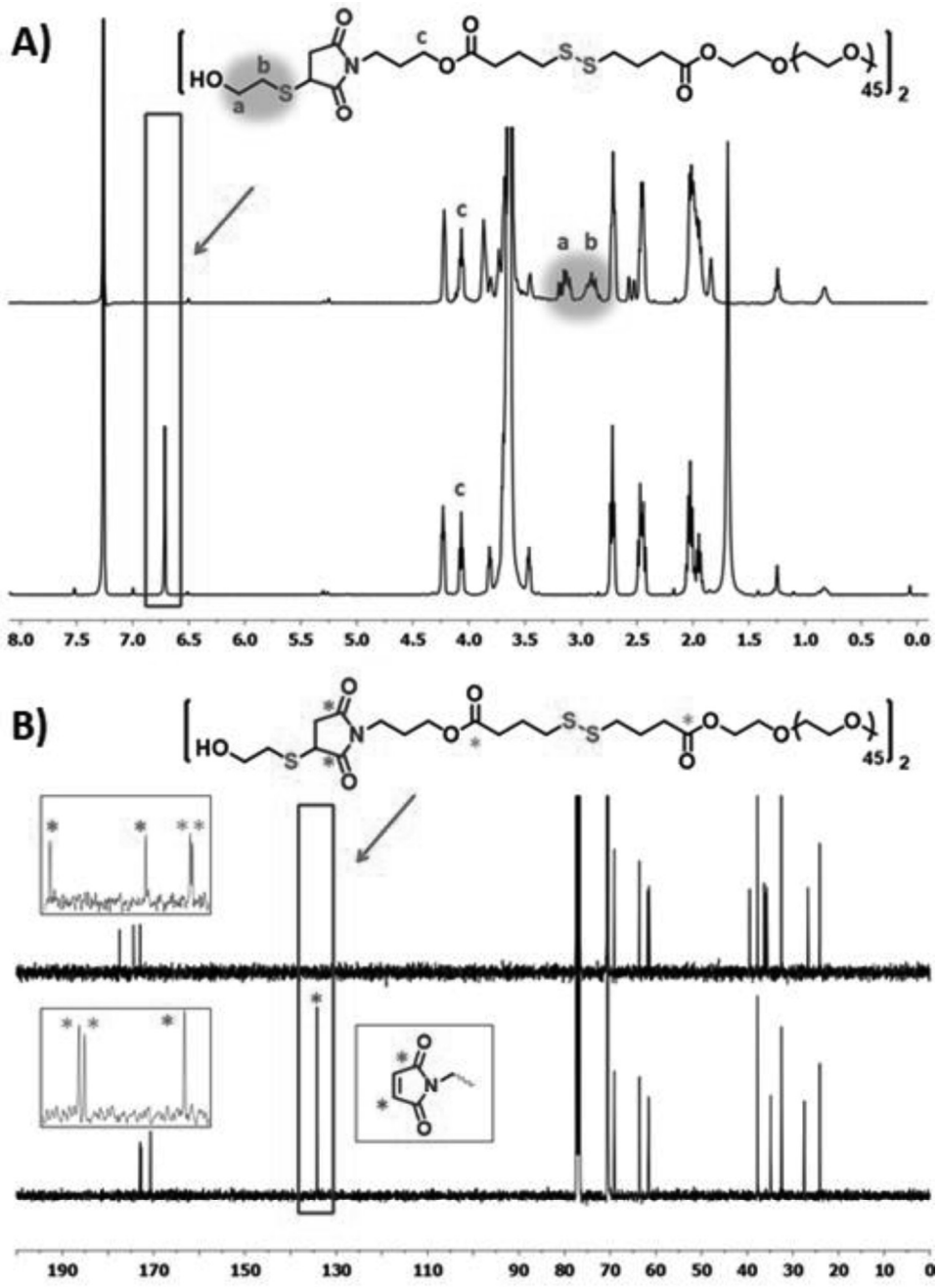

Figure 5.10. Comparison of (a) ^{1}H and (b) ^{13}C NMR spectrums of PEG bis-maleimide polymer and thiol-conjugated bis-maleimide polymers.

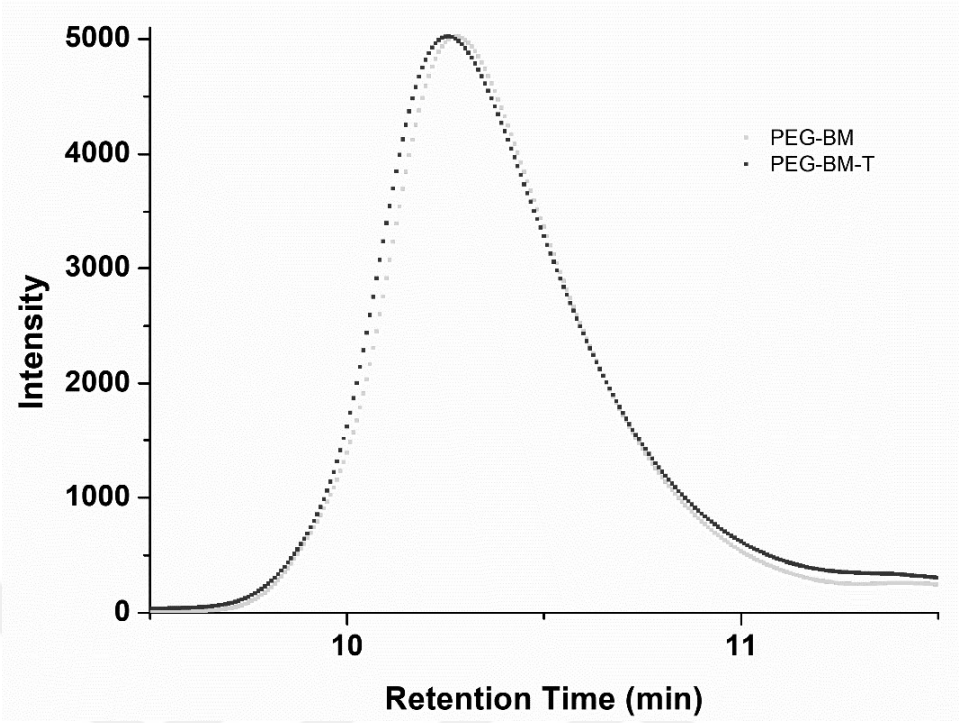

Figure 5.11. SEC chromatographs of PEG polymers before and after addition of 2-mercaptoethanol.

5.3.3. Preparation and Characterization of HGs

For the preparation of hydrogels, the disulfide-containing bis-maleimide PEG polymer was mixed with a tetra-arm thiol-containing PEG polymer in PBS solution at 37 ºC, with the equimolar stoichiometry of the thiol and maleimide functional groups. Figure 5.12a showed clear and transparent hydrogels formed within a minute of mixing the polymers, with near quantitative conversions. The morphology of the obtained hydrogel was investigated using scanning electron microscopy, and a highly porous structure was observed in Figure 5.12b. Lack of the appearance of any characteristic UV–vis absorbance peak upon treatment of HGs with Ellman's reagent suggested that no significant amount of free thiol groups were present in the obtained HGs, as opposed to the peak observed at 411 cm^{-1} for the tetra-thiol polymeric precursor as seen in Figure 5.13. The gelation product was analyzed using FTIR spectroscopy, where it was observed that the characteristic peak of imide carbonyl groups shifted from 1704 to 1706 cm^{-1} and appeared as a smaller peak, as well as the absorbance of a maleimide moiety at 696 cm^{-1} disappeared as seen in Figure 5.14, which are in accordance

with the results of a previous work related to thiol-maleimide additions To investigate the stability and degradation profile of the HG, rheological behaviors of a water-swollen HG were studied via a strain sweep test and frequency sweep test. A strain sweep test was performed to investigate the linear viscoelastic limits of hydrogels. When a 0.01 to 100% strain was applied to the hydrogel, a linear viscoelastic behavior was observed up to 4% strain under ten rad/s frequency in Figure 5.15, indicating a lack of structural breakdowns. Figure 5.12c demonstrates the response of hydrogels to scaled frequency that was measured using a frequency sweep test from 0.01 to 100 rad/s by using a constant strain of 1%. As expected for gels prepared with hydrophilic PEG polymers, hydrogels exhibited a rapid high water uptake within a few minutes, as seen in Figure 5.12d.

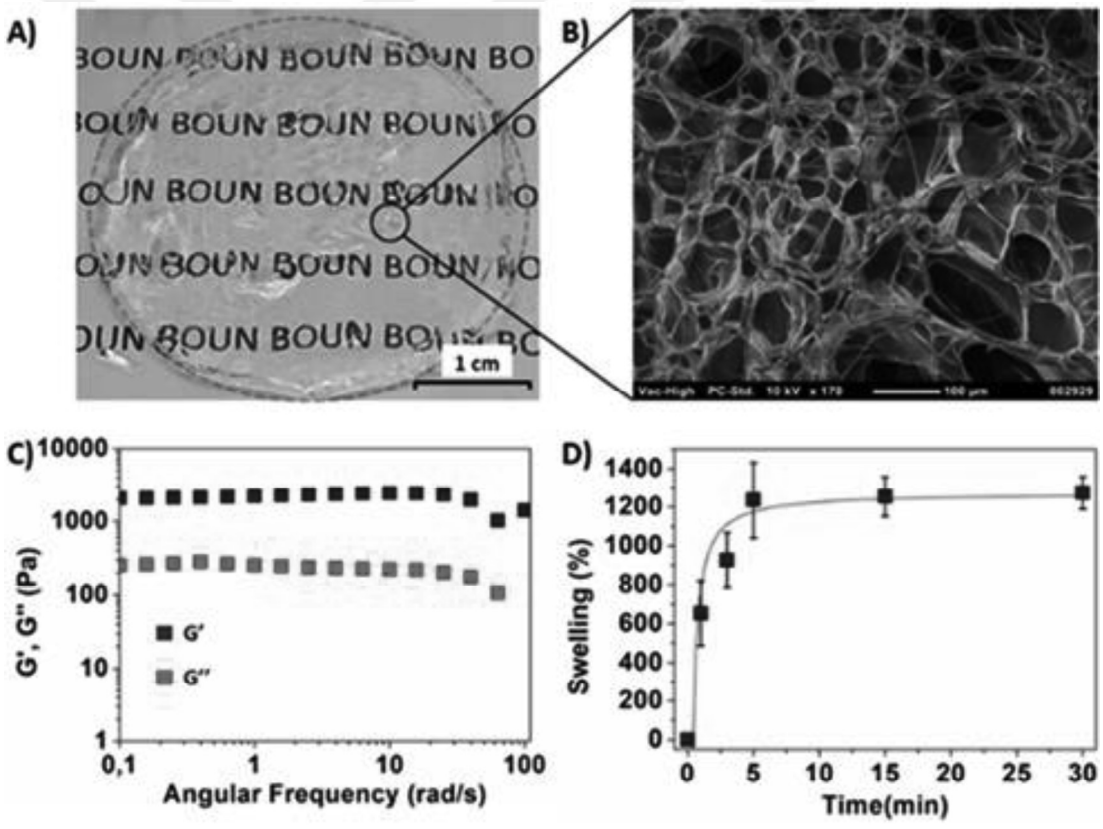

Figure 5.12. (a) Photographic image of a wet hydrogel sample, (b) SEM image of a dry hydrogel sample (scale bar: 100 μm), (c) frequency sweep test, and (d) water uptake swelling profile.

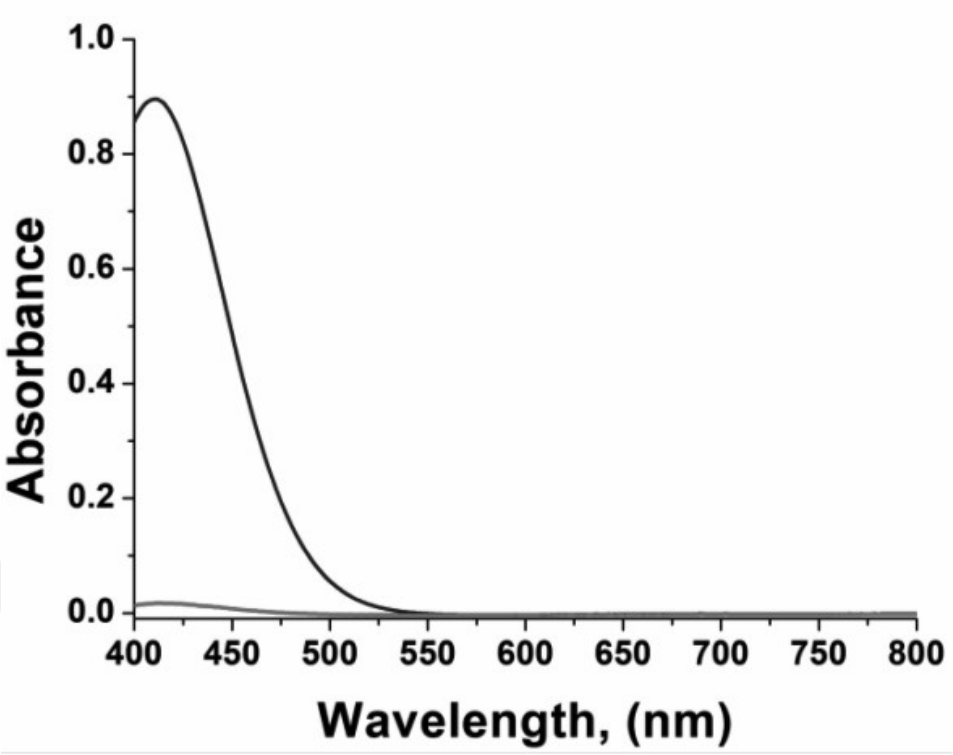

Figure 5.13. UV-vis spectra of Ellman's reagent solution incubated with hydrogel (red) and tetra-thiol polymer (blue).

5.3.4. Degradation of HGs

To monitor the degradation behavior in reductive and nonreductive environments, HGs loaded with a fluorescent dye-labeled protein, namely, FITC–BSA were prepared. To investigate the effect of FITC–BSA loading on the rheological properties of HG, strain and frequency sweep tests were undertaken, and no significant change compared to the protein-free HGs was observed, as seen in Figure 5.16. Obtained FITC-BSA loaded swollen disk-shaped hydrogel was cut into two pieces, and one of these pieces was immersed in PBS solution, while the other one was immersed in DTT solution (0.2 M) at 37 $^{\circ}$C as seen in Figure 5.17a. As expected, while the hydrogel kept in PBS did not show any visible degradation over a prolonged period, the hydrogel immersed in DTT solution degraded completely, and the solution became fluorescent within 10 minutes. Hence, as expected from the molecular design of these materials, they undergo rapid gelation to provide stable hydrogels and undergo rapid dissolution in the presence of a thiol-based reducing agent.

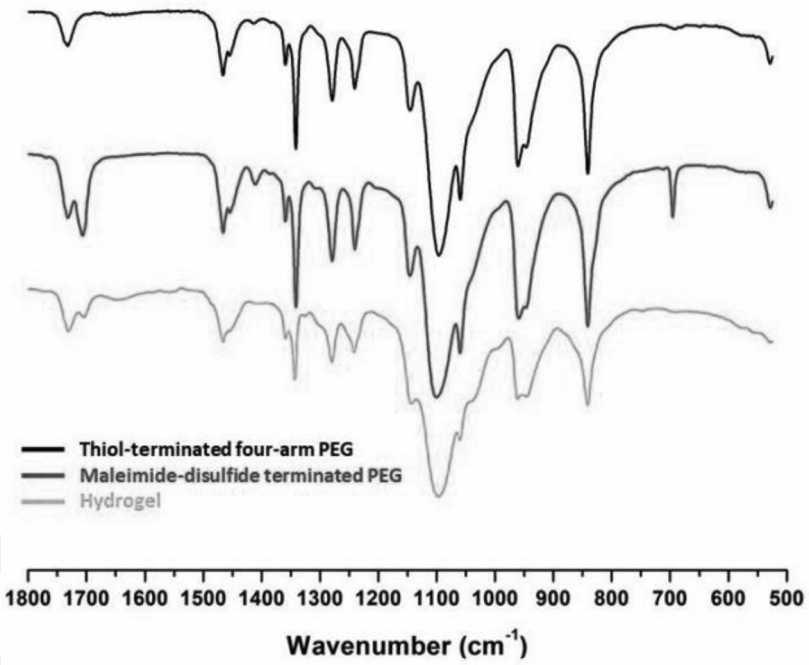

Figure 5.14. FTIR spectra of thiol-terminated four arm PEG, maleimide-disulfide terminated PEG, and hydrogel.

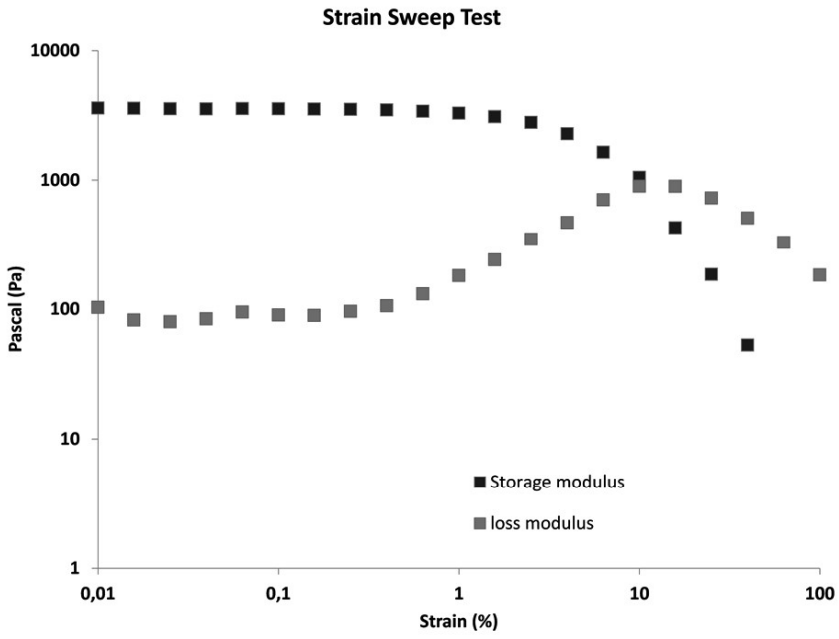

Figure 5.15. Strain sweep test of hydrogel.

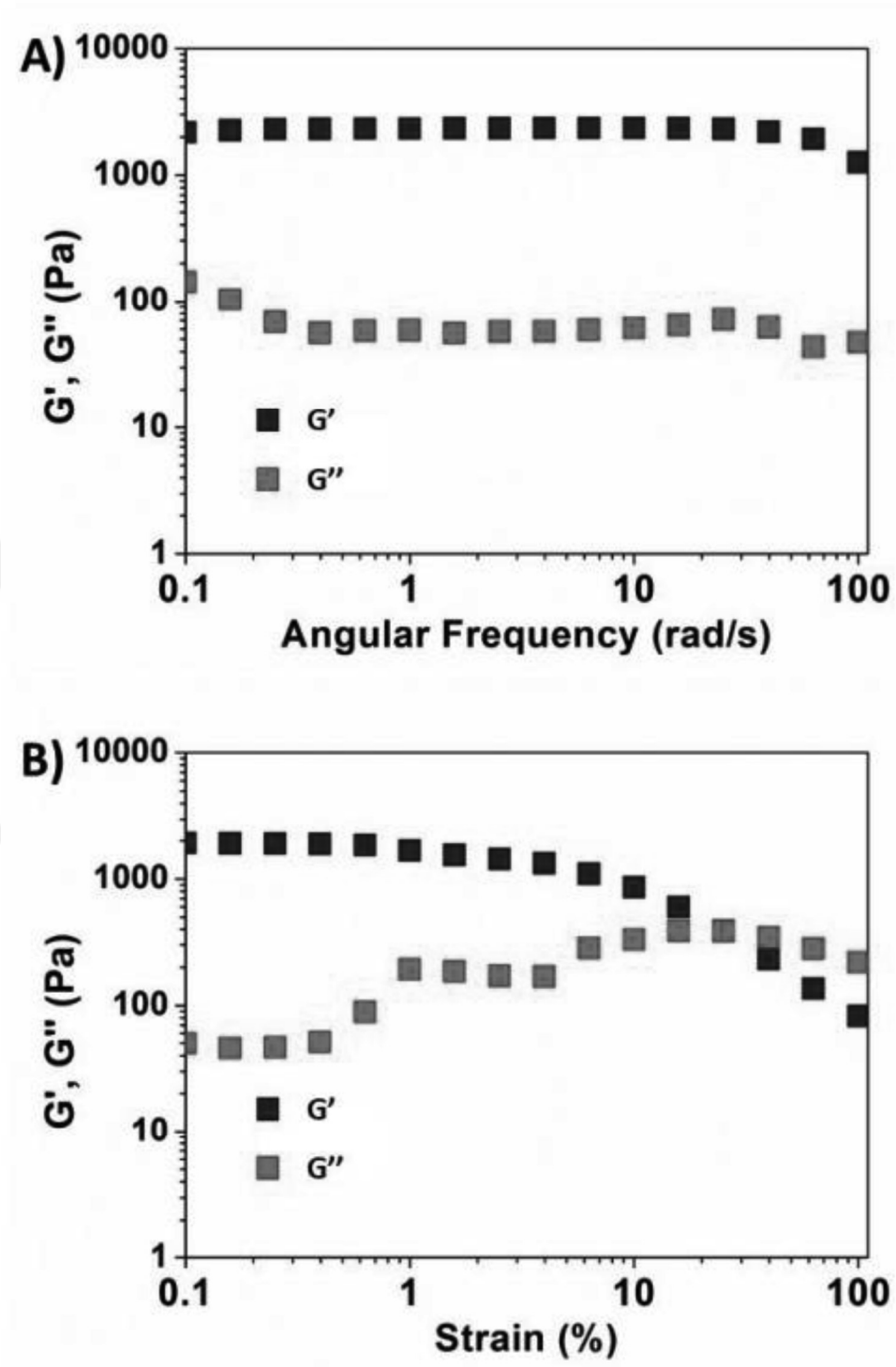

Figure 5.16. (a) Frequency sweep test and (b) strain sweep test of the FITC-BSA loaded hydrogel.

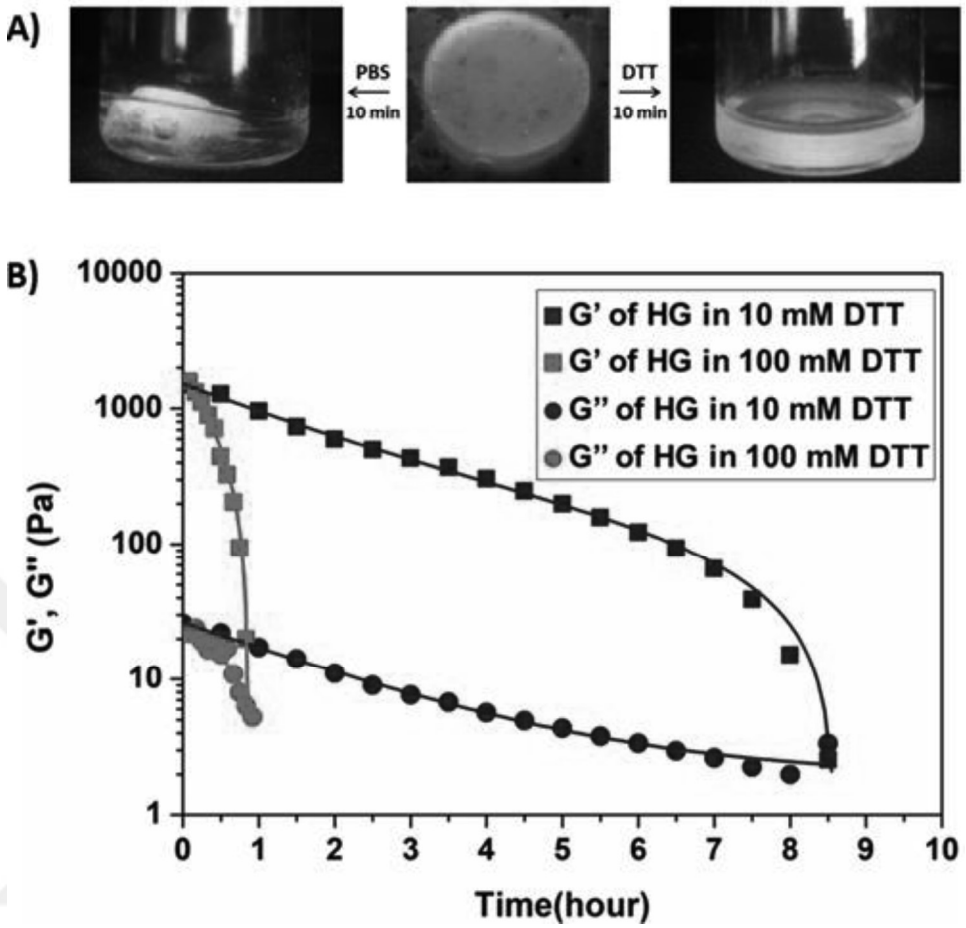

Figure 5.17. (a) Behavior of disulfide-containing hydrogel in PBS and DTT (200 mM) solutions, and (b) rheological analysis of the degradation of hydrogel in DTT solutions (10 and 100 mM).

Degradation of hydrogels was also probed using the time sweep test in a rheometer. For the time sweep test, the hydrogel sample was placed between parallel plates, and the chamber around the hydrogel was filled with DTT or PBS solution. In Figure 5.18, it was observed that the elastic modulus of hydrogel remained constant when the chamber was filled with PBS solution. However, a drastic decrease in elastic modulus was observed for the hydrogel that was incubated in the DTT solution. While in 10 mM DTT solution, it takes 8 hours, in 100 mM DTT solution, it takes only 40 mins for complete degradation of the hydrogel, as seen in Figure 5.18b. As expected, glutathione works relatively slower than DTT in disulfide bond cleavage. In Figure 5.18, it was observed that complete degradation took 30 hours when the hydrogel was placed in 10 mM glutathione solution.

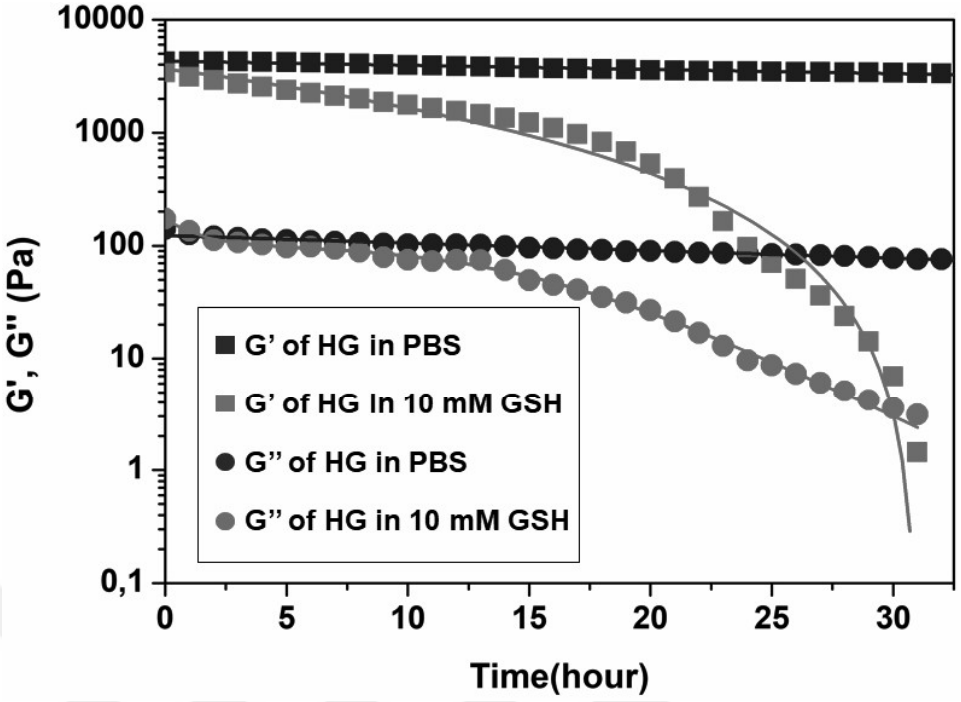

Figure 5.18. Time sweep test of hydrogel in the presence and absence of glutathione (GSH).

5.3.5. Macromolecular Release from HGs

Obtained hydrogels were utilized to study the release of macromolecules such as polymers and proteins, which are often employed as macromolecular therapeutics. First, FITC-labeled dextran polymers (20 and 150 kDa) were used to probe release from the hydrogel network. Two different molecular weights of FITC-labeled dextran were used to ascertain the effect of molecular weight on release. Briefly, FITC-labeled dextran polymers, thiol-terminated four-arm PEG polymer, and disulfide-containing PEG bis-maleimide polymers were dissolved in separate vials. This solution was quickly mixed with a thiol-terminated PEG polymer dissolved in PBS. A solid and freestanding transparent HG was obtained. Thereafter, HGs were immersed in DTT (10 mM) and PBS solutions to investigate the release of the FITC-dextran polymer. It was noticeable that the cumulative release of FITC-dextran was considerably higher in DTT solution than in PBS, as seen in Figure 5.19. As expected, relatively less release was observed for the 150 kDa FITC-dextran polymer, while more dextran release was observed for the lower molecular weight 20 kDa FITC-

dextran. HGs were treated with a concentrated DTT solution to demonstrate the on-demand release. For this purpose, the release solution of HGs was exchanged with a 200 mM DTT solution after 20 h. Under this highly reducing environment, HGs degraded rapidly and released all of the encapsulated FITC-labeled polymers.

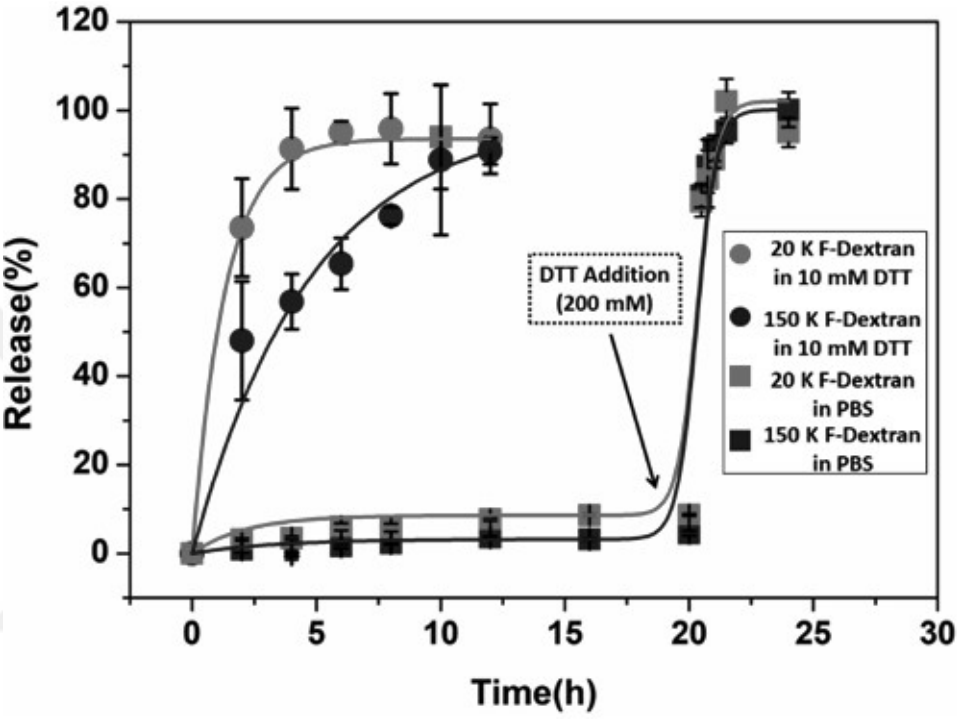

Figure 5.19. Release of 150 kDa and 20 kDa FITC-label dextran from hydrogels in DTT and PBS solutions.

Additionally, as a model protein, FITC–BSA was utilized to investigate the release profile of biomacromolecules. HGs were prepared to obtain a freestanding HG loaded with FITC–BSA using the above-mentioned protocol. Obtained HGs were immersed in DTT (10 mM) and PBS solutions. As seen in Figure 5.20, the cumulative release of FITC–BSA was substantially higher in the DTT solution than in the PBS solution. While the release in PBS solution was slow, the addition of a 200 mM DTT solution initiated the forced release, whereby the HG degraded completely and released all of the encapsulated protein within a few minutes. It should be noted that FITC–BSA was used here as a model example to demonstrate that tunable release of large biomacromolecules from such gels is possible. One can envision that the concept can be extended to release of other large macromolecules such

as oligonucleotide sequences, as well as drug-conjugated polymers encapsulated within such HGs, but may be limited to biomolecules that do not possess susceptible disulfide units whose cleavage under reducing conditions may lead to loss of activity unless they are able to refold to their original structure after release from the reducing environment.

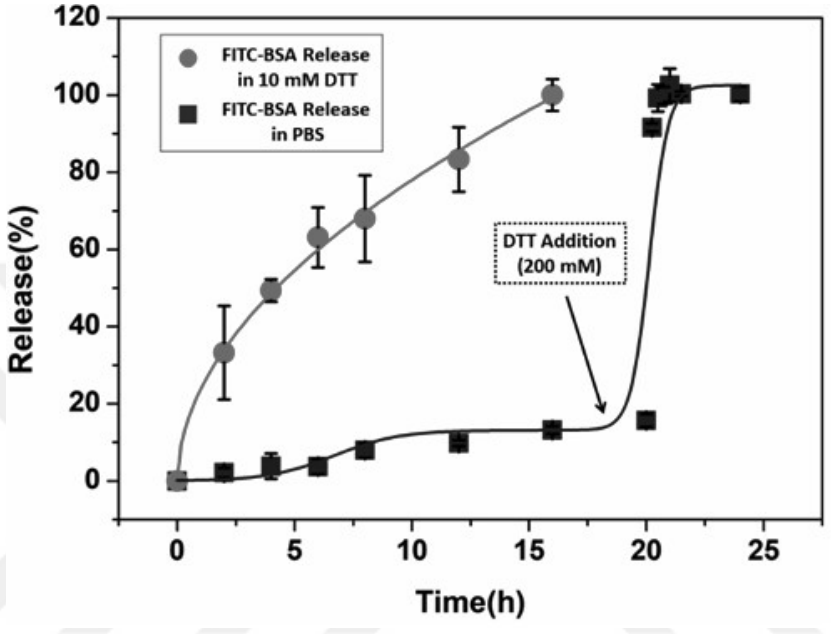

Figure 5.20. The prelease profile of FITC-labeled BSA from hydrogels in DTT and PBS solutions.

5.3.6. Cell Studies

The in vitro cytotoxicity of the HG was evaluated on a L929 fibroblast cell line using the CCK-8 cell viability assay and live/dead assay. The results CCK-8 and live/dead cell viability assays in Figures 5.21a, and b showed no significant cytotoxicity when cells were treated with varying amounts of HGs. Furthermore, to evaluate the cytotoxicity of degradation products (HG-d), an HG sample was incubated in DTT solution (10 mM) for six h at 37 °C. The cytotoxicity of the supernatant was evaluated on the L929 fibroblast cell line using the CCK-8 cell viability assay and live/dead cell viability assay in Figure 5.21c. No significant cytotoxicity was observed in either of the experiments, which suggests the benign nature of these materials.

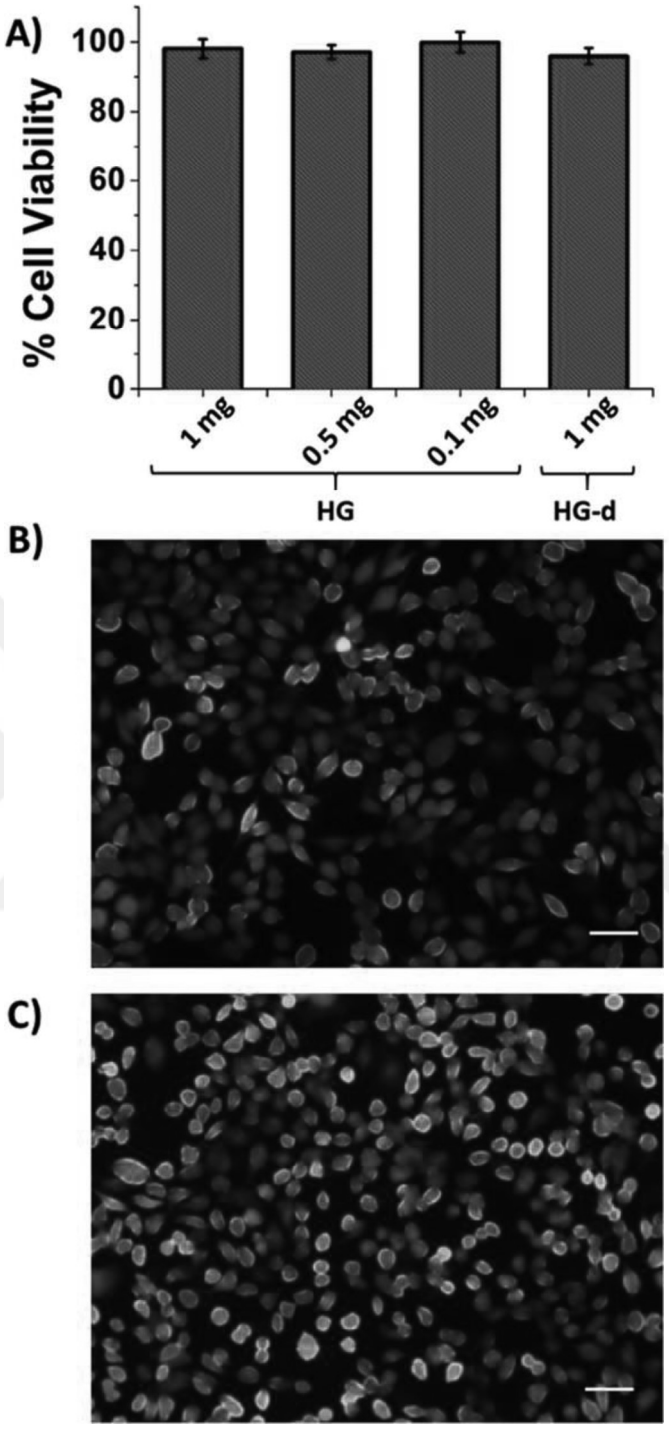

Figure 5.21. (a) Cell viability of L929 fibroblasts upon treatment with varying amounts of HGs and with the degradation product of the HG (HG-d). Fluorescence microscopy images of the live/dead cell viability assay upon treatment with the (b) HG and (c) with the degradation product of hydrogel (scale bar in images: 50 μm).

5.4. Conclusion

In conclusion, redox-responsive HGs were fabricated using tetra-arm PEG thiol and maleimide disulfide-terminated telechelic linear PEG polymers. Efficient crosslinking between these polymers was accomplished through the Michael addition reaction without the need for any additional catalyst. Fluorescent dye-labeled macromolecules and proteins could be efficiently encapsulated under mild conditions. While these macromolecules were slowly released in a nonreducing environment, exposure to a reducing milieu accelerated the process. Notably, the entire HG construct can be rapidly dissolved upon the addition of a concentrated DTT solution. One can envision that such control over the release of macromolecular agents and on-demand HG dissolution would be attractive for adapting these materials for different biomedical applications.

6. REDOX-RESPONSIVE NANOGELS FOR DRUG-DELIVERY: THIOL-MALEIMIDE AND DISULFIDE-EXCHANGE CHEMISTRY AS ORTHOGONAL TOOLS FOR FABRICATION AND DEGRADATION

6.1. Introduction

The past decades have witnessed the progressive development of responsive polymeric nanoparticles [270,271]. One of the fundamental reasons for the emergence of broad interest in nanoparticles stems from their ability to increase the bioavailability of hydrophobic drug molecules, many of which are insoluble in the aqueous biological milieu [272-274]. Additionally, utilizing these nanosized delivery agents also addresses the pharmacokinetic limitations of conventional medication, such as short circulation time and rapid systematic clearance. As alternatives between soft polymeric versus hard inorganic nanoparticles, polymer-based systems such as micelles [275], polymeric nanoparticles [276], and nanogels [277] are more prone to deformability and degradation compared to their rigid inorganic counterparts, which assists in their overcoming biological barriers to increase circulation time, escape immune cell uptake and reduce accumulation in the spleen [278-280]. In recent years, nanogels have emerged as an attractive soft nanoparticle platform for various drug delivery applications due to their high drug-loading capacity, multi-functional nature, and high stability [281-285]. Their nanoscale size offers passive tumor targeting through enhanced permeation and retention effect [286], as well as installation of appropriate targeting ligands, which offers active targeting of the disease cells [287,288]. Furthermore, employing "smart" or environmentally sensitive nanogels provides an opportunity to facilitate the release of the therapeutic agent predominantly at the disease site [289].

In general, the fabrication of nanogels can be achieved using one of the two common approaches: polymerization of monomers and crosslinking of polymer precursors. For example, in a seminal contribution, Matyjaszewski and coworkers utilized the inverse miniemulsion atom transfer radical polymerization method to fabricate redox-responsive

nanogels using direct polymerization of oligo(ethylene oxide) monomethyl ether methacrylate in the presence of a disulfide-containing dimethyl methacrylate crosslinker [290]. In the second approach, a well-defined functional polymer is used as a nanogel precursor and crosslinked after assembly as a nanosized aggregate [291]. In general, polymeric precursors are stabilized as nanosized aggregates using surfactants, followed by crosslinking [292-294]. Thayumanavan and coworkers reported a clever approach to fabricating nanogels without surfactants [103]. They utilized the thermally promoted self-assembly of copolymers composed of oligo(ethylene glycol) and pyridyl-disulfide side chains, which undergo *in situ* generated thiol-disulfide exchange upon partial reduction of the disulfide groups to thiols. The monomer and polymer-based methods continue to be extensively utilized in fabricating nanogels for various biomedical applications.

Stimuli-responsive nanogels change their physicochemical properties, such as size, hydrophobicity, and crosslinking density, under various environmental conditions [295]. Degradable linkages in the nanogels are critical in manipulating these physicochemical properties. In this regard, stimuli-responsive linkages sensitive to stimuli such as pH, temperature, and redox have been used in designing drug delivery systems [296-305]. Common degradable linkages employed are acetals [306], imines [307], hydrazones [308] , dithioketals [309], and disulfide bonds [310-318]. In recent years, redox-responsive disulfide bonds have been used for crosslinking nanogel because of their preferential degradation in cancer cells due to the high intracellular GSH concentration in the cytosol [319-321].

Reactions with high efficiency are utilized to ensure the rapid crosslinking of polymeric nanogel precursors to obtain stimuli-responsive nanogels. While many 'click' reactions have been used to fabricate stimuli-responsive nanogels [322,323], utilization of the highly efficient thiol-maleimide reaction is rare. Maleimide-thiol reaction is a highly efficient reaction used in the functionalization and crosslinking of polymers [324-330]; however, maleimide-thiol conjugation is generally not easily cleavable, apart from when using specific thiols are employed [331]. We envision integrating a disulfide linkage into the maleimide-thiol conjugation system will provide advantages for rapid maleimide-thiol conjugation and disulfide-based degradation. We recently demonstrated that the thiol-maleimide conjugation proceeded with a high level of selectivity in the presence of disulfide

linkages and utilized this selectivity to engineer fast-forming dissolvable bulk hydrogels [239]. Importantly, the thiol-maleimide conjugation proceeds with high efficiency in aqueous media without releasing any byproducts, so the approach is quite benign. We envisioned that the selective thiol-based chemistry could be exploited to fabricate redox-responsive nanogels that are amenable to non-covalent and covalent functionalization for engineering targeted drug delivery systems.

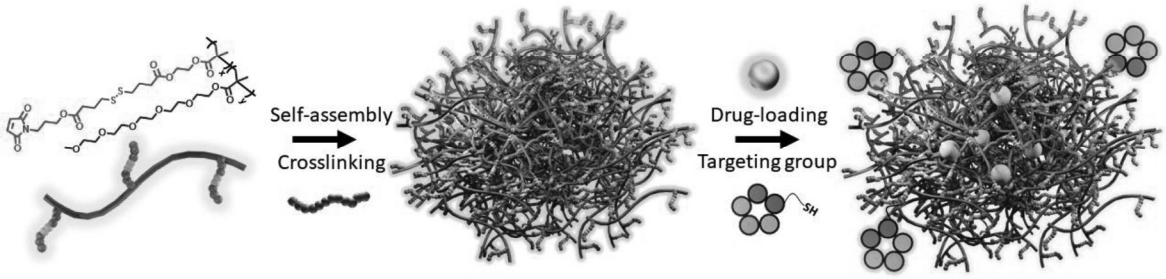

Figure 6.1. Schematic illustration of the fabrication of drug-loaded targeted nanogel.

Herein, we report the synthesis and evaluation of redox-responsive nanogels obtained using the thiol-maleimide conjugation. For this purpose, a novel disulfide-containing maleimide side chain polymer was synthesized using reversible addition-fragmentation chain transfer (RAFT) polymerization. An oligo ethylene glycol-based comonomer was used to provide aqueous solubility and undergo thermally-promoted self-assembly to yield nanoaggregates. The otherwise unstable nanoaggregates were crosslinked using a water-soluble bis-thiol crosslinker to produce stable nanogels. These nanogels could be loaded with hydrophobic dyes and drugs and conjugated with peptide-based cancer cell targeting motifs, as illustrated in Figure 6.1. Nanogels were prone to degradation under reducing environments, releasing their encapsulated cargo. Finally, a clinically used anticancer drug, docetaxel, was loaded into the targeting group appended nanogels, and their cellular internalization and toxicity were investigated.

6.2. Experimental

6.2.1. Materials

Diethyl ether was purchased from Merck. 1,4-Dithio-DL-threitol (DTT) (98%), were purchased from Alfa Aesar. Furan (>99%), maleic anhydride (99%), 3-amino-1-propanol (99%), 2-hydroxymethyl methacrylate (HEMA, 98%), 4-(dimethylamino)pyridine (DMAP, >99%), 4,4'-dithiodibutyric acid (95%), *N*,*N*′-dicyclohexylcarbodiimide (DCC), poly(ethylene glycol) methyl ether methacrylate (PEGMEMA, M_n=300), 2,2′-azobis(2-methylpropionitrile) (AIBN), 4-cyano-4-(phenylcarbonothioylthio)pentanoic acid (CTA), 2,2'-(ethylenedioxy)-diethanethiol, Nile red (NR), 1,4-dithiothreitol (DTT), docetaxel, and glutathione were purchased from Sigma-Aldrich. All solvents were purchased from Merck and used as received. The furan-protected maleimide-disulfide acid was prepared according to literature procedures [239].

6.2.2. Methods

Ultra-pure water was obtained via MilliQ Water Purification System (Merck Millipore, USA). FTIR spectroscopy measurements were done on a Thermo Scientific Nicolet 380 FTIR spectrometer. The size of nanogels was measured using a Zetasizer Nano particle analyzer (Malvern). NMR analysis was carried out using a 400 MHz Bruker spectrometer. Molecular weights of the polymers were monitored using a gel permeation chromatography using a PSS-SDV (gram linear, length/ID 8 × 300 mm, ten μm particle size) column calibrated with poly(methyl methacrylate) standards (1−175 kDa) using a refractive index detector. Dimethylacetamide with 0.05% lithium bromide was used as an eluent at a flow rate of 1.0 mL/min at 30 °C. Side products of reactions were analyzed by LC-MS analysis using an LC-MS-2020- spectroscopy (Shimadzu, Japan) equipped with a C-18, five μm, 150 × 4.6 mm column. ACN; 25.01-30 min, 50% ACN. Drug concentrations were analyzed LC-MS analysis using LC-MS-8030 mass spectroscopy (Shimadzu, Japan), which contains a C-18, 2.7 μm, 100 × 3 mm column. Transmittance measurements were carried out using a UV-vis spectrophotometer (Varian Cary Eclipse, Agilent, USA). Nile Red

concentrations were quantified using a fluorescence spectrophotometer (Varian Cary Eclipse, Agilent, USA). During the internalization experiments, cells were visualized using Zeiss Axio Observer inverted fluorescence microscope (Carl Zeiss Canada Ltd., Canada). The dry nano-constructs were visualized on a holey carbon film-coated 300 mesh Cu-grid (Pacific Grid Tech, USA) using an LVEM5 electron microscope on transmission electron microscopy (TEM) mode (Delong Instruments, USA).

6.2.3. Cell Lines

MDA-MB-231 was purchased from ATCC (LGC Standards, Germany) and grown according to the cell culture methods requirements of the manufacturer. Cells were kept in the logarithmic phase of cell growth for the duration of experiments and incubated in a humidified atmosphere of 5% CO2 at 37 °C. Cytotoxicity experiments were done with a plate reader (Multiscan FC, Thermo Scientific, USA), and Cell Counting Kit8 (CCK-8, Fluka) was obtained from Sigma-Aldrich.

6.2.4. Synthesis of Masked Maleimide-Disulfide-Containing Monomer (FMDSMA)

Masked maleimide-disulfide acid (0.854 g 0.002 mol), HEMA (1.00 g, 0.007 mol), and DMAP (0.565 g, 0.004 mol) were added to a round bottom flask and dissolved in anhydrous CH_2Cl_2 (1.5 mL). DCC (0.397 g, 0.002 mol) was dissolved in another flask in anhydrous CH_2Cl_2 (1 mL). The DCC solution was slowly added to the first flask at 0 °C. The reaction mixture was stirred at room temperature for 24 hours. Cold CH_2Cl_2 (25 mL) was then added to the reaction mixture and precipitated dicyclohexylurea was removed by filtration. The concentrated solution was purified using a SiO_2 column on, using EtOAc and CH_2Cl_2 (1:1) as eluents yielding 0.9 g product (82 % yield). ^{1}H NMR ($CDCl_3$, δ, ppm), 6.51 (s, 2H, C*H*=C*H*), 6.12 (s, 1H, CH_2=C), 5.60 (s, 1H CH_2=C), 5.26 (s, 2H, bridgehead protons), 4.34 (s, 4H, C(O)OCH_2CH_2O(O)C), 4.04 (t, 2H, C(O)OCH_2CH$_2$), 3.57 (t, 2H, NCH_2CH$_2$), 2.84 (s, 2H, bridge protons), 2.72 (t, 4H, SCH_2CH$_2$), 2.44 (t, 4H, C(O)CH_2CH$_2$), 2.03 (m, 4H, SCH$_2$CH_2CH$_2$), 1.94 (m, 2H, NCH$_2$CH_2CH$_2$), 1.53 (s, 3H, CCH_3). ^{13}C NMR ($CDCl_3$, δ, ppm), 176.20, 172.80, 172.71, 167.12, 136.54, 135.92, 126.13, 80.96, 62.38, 62.16, 61.37, 47.42, 37.77, 37.68, 35.75, 32.50, 32.42, 26.67, 24.14, 24.10, 18.30.

6.2.5. Synthesis of Masked Maleimide-Disulfide-Containing Copolymer

PEGMEMA (0.500 g, 1.60 mmol), FMDSMA (0.185 g, 0.3 mmol), AIBN (1.02 mg, 0.006 mmol), and CTA (0.015 g, 0.050 mmol) were added to a round bottom flask and dissolved in DMF (1.5 mL). The solution was purged with N_2 for 45 minutes. The reaction vessel was immersed in a preheated oil bath at 70 °C. After 24 hours, the solution was concentrated on a rotary evaporator, and the residue was precipitated in cold ether. The precipitated polymer was then collected and dried under a high vacuum affording 0.700 g product (73% yield). $M_{n,theo}$ = 12800 g/mol, $M_{n,GPC}$ = 10 800 g/mol M_w/Mn = 1.20. ^{1}H NMR (CDCl3, δ, ppm), 6.51 (s, C*H*=C*H*), 5.25 (s, CH bridgehead protons), 4.26 (s, C(O)OCH_2CH_2OC(O)), 4.08 (t, (O)COCH_2CH_2), 3.60 (m, OCH_2CH_2O), 3.38 (s, 3H, CCH_3), 2.85 (s, bridge protons), 2.73 (t, SCH_2CH_2), 2.47 (t, 4H, C(O)CH_2CH_2). Retro Diels-Alder reaction was carried out by dissolving the product (0.7 g) in anhydrous toluene (25 mL), and the solution was heated to reflux for 8 hours. The solution was then concentrated, and the residue precipitated in cold ether and dried under a high vacuum to yield 0.650 g of product (92% yield). ^{1}H NMR ($CDCl_3$, δ, ppm), 6.72 (s, C*H*=C*H*), 4.26 (s, C(O)OCH_2CH_2O(O)C), 4.08 (t, C(O)OCH_2CH_2), 3.60 (m, OCH_2CH_2O), 3.38 (s, CH_3C), 2.73 (t, SCH_2CH_2), 2.47 (t, C(O)CH_2CH_2).

6.2.6. Orthogonality of the Thiol-Disulfide Exchange and Thiol-Maleimide Reaction

For an equivalent amount of thiol and maleimide reaction, copolymer (10 mg, 0.0007 mmol) and 2-mercapto-ethanol (0.78 mg, 0.0042 mmol) were reacted in PBS (0.10 mL) in a thermal shaker with a constant shake (100 rpm) for 30 minutes at 37 °C. The solution was freeze-dried, and the polymer was redissolved in CH_2Cl_2 (0.2 μL) and precipitated in diethyl ether (1.5 mL). The solution was centrifuged at 13000 rpm for five minutes, and the supernatant was separated. The polymer part was analyzed using a ^{1}H NMR spectroscopy. The supernatant was redissolved in CH_2Cl_2 (0.50 mL) and filtered through a silica oxide plug using methanol as eluent. The filtered solution was then evaporated, redissolved in acetonitrile, and analyzed using LC-MS. The same procedure was applied to the control experiment, where four equivalents of thiol were used.

6.2.7. Determination of LCST of Copolymer

LCST of copolymer solution (0.1 M PBS) was determined by measuring the transmittance values of polymer solution between 20 and 80 °C via UV-vis spectrophotometer. The size of polymeric particles at room temperature (25 °C) and above LCST (60 °C) was measured by Dynamic Light Scattering (DLS).

6.2.8. Preparation of Nanogels

For nanogel preparation, nanoaggregates were first prepared by dissolving the copolymer (5 mg, 0.357 mmol) in PBS (1 mL, 0.1 M) at 60 °C. After ten minutes at 60 °C, 2,2'-(ethylenedioxy)-diethanethiol as crosslinker (0.072 mg, 0.396 mmol) was added to the solution, and the reaction was stirred for 30 minutes at 60 °C affording 4.80 mg nanogel (96 % yield).

6.2.9. Loading and Release of NR

For Nile Red (NR) loading, NR was dissolved in acetone (37 µg/mL), and this solution (1 mL) was added to the NG solution (1 mL, 5 mg/mL). After mixing the polymer and NR solution, acetone was allowed to evaporate slowly at 25 °C for 24 hours. The solution was filtered through filters (0.45 µm pore size) to remove excess insoluble NR. The amount of loaded-NR was calculated as follows; nanogels were first incubated in DTT solution (0.20 M) for one hour. The solution was then freeze-dried and redissolved in DMSO. The fluorescence signal at 623 nm was measured using a spectrometer, and the content was quantified employing an NR calibration curve. To visualize the degradation of NGs, DTT (0.20 M) was added to an NR-loaded NG solution. Digital photographs of this solution under UV light were taken before and after ten minutes of DTT addition. NR release from NG was also monitored by incubating them in reductive (0.01 M GSH) and non-reductive environments. The released amount was quantified at different time points using a fluorescence spectrophotometer.

6.2.10. Conjugation of cRGDfC to Nanogels

To the nanogel solution (1 mL, 5 mg/mL) in PBS, cRGDfC (250 µg, 0.430 µmol) was added, and the mixture was stirred for 24 hours at room temperature. Unreacted peptides were removed using a dialysis bag (cutoff:12 kDa). After purification of the nanogels, 100 µL of the nanogel solution was used against the BCA working reagent (2 mL) for the determination of conjugated peptide. The blue mixture was incubated for 30 minutes at 60 °C. After 30 minutes, the blue color mixture turned purple, and its absorbance was measured at 562 nm via UV spectroscopy.

6.2.11. Loading and Release of DTX

To calculate the DTX loading, NG solution (0.1 mL, 5 mg/mL) was diluted with PBS solution (0.9 mL, 0.1 M). DTX (0.25 mg) was then dissolved in acetone (1.0 mL). DTX solution (1.0 mL, 0.25 mg/mL) was then added to the NG solution. Acetone in the final solution was allowed to evaporate at 25 °C for 24 hours slowly. Unloaded-DTX was removed by filtration method (0.45 µm pore size). The DTX content was calculated after treating the NG solution with DTT (0.20 M) for one hour. The final solution was diluted with CH_3CN (1:1) and analyzed using LC-MSMS, and DTX content was calculated as 28 (±2) wt %. For DTX release studies, DTX-loaded NG solution (1 mL, 5mg/mL) was put in a dialysis bag (Cutoff: 3.5 kDa), and release was started in 40 mL PBS and 40 mL GSH solution (10 mM) in a thermal shaker with a constant shake (100 rpm) at 37 °C. Samples (1 mL) were taken, and the new solution was added at every time point; samples were analyzed using LC-MSMS.

6.2.12. Cell Experiments

Cytotoxicity of the nanogels was investigated via CCK-8 viability assay on MDA-MB-231 cancer cells. Cells (6000 cells/well) were seeded on a 96-well plate in quadruplicate with a culture medium (100 µL) and incubated for 24 hours at 37 °C for cell growth and adhesion. After incubation, one part of the cells was treated with GSH solution (5 mM) for one hour at 37 °C. After one hour, the GSH solution was removed and washed three times

with a cell medium. Cells were then treated with cellular media containing different concentrations of free drug, empty NG, drug-loaded NG, and drug-loaded and cRGDfC-conjugated nanogels. For free drug treatment, DTX (10^{-4} M) was dissolved in culture media containing DMSO (2.5 %), then serial dilutions were made from stock solution (10^{-4} M) using cell media; in that way, DMSO concentration in each well was kept below 0.5% (v/v). For control, an empty NG solution in cell media (1 mL, 0.4 mg/mL) was prepared and diluted with fresh cell media to add to wells. For drug-loaded nanogels, nanogels with different DTX concentrations (10^{-6}-10^{-11} M) were prepared. cRGDfC-conjugated nanogels solution (0.4 mg/mL) with varying concentrations of DTX was prepared in cell media and added to cells treated with GSH and without GSH. The plate was kept with the corresponding solutions for 48 hours. For the pulse-chase experiment, the same sample preparation and procedure were used; however, cells containing drug solutions were replaced with fresh media after four hours. After 20 h, CCK-8 solution was added to each well to culture for four hours. After incubation with CCK-8, the absorbance values at 450 nm were measured via a microplate reader. Results were obtained by GraphPad prism software using nonlinear regression mode.

6.2.13. Internalization Experiments

For the cellular internalization experiment, MDA-MB-231 adenocarcinoma cells (150 000 cells/well) were seeded in a 12-well plate as duplicates in culture media (1 mL). The cells were incubated at 37 °C for 24 hours. Cells were then incubated with nonconjugated nanogels, cRGDfC-conjugated, free cRGDfV (10 µg/mL) containing cRGDfC-conjugated NG that containing the same amount of Nile Red dye (5.16×10^{-4} mmol) at 37 °C for a related time. After several time points (3, 6, and 24 h), cellular media were removed and washed two times with PBS (500 µL), and 4% of formaldehyde solution (300 µL) was added to wells at 37 °C for 10 minutes. After removing the solution and washing process, DAPI (300 µL) containing PBS was added to wells for 15 minutes at room temperature for nuclei staining. After washing cells with PBS, cell images were obtained using a Zeiss Observer Z1 fluorescence microscope. For the flow cytometry experiment, MDA-MB-231 adenocarcinoma cells (200 000 cells/well) were seeded into a 12-well plate as duplicates in culture media (1 mL) and incubated at 37 °C for 24 hours. The properties of the sample were the same as those used in the cellular internalization experiment. After 24 hours, cell media

was removed, and the cells were trypsinized with 0.05% trypsin solution for two minutes at 37 °C. After two minutes, culture media (700 μL) was added to wells, and Nile Red intensities were determined by flow cytometry (Guava easyCyte).

6.3. Results and Discussion

6.3.1. Synthesis of Masked Maleimide-Disulfide-Containing Monomer

Due to our interest in making redox-responsive crosslinked nanoparticles, furan-protected maleimide and disulfide-bearing monomers were utilized as functional and degradable blocks in polymers. As monomer precursors, masked maleimide-disulfide acid was prepared according to the previously reported protocol.[239] An esterification reaction was used for coupling masked maleimide-disulfide acid with 2-hydroxyethyl methacrylate to produce FMDSMA, as drawn in Figure 6.2a. The synthesized monomer's composition was deduced from the ^{13}C NMR spectrum shown in Figure 6.3, where the carbon resonance at 172.80 ppm and 172.71 ppm belonging to carbonyl carbons of the ester groups and at 167.12 ppm for the carbonyl in the methacrylate group corroborated the structure. ^{1}H NMR spectrum in Figure 6.2b also confirmed the structure; the proton resonances at 5.60 and 6.12 ppm belonging to a methacrylic double bond, and at 6.51 and 5.26 ppm belonging to protons on the bicyclic moiety confirmed the structure. . As expected, the carbonyl bond stretches around 1700 cm-1 were present in the FTIR spectrum as seen in Figure 6.4.

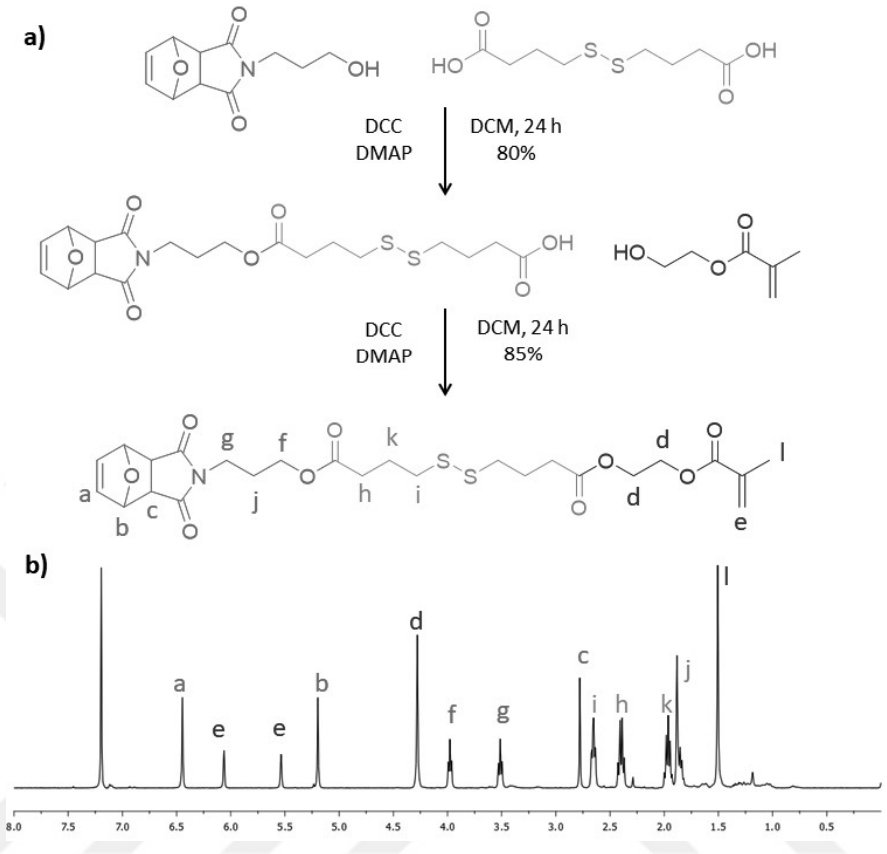

Figure 6.2. (a) Synthetic pathway and (b) ^{1}H NMR spectrum of the masked maleimide-disulfide-containing monomer.

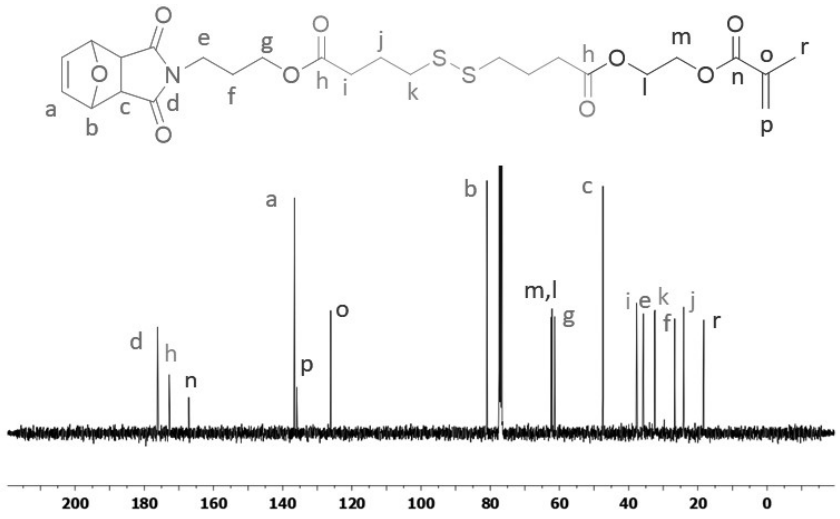

Figure 6.3. ^{13}C NMR spectrum of the masked maleimide-disulfide-containing monomer.

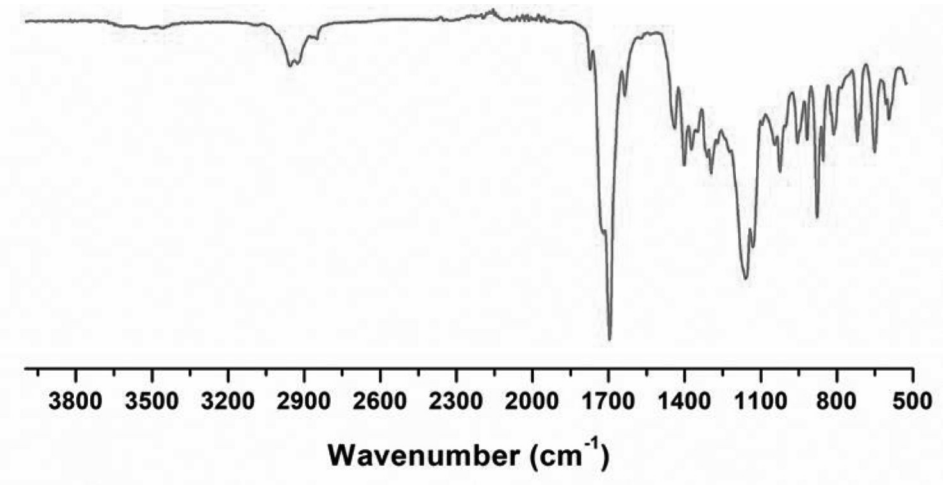

Figure 6.4. FTIR spectra of masked maleimide-disulfide-containing monomer.

6.3.2. Synthesis of the Redox-Responsive Copolymer

A copolymer of FMDSMA and PEGMEMA as a building block of nanogels was synthesized using RAFT polymerization to yield well-defined polymers, as drawn in Figure 6.7a. A polymer that would contain enough functionality for crosslinking and functionalization yet be water-soluble was targeted using an FMDSMA: PEGMEMA ratio of 1:5. The experimental monomer ratio in the copolymer was calculated to be 1:6 from its ^{1}H NMR spectrum in Figure 6.5, and the number average molecular weight was deduced to be 10 800 gmol^{-1} with 1.2 PDI using size exclusion chromatography (SEC), as seen in Figure 6.6. The furan-protected maleimide moieties were unmasked via retro Diels-Alder reaction by refluxing polymer solution in toluene. The formation of maleimide groups was confirmed using ^{1}H NMR spectrum in Figure 6.7b; the appearance of vinylic proton resonance at 6.7 ppm and the disappearance of protons at 6.5 and 5.2 ppm proves the presence of a maleimide ring.

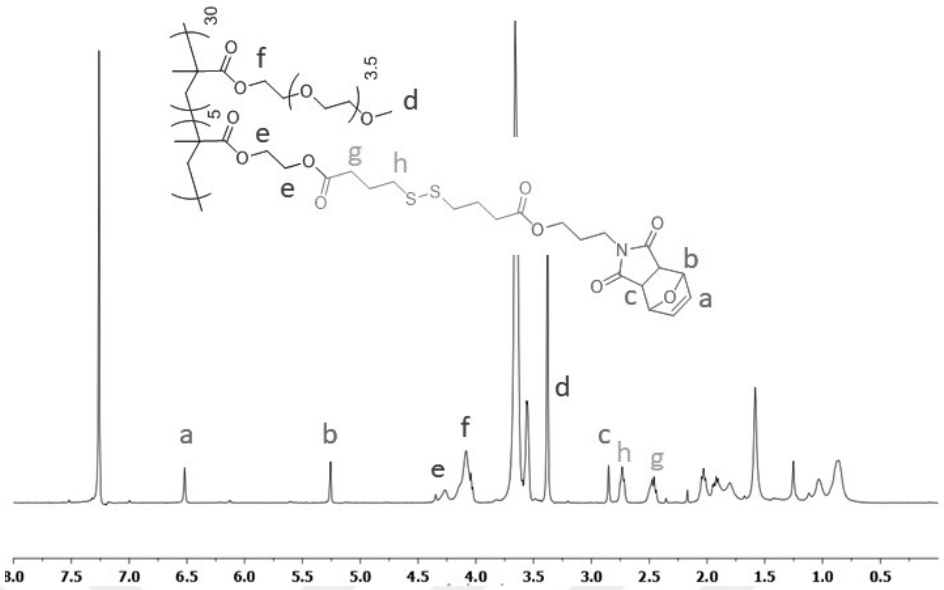

Figure 6.5. ^{1}H NMR spectrum of the redox-responsive polymer.

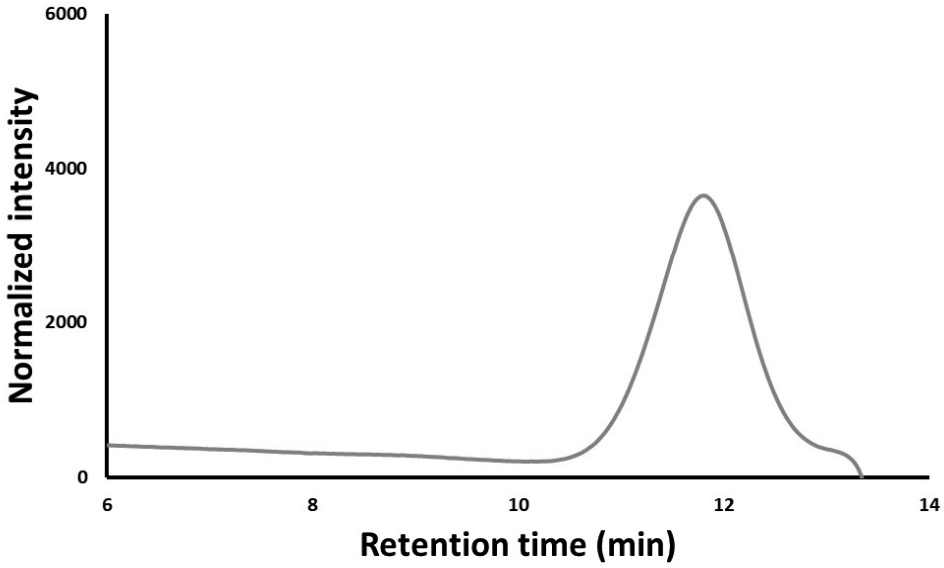

Figure 6.6. SEC chromatographs of the redox-responsive copolymer.

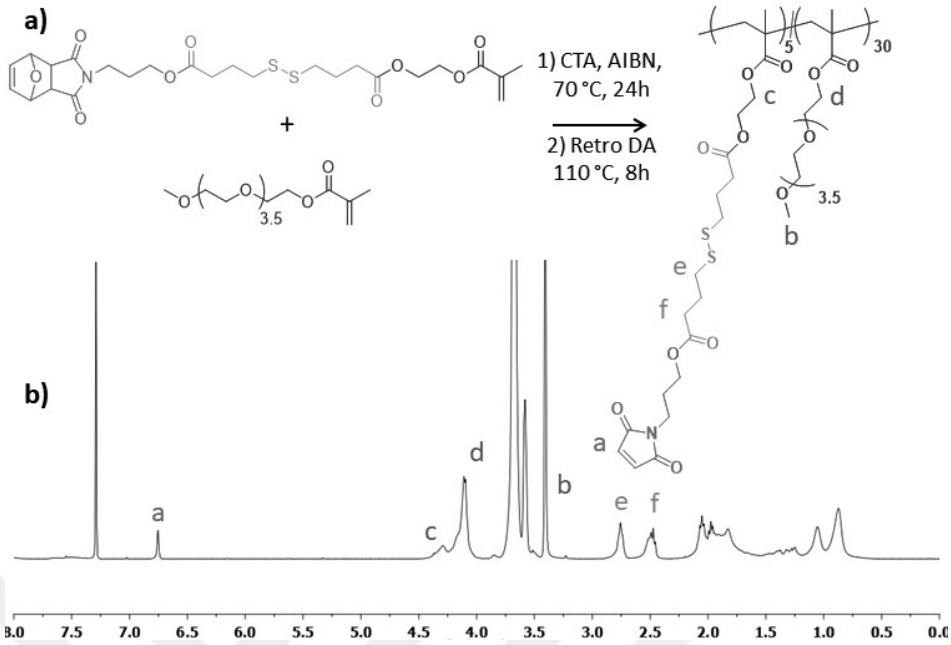

Figure 6.7. (a) Synthesis, and (b) ^{1}H NMR of the copolymer.

6.3.3. The Selectivity of Thiol-Maleimide reaction Over Thiol-Disulfide Exchange Reaction

For well-defined crosslinking, it is crucial to explore the reactivity of free thiol moieties of the crosslinker against maleimide moieties and disulfide bonds on the polymer. Our previous study[239] showed that thiol moieties selectively undergo a Michael addition reaction with maleimide groups on the side chains instead of a thiol-exchange reaction with disulfide groups. In this study, reactivities of the copolymer were also investigated; maleimide and disulfide-containing polymer were reacted with the stoichiometric equivalent of 2-mercaptoethanol. ^{1}H NMR analysis of the final product shows that the vinylic proton resonance of the maleimide ring at 6.72 ppm disappeared and reappeared at 3.87 ppm, which proves the thiol-maleimide reaction, as seen in Figure 6.8. Furthermore, the supernatant of the reaction above was analyzed using LC-MS for possible side products that may form through the thiol-disulfide exchange reaction. The reaction between copolymer and the stoichiometric equivalent of 2-mercaptoethanol did not contain any significant amount of side-product, which may be formed due to the thiol-disulfide exchange reaction, as seen in Figure A.2a. On the other hand, Figure A.2b showed that the reaction between copolymer

and four equivalent of 2-mercaptoethanol led to several side products, proving that thiols first react with maleimide and then disulfide bonds.

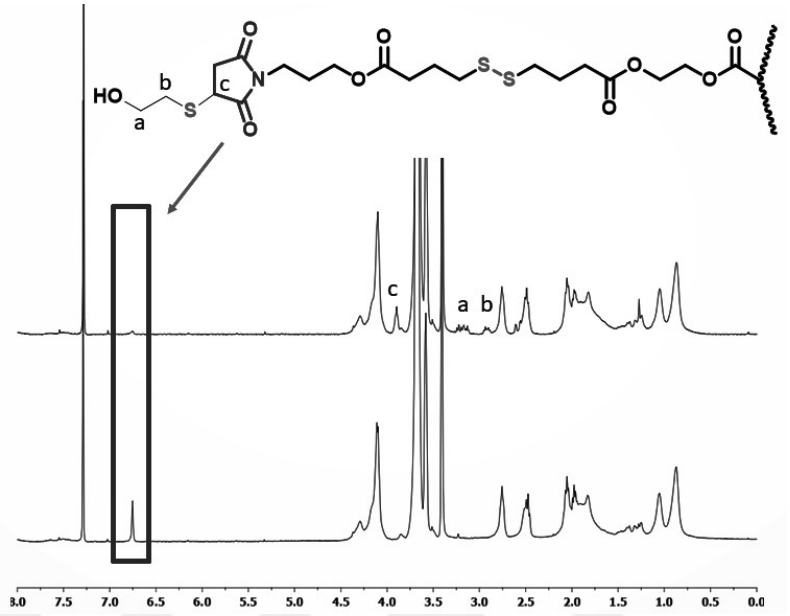

Figure 6.8. ^{1}H NMR spectrum of the polymer after and before treated with 2-mercaptoethanol.

6.3.4. Fabrication of Redox-Responsive NGs

It is well-established that polymers containing oligo ethylene side chains demonstrate a thermoresponsive behavior and can self-assemble to yield nanoaggregates in an aqueous solution above their lower critical solution temperature (LCST). Due to our interest in the fabrication of nanoaggregates, the LCST behavior of copolymers was studied. Clear polymer solution at 25 °C and cloudy polymer solution above 60 °C in Figure 6.9a indicated that copolymer reversibly undergoes self-assembly to nanoaggregates. Figure 6.9b showed the DLS measurement that also confirmed that polymeric nanoaggregates were formed with an average 86 nm diameter at 60 °C. **T**he nanoaggregates were crosslinked with this ratio at 60 °C upon adding a small bis-thiol molecule, 2,2'-(ethylenedioxy)-diethanethiol into the solution. At this point, it was essential to investigate the degree of crosslinking to obtain stable but degradable nanogels. The optimum crosslinking ratio for maleimide to thiol was determined as 37%, which afforded stable hydrogels which could be degraded in a reducing

environment. The hydrodynamic diameter of the crosslinked particles was determined as 18 nm using TEM image in Figure 6.9c and 67 nm diameter using DLS measurement in Figure 6.9d at 25 °C. The smaller size was obtained using TEM as compared to DLS measurements, presumably due to the dry dehydrated state of nanogels during the TEM measurements. Figure 6.10 showed that Ellman's analysis of obtained nanogels confirmed that only 2% of free thiol moieties remained unreacted.

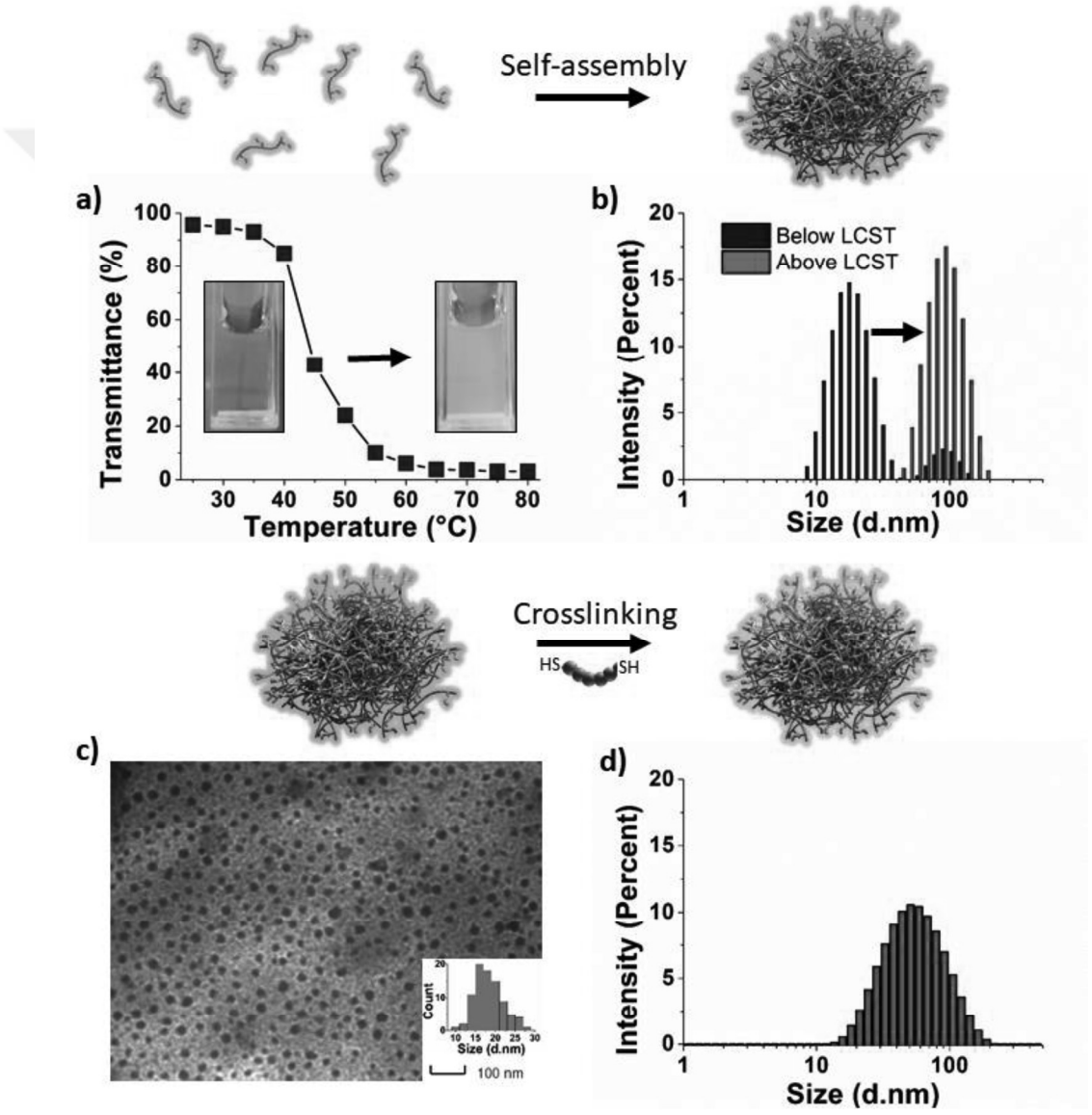

Figure 6.9. (a) Change in % transmittance of copolymer solution with temperature change, (b) hydrodynamic size as determined by DLS analysis of copolymer solution at 25 and 60 °C, (c) TEM image, and (d) DLS analysis of NG.

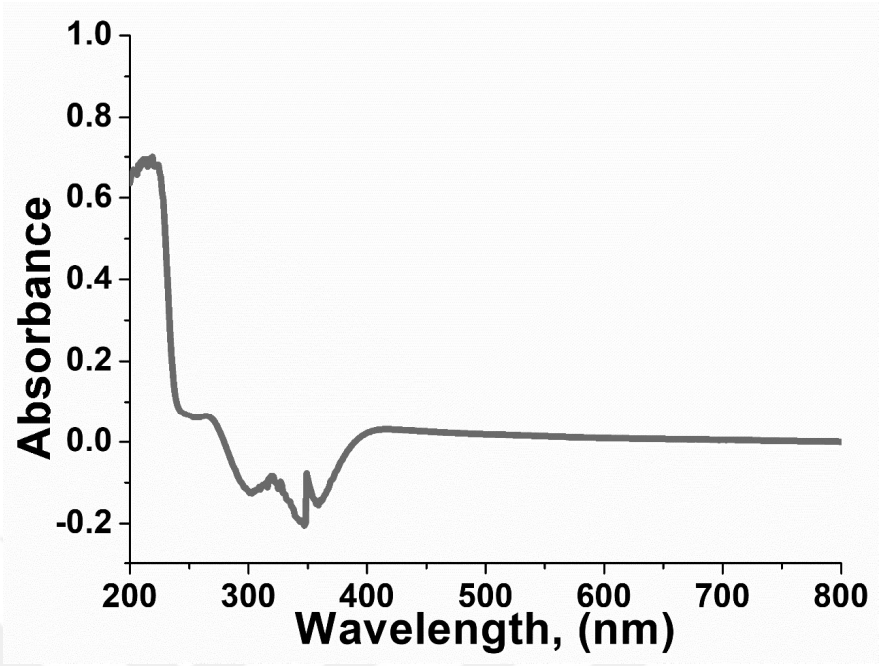

Figure 6.10. UV-vis spectra of Ellman's reagent solution incubated with nanogel.

6.3.5. NR-Loading and Redox-Responsive NR Release From Nanogels

Due to our interest in hydrophobic drug delivery, nanogels were loaded with dye molecule NR. Loading of water-insoluble NR is carried out by the co-solvent (acetone) evaporation method (0.1 wt %). The degradability of nanogels in a reducing environment was evaluated with NR-loaded nanogels (NR@NG). Under UV light, NR@NG gave a nice pink color, but the color disappeared when nanogels were incubated in DTT solution (0.20 M) for ten minutes due to the release of water-insoluble molecule NR upon NG degradation under a reducing environment, as seen in Figure 6.11a. To evaluate NR release under milder conditions for a period of time, the fluorescence intensity of NR-loaded nanogels was monitored for five days. While there was no significant fluorescence intensity change in PBS solution, as seen in Figure 6.11b, Figure 6.11c showed that it dramatically decreased in GSH solutions (0.010 M), indicating that nanogels were degrading and releasing their water-insoluble cargo DLS measurements also indicated that NGs started to disintegrate in GSH solution (10 mM) after four hours at 37 °C, while remained stable in PBS solution during the same time as seen in Figure 6.11d and e.

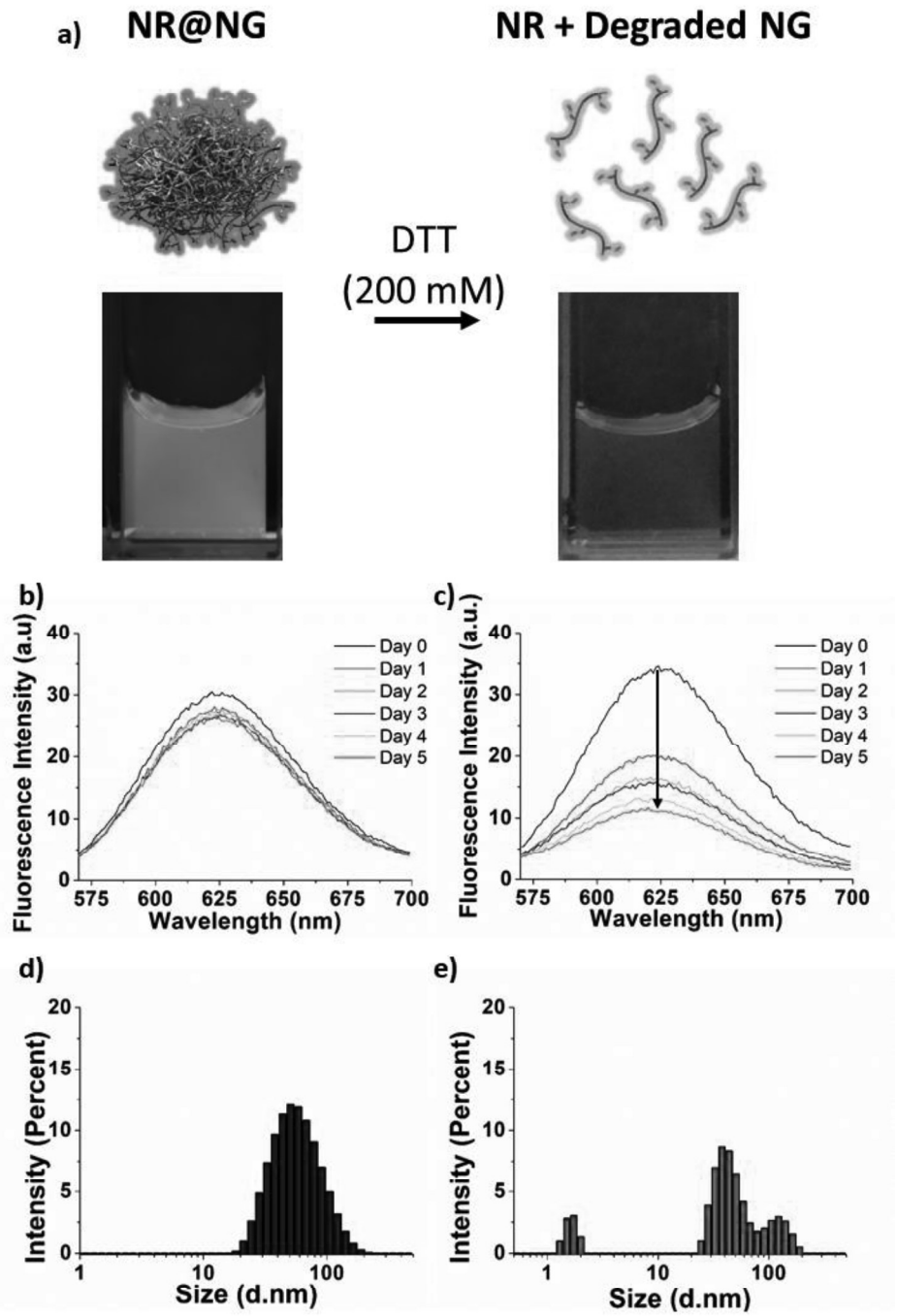

Figure 6.11. (a) Schematic representation of degradation and visual images of redox-responsive degradation of hydrophobic dye NR-containing nanogels under UV light. Fluorescence intensity of NR-containing nanogel solutions incubated in (b) PBS and (c) 10 mM GSH solution for five days. Stability of nanogels after 4 hours in (d) PBS and (e) GSH solution (10 mM).

6.3.6. DTX Release, Cytotoxicity, and Cell Uptake

DTX-loaded NGs were prepared by the co-solvent (acetone) evaporation method. The DTX loading was calculated after degrading NGs in DTT solution (0.20 M) and determined by the weight percentage ratio of the encapsulated drug to polymer amount and found to be 36 (±2) wt %. Next, we monitored the DTX release profile of NG at pH in neutral (pH 7.4, PBS), acidic (pH 5.5), reductive (0.01 M GSH), and acidic-reductive environments (pH 5.5, 0.01 M GSH). As shown in Figure 6.12a, there is a significant difference in releases between neutral and reductive environments. It was hypothesized that NGs lose their structural integrity in GSH solution (0.010 M) and start to release their cargo. As a comparison, DTX release from NGs at pH 7.4 plateaus at 11% after 2 hours. Additionally, the pH of the environment plays a critical role in the release of DTX; an acidic environment (pH 5.5) boosts the release compared to the release in 10 mM GSH alone.

The antitumor efficacy of DTX-loaded NGs was assesed using human breast carcinoma MDA-MB-231 cells. Due to our interest in active targeting and redox-respoonsive degradation of NG, a cell viability test was performed with free DTX, NG-DTX, cRGDfC-NG-DTX, and cRGDfC-NG-DTX+GSH. For the latter, MDB-MB-231 cells were previously treated with GSH to reach efficient intracellular GSH concentration. Results showed that the EC50 value of cRGDfC-NG-DTX is higher than NG-DTX, indicating that the targeting ability of NG improved the drug uptake by the cancer cells. In particular, the cRGDfC-NG-DTX+GSH showed remarkable cytotocix efficacy on MDB-MB-231 cells when GSH was present in the intracellular environment, as shown in Figure 6.12b. These results demonstrated that NG degradation and targeting ability were vital for advanced drug delivery of NGs. The in vitro cellular internalization of cRGDfC conjugated NG loaded with fluorescent dye NR was also assessed with MDA-MB-231 cells. Cells were treated with an equivalent amount of NR-containing NG, cRGDfC-NG, and cRGDfV + cRGDfC-NG for 6 hours, where cRGDfV peptide which has higher affinity for the integrin receptors was introduced as a competitive inhibitor, to establish that the enhanced uptake was due to receptor-mediated internalization. Figure 6.13a showed that NR-loaded NGs were gradually internalized by the MDA-MB-231 cells as suggested by the increase in red fluorescence**.** The presence of cRGDfC on the surface of the NG (cRGDfC-NG) increased the NR

internalization compared to NG without cRGDfC (NG) motif. Addition of the competitive integrin targeting peptide cRGDfV resulted in lower NR internalization as indicated by fluorescence microscopy. The uptake of cRGDfC-NG was also investigated and quantified using flow cytometry. The mean fluorescence intensity values of MDA-MB-231 cells treated with NR-loaded cRGDfC-NG compared NG (non-targeted) showed that the targeting-group bearing nanogels were preferentially internalized as seen in Figure 6.13b.

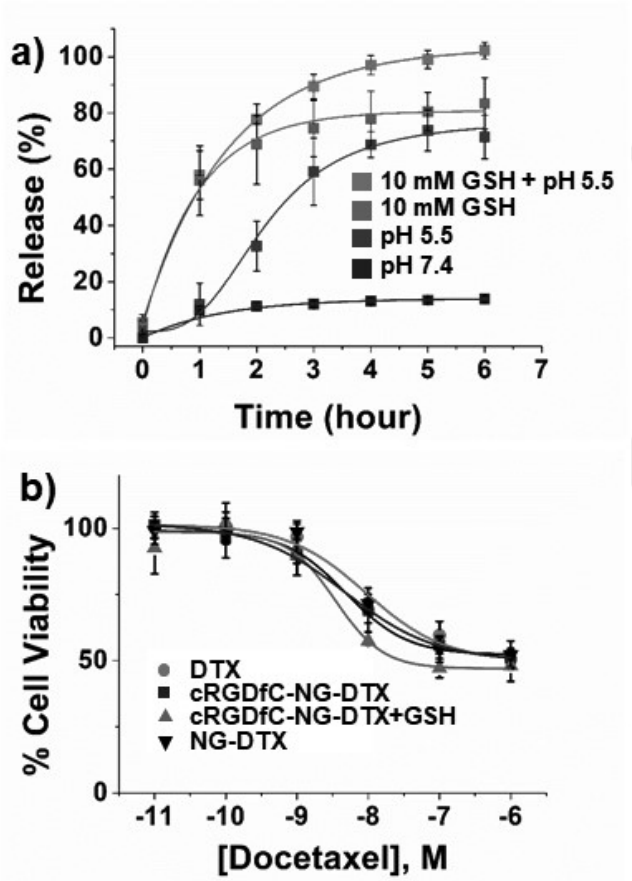

DTX	cRGDfC-NG-DTX	cRGDfC-NG-DTX+GSH	NG-DTX
5.696×10^{-9}	5.423×10^{-9}	3.221×10^{-9}	7.774×10^{-9}

Figure 6.12. (a) DTX release in a reductive and non-reductive environment for 24 hours at 37 °C, (b) Cell viabilities of MDA-MB-231 tumor cells treated with the DTX, cRGDfC-NG-DTX, cRGDfC-NG-DTX+GSH, and NG-DTX.

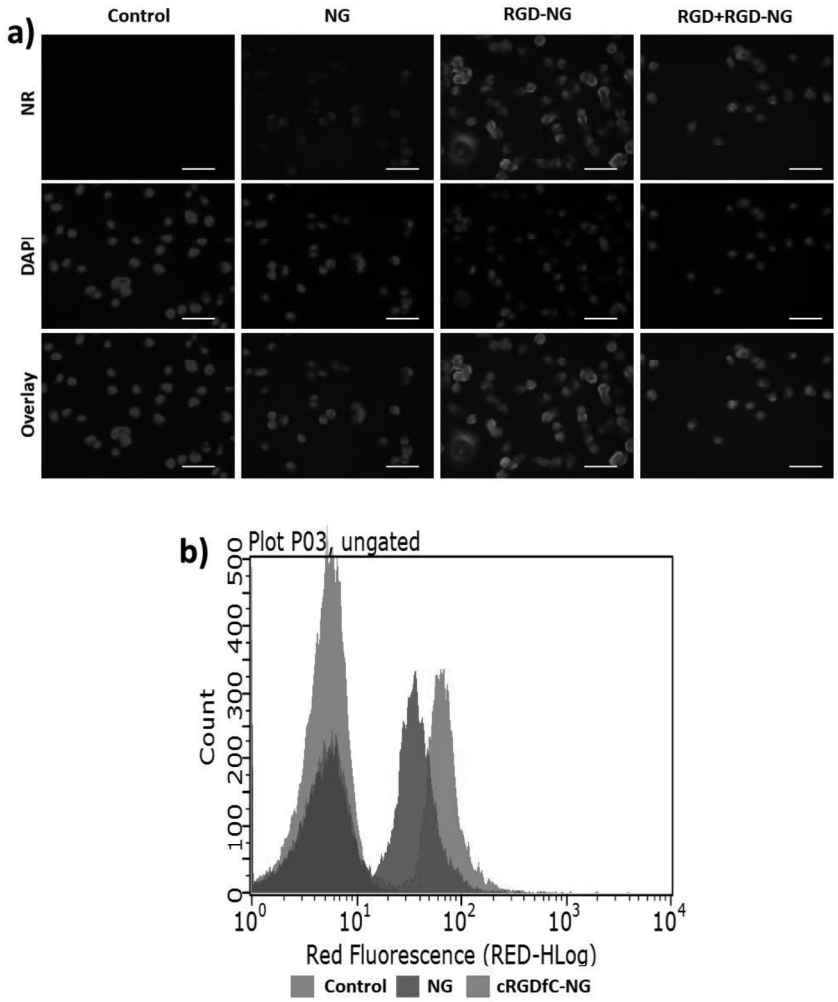

Figure 6.13. (a) NR-internalization of NG, RGD-NG, and RGD+RGD-NG into MDA-MB-231 cells after six hours. NR provides a red fluorescent signal, whereas the cell nuclei are blue due to DAPI staining (Scale bar 50 μm). (b) Overlapping histograms of the control, NG, and cRGDfC-NG treatment.

6.4. Conclusion

In summary, a redox-responsive nanogel system for application in targeted drug delivery was fabricated using the reactivity differences between the thiol-maleimide and disulfide-thiol exchange chemistry. A new monomer containing a disulfide linkage and a masked maleimide group was designed for this purpose. Copolymers of this unique

monomer with oligo(ethylene glycol)-based monomers furnish a thermoresponsive polymer that yields nano-sized aggregates upon heating in aqueous media. The difference in the reactivity of the disulfide and maleimide groups towards thiols enables crosslinking of aggregates using bis-thiol-based crosslinkers. Some of the residual maleimide groups in the nanogels are functionalized by the peptide-targeting ligand cRGDfC through a thiol-maleimide addition reaction. Nanogels could be loaded with hydrophobic dyes and drugs, and a redox-responsive release was observed under a reducing environment. Preferential cellular internalization and enhanced cytotoxicity against MDA-MB-231 were observed for the targeting group constructs. Overall, the robust fabrication of these redox-responsive and functionalizable nanogels offers a reliable targeted drug delivery platform that is versatile enough to be evaluated for the treatment of various cancers by loading and conjugating appropriate drugs and targeting moieties.

7. COMBINATION OF COVALENT AND NON-COVALENT DRUG-LOADING ON pH-RESPONSIVE MICELLAR STRUCTURE FOR TARGETED DRUG-DELIVERY

7.1. Introduction

Over the past few decades, the vital problems of conventional cancer medications, such as systematic toxicity, rapid clearance, poor solubility, and lack of selectivity, have been trying to overcome [332]. Incorporating polymeric structures into the chemotherapeutic agents significantly improved the therapeutic efficacy of drugs by increasing solubility and circulation time and minimizing undesired toxicity [333-335]. These enhancements allow administering a high quantity of toxic drugs bypassing the maximum tolerated dose to combat overspread tumors. Polymeric nanoparticles offer even more advantages, such as targeting ability [336-338] and stimuli-responsive control [339-341] over drug release to improve the selective delivery of highly toxic chemotherapeutic agents.

Polymeric micelles have been studied extensively in drug delivery applications for cancer therapy because they improve chemotherapeutic agents' solubility and circulation time in blood and have a high loading capacity [342-344]. Equally important, the micelles' passive targeting ability through enhanced permeability and retention (EPR) effect due to their nano-scale size also provides selective delivery to tumor tissue [345-347]. Additionally, the versatility of the polymer structures used in micelle synthesis brings functionality opportunities that have been widely used in conjugating targeting groups for enhanced accumulation into cancer cells [348-351].

The majority of the studies now focus on the non-covalent loading of the chemotherapeutic agents [4,352], and only a few have explored the covalent conjugation of drug molecules [124,353]. Non-covalent loading of cancer drugs is relatively easier to prepare; poor water-soluble drugs tend to escape in the hydrophobic core of the micelle. However, the control over the release of physically loaded drugs is generally limited. Higher

control over drug release can be obtained with covalent conjugation of a drug, in which it is attached to polymer backbones through stimuli-responsive bonds. The polymeric precursor for making micelle is mostly diblock, where the hydrophobic block gets together in the core. The hydrophobic block can be designed to play a role beyond gaining hydrophobicity. Since most anticancer drugs are hydrophobic, one can utilize a hydrophobic drug-based monomer that constructs the hydrophobic block of the copolymer. The activation of conjugated drug molecules relies on a cleavable bond between drug molecules and the polymer backbone. The cleavable bonds are generally chosen among stimuli-responsive bonds triggered by pH [354,355], redox, temperature [356], and enzyme [357] for a controlled drug profile. Furthermore, designing the drug-based hydrophobic block to be responsive to endogenous stimuli will enable the disintegration of the micellar structure due to disturbance of the hydrophobicity/hydrophilicity balance. This stabilization of the micellar system will also be accompanied by drug releases. The drug release system can be further elaborated through non-covalent encapsulation of the additional drug at the core of the micelle structure obtained using a drug-conjugated copolymer. This strategy allows for delivering a combination of medications at the same site simultaneously. Furthermore, the conjugation of different drugs through a covalent and non-covalent manner may be tuned to provide other release characteristics at the disease site. For example, Cai, Lin et al. synthesized poly(propylene oxide)-b-poly(γ-benzyl-L-glutamate)-b-poly(ethylene glycol) (PPO-b-PBLG-b-PEG) triblock terpolymers, in which doxorubicin was attached to PBLG block through acid-sensitive hydrazone bone. They prepared micelle structures with triblock terpolymer, in which naproxen is loaded physically in the core. It was found that the release of chemically and physically loaded drugs differs at different pH and temperatures [358].

5-Fluorouracil (5-FU) is one of the most common chemotherapeutic agents which inhibits DNA synthesis, and it is known for efficiency in the treatment of OSCC, colorectal, gastric, and oesophageal cancer [359-363]. The monomer version of 5-FU has been synthesized in several different studies [364-367], but it has not been used as a hydrophobic block of micellar structure. On the other hand, docetaxel (DTX) is another common anticancer drug that promotes abnormal microtubule stabilization and shows activity against similar tumor types as 5-FU [368]. The sequential administration 5-Fu and DTX demonstrated high potential in treating oral cancer because DTX improves the efficiency of

5-FU [369]. Herein, we report the fabrication of a micellar structure through the self-assembly of a drug-conjugated copolymer of poly(ethylene glycol) methacrylate and 5-fluorouracil methacrylate, as illustrated in Figure 7.1. Anticancer drug 5-fluorouracil was modified with a methacrylate group through a pH-sensitive hemiacetal bond. The hydrophobic monomer, 5-fluorouracil methacrylate, was then polymerized from a poly(ethylene glycol)-based macroinitiator via reversible addition-fragmentation chain-transfer (RAFT) polymerization. The obtained diblock copolymer-bearing activated ester groups were modified with an amine-containing peptide-based targeted group, cRGDfK, which targets the $\alpha_v\beta_3$ integrin receptors overexpressed in most of the cancer cells. The final modified copolymer was then used to prepare micelles non-covalently loaded with docetaxel, a clinically administered chemotherapeutic agent. The stability and release characteristics of the dual-drug loaded micelles were evaluated under neutral and acidic environments. Finally, in vitro cytotoxicity and internalization experiments, micelles were assessed against squamous carcinoma cells CAL-27.

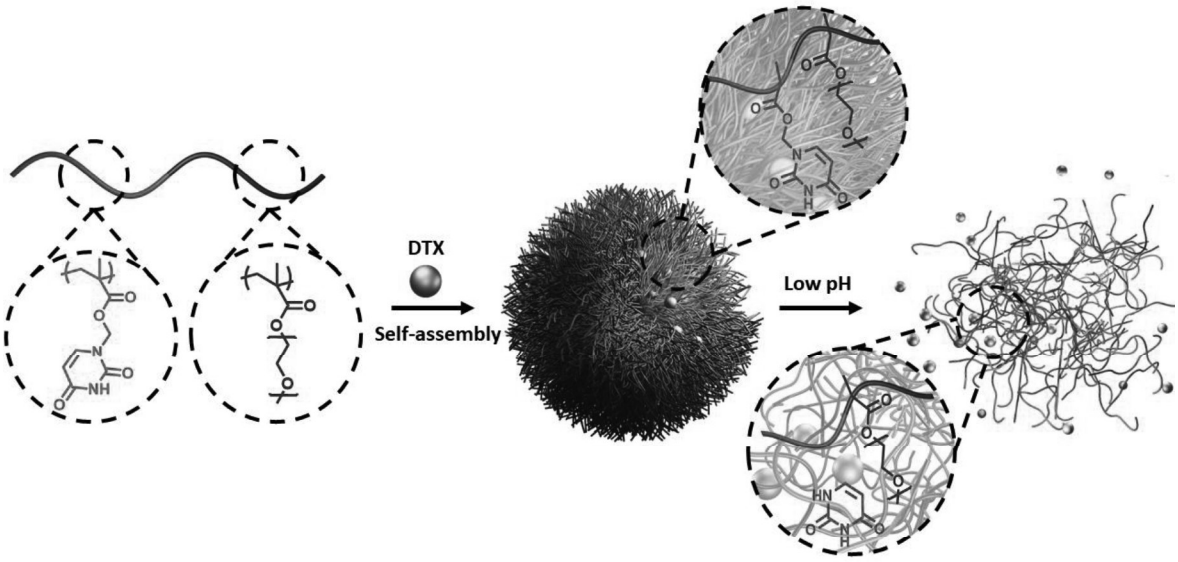

Figure 7.1. Schematic illustration of the formation and degradation of the pH-sensitive micelle.

7.2. Experimental

7.2.1. Materials

Diethyl ether was purchased from Merck. Poly(ethylene glycol) methyl ether methacrylate (PEGMEMA, Mn 300), 2,2′-Azobis(2-methylpropionitrile) (AIBN), 4-Cyano-4-(phenylcarbonothioylthio)pentanoic acid (CTA), formaldehyde solution (>36.0% in H_2O), methacryloyl chloride, triethyl amine (>99%), pyrene (98%), *N*,*N*′-dicyclohexylcarbodiimide (DCC), diisopropylcarbodiimide (DIC), Nile red (NR), cRGDfK, toluene, *N*,*N*′-dimethylformamide (DMF), *N*,*N*′-dimethylacetamide, acetonitrile (ACN), acetone, diethyl ether, dichloromethane (CH_2Cl_2), and docetaxel were purchased from Sigma-Aldrich. 5-Fluorouracil was purchased from Tokyo Chemical Industry. *N*-hydroxysuccinimide (NHS, 98+%) was purchased from Alfa Aesar.

7.2.2. Method

Ultra-pure water was obtained via MilliQ Water Purification System (Merck Millipore, USA). FTIR spectroscopy measurements were done on a Thermo Scientific Nicolet 380 FTIR spectrometer. The size of micelles was measured using a Zetasizer Nano particle analyzer (Malvern). NMR analysis was carried out using a 400 MHz Bruker spectrometer. Molecular weights of the polymers were monitored using a gel permeation chromatography using a PSS-SDV (gram linear, length/ID 8 × 300 mm, ten μm particle size) column calibrated with poly(methyl methacrylate) standards (1−175 kDa) using a refractive index detector. Dimethylacetamide with 0.05% lithium bromide was used as an eluent at a flow rate of 1.0 mL/min at 30 °C. Drug concentrations were analyzed by LC-MS analysis using LC-MS-8030-mass spectroscopy (Shimadzu, Japan) equipped with a C-18, 2.7 μm, 100×3 mm column. Nile Red concentrations were quantified using a fluorescence spectrophotometer (Varian Cary Eclipse, Agilent, USA). For the internalization experiments, cells were monitored using Zeiss Axio Observer inverted fluorescence microscope (Carl Zeiss Canada Ltd., Canada).

7.2.3. Cell Lines

Cal27 was purchased from ATCC (LGC Standards, Germany) and grown according to the culture methods requirements of the manufacturer. Cells were kept in the logarithmic phase of cell growth for the duration of experiments and incubated in a humidified atmosphere of 5% CO2 at 37 °C. Cytotoxicity experiments were done with a plate reader (Multiscan FC, Thermo Scientific, USA) and Cell Counting Kit8 (CCK-8, Fluka) was obtained from Sigma-Aldrich.

7.2.4. Synthesis of 5-Fluorouracil-Containing Monomer

5-Fluorouracil (1.50 g, 0.012 mol) and formaldehyde (1.46 g, 0,018 mol) were mixed in a round bottom. The reaction solution was stirred at room temperature for two hours at 60 °C. The solution was then lypolyzed and redissolved in ACN (18 mL) under N_2 gas. Triethyl amine (2.50 g, 0.024 mol) was then added to the mixture. Methacryloyl chloride (1.20 g, 0.012 mol) was then added into this ice-cold mixture dropwise, and the reaction was stirred for 24 hours at 25 °C. After 24 hours, the reaction solution was filtered and concentrated on a rotary evaporator. The concentrated solution was purified by preparative HPLC using ACN and water (1:1) as eluents affording 1.5 g product (50 % yield). ^{1}H NMR ($CDCl_3$, δ, ppm), 9.11 (s, 1H, CH_2-NH-CH_2), 7.70 (d, 1H, N-CH-CF), 6.24 (s 1H, CH_2=C), 5.72 (s 1H, CH_2=C), 5.72 (s, 2H, O-CH_2-N), 1.95 (s, 3H, CH_3-C). ^{13}C NMR ($CDCl_3$, δ, ppm), 167.35, 157.06, 156.79, 149.33, 141.46, 139.07, 134.86, 128.97, 128.73, 128.63, 70.06, 18.20.

7.2.5. Synthesis of PEG-Based Macro-Initiator

PEGMEMA (0.50 g, 1.0 mmol), AIBN (0.001 mg, 0,00625 mmol), and CTA (0.014 g, 0.05 mmol) were added to a round bottom flask and dissolved in DMF (1.0 mL). The solution was then purged with N_2 for 30 minutes. The reaction was then started at 70 °C. After 24 hours, the reaction solution was concentrated on a rotary evaporator, and the final solution was precipitated in diethyl ether. The precipitated polymer was dried under a high vacuum affording 0.46 g product (92% yield). $M_{n,\,theo}$ = 6000 g/mol, $M_{n,\,GPC}$ = 6300 g/mol,

$M_{n,\ NMR}$ = 6400 g/mol, M_w/M_n = 1.1. ^{1}H NMR (CDCl3, δ, ppm), 4.08 (s, 2H, C(O)-O-CH_2-CH_2), 3.65 (s, 4H, O-CH_2-CH_2-O), 3.38 (s, 3H, CH_3-O).

7.2.6. Synthesis of 5FMA Containing Diblock Copolymer

5FMA (0.20 g, 0.87 mmol), AIBN (0.51 mg, 0.0031 mmol), and macro-initiator (0.19 g, 0.029 mmol) was added to a round bottom flask and dissolved in DMF (0.75 mL). The solution was then purged with N_2 for 30 minutes. The reaction was then started at 70 °C. After 24 hours, the reaction solution was concentrated using a rotary evaporator. The remaining solution was then precipitated in diethyl ether. The solid product was dried under vacuum affording 0.31 g product (86% yield). $M_{n,\ theo}$ = 130000 g/mol, $M_{n,\ GPC}$ = 12000 g/mol, M_w/M_n = 1.3. ^{1}H NMR ($CDCl_3$, δ, ppm), 12.05 (s, CH_2NH-CH_2), 8.11 (d, NCHCF), 5.49 (s, C(O)OCH_2N), 4.01 (s, C(O)OC$H_2$$CH_2$), 3.52 (s, OC$H_2CH_2$O), 3.24 (s, C$H_3$O).

7.2.7. End Group Modification of Diblock Copolymer With cRGDfK

Firstly, the end group of the diblock copolymer was activated with NHS. The diblock copolymer (0.20 g, 0.016 mmol) and NHS (0.009 mg, 0.08 mmol) were dissolved in DMF (4.16 mL) under N_2. DCC (0.016 mg, 0.08 mmol) was dissolved in DMF (1.6 mL) under N_2. DCC solution was then added dropwise into an ice-cold solution of polymer and NHS. The reaction was then stirred at 25 °C for 24 hours. After the reaction, the solution was filtered and concentrated on a rotary evaporator. The final solution was precipitated in diethyl ether and dried under a vacuum, producing 0.20 g product (99 % yield). ^{1}H NMR ($CDCl_3$, δ, ppm), 12.05 (s, CH_2N$H$$CH_2$), 8.11 (d, N-C$H$-CF), 5.49 (s, C(O)OC$H_2$N), 4.01 (s, C(O)OC$H_2$$CH_2$), 3.52 (s, OC$H_2CH_2$O), 3.24 (s, C$H_3$-O), 2.81 (s, CC$H_2CH_2$C). Secondly, NHS-activated diblock copolymer was modified with cRGDfK. NHS-modified copolymer (50 mg, 0.004 mmol), cRGDfK (2.5 mg, 0.004 mmol), DIC (1.1 mg, 0.008 mmol), and DMAP (0.61 mg, 0.005 mmol) were dissolved in H_2O (0.5 mL). The reaction mixture was stirred for 24 hours at 25 °C. After the reaction, the product was purified using a dialysis membrane (MWCO: 3500) against H_2O for three days. The solution inside the bag was then lypolyzed, affording 43 mg of product (86% yield). ^{1}H NMR ($CDCl_3$, δ, ppm), 8.11 (d,

NC*H*CF), 7.62 (m, 5H, aromatic ring of CTA), 7.16 (m, 5H, aromatic ring of cRGDfK), 5.49 (s, C(O)OCH_2N), 4.01 (s, C(O)OCH_2CH$_2$), 3.52 (s, OCH_2CH_2O), 3.24 (s, CH_3O).

7.2.8. Preparation of Micelles

Critical micelle concentration (CMC) was determined at 25 °C by measuring the intensity of pyrene in the polymer solution via fluorescence spectroscopy. The Cosolvent evaporation method was used to prepare micelles and to load pyrene. Briefly, 15 samples with various amounts of polymers were prepared and dissolved in acetone (0.7 mL). The exact amount of pyrene was added to each sample. Each sample was then added dropwise into H_2O (3 mL). The solution was then left in the open air to evaporate cosolvent slowly. After 16 hours, the final concentration of the polymer sample was found to be between 8.33×10^{-9} M and 1.72×10^{-5} M. Samples were analyzed with fluorescence spectroscopy to calculate the CMC. Micelle samples were monitored using pyrene excitation spectra at emission wavelength (390 nm), and the CMC value was then calculated using the I_{338}/I_{334} ratio. Targeted and non-targeted micelles were prepared using the cosolvent evaporation method. For targeted micellar structure, cRGDfK modified (20 wt %) and non-modified (80 wt %) polymer (3 mg, 0.25 mmol) was dissolved in acetone (0.7 mL). The polymer solution was then added to 3 mL of H_2O. The mixture was left in the open air for slow evaporation of organic solvent to obtain a micellar structure for 24 hours. For non-targeted micellar structure, only non-modified polymer was used. For determination of the size of the micelle structure, **t**argeted, non-targeted and drug-loaded micelles were prepared with polymer solution (1 mg/mL), and their dynamic size diameter was measured at 25 °C and 37 °C in water using DLS. Zeta potential analysis was also done at 37 °C in water and phosphate buffer saline (PBS) at pH 7.4.

7.2.9. Docetaxel Loading into Micelles

Docetaxel (1 mg, 0.001 mmol) was dissolved in acetone (2 mL). In a different place, the polymer (3 mg, 0.25 mmol) was dissolved in acetone (0.7 mL) and slowly added to H_2O (3 mL). Docetaxel solution (0.3 mL, 0.5 mg/mL) was then added to polymer solution. The mixture was then left in the open air for 24 hours to evaporate the organic solvent. The

diameter of micellar structures was analyzed using DLS. The final solution was passed through a filter (0.45 μm pore size) to remove unloaded and aggregated drug molecules if it is needed. For the analysis of docetaxel content, the micelle solution (0.1 mL, 1 mg/mL) was diluted with acetonitrile (0.9 mL) and vortexed for 10 minutes for the complete disassembly of the micellar structure. Disassembled polymer/drug solution was analyzed using LC-MS, and docetaxel content was calculated.

7.2.10. DTX Release, Cytotoxicity, and Cell Uptake

Cytotoxicity Experiments. Cytotoxicity of the micelles was investigated via CCK-8 viability assay on CAL 27 cancer cells. Cells (25000 cells/well) were seeded on a 96-well plate in quadruplicate as 100 μL of culture medium and incubated at 37 °C for overnight to cells to grow and adhere completely. Cells were treated with cellular media containing different concentration of free drugs (DTX and 5-FU), micelle containing 5-FU, micelle containing 5-FU and DTX and micelles containing different drugs conjugated with RGD. The plates were kept with the corresponding solutions for 48 h. After 48 h, CCK-8 solution was added to into each well to culture for 2 h. After incubation with CCK-8, the absorbance values at 450 nm were measured via microplate reader. Results were obtained by GraphPad prism software using in nonlinear regression mode.

Internalization Experiments. For the cellular internalization experiment, CAL27 cells (50 000 cells/well) were seeded in 24-well plate as dublicate in 1 mL of culture media. The cells were incubated at 37 °C for 18 h. Cells were incubated with micelles containing the same amount of Nile Red dye (5.16x10-4 mmol) and micelles with cRGDfV (10 mg/mL) to make a comparison between targeted group at 37 °C for related time. After at several time points (8 and 24 h) cellular media were removed and washed three times with PBS (500 μL) and 4% of formaldehyde solution (300 μL) was added to wells at 37 °C for 10 min. After the removing solution and washing process, DAPI (300 μL) containing PBS were added to wells for 15 min at room temperature for nuclei staining. After washing cells three times with PBS, cell images were obtained by using Zeiss Observer Z1 fluorescence microscope. For flow cytometry experiment CAL27 cancer cells (100 000 cells/well) were seeded into 12-well plate as duplicates in 1 mL of culture media and incubated at 37 °C for overnight.

The samples' properties were the same with used in the cellular internalization experiment. After 24 h, cell media were removed, and the cells were trypsinized with 0.05% trypsin solution for 2 min at 37 °C. After 2 min, culture media (700 μL) was added to wells and Nile Red intensities were determined by flow cytometry (Guava easyCyte).

7.3. Results and Discussion

7.3.1. Synthesis and Characterization of 5-Fluorouracil Monomer

As a hydrophobic construct of the diblock copolymer, a methacrylic monomer of 5-fluorouracil was synthesized. Due to our interest in making redox-sensitive drug release, a pH-responsive linker was incorporated between the 5-fluorouracil molecule and the methacrylate group. The amine group adjacent to the double bond on 5-fluorouracil molecules was reacted with formaldehyde solution to obtain an alcohol derivative of 5-fluorouracil. The product was used without further purification and reacted with methacryloyl chloride to produce a 5-fluorouracil monomer, as shown in Figure 7.2a. The composition of the synthesized monomer was characterized by ^{1}H NMR spectrum in Figure 7.2b, where the resonance at 7.70 ppm belonging to vinylic proton on the ring, 6.24 and 5.72 belonging to protons on the double bond, 5.72 ppm belonging to protons on the methylene group and 1.95 ppm belonging to the protons of the methyl group. ^{13}C NMR spectrum in Figure 7.2c also confirmed the structure; the carbon resonance at 167.35 belonging to carbonyl on the ester bond, 149.33 belonging to carbonyl on the ring, and 70.06 belonging to methylene carbon. The 5-Fluorouracil monomer was chosen as a hydrophobic compartment of the diblock copolymer as well as the chemotherapeutic activity of 5-fluorouracil against oral squamous cell carcinoma. The 5-Fluorouracil monomer was designed to activate the drug by the cleavage of a responsive linker. Degradation of this linker will cause the release of not only the 5-fluorouracil but also the second drug due to the unbalanced hydrophobicity/hydrophilicity in the micellar structure.

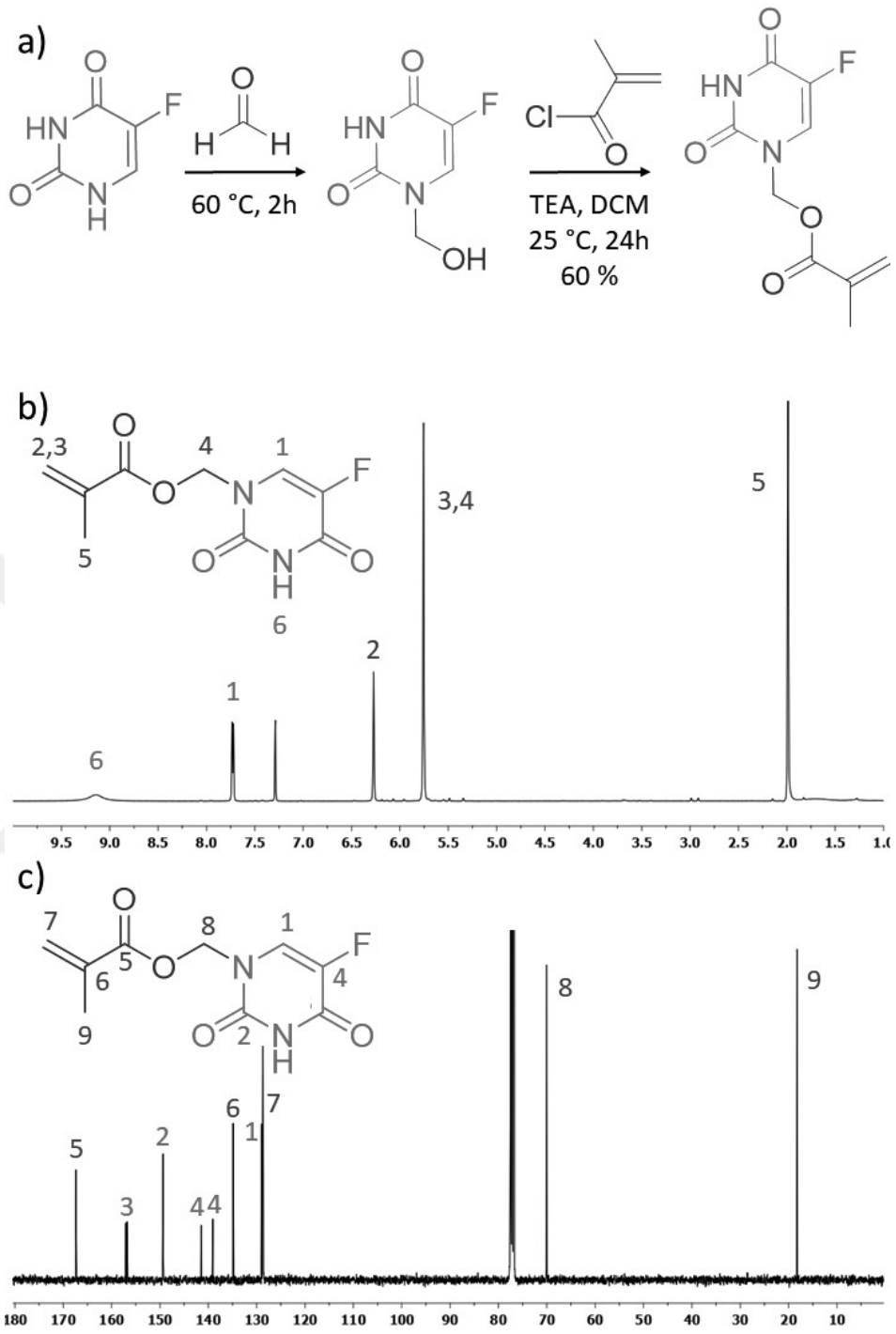

Figure 7.2. (a) Synthetic pathway, (b) ^{1}H NMR spectrum, and (c) ^{13}C NMR spectrum of 5-fluorouracil monomer.

7.3.2. Synthesis of the Diblock Copolymer

PEGMEMA was polymerized using RAFT polymerization to yield a macroinitiator as a hydrophilic block of the copolymer. A polymer chain that would be hydrophilic enough for a micellar structure was targeted using PEGMEMA:CTA ratio of 20:1. The experimental number of monomers in the polymer chain was calculated to be 21:1 from its ^{1}H NMR spectrum in Figure 7.3, and the number of the average weight of macroinitiator was calculated to be 6300 gmol^{-1} using size exclusion chromatography, as seen in Figure 7.4. As a second block of the copolymer, the 5-fluorouracil monomer was polymerized on a macroinitiator using RAFT polymerization to yield a diblock copolymer. Hydrophobic block that would be long enough for chemotherapeutic efficiency yet balance the hydrophilicity of diblock copolymer was targeted using a 5-fluorouracil:macroinitiator ratio of 30:1. The experimental ratio in the diblock copolymer was determined to be 26:1 from its ^{1}H NMR spectrum in Figure 7.5, and the number average of molecular weight was deduced to be 12 000 gmol^{-1} using size exclusion chromatography, as seen in Figure 7.6.

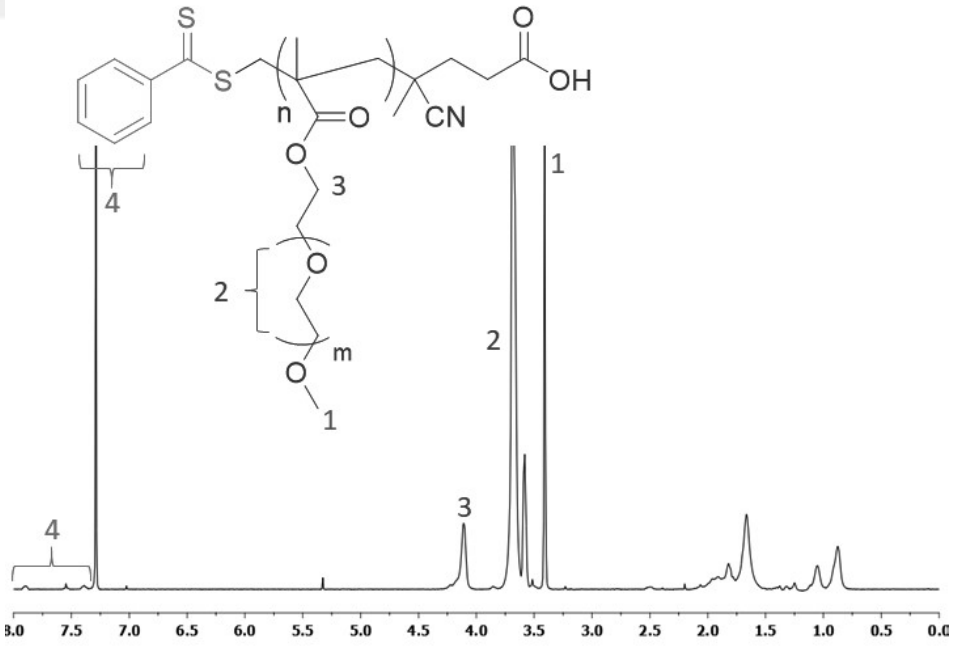

Figure 7.3. ^{1}H NMR spectrum of macroinitiator

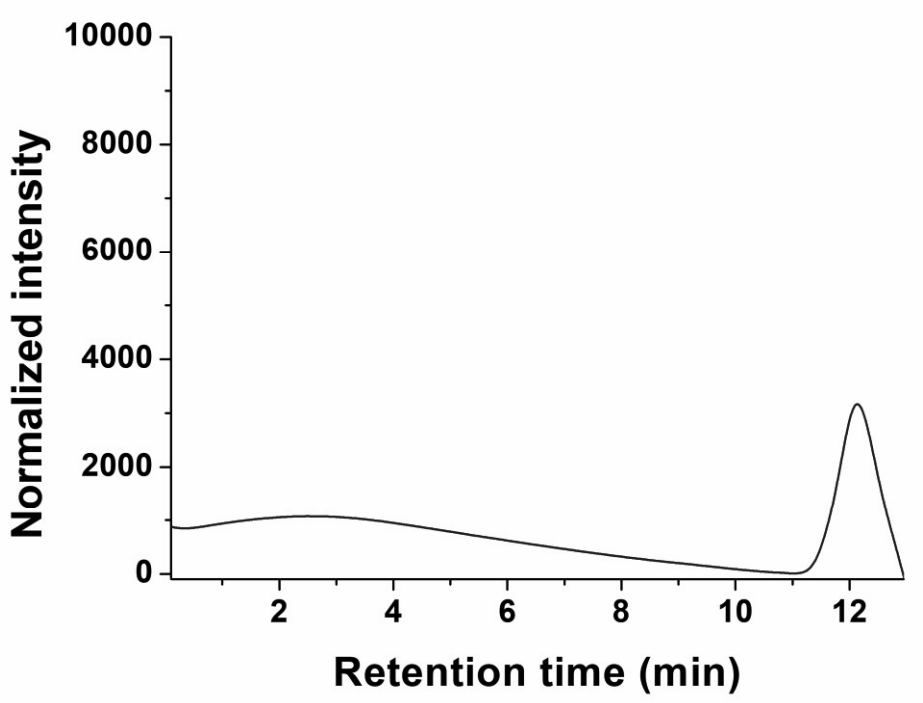

Figure 7.4. SEC chromatographs of the macroinitiator.

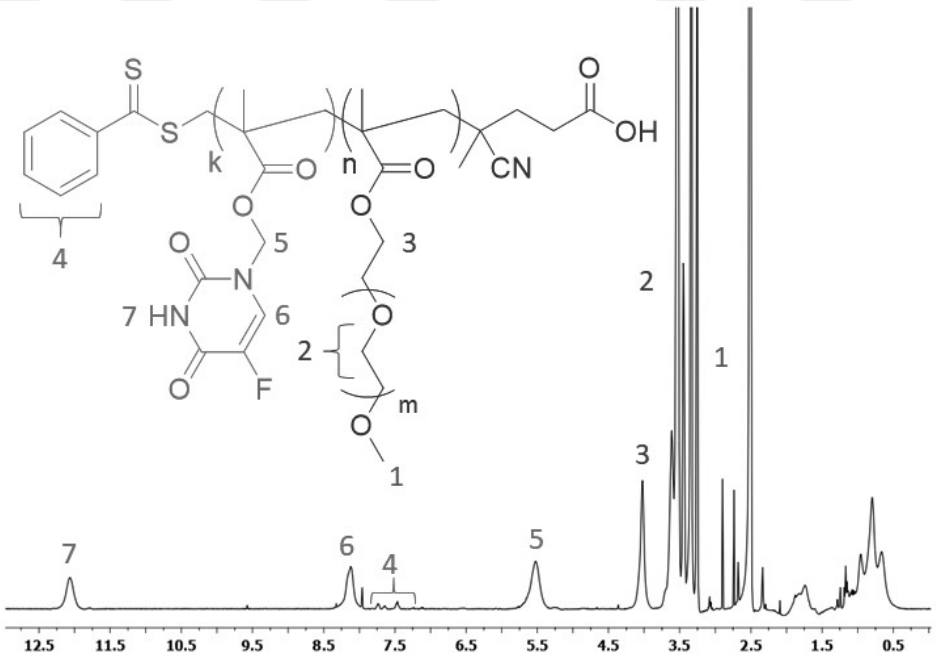

Figure 7.5. ^{1}H NMR spectrum of diblock copolymer.

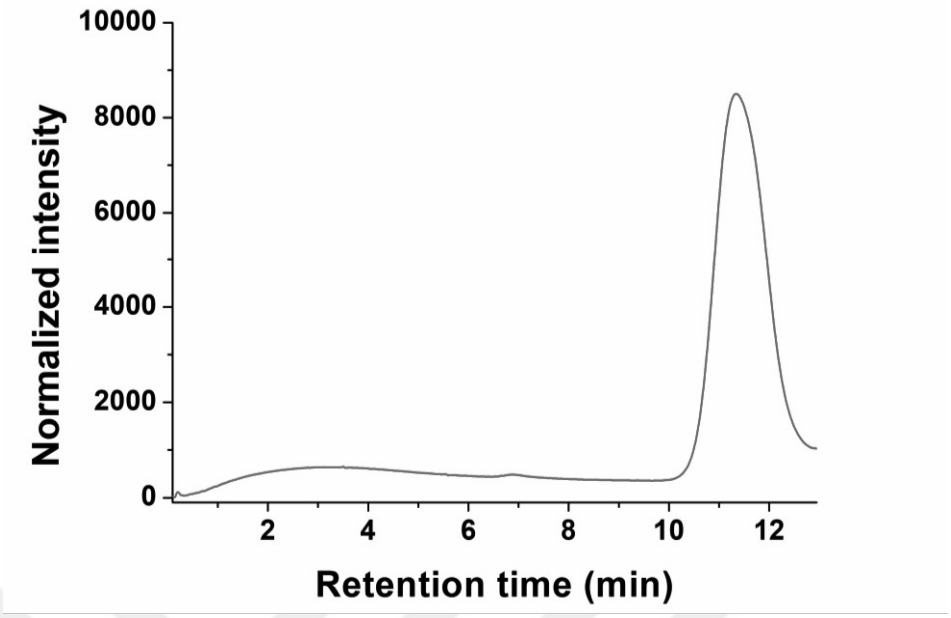

Figure 7.6. SEC chromatographs of the diblock copolymer.

Due to our interest in targeting CAL-27 squamous carcinoma cells with integrin αvβ3 expression, the hydrophilic end of the diblock copolymer was modified with cRGDfK. For efficient conjugation, the carboxylic acid moiety of the copolymer was activated using NHS, and the success of the modification through amidation reaction was deduced from ^{1}H NMR spectrum in Figure 7.7 where the resonance at 2.81 ppm belonging to methylene protons on the NHS. End group modification was carried out by reacting NHS-activated diblock copolymer and cRGDfK; the final structure was characterized using ^{1}H NMR spectrum in Figure 7.8 where the resonance at 7.16 ppm belonging to protons on the aromatic ring of cRGDfK**.**

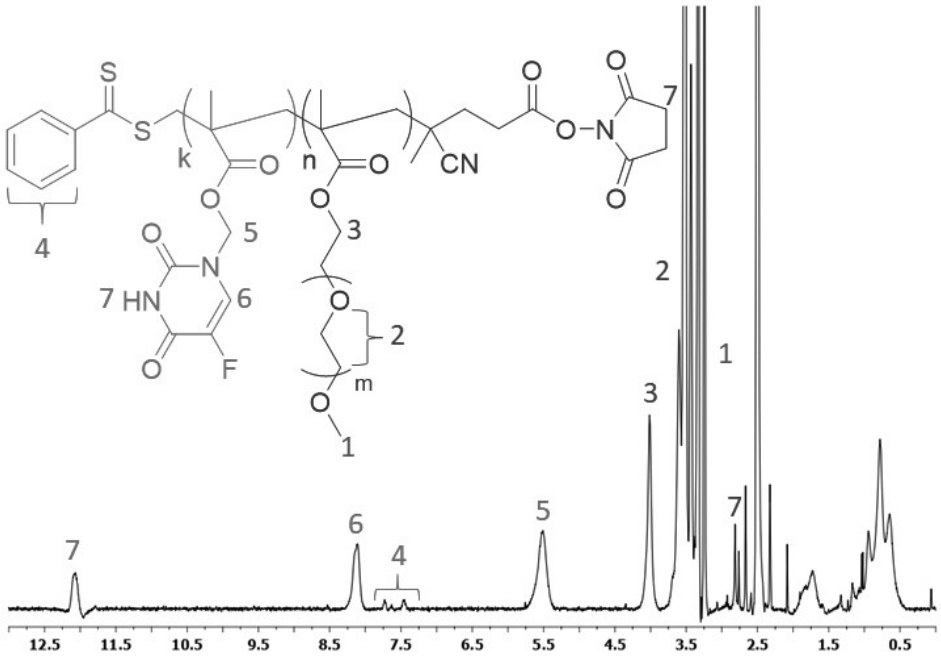

Figure 7.7. ^{1}H NMR spectrum of NHS-activated diblock copolymer.

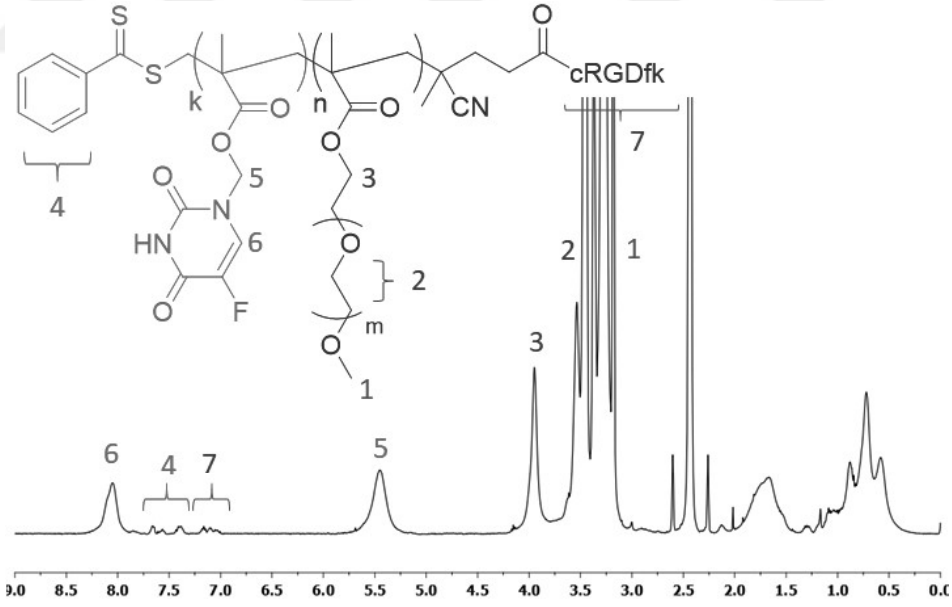

Figure 7.8. ^{1}H NMR spectrum of cRGDfK diblock copolymer.

7.3.3. Fabrication and Characterization of Micelles

Critical micelle concentration of diblock copolymer was monitored using the pyrene as a probe. Upon micelle formation at a suitable concentration, water-insoluble pyrene was encapsulated inside the micellar structure, causing an increase in pyrene intensity and the shift of maxima from 334 nm to 338 nm because of the formation of pyrene excimers. Using this approach, the CMC value of the micellar structure was determined as 3.6×E-07 M as shown in Fgure 7.9a. polydispersity index (PDI) and Z-average values at different concentrations where pyrene intensities measured were shown in Figure 7.9b and c. For further studies, micellar structures were prepared at 8.3E-5 M using acetone as a cosolvent. After the cosolvent was evaporated, the Z-average size of particles was determined as 130 nm using DLS analysis as shown in Figure 7.10.

At this point, it was crucial to investigate the stability of micellar structures in dilute environments; hence they will face extreme dilutions upon injection in potential *in vivo* applications. For this purpose, the colloidal stability of micellar structures was analyzed using DLS. Micelle solution (8.3E-7 M) was extensively diluted with water, and the Z-average size and content % of micelles were analyzed. The results showed that the particle's size and content % of particle did not change significantly up to 40 times dilution. The Z-average size and PDI slightly increased for further dilutions up to 2000 times, as seen in Figure 7.11b, and c. Additionally, the contents of micelle were around 100 % up to 40 times dilution and started to decrease slightly upon increased dilutions indicating that micellar structures preserved their physical integrity in dilute environments, as noticed in Figure 7.11a.

Docetaxel encapsulated targeted, and non-targeted micellar structures were prepared using the cosolvent evaporation method. Targeted micellar structures were prepared using 20 wt % cRGDfK-modified polymers, while only non-modified polymers were used for the non-targeted micellar structure. The amount of loaded-docetaxel was calculated using LC-MSMS after micellar structure disessambled by addition of acetonitrile and docetaxel content was calculated as 11 wt %.

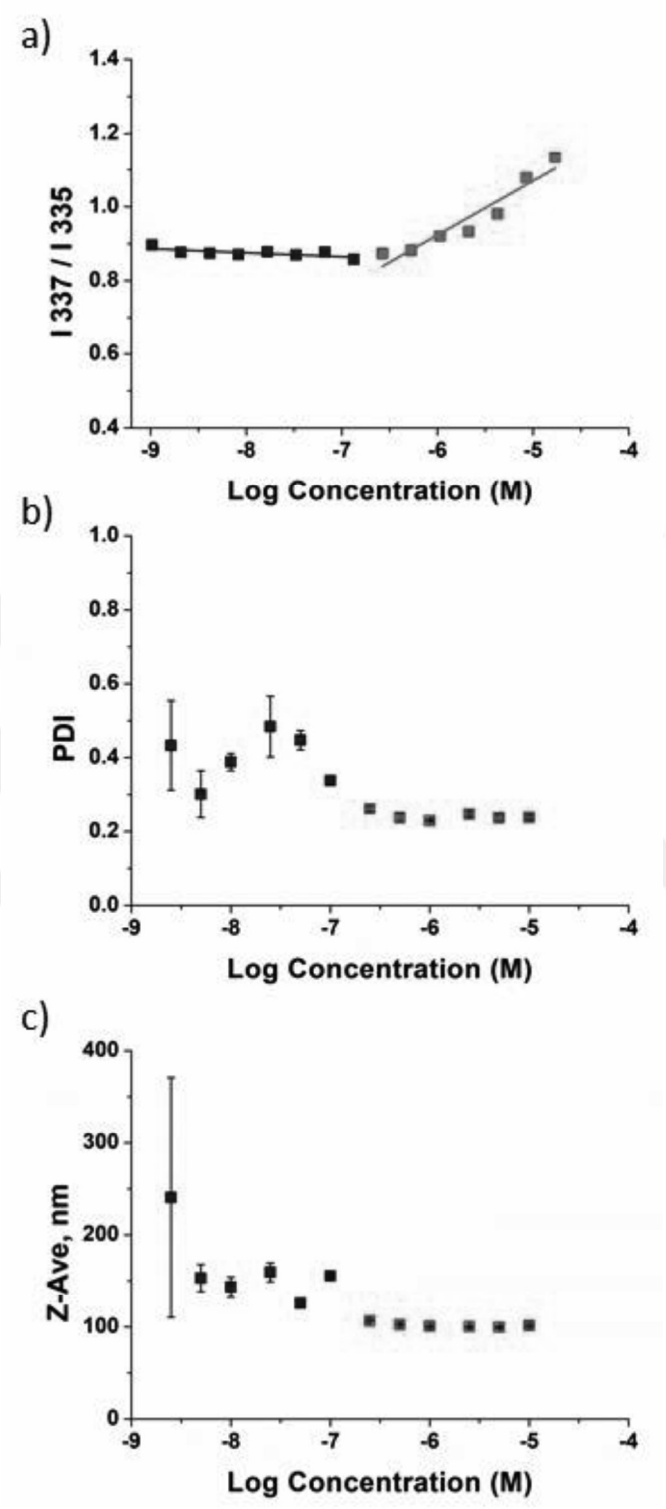

Figure 7.9. (a) CMC, (b) PDI, and (c) Z-ave valuse of polymer solutions at various concentrations.

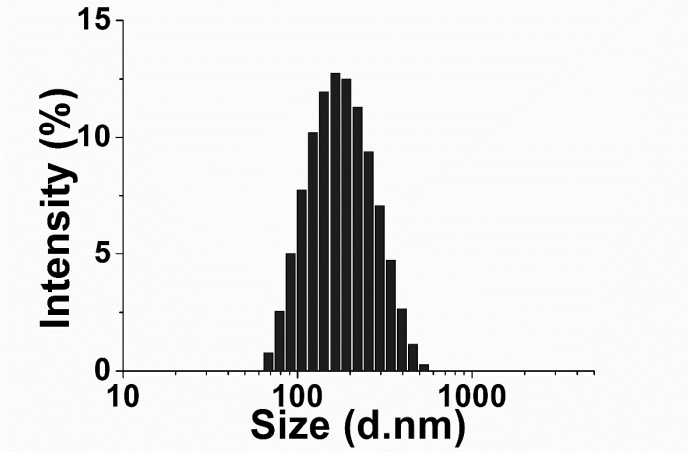

Figure 7.10. DLS measurement of micellar structures at CMC.

7.3.4. pH-Responsive Docetaxel and 5-Fluorouracil Release

pH-responsive drug delivery is one of the widely investigated methods for selective drug delivery to tumors due to the acidic environment of tumor tissue. pH-responsive nano-structures took advantage of pH differences between healthy tissue (pH 7.4) and tumor tissue (pH < 7.0) to release their cargo selectively. More acidic intracellular environments such as endosomes (pH ~ 5-6), which encapsulate nano-structure after internalization, also lead to pH-responsive drug release [370]. Prior to drug release studies, the stability of the micellar structure in neutral and acidic pH was monitored. Figure 7.12a showed that micellar structures were relatively stable in a neutral environment, while the hydrodynamic size notably increased at pH 5.5, as seen in Figure 7.12c. The release of 5-fluorouracil was around ~ 10 %, as seen in Figure 7.12b. Figure 7.12d showed that Docetaxel release was also quite low (~ 10 %) in a neutral environment (pH 7.4) for 5 hours, suggesting that only a few amounts of the drug escaped from the micellar structure due to the stability of nano-assembly. On the other hand, the decrease in stability of micellar structure contributed to the release of physically-loaded docetaxel, reaching around 100 % release.

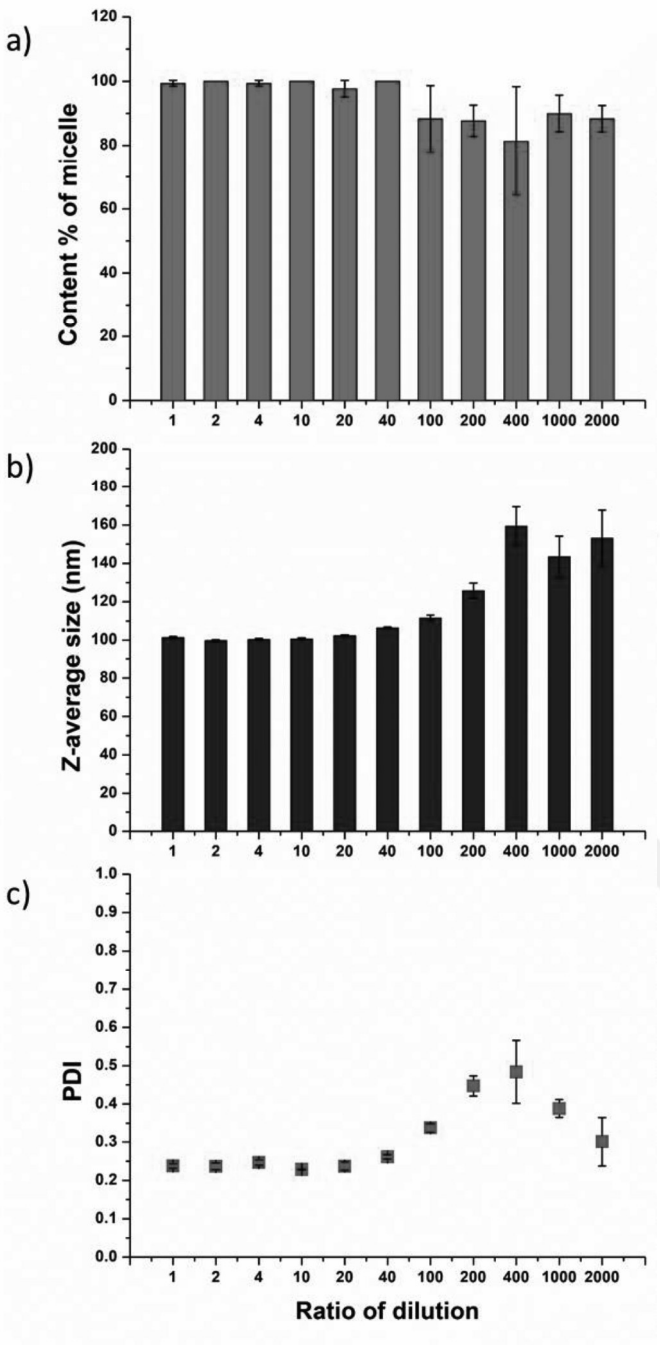

Figure 7.11. (a) Cell viability results of Drug, micelle and RGD combinations and (b) internalization experiment results of NR-loaded RGD-bearing and non-bearing micelles.

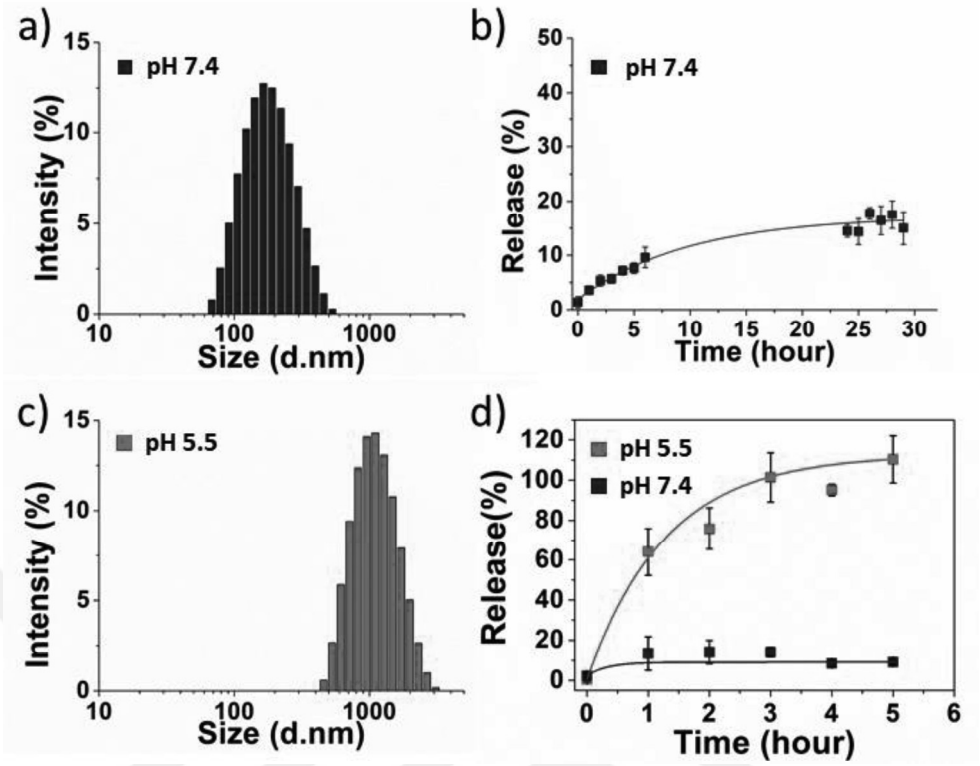

Figure 7.12. (a) Z-average size of micelles in pH 7.4 and (c) in pH 5.5. The release of (b) 5-fluorouracil and (c) docetaxel in pH 5.5 and 7.4.

7.3.5. Cytotoxicity and Internalization Experiments for Drug Conjugates on CAL 27

The antitumor efficacy of DTX-loaded micelles was monitored using squamous carcinoma cells CAL-27. Due to our interest in active targeting and selective delivery of drug-loaded micelles, a cell viability test was performed with free DTX, free 5-FU, micelle, RGD-micelle, micelle-DTX, RGD-micelle-DTX. As expected, the micelle-DTX showed less antitumor efficacy on CAL 27 cells compared to free DTX after 48 h, as shown in Figure 7.13a. Results showed that the EC50 value of cRGDfV-micelle-DTX is higher than micelle-DTX, indicating that the targeting ability of micelles improved the drug delivery. Additionally, micelles showed less toxicity compared to free 5-FU which is expected due to physical conjugation of 5-FU to polymers.

The in vitro cellular internalization of cRGDfV conjugated micelle was also monitored on squamous carcinoma cells CAL-27. Cells were continuously treated with an equivalent

amount of NR-containing micelles, cRGDfV-micelle, and cRGDfV + cRGDfV-micelle for six hours, and Figure 7.13b showed that micelless were gradually internalized by the squamous carcinoma cells CAL-27 as monitored by the increase in red fluorescence provided by NR. The presence of cRGDfV on the surface of the micelles (cRGDfV-micelle) increased the NR internalization compared to micelle without cRGDfC (micelle). To further investigate the role of the cRGDfV ligand on the internalization of the NR, free cRGDfV was added to the media (cRGDfV+ cRGDfV-micelle) and resulted in lower NR internalization as monitored by fluorescence microscopy. The competitive binding of free cRGDfV can explain this with integrin receptors on the cell surface, which negatively affected the binding of cRGDfV-micelle. The uptake of cRGDfV-micelle was also investigated and quantified using flow cytometry. The mean fluorescence intensity values of CAL-27 cells treated with NR-loaded cRGDfV-micelle compared to micelle (non-targeted) in Figure 7.13b showed that the targeting-group bearing micelles were preferentially internalization.

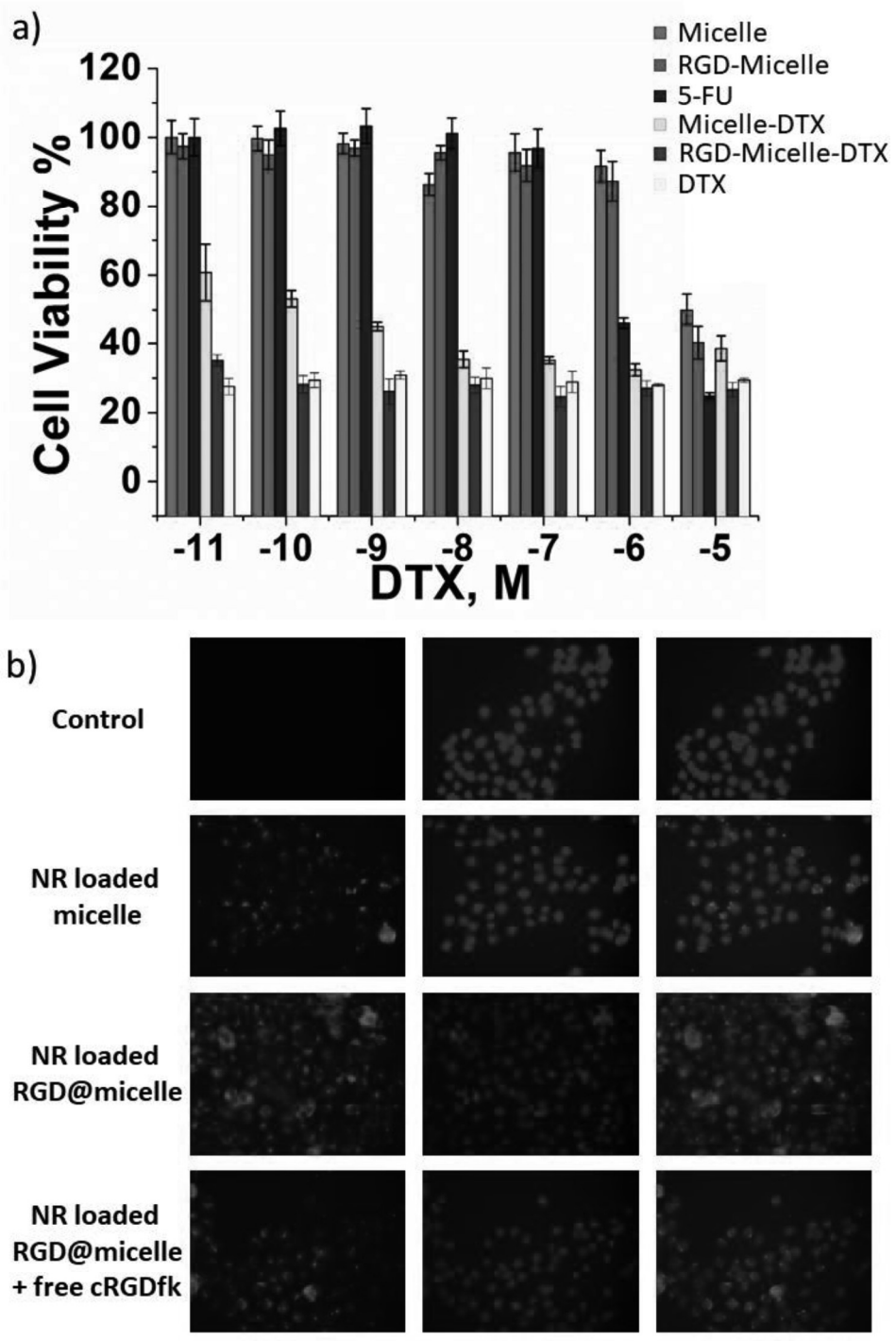

Figure 7.13. (a) Cell viability results of Drug, micelle and RGD combinations and (b) internalization experiment results of NR-loaded RGD-bearing and non-bearing micelles.

7.4. Conclusion

A diblock polymer of 5-Fluorouracil monomer and PEGMEMA were synthesized and conjugated with targeting group cRGDfK. The targeted polymer-drug conjugate was employed to generate micellar structures characterized by DLS and TEM analysis. Micellar structures demonstrated high stability in neutral pH, whereas self-assembly was quickly disrupted at pH 5.5 due to the pH-sensitive linker between the 5-fluorouracil molecule and polymer backbone. The micellar structure did not show any significant stability problem in a highly dilute environment indicating that they will preserve their form upon possible *in vivo* injections. As a second drug, docetaxel was loaded to micellar structures, and the release of both drugs was found to be pH-responsive. Targeted and docetaxel-loaded micellar structures were shown to display higher cytotoxicity *in vitro* than non-targeted docetaxel-loaded particles and targeted nanoparticles. Targeted and docetaxel-loaded particles were also shown similar cytotoxicity as free docetaxel. Flow cytometry and internalization experiments demonstrated that targeted particles internalized more efficiently compared to non-targeted counterparts. Moreover, internalization significantly decreased in the presence of free RGD, indicating receptor-mediated uptake.

8. CONCLUSION

In this thesis, we investigated the design and fabrication of macro- and nano-scale polymeric materials for drug delivery applications. Hydrogels were explored as macroscopic, while nanofibers, nanogels, and micelles were investigated as nanosized polymeric materials. All polymeric systems were designed as stimuli-responsive to increase the control over the drug delivery profile. While the hydrogels and nanogels were designed to be redox-responsive using disulfide-containing crosslinkers and polymers, pH-responsive linkages were used in nanofibers and micelles to control the drug release. Also, a light-triggered, temperature-driven drug release system was developed using an rGO-embedded nanofiber system. Different chemistries were utilized to design the novel stimuli-responsive materials explored in this thesis. For example, the thiol-maleimide reaction was employed for crosslinking of hydrogels, and the thiol-disulfide exchange chemistry was used to impart them with on-demand dissolution. Similarly, the orthogonality of the thiol-maleimide and the thiol-disulfide reaction was also used for obtaining redox-responsive nanogels. Likewise, acid-sensitive linkages such as acetals were used for obtaining redox-responsive polymeric materials.

The first chapter of the thesis provided background information about the importance of stimuli-responsive drug delivery systems. The chapter also gives a general overview of the numerous stimuli-responsive chemistries used in drug-delivery applications for hydrogels, nanogels, nanofibers, and micelles. The second chapter briefly mentioned the aim of the research projects conducted in this thesis.

The following two chapters report exogenous and endogenous stimuli-responsive polymeric nanofibers with antibiotic agents and chemotherapeutic drugs. The third chapter described the fabrication of the rGO-embedded PAA nanofibers. Water soluble PAA nanofibers were crosslinked using β-CD at high temperatures under vacuum. The photothermal activity of these nanofiber mats was demonstrated under NIR light using a thermal camera. It was also shown that the antibiotic agents loaded in the nanofibers were forced to diffuse outside through the heating of the nanofiber mat upon NIR irradiation.

Additionally, it was demonstrated that antibiotic agents released at elevated temperatures were still active against various bacteria. Furthermore, in vivo studies established that the antibiotic-loaded nanofiber mat was effective in curing bacterial infection in mice.

The fourth chapter reports pH-sensitive nanofibers obtained using electrospinning of a homopolymer comprised of an acrylic backbone with acid-sensitive hydrolyzable side chains. In slightly acidic conditions, the nanofiber buttresses undergo a pH-responsive transformation from hydrophobic to hydrophilic. Importantly, it was demonstrated that the release profile of the encapsulated cargo could be tuned by adjusting the nanofiber diameter. Additionally, chemotherapeutic agent release was highly selective to slight decreases in the pH of the environment. Lastly, it was established that released drugs were still cytotoxic to several cancer cell lines. The nanofiber mat could be used with a clinically utilized surgical stapler and localized at the surgical site using an ex vivo porcine lung.

The fifth chapter reports redox-responsive, fast-forming, and dissolvable hydrogels' design and fabrication. A disulfide-containing maleimide-terminated PEG polymer and a four-arm PEG-thiol were crosslinked through Michael-type conjugation to obtain hydrogels. The orthogonality of the thiol-maleimide and thiol-disulfide exchange reaction was investigated; it was observed that the thiol reacts with the maleimide group in preference to the disulfide group. After gelation through the thiol-maleimide reaction, hydrogels were exposed to various reducing agents, and redox-responsive degradation was observed. Finally, the FITC-BSA protein was encapsulated within hydrogels, and its release in a reducing environment was analyzed. Cell viability experiments demonstrated that hydrogels and their degradation products were non-toxic.

Targeted and stimuli-responsive drug delivery with polymeric nanoparticles was the topic of the following two chapters. The sixth chapter reports the fabrication and functionalization of polymeric nanogels. A novel disulfide- and maleimide-containing monomer was copolymerized with PEGMEMA using RAFT polymerization to obtain a thiol-reactive thermoresponsive copolymer. Nano-size aggregates were formed from the obtained polymer using their self-assembly in aqueous media above their LCST. Through the Michael-type conjugation, self-assembled nano-aggregates were crosslinked using a

small dithiol-containing linker. Nanogels were further functionalized with a cell-adhesive peptide through a thiol-maleimide reaction. Nanogels were loaded with a fluorescent dye, and the degradation of nanogels in the reducing environment was investigated. Additionally, the stability of nanogels in different environments was investigated using DLS, and it was observed that nanogels were not stable in a GSH solution (10 mM). Importantly, in vitro drug release studies showed that enhanced drug release occurs in the reducing environment compared to the non-reducing environment. Finally, cytotoxicity and internalization studies showed that drug-loaded nanogel formulations were more toxic in reductive cell environments, and targeted-nanogels were internalized more than their non-targeted counterparts.

In the seventh chapter, a targeted-micellar nanostructure that can deliver two drugs, one loaded chemically and the other physically, was designed. A 5-fluorouracil-based monomer was synthesized and polymerized to obtain the first block, followed by extension with a PEGMEMA-based second block through RAFT polymerization. A micellar nanostructure was prepared using the self-assembly of this diblock copolymer in aqueous media and loaded with docetaxel. Finally, the nanostructure was functionalized with cRGDfK, a cell-targeting peptide. Obtained micellar nanoaggregate was found to be stable under physiological conditions and against serial dilutions. Interestingly, self-assembly was quickly disrupted at lower pH and caused the release of the physically loaded cargo. The dual-drug-loaded micelles demonstrated good therapeutic efficacy against the CAL-27 cell line. DTX-loaded micelles showed similar cytotoxicity with free docetaxel, and the targeted group's presence improved the cytotoxicity.

REFERENCES

1. Xu, X., L. He, B. Zhu, Jiyao Li, and Jianshu Li, “Advances In Polymeric Materials For Dental Applications.”, *Polymer Chemistry*, Vol. 8, No. 5, pp. 807–823, 2017.

2. Fenton, O.S., K.N. Olafson, P.S. Pillai, M.J. Mitchell, and R. Langer, “Advances In Biomaterials For Drug Delivery.”, *Advanced Materials*, Vol. 30, No. 29, p. 1705328, 2018.

3. Bordat, A., T. Boissenot, J. Nicolas, and N. Tsapis, “Thermoresponsive Polymer Nanocarriers For Biomedical Applications.”, *Advanced Drug Delivery Reviews*, Vol. 138, pp. 167–192, 2019.

4. Calik, F., A. Degirmenci, M. Eceoglu, A. Sanyal, and R. Sanyal, “Dendron-Polymer Conjugate Based Cross-Linked Micelles: A Robust And Versatile Nanosystem For Targeted Delivery.”, *Bioconjugate Chemistry*, Vol. 30, No. 4, pp. 1087–1097, 2019.

5. Chambre, L., W.S. Saw, G. Ekineker, L.V. Kiew, W.Y. Chong, H.B. Lee, L.Y. Chung, Y. Bretonnière, F. Dumoulin, and A. Sanyal, “Surfactant-Free Direct Access To Porphyrin-Cross-Linked Nanogels For Photodynamic And Photothermal Therapy.”, *Bioconjugate Chemistry*, Vol. 29, No. 12, pp. 4149–4159, 2018.

6. Bolu, B., R. Sanyal, and A. Sanyal, “Drug Delivery Systems From Self-Assembly Of Dendron-Polymer Conjugates.”, *Molecules*, Vol. 23, No. 7, p. 1570, 2018.

7. Adepu, S., and S. Ramakrishna, “Controlled Drug Delivery Systems: Current Status And Future Directions.”, *Molecules*, Vol. 26, No. 19, p. 5905, 2021.

8. Senaratne, W., L. Andruzzi, and C.K. Ober, “Self-Assembled Monolayers And Polymer Brushes In Biotechnology: Current Applications And Future Perspectives.”, *Biomacromolecules*, Vol. 6, No. 5, pp. 2427–2448, 2005.

9. Jhaveri, S.J., M.R. Hynd, N. Dowell-Mesfin, J.N. Turner, W. Shain, and C.K. Ober, “Release Of Nerve Growth Factor From HEMA Hydrogel-Coated Substrates And Its Effect On The Differentiation Of Neural Cells.”, *Biomacromolecules*, Vol. 10, No. 1, pp. 174–183, 2009.

10. Hoffman, A.S., “The Origins And Evolution Of ‘Controlled’ Drug Delivery Systems.”, *Journal of Controlled Release*, Vol. 132, No. 3, pp. 153–163, 2008.

11. Bayer, C.L., and N.A. Peppas, “Advances In Recognitive, Conductive And Responsive Delivery Systems.”, *Journal of Controlled Release*, Vol. 132, No. 3, pp. 216–221, 2008.

12. Fleige, E., M.A. Quadir, and R. Haag, “Stimuli-Responsive Polymeric Nanocarriers For The Controlled Transport Of Active Compounds: Concepts And Applications.”, *Advanced Drug Delivery Reviews*, Vol. 64, No. 9, pp. 866–884, 2012.

13. Colson, Yolonda L, Mark W Grinstaff, Y L Colson, and M W Grinstaff, “Biologically Responsive Polymeric Nanoparticles For Drug Delivery.”, *Advanced Materials*, Vol. 24, No. 28, pp. 3878–3886, 2012.

14. Basel, M.T., T.B. Shrestha, D.L. Troyer, and S.H. Bossmann, “Protease-Sensitive, Polymer-Caged Liposomes: A Method For Making Highly Targeted Liposomes Using Triggered Release.”, *ACS Nano*, Vol. 5, No. 3, pp. 2162–2175, 2011.

15. Zhang, R., M. Tang, A. Bowyer, R. Eisenthal, and J. Hubble, “A Novel PH- And Ionic-Strength-Sensitive Carboxy Methyl Dextran Hydrogel.”, *Biomaterials*, Vol. 26, No. 22, pp. 4677–4683, 2005.

16. Tagliazucchi, M., M.G. Blaber, G.C. Schatz, E.A. Weiss, and I. Szleifer, “Optical Properties Of Responsive Hybrid Au@Polymer Nanoparticles.”, *ACS Nano*, Vol. 6, No. 9, pp. 8397–8406, 2012.

17. Jochum, F.D., and P. Theato, “Temperature- And Light-Responsive Smart Polymer

Materials.”, *Chemical Society Reviews*, Vol. 42, No. 17, pp. 7468–7483, 2013.

18. Wang, M., H. Singh, T.A. Hatton, and G.C. Rutledge, “Field-Responsive Superparamagnetic Composite Nanofibers By Electrospinning.”, *Polymer*, Vol. 45, No. 16, pp. 5505–5514, 2004.

19. Paris, J.L., M. Manzano, M.V. Cabañas, and M. Vallet-Regí, “Mesoporous Silica Nanoparticles Engineered For Ultrasound-Induced Uptake By Cancer Cells.”, *Nanoscale*, Vol. 10, No. 14, pp. 6402–6408, 2018.

20. Filipcsei, G., J. Fehér, and M. Zrínyi, “Electric Field Sensitive Neutral Polymer Gels.”, *Journal of Molecular Structure*, Vol. 554, No. 1, pp. 109–117, 2000.

21. Sun, X., S. Agate, K.S. Salem, L. Lucia, and L. Pal, “Hydrogel-Based Sensor Networks: Compositions, Properties, And Applications - A Review.”, *ACS Applied Bio Materials*, Vol. 4, No. 1, pp. 140–162, 2021.

22. Raza, A., T. Rasheed, F. Nabeel, U. Hayat, M. Bilal, and H.M.N. Iqbal, “Endogenous And Exogenous Stimuli-Responsive Drug Delivery Systems For Programmed Site-Specific Release.”, *Molecules*, Vol. 24, No. 6, p. 1117, 2019.

23. Peppas, N.A., P. Bures, W. Leobandung, and H. Ichikawa, “Hydrogels In Pharmaceutical Formulations.”, *European Journal of Pharmaceutics and Biopharmaceutics*, Vol. 50, No. 1, pp. 27–46, 2000.

24. Ahadian, S., R.B. Sadeghian, S. Salehi, S. Ostrovidov, H. Bae, M. Ramalingam, and A. Khademhosseini, “Bioconjugated Hydrogels For Tissue Engineering And Regenerative Medicine.”, *Bioconjugate Chemistry*, Vol. 26, No. 10, pp. 1984–2001, 2015.

25. Peppas, N.A., J.Z. Hilt, A. Khademhosseini, and R. Langer, “Hydrogels In Biology And Medicine: From Molecular Principles To Bionanotechnology.”, *Advanced Materials*, Vol. 18, No. 11, pp. 1345–1360, 2006.

26. Ratner, B.D., and A.S. Hoffman, “Synthetic Hydrogels For Biomedical Applications.”, pp. 1–36, 1976.

27. Hoffman, A.S., “Hydrogels For Biomedical Applications.”, *Advanced Drug Delivery Reviews*, Vol. 54, No. 1, pp. 3–12, 2002.

28. Liu, Xiaowei, Haojie Yu, Li Wang, Zhikun Huang, Fazal Haq, Lisong Teng, Meijin Jin, Binbin Ding, X Liu, H Yu, L Wang, Z Huang, F Haq, L Teng, M Jin, and B Ding, “Recent Advances On Designs And Applications Of Hydrogel Adhesives.”, *Advanced Materials Interfaces*, Vol. 9, No. 2, p. 2101038, 2022.

29. Song, G., L. Zhang, C. He, D.C. Fang, P.G. Whitten, and H. Wang, “Facile Fabrication Of Tough Hydrogels Physically Cross-Linked By Strong Cooperative Hydrogen Bonding.”, *Macromolecules*, Vol. 46, No. 18, pp. 7423–7435, 2013.

30. Hu, Y., Z. Du, X. Deng, T. Wang, Z. Yang, W. Zhou, and C. Wang, “Dual Physically Cross-Linked Hydrogels With High Stretchability, Toughness, And Good Self-Recoverability.”, *Macromolecules*, Vol. 49, No. 15, pp. 5660–5668, 2016.

31. Lin, Peng, Shuanhong Ma, Xiaolong Wang, Feng Zhou, P Lin, S Ma, X Wang, and F Zhou, “Molecularly Engineered Dual-Crosslinked Hydrogel With Ultrahigh Mechanical Strength, Toughness, And Good Self-Recovery.”, *Advanced Materials*, Vol. 27, No. 12, pp. 2054–2059, 2015.

32. Edwards, C.E.R., D.J. Mai, S. Tang, and B.D. Olsen, “Molecular Anisotropy And Rearrangement As Mechanisms Of Toughness And Extensibility In Entangled Physical Gels.”, *Physical Review Materials*, Vol. 4, No. 1, p. 015602, 2020.

33. Tuncaboylu, D.C., M. Sari, W. Oppermann, and O. Okay, “Tough And Self-Healing Hydrogels Formed Via Hydrophobic Interactions.”, *Macromolecules*, Vol. 44, No. 12, pp. 4997–5005, 2011.

34. Mathur, A.M., S.K. Moorjani, and A.B. Scranton, “Methods For Synthesis Of

Hydrogel Networks: A Review.", *Journal of Macromolecular Science, Part C: Polymer Reviews*, Vol. 36, No. 2, pp. 405–430, 1996.

35. Macret, M., and G. Hild, "Hydroxyalkyl Methacrylates: Kinetic Investigations Of Radical Polymerizations Of Pure 2-Hydroxyethyl Methacrylate And 2, 3-Dihydroxypropyl Methacrylate And The Radical Copolymerization Of Their Mixtures.", *Polymer*, Vol. 23, No. 1, pp. 81–90, 1982.

36. Wu, X.S., A.S. Hoffman, and P. Yager, "Synthesis And Characterization Of Thermally Reversible Macroporous Poly(N-Isopropylacrylamide) Hydrogels.", *Journal of Polymer Science Part A: Polymer Chemistry*, Vol. 30, No. 10, pp. 2121–2129, 1992.

37. Andreopoulos, A.G., "Preparation And Swelling Of Polymeric Hydrogels.", *Journal of Applied Polymer Science*, Vol. 37, No. 8, pp. 2121–2129, 1989.

38. Kureha, T., K. Hayashi, M. Ohira, X. Li, and M. Shibayama, "Dynamic Fluctuations Of Thermoresponsive Poly(Oligo-Ethylene Glycol Methyl Ether Methacrylate)-Based Hydrogels Investigated By Dynamic Light Scattering.", *Macromolecules*, Vol. 51, No. 21, pp. 8932–8939, 2018.

39. Yigit, S., R. Sanyal, and A. Sanyal, "Fabrication And Functionalization Of Hydrogels Through 'Click' Chemistry.", *Chemistry – An Asian Journal*, Vol. 6, No. 10, pp. 2648–2659, 2011.

40. Nimmo, C.M., and M.S. Shoichet, "Regenerative Biomaterials That 'Click': Simple, Aqueous-Based Protocols For Hydrogel Synthesis, Surface Immobilization, And 3D Patterning.", *Bioconjugate Chemistry*, Vol. 22, No. 11, pp. 2199–2209, 2011.

41. DeForest, C.A., B.D. Polizzotti, and K.S. Anseth, "Sequential Click Reactions For Synthesizing And Patterning Three-Dimensional Cell Microenvironments.", *Nature Materials*, Vol. 8, No. 8, pp. 659–64, 2009.

42. Malkoch, M., R. Vestberg, N. Gupta, L. Mespouille, P. Dubois, A.F. Mason, J.L.

Hedrick, Q. Liao, C.W. Frank, K. Kingsbury, and C.J. Hawker, "Synthesis Of Well-Defined Hydrogel Networks Using Click Chemistry.", *Chemical Communications,* No. 26, pp. 2774–2776, 2006.

43. Ossipov, D. a., and J. Hilborn, "Poly(Vinyl Alcohol)-Based Hydrogels Formed By 'Click Chemistry.'", *Macromolecules*, Vol. 39, No. 5, pp. 1709–1718, 2006.

44. Clark, M., and P. Kiser, "In Situ Crosslinked Hydrogels Formed Using Cu(I)-Free Huisgen Cycloaddition Reaction.", *Polymer International*, Vol. 58, No. 10, pp. 1190–1195, 2009.

45. Gupta, N., B.F. Lin, L.M. Campos, M.D. Dimitriou, S.T. Hikita, N.D. Treat, M. V Tirrell, D.O. Clegg, E.J. Kramer, and C.J. Hawker, "A Versatile Approach To High-Throughput Microarrays Using Thiol-Ene Chemistry.", *Nature Chemistry*, Vol. 2, No. 2, pp. 138–145, 2010.

46. Campos, L.M., I. Meinel, R.G. Guino, M. Schierhorn, N. Gupta, G.D. Stucky, and C.J. Hawker, "Highly Versatile And Robust Materials For Soft Imprint Lithography Based On Thiol-Ene Click Chemistry.", *Advanced Materials*, Vol. 20, No. 19, pp. 3728–3733, 2008.

47. Chujo, Y., K. Sada, and T. Saegusa, "Reversible Gelation Of Polyoxazoline By Means Of Diels-Alder Reaction.", *Macromolecules*, Vol. 23, No. 10, pp. 2636–2641, 1990.

48. Gillette, J.R., "Factors Affecting Drug Metabolism.", *Annals of the New York Academy of Sciences*, Vol. 179, No. 1, pp. 43–66, 1971.

49. Altinbasak, I., R. Sanyal, and A. Sanyal, "Best Of Both Worlds: Diels–Alder Chemistry Towards Fabrication Of Redox-Responsive Degradable Hydrogels For Protein Release.", *RSC Advances*, Vol. 6, No. 78, pp. 74757–74764, 2016.

50. Patenaude, M., and T. Hoare, "Injectable, Degradable Thermoresponsive Poly(Nisopropylacrylamide) Hydrogels.", *ACS Macro Letters*, Vol. 1, No. 3, pp. 409–

413, 2012.

51. Gan, J., X.X. Guan, J. Zheng, H. Guo, K. Wu, L. Liang, and M. Lu, “Biodegradable, Thermoresponsive PNIPAM-Based Hydrogel Scaffolds For The Sustained Release Of Levofloxacin.”, *RSC Advances*, Vol. 6, No. 39, pp. 32967–32978, 2016.

52. Sun, S., and P. Wu, “A One-Step Strategy For Thermal- And PH-Responsive Graphene Oxide Interpenetrating Polymer Hydrogel Networks.”, *Journal of Materials Chemistry*, Vol. 21, No. 12, pp. 4095–4097, 2011.

53. Cong, Huai-Ping, Jia-Hua Qiu, Shu-Hong Yu, H.-P Cong, J.-H Qiu, and S.-H Yu, “Thermoresponsive Poly(N-Isopropylacrylamide)/Graphene/Au Nanocomposite Hydrogel For Water Treatment By A Laser-Assisted Approach.”, *Small*, Vol. 11, No. 9–10, pp. 1165–1170, 2015.

54. Rosselle, L., A.R. Cantelmo, A. Barras, N. Skandrani, M. Pastore, D. Aydin, L. Chambre, R. Sanyal, A. Sanyal, R. Boukherroub, and S. Szunerits, “An ‘On-Demand’ Photothermal Antibiotic Release Cryogel Patch: Evaluation Of Efficacy On An Ex Vivo Model For Skin Wound Infection.”, *Biomaterials Science*, Vol. 8, No. 21, pp. 5911–5919, 2020.

55. Teodorescu, F., Y. Oz, G. Quéniat, A. Abderrahmani, C. Foulon, M. Lecoeur, R. Sanyal, A. Sanyal, R. Boukherroub, and S. Szunerits, “Photothermally Triggered On-Demand Insulin Release From Reduced Graphene Oxide Modified Hydrogels.”, *Journal of Controlled Release*, Vol. 246, pp. 164–173, 2017.

56. Liu, W., X. Zhang, L. Zhou, L. Shang, and Z. Su, “Reduced Graphene Oxide (RGO) Hybridized Hydrogel As A Near-Infrared (NIR)/PH Dual-Responsive Platform For Combined Chemo-Photothermal Therapy.”, *Journal of Colloid and Interface Science*, Vol. 536, pp. 160–170, 2019.

57. Chambre, L., L. Rosselle, A. Barras, D. Aydin, A. Loczechin, S. Gunbay, R. Sanyal, N. Skandrani, N. Metzler-Nolte, J.E. Bandow, R. Boukherroub, S. Szunerits, and A.

Sanyal, “Photothermally Active Cryogel Devices For Effective Release Of Antimicrobial Peptides: On-Demand Treatment Of Infections.”, *ACS Applied Materials and Interfaces*, Vol. 12, No. 51, pp. 56805–56814, 2020.

58. Golba, B., O.I. Kalaoglu-Altan, R. Sanyal, and A. Sanyal, “Hydrophilic Cross-Linked Polymeric Nanofibers Using Electrospinning: Imparting Aqueous Stability To Enable Biomedical Applications.”, *ACS Applied Polymer Materials*, Vol. 4, No. 1, pp. 1–17, 2022.

59. Greiner, A., and J.H. Wendorff, “Electrospinning: A Fascinating Method For The Preparation Of Ultrathin Fibers.”, *Angewandte Chemie International Edition*, Vol. 46, No. 30, pp. 5670–5703, 2007.

60. Li, D., and Y. Xia, “Electrospinning Of Nanofibers: Reinventing The Wheel?”, *Advanced Materials*, Vol. 16, No. 14, pp. 1151–1170, 2004.

61. Liu, Yanbo, M. Hao, Z. Chen, L. Liu, Yao Liu, W. Yang, and S. Ramakrishna, “A Review On Recent Advances In Application Of Electrospun Nanofiber Materials As Biosensors.”, *Current Opinion in Biomedical Engineering*, Vol. 13, pp. 174–189, 2020.

62. Xu, Y., X. Li, H.-F. Xiang, Q.-Q. Zhang, X.-X. Wang, M. Yu, L.-Y. Hao, and Y.-Z. Long, “Large-Scale Preparation Of Polymer Nanofibers For Air Filtration By A New Multineedle Electrospinning Device.”, *Journal of Nanomaterials*, Vol. 2020, pp. 1–7, 2020.

63. Maver, T., M. Kurečič, T. Pivec, U. Maver, L. Gradišnik, P. Gašparič, B. Kaker, A. Bratuša, S. Hribernik, and K. Stana Kleinschek, “Needleless Electrospun Carboxymethyl Cellulose/Polyethylene Oxide Mats With Medicinal Plant Extracts For Advanced Wound Care Applications.”, *Cellulose*, Vol. 27, No. 8, pp. 4487–4508, 2020.

64. Hirsch, E., P. Vass, B. Démuth, Z. Pethő, E. Bitay, S.K. Andersen, T. Vigh, G.

Verreck, K. Molnár, Z.K. Nagy, and G. Marosi, “Electrospinning Scale-Up And Formulation Development Of PVA Nanofibers Aiming Oral Delivery Of Biopharmaceuticals.”, *Express Polymer Letters*, Vol. 13, No. 7, pp. 590–603, 2019.

65. Ogueri, K.S., and C.T. Laurencin, “Nanofiber Technology For Regenerative Engineering.”, *ACS Nano*, Vol. 14, No. 8, pp. 9347–9363, 2020.

66. Dos Santos, D.M., D.S. Correa, E.S. Medeiros, J.E. Oliveira, and L.H.C. Mattoso, “Advances In Functional Polymer Nanofibers: From Spinning Fabrication Techniques To Recent Biomedical Applications.”, *ACS Applied Materials & Interfaces*, Vol. 12, No. 41, pp. 45673–45701, 2020.

67. Boda, S.K., N.G. Fischer, Z. Ye, and C. Aparicio, “Dual Oral Tissue Adhesive Nanofiber Membranes For PH-Responsive Delivery Of Antimicrobial Peptides.”, *Biomacromolecules*, Vol. 21, No. 12, pp. 4945–4961, 2020.

68. Kalaoglu-Altan, O.I., R. Sanyal, and A. Sanyal, “Orthogonally ‘Clickable’ Biodegradable Nanofibers: Tailoring Biomaterials For Specific Protein Immobilization.”, *ACS Omega*, Vol. 4, No. 1, pp. 121–129, 2019.

69. Halicka, K., and J. Cabaj, “Electrospun Nanofibers For Sensing And Biosensing Applications—A Review.”, *International Journal of Molecular Sciences*, Vol. 22, No. 12, p. 6357, 2021.

70. Kalaoglu-Altan, O.I., R. Sanyal, and A. Sanyal, “Micropatterned Reactive Nanofibers: Facile Fabrication Of A Versatile Biofunctionalizable Interface.”, *ACS Applied Polymer Materials*, Vol. 2, No. 9, pp. 4026–4036, 2020.

71. Luraghi, A., F. Peri, and L. Moroni, “Electrospinning For Drug Delivery Applications: A Review.”, *Journal of Controlled Release*, Vol. 334, pp. 463–484, 2021.

72. Ghosal, K., R. Augustine, A. Zaszczynska, M. Barman, A. Jain, A. Hasan, N. Kalarikkal, P. Sajkiewicz, and S. Thomas, “Novel Drug Delivery Systems Based On

Triaxial Electrospinning Based Nanofibers.", *Reactive and Functional Polymers*, Vol. 163, p. 104895, 2021.

73. Sisson, K., C. Zhang, M.C. Farach-Carson, D.B. Chase, and J.F. Rabolt, "Evaluation Of Cross-Linking Methods For Electrospun Gelatin On Cell Growth And Viability.", *Biomacromolecules*, Vol. 10, No. 7, pp. 1675–1680, 2009.

74. Meng, L., W. Klinkajon, P.R. K-hasuwan, S. Harkin, P. Supaphol, and G.E. Wnek, "Electrospun Crosslinked Poly(Acrylic Acid) Fiber Constructs: Towards A Synthetic Model Of The Cortical Layer Of Nerve.", *Polymer International*, Vol. 64, No. 1, pp. 42–48, 2015.

75. Mofidfar, M., E.S. Kim, E.L. Larkin, L. Long, W.D. Jennings, S. Ahadian, M.A. Ghannoum, and G.E. Wnek, "Antimicrobial Activity Of Silver Containing Crosslinked Poly(Acrylic Acid) Fibers.", *Micromachines*, Vol. 10, No. 12, p. 829, 2019.

76. Zhang, S., Y. Huang, X. Yang, F. Mei, Q. Ma, G. Chen, S. Ryu, and X. Deng, "Gelatin Nanofibrous Membrane Fabricated By Electrospinning Of Aqueous Gelatin Solution For Guided Tissue Regeneration.", *Journal of Biomedical Materials Research Part A*, Vol. 90A, No. 3, pp. 671–679, 2009.

77. Li, M., Y. Guo, Y. Wei, A.G. MacDiarmid, and P.I. Lelkes, "Electrospinning Polyaniline-Contained Gelatin Nanofibers For Tissue Engineering Applications.", *Biomaterials*, Vol. 27, No. 13, pp. 2705–2715, 2006.

78. Ji, Y., K. Ghosh, X.Z. Shu, B. Li, J.C. Sokolov, G.D. Prestwich, R.A.F. Clark, and M.H. Rafailovich, "Electrospun Three-Dimensional Hyaluronic Acid Nanofibrous Scaffolds.", *Biomaterials*, Vol. 27, No. 20, pp. 3782–3792, 2006.

79. Kalaoglu-Altan, O.I., B. Verbraeken, K. Lava, T.N. Gevrek, R. Sanyal, T. Dargaville, K. De Clerck, R. Hoogenboom, and A. Sanyal, "Multireactive Poly(2-Oxazoline) Nanofibers Through Electrospinning With Crosslinking On The Fly.", *ACS Macro*

Letters, Vol. 5, No. 6, pp. 676–681, 2016.

80. Cao, S., B. Hu, and H. Liu, "Synthesis Of PH-Responsive Crosslinked Poly[Styrene-Co-(Maleic Sodium Anhydride)] And Cellulose Composite Hydrogel Nanofibers By Electrospinning.", *Polymer International*, Vol. 58, No. 5, pp. 545–551, 2009.

81. Rockwood, D.N., D.B. Chase, R.E. Akins, and J.F. Rabolt, "Characterization Of Electrospun Poly(N-Isopropyl Acrylamide) Fibers.", *Polymer*, Vol. 49, No. 18, pp. 4025–4032, 2008.

82. Wang, X., Y.G. Kim, C. Drew, B.C. Ku, J. Kumar, and L.A. Samuelson, "Electrostatic Assembly Of Conjugated Polymer Thin Layers On Electrospun Nanofibrous Membranes For Biosensors.", *Nano Letters*, Vol. 4, No. 2, pp. 331–334, 2004.

83. Linge Wang, B., Chengming Li, Anthony J Ryan, Steven P Armes, S P Armes, L. Wang, C Li, and A J Ryan, "Synthesis And Peptide-Induced Degradation Of Biocompatible Fibers Based On Highly Branched Poly(2-Hydroxyethyl Methacrylate).", *Advanced Materials*, Vol. 18, No. 12, pp. 1566–1570, 2006.

84. Cui, W., M. Qi, X. Li, S. Huang, S. Zhou, and J. Weng, "Electrospun Fibers Of Acid-Labile Biodegradable Polymers With Acetal Groups As Potential Drug Carriers.", *International Journal of Pharmaceutics*, Vol. 361, No. 1–2, pp. 47–55, 2008.

85. Alexander, C., "Temperature- And PH-Responsive Smart Polymers For Gene Delivery.", *Expert Opinion on Drug Delivery*, Vol. 3, No. 5, pp. 573–581, 2006.

86. Azerbaijan, M.H., E. Bahmani, M.H. Jouybari, A. Hassaniazardaryani, P. Goleij, M. Akrami, and M. Irani, "Electrospun Gold Nanorods/Graphene Oxide Loaded-Core-Shell Nanofibers For Local Delivery Of Paclitaxel Against Lung Cancer During Photo-Chemotherapy Method.", *European Journal of Pharmaceutical Sciences*, Vol. 164, 2021.

87. Jiang, Y., J. Chen, C. Deng, E.J. Suuronen, and Z. Zhong, "Click Hydrogels, Microgels

And Nanogels: Emerging Platforms For Drug Delivery And Tissue Engineering.", *Biomaterials*, Vol. 35, No. 18, pp. 4969–4985, 2014.

88. Oh, J.K., R. Drumright, D.J. Siegwart, and K. Matyjaszewski, "The Development Of Microgels/Nanogels For Drug Delivery Applications.", *Progress in Polymer Science*, Vol. 33, No. 4, pp. 448–477, 2008.

89. Neamtu, I., A.G. Rusu, A. Diaconu, L.E. Nita, and A.P. Chiriac, "Basic Concepts And Recent Advances In Nanogels As Carriers For Medical Applications.", *Drug Delivery*, Vol. 24, No. 1, pp. 539–557, 2017.

90. Mauri, E., G. Perale, and F. Rossi, "Nanogel Functionalization: A Versatile Approach To Meet The Challenges Of Drug And Gene Delivery.", *ACS Applied Nano Materials*, Vol. 1, No. 12, pp. 6525–6541, 2018.

91. Molina, M., M. Asadian-Birjand, J. Balach, J. Bergueiro, E. Miceli, and M. Calderón, "Stimuli-Responsive Nanogel Composites And Their Application In Nanomedicine.", *Chemical Society Reviews*, Vol. 44, No. 17, pp. 6161–6186, 2015.

92. Díaz-Moscoso, A., "Soft Versus Hard Nanoparticles In The Delivery Of Aromatic Macrocycles For Photodynamic Therapy Of Cancer.", *International Journal of Medicine and Biomedical Research*, Vol. 1, No. 1, pp. 12–23, 2012.

93. Latreille, P.-L., V. Adibnia, A. Nour, J.-M. Rabanel, A. Lalloz, J. Arlt, W.C.K. Poon, P. Hildgen, V.A. Martinez, and X. Banquy, "Spontaneous Shrinking Of Soft Nanoparticles Boosts Their Diffusion In Confined Media.", *Nature Communications*, Vol. 10, No. 1, p. 4294, 2019.

94. Rancan, F., M. Asadian-Birjand, S. Dogan, C. Graf, L. Cuellar, S. Lommatzsch, U. Blume-Peytavi, M. Calderón, and A. Vogt, "Effects Of Thermoresponsivity And Softness On Skin Penetration And Cellular Uptake Of Polyglycerol-Based Nanogels.", *Journal of Controlled Release*, Vol. 228, pp. 159–169, 2016.

95. Anselmo, A.C., M. Zhang, S. Kumar, D.R. Vogus, S. Menegatti, M.E. Helgeson, and S. Mitragotri, “Elasticity Of Nanoparticles Influences Their Blood Circulation, Phagocytosis, Endocytosis, And Targeting.”, *ACS Nano*, Vol. 9, No. 3, pp. 3169–3177, 2015.

96. Anselmo, A.C., and S. Mitragotri, “Impact Of Particle Elasticity On Particle-Based Drug Delivery Systems.”, *Advanced Drug Delivery Reviews*, Vol. 108, pp. 51–67, 2017.

97. Zhang, X., S. Malhotra, M. Molina, and R. Haag, “Micro- And Nanogels With Labile Crosslinks – From Synthesis To Biomedical Applications.”, *Chemical Society Reviews*, Vol. 44, No. 7, pp. 1948–1973, 2015.

98. Deen, G.R., and L.H. Gan, “Study Of Microemulsion Polymerization Conditions On The Preparation Of ‘Stimuli’ Responsive Copolymer Nanogels Of N-Acryloyl-N′-Methyl Piperazine And Methyl Methacrylate.”, *Journal of Dispersion Science and Technology*, Vol. 29, No. 3, pp. 431–435, 2008.

99. Raghupathi, K., S.J. Eron, F. Anson, J.A. Hardy, and S. Thayumanavan, “Utilizing Inverse Emulsion Polymerization To Generate Responsive Nanogels For Cytosolic Protein Delivery.”, *Molecular Pharmaceutics*, Vol. 14, No. 12, pp. 4515–4524, 2017.

100. Ryu, J.H., S. Jiwpanich, R. Chacko, S. Bickerton, and S. Thayumanavan, “Surface-Functionalizable Polymer Nanogels With Facile Hydrophobic Guest Encapsulation Capabilities.”, *Journal of the American Chemical Society*, Vol. 132, No. 24, pp. 8246–8247, 2010.

101. González-Toro, D.C., J.H. Ryu, R.T. Chacko, J. Zhuang, and S. Thayumanavan, “Concurrent Binding And Delivery Of Proteins And Lipophilic Small Molecules Using Polymeric Nanogels.”, *Journal of the American Chemical Society*, Vol. 134, No. 16, pp. 6964–6967, 2012.

102. Ryu, J.H., S. Bickerton, J. Zhuang, and S. Thayumanavan, “Ligand-Decorated

Nanogels: Fast One-Pot Synthesis And Cellular Targeting.", *Biomacromolecules*, Vol. 13, No. 5, pp. 1515–1522, 2012.

103. Ryu, J.-H., R.T. Chacko, S. Jiwpanich, S. Bickerton, R.P. Babu, and S. Thayumanavan, "Self-Cross-Linked Polymer Nanogels: A Versatile Nanoscopic Drug Delivery Platform.", *Journal of the American Chemical Society*, Vol. 132, No. 48, pp. 17227–17235, 2010.

104. Podgórna, K., K. Szczepanowicz, M. Piotrowski, M. Gajdošová, F. Štěpánek, and P. Warszyński, "Gadolinium Alginate Nanogels For Theranostic Applications.", *Colloids and Surfaces B: Biointerfaces*, Vol. 153, pp. 183–189, 2017.

105. Cao, X.T., H. Vu-Quang, V.D. Doan, and V.C. Nguyen, "One-Step Approach Of Dual-Responsive Prodrug Nanogels Via Diels-Alder Reaction For Drug Delivery.", *Colloid and Polymer Science*, Vol. 299, No. 4, pp. 675–683, 2021.

106. Kou, L., Y.D. Bhutia, Q. Yao, Z. He, J. Sun, and V. Ganapathy, "Transporter-Guided Delivery Of Nanoparticles To Improve Drug Permeation Across Cellular Barriers And Drug Exposure To Selective Cell Types.", *Frontiers in Pharmacology*, Vol. 9, p. 27, 2018.

107. Blanco, E., H. Shen, and M. Ferrari, "Principles Of Nanoparticle Design For Overcoming Biological Barriers To Drug Delivery.", *Nature Biotechnology*, Vol. 33, No. 9, pp. 941–951, 2015.

108. Mohan, P., and N. Rapoport, "Doxorubicin As A Molecular Nanotheranostic Agent: Effect Of Doxorubicin Encapsulation In Micelles Or Nanoemulsions On The Ultrasound-Mediated Intracellular Delivery And Nuclear Trafficking.", *Molecular Pharmaceutics*, Vol. 7, No. 6, pp. 1959–1973, 2010.

109. Eckmann, D.M., R.J. Composto, A. Tsourkas, and V.R. Muzykantov, "Nanogel Carrier Design For Targeted Drug Delivery.", *Journal of Materials Chemistry B*, Vol. 2, No. 46, pp. 8085–8097, 2014.

110. Fadeel, B., “Hide And Seek: Nanomaterial Interactions With The Immune System.”, *Frontiers in Immunology*, Vol. 10, p. 133, 2019.

111. Mitragotri, S., T. Lammers, Y.H. Bae, S. Schwendeman, S. De Smedt, J.-C. Leroux, D. Peer, I.C. Kwon, H. Harashima, A. Kikuchi, Y.-K. Oh, V. Torchilin, W. Hennink, J. Hanes, and K. Park, “Drug Delivery Research For The Future: Expanding The Nano Horizons And Beyond.”, *Journal of Controlled Release*, Vol. 246, pp. 183–184, 2017.

112. Movassaghian, S., O.M. Merkel, and V.P. Torchilin, “Applications Of Polymer Micelles For Imaging And Drug Delivery.”, *Wiley Interdisciplinary Reviews: Nanomedicine and Nanobiotechnology*, Vol. 7, No. 5, pp. 691–707, 2015.

113. Croy, S.R., and G.S. Kwon, “Polymeric Micelles For Drug Delivery.”, *Current Pharmaceutical Design*, Vol. 12, No. 36, pp. 4669–4684, 2006.

114. Gong, J., M. Chen, Y. Zheng, S. Wang, and Y. Wang, “Polymeric Micelles Drug Delivery System In Oncology.”, *Journal of Controlled Release*, Vol. 159, No. 3, pp. 312–323, 2012.

115. Mikhail, A.S., and C. Allen, “Block Copolymer Micelles For Delivery Of Cancer Therapy: Transport At The Whole Body, Tissue And Cellular Levels.”, *Journal of Controlled Release*, Vol. 138, No. 3, pp. 214–223, 2009.

116. Kedar, U., P. Phutane, S. Shidhaye, and V. Kadam, “Advances In Polymeric Micelles For Drug Delivery And Tumor Targeting.”, *Nanomedicine: Nanotechnology, Biology and Medicine*, Vol. 6, No. 6, pp. 714–729, 2010.

117. Espelin, C.W., S.C. Leonard, E. Geretti, T.J. Wickham, and B.S. Hendriks, “Dual HER2 Targeting With Trastuzumab And Liposomal-Encapsulated Doxorubicin (MM-302) Demonstrates Synergistic Antitumor Activity In Breast And Gastric Cancer.”, *Cancer Research*, Vol. 76, No. 6, pp. 1517–1527, 2016.

118. Valabrega, G., F. Montemurro, and M. Aglietta, “Trastuzumab: Mechanism Of

Action, Resistance And Future Perspectives In HER2-Overexpressing Breast Cancer.", *Annals of Oncology*, Vol. 18, No. 6, pp. 977–984, 2007.

119. Sumer Bolu, B., B. Golba, A. Sanyal, and R. Sanyal, "Trastuzumab Targeted Micellar Delivery Of Docetaxel Using Dendron–Polymer Conjugates.", *Biomaterials Science*, Vol. 8, No. 9, pp. 2600–2610, 2020.

120. Pfaff, M., K. Tangemann, B. Müller, M. Gurrath, G. Müller, H. Kessler, R. Timpl, and J. Engel, "Selective Recognition Of Cyclic RGD Peptides Of NMR Defined Conformation By Alpha IIb Beta 3, Alpha V Beta 3, And Alpha 5 Beta 1 Integrins.", *Journal of Biological Chemistry*, Vol. 269, No. 32, pp. 20233–20238, 1994.

121. Mondal, G., S. Barui, and A. Chaudhuri, "The Relationship Between The Cyclic-RGDfK Ligand And Avβ3 Integrin Receptor.", *Biomaterials*, Vol. 34, No. 26, pp. 6249–6260, 2013.

122. Zhou, D., G. Zhang, and Z. Gan, "C(RGDfK) Decorated Micellar Drug Delivery System For Intravesical Instilled Chemotherapy Of Superficial Bladder Cancer.", *Journal of Controlled Release*, Vol. 169, No. 3, pp. 204–210, 2013.

123. Calik, F., A. Degirmenci, M. Eceoglu, A. Sanyal, and R. Sanyal, "Dendron-Polymer Conjugate Based Cross-Linked Micelles: A Robust And Versatile Nanosystem For Targeted Delivery.", *Bioconjugate Chemistry*, Vol. 30, No. 4, pp. 1087–1097, 2019.

124. Takahashi, A., Y. Yamamoto, M. Yasunaga, Y. Koga, J.I. Kuroda, M. Takigahira, M. Harada, H. Saito, T. Hayashi, Y. Kato, T. Kinoshita, N. Ohkohchi, I. Hyodo, and Y. Matsumura, "NC-6300, An Epirubicin-Incorporating Micelle, Extends The Antitumor Effect And Reduces The Cardiotoxicity Of Epirubicin.", *Cancer Science*, Vol. 104, No. 7, pp. 920–925, 2013.

125. Zhang, S., J. Zou, M. Elsabahy, A. Karwa, A. Li, D.A. Moore, R.B. Dorshow, and K.L. Wooley, "Poly(Ethylene Oxide)-Block-Polyphosphester-Based Paclitaxel Conjugates As A Platform For Ultra-High Paclitaxel-Loaded Multifunctional

Nanoparticles.", *Chemical Science*, Vol. 4, No. 5, pp. 2122–2126, 2013.

126. Vetvicka, D., M. Hruby, O. Hovorka, T. Etrych, M. Vetrik, L. Kovar, M. Kovar, K. Ulbrich, and B. Rihova, "Biological Evaluation Of Polymeric Micelles With Covalently Bound Doxorubicin.", *Bioconjugate Chemistry*, Vol. 20, No. 11, pp. 2090–2097, 2009.

127. Rao N, V., M.N. Ganivada, S. Sarkar, H. Dinda, K. Chatterjee, T. Dalui, J. Das Sarma, and R. Shunmugam, "Magnetic Norbornene Polymer As Multiresponsive Nanocarrier For Site Specific Cancer Therapy.", *Bioconjugate Chemistry*, Vol. 25, No. 2, pp. 276–285, 2014.

128. Vijayakameswara Rao, V., S.R. Mane, A. Kishore, J. Das Sarma, and R. Shunmugam, "Norbornene Derived Doxorubicin Copolymers As Drug Carriers With PH Responsive Hydrazone Linker.", *Biomacromolecules*, Vol. 13, No. 1, pp. 221–230, 2012.

129. Altinbasak, I., R. Jijie, A. Barras, B. Golba, R. Sanyal, J. Bouckaert, D. Drider, R. Bilyy, T. Dumych, S. Paryzhak, V. Vovk, R. Boukherroub, A. Sanyal, and S. Szunerits, "Reduced Graphene-Oxide-Embedded Polymeric Nanofiber Mats: An 'On-Demand' Photothermally Triggered Antibiotic Release Platform.", *ACS Applied Materials & Interfaces*, Vol. 10, No. 48, pp. 41098–41106, 2018.

130. GuhaSarkar, S., and R. Banerjee, "Intravesical Drug Delivery: Challenges, Current Status, Opportunities And Novel Strategies.", *Journal of Controlled Release*, Vol. 148, No. 2, pp. 147–159, 2010.

131. Liu, D., F. Yang, F. Xiong, and N. Gu, "The Smart Drug Delivery System And Its Clinical Potential.", *Theranostics*, Vol. 6, No. 9, pp. 1306, 2016.

132. Tiwari, G., R. Tiwari, B. Sriwastawa, L. Bhati, S. Pandey, P. Pandey, and S.K. Bannerjee, "Drug Delivery Systems: An Updated Review.", *International Journal of Pharmaceutical Investigation*, Vol. 2, No. 1, p. 2, 2012.

133. Szunerits, S., F. Teodorescu, and R. Boukherroub, “Electrochemically Triggered Release Of Drugs.”, *European Polymer Journal*, Vol. 83, pp. 467–477, 2016.

134. Ganta, S., H. Devalapally, A. Shahiwala, and M. Amiji, “A Review Of Stimuli-Responsive Nanocarriers For Drug And Gene Delivery.”, *Journal of Controlled Release*, Vol. 126, No. 3, pp. 187–204, 2008.

135. Kamaly, N., B. Yameen, J. Wu, and O.C. Farokhzad, “Degradable Controlled-Release Polymers And Polymeric Nanoparticles: Mechanisms Of Controlling Drug Release.”, *Chemical Reviews*, Vol. 116, No. 4, pp. 2602–2663, 2016.

136. Karimi, M., P. Sahandi Zangabad, Alireza Ghasemi, M. Amiri, M. Bahrami, H. Malekzad, H. Ghahramanzadeh Asl, Z. Mahdieh, M. Bozorgomid, Amir Ghasemi, M.R. Rahmani Taji Boyuk, and M.R. Hamblin, “Temperature-Responsive Smart Nanocarriers For Delivery Of Therapeutic Agents: Applications And Recent Advances.”, *ACS Applied Materials and Interfaces*, Vol. 8, No. 33, pp. 21107–21133, 2016.

137. Li, Y., G. Liu, X. Wang, J. Hu, and S. Liu, “Enzyme-Responsive Polymeric Vesicles For Bacterial-Strain-Selective Delivery Of Antimicrobial Agents.”, *Angewandte Chemie International Edition*, Vol. 55, No. 5, pp. 1760–1764, 2016.

138. Weng, L., and J. Xie, “Smart Electrospun Nanofibers For Controlled Drug Release: Recent Advances And New Perspectives.”, *Current Pharmaceutical Design*, Vol. 21, No. 15, pp. 1944–1959, 2015.

139. Muñoz-Bonilla, A., and M. Fernández-García, “Polymeric Materials With Antimicrobial Activity.”, *Progress in Polymer Science*, Vol. 37, No. 2, pp. 281–339, 2012.

140. Xiong, M.H., Y. Bao, X.Z. Yang, Y.H. Zhu, and J. Wang, “Delivery Of Antibiotics With Polymeric Particles.”, *Advanced Drug Delivery Reviews*, Vol. 78, pp. 63–76, 2014.

141. Chiang, W.L., T.T. Lin, R. Sureshbabu, W.T. Chia, H.C. Hsiao, H.Y. Liu, C.M. Yang, and H.W. Sung, “A Rapid Drug Release System With A NIR Light-Activated Molecular Switch For Dual-Modality Photothermal/Antibiotic Treatments Of Subcutaneous Abscesses.”, *Journal of Controlled Release*, Vol. 199, pp. 53–62, 2015.

142. Stebbins, N.D., M.A. Ouimet, and K.E. Uhrich, “Antibiotic-Containing Polymers For Localized, Sustained Drug Delivery.”, *Advanced Drug Delivery Reviews*, Vol. 78, pp. 77–87, 2014.

143. Ng, V.W.L., J.M.W. Chan, H. Sardon, R.J. Ono, J.M. García, Y.Y. Yang, and J.L. Hedrick, “Antimicrobial Hydrogels: A New Weapon In The Arsenal Against Multidrug-Resistant Infections.”, *Advanced Drug Delivery Reviews*, Vol. 78, pp. 46–62, 2014.

144. Gustafson, C.T., F. Boakye-Agyeman, C.L. Brinkman, J.M. Reid, R. Patel, Z. Bajzer, M. Dadsetan, and M.J. Yaszemski, “Controlled Delivery Of Vancomycin Via Charged Hydrogels.”, *Public Library of Science ONE*, Vol. 11, No. 1, p. e0146401, 2016.

145. Pritchard, E.M., T. Valentin, B. Panilaitis, F. Omenetto, and D.L. Kaplan, “Antibiotic-Releasing Silk Biomaterials For Infection Prevention And Treatment.”, *Advanced Functional Materials*, Vol. 23, No. 7, pp. 854–861, 2013.

146. Wang, C., G. Zhang, G. Liu, J. Hu, and S. Liu, “Photo- And Thermo-Responsive Multicompartment Hydrogels For Synergistic Delivery Of Gemcitabine And Doxorubicin.”, *Journal of Controlled Release*, Vol. 259, pp. 149–159, 2017.

147. Khanal, A., and K. Nakashima, “Incorporation And Release Of Cloxacillin Sodium In Micelles Of Poly(Styrene-B-2-Vinyl Pyridine-B-Ethylene Oxide).”, *Journal of Controlled Release*, Vol. 108, No. 1, pp. 150–160, 2005.

148. Coll Ferrer, M.C., S. Dastgheyb, N.J. Hickok, D.M. Eckmann, and R.J. Composto, “Designing Nanogel Carriers For Antibacterial Applications.”, *Acta Biomaterialia*, Vol. 10, No. 5, pp. 2105–2111, 2014.

149. Forier, K., K. Raemdonck, S.C. De Smedt, J. Demeester, T. Coenye, and K. Braeckmans, “Lipid And Polymer Nanoparticles For Drug Delivery To Bacterial Biofilms.”, *Journal of Controlled Release*, Vol. 190, pp. 607–623, 2014.

150. Calamak, S., R. Shahbazi, I. Eroglu, M. Gultekinoglu, and K. Ulubayram, “An Overview Of Nanofiber-Based Antibacterial Drug Design.”, *Expert Opinion on Drug Discovery*, Vol. 12, No. 4, pp. 391–406, 2017.

151. Frykberg, R.G., and J. Banks, “Challenges In The Treatment Of Chronic Wounds.”, *Advances in Wound Care*, Vol. 4, No. 9, pp. 560–582, 2015.

152. Han, G., and R. Ceilley, “Chronic Wound Healing: A Review Of Current Management And Treatments.”, *Advances in Therapy*, Vol. 34, No. 3, pp. 599–610, 2017.

153. Warriner, R., and R. Burrell, “Infection And The Chronic Wound: A Focus On Silver.”, *Advances in Skin & Wound Care*, Vol. 18 Suppl 1, pp. 2–12, 2005.

154. Draelos, Z.D., R.L. Rizer, and N.S. Trookman, “A Comparison Of Postprocedural Wound Care Treatments: Do Antibiotic-Based Ointments Improve Outcomes?”, *Journal of the American Academy of Dermatology*, Vol. 64, No. 3, pp. S23–S29, 2011.

155. Kalaoglu Altan, O.I., R. Sanyal, and A. Sanyal, “Reactive And ‘clickable’ Electrospun Polymeric Nanofibers.”, *Polymer Chemistry*, Vol. 6, No. 18, pp. 3372–3381, 2015.

156. Teo, W.E., and S. Ramakrishna, “A Review On Electrospinning Design And Nanofibre Assemblies.”, *Nanotechnology*, Vol. 17, No. 14, p. R89, 2006.

157. Agarwal, S., J.H. Wendorff, and A. Greiner, “Use Of Electrospinning Technique For Biomedical Applications.”, *Polymer*, Vol. 49, No. 26, pp. 5603–5621, 2008.

158. Qi, R., R. Guo, F. Zheng, H. Liu, J. Yu, and X. Shi, “Controlled Release And Antibacterial Activity Of Antibiotic-Loaded Electrospun Halloysite/Poly(Lactic-Co-Glycolic Acid) Composite Nanofibers.”, *Colloids and Surfaces B: Biointerfaces*, Vol.

110, pp. 148–155, 2013.

159. Kim, K., Y.K. Luu, C. Chang, D. Fang, B.S. Hsiao, B. Chu, and M. Hadjiargyrou, “Incorporation And Controlled Release Of A Hydrophilic Antibiotic Using Poly(Lactide-Co-Glycolide)-Based Electrospun Nanofibrous Scaffolds.”, *Journal of Controlled Release*, Vol. 98, No. 1, pp. 47–56, 2004.

160. Son, Y.J., Y. Kim, W.J. Kim, S.Y. Jeong, and H.S. Yoo, “Antibacterial Nanofibrous Mats Composed Of Eudragit For PH-Dependent Dissolution.”, *Journal of Pharmaceutical Sciences*, Vol. 104, No. 8, pp. 2611–2618, 2015.

161. Demirci, S., A. Celebioglu, Z. Aytac, and T. Uyar, “PH-Responsive Nanofibers With Controlled Drug Release Properties.”, *Polymer Chemistry*, Vol. 5, No. 6, pp. 2050–2056, 2014.

162. Cheng, M., H. Wang, Z. Zhang, N. Li, X. Fang, and S. Xu, “Gold Nanorod-Embedded Electrospun Fibrous Membrane As A Photothermal Therapy Platform.”, *ACS Applied Materials and Interfaces*, Vol. 6, No. 3, pp. 1569–1575, 2014.

163. Maity, S., W.C. Wu, C. Xu, J.B. Tracy, K. Gundogdu, J.R. Bochinski, and L.I. Clarke, “Spatial Temperature Mapping Within Polymer Nanocomposites Undergoing Ultrafast Photothermal Heating Via Gold Nanorods.”, *Nanoscale*, Vol. 6, No. 24, pp. 15236–15247, 2014.

164. Chen, L., L. Si, F. Wu, S.Y. Chan, P. Yu, and B. Fei, “Electrical And Mechanical Self-Healing Membrane Using Gold Nanoparticles As Localized ‘Nano-Heaters.’”, *Journal of Materials Chemistry C*, Vol. 4, No. 42, pp. 10018–10025, 2016.

165. Zhang, Z., S. Liu, H. Xiong, X. Jing, Z. Xie, X. Chen, and Y. Huang, “Electrospun PLA/MWCNTs Composite Nanofibers For Combined Chemo- And Photothermal Therapy.”, *Acta Biomaterialia*, Vol. 26, pp. 115–123, 2015.

166. Zhang, J., T. Zheng, E. Alarçin, B. Byambaa, X. Guan, J. Ding, Y.S. Zhang, and Z.

Li, “Porous Electrospun Fibers With Self-Sealing Functionality: An Enabling Strategy For Trapping Biomacromolecules.”, *Small*, Vol. 13, No. 47, p. 1701949, 2017.

167. Li, Y., Y. Fu, Z. Ren, X. Li, C. Mao, and G. Han, “Enhanced Cell Uptake Of Fluorescent Drug-Loaded Nanoparticles Via An Implantable Photothermal Fibrous Patch For More Effective Cancer Cell Killing.”, *Journal of Materials Chemistry B*, Vol. 5, No. 36, pp. 7504–7511, 2017.

168. Wang, X., F. Lv, T. Li, Y. Han, Z. Yi, M. Liu, J. Chang, and C. Wu, “Electrospun Micropatterned Nanocomposites Incorporated With Cu2S Nanoflowers For Skin Tumor Therapy And Wound Healing.”, *ACS Nano*, Vol. 11, No. 11, pp. 11337–11349, 2017.

169. Qi, K., J. He, H. Wang, Y. Zhou, X. You, N. Nan, W. Shao, L. Wang, B. Ding, and S. Cui, “A Highly Stretchable Nanofiber-Based Electronic Skin With Pressure-, Strain-, And Flexion-Sensitive Properties For Health And Motion Monitoring.”, *ACS Applied Materials and Interfaces*, Vol. 9, No. 49, pp. 42951–42960, 2017.

170. Luo, Y., H. Shen, Y. Fang, Y. Cao, J. Huang, M. Zhang, J. Dai, X. Shi, and Z. Zhang, “Enhanced Proliferation And Osteogenic Differentiation Of Mesenchymal Stem Cells On Graphene Oxide-Incorporated Electrospun Poly(Lactic-Co-Glycolic Acid) Nanofibrous Mats.”, *ACS Applied Materials and Interfaces*, Vol. 7, No. 11, pp. 6331–6339, 2015.

171. Wang, S.D., Q. Ma, K. Wang, and H.W. Chen, “Improving Antibacterial Activity And Biocompatibility Of Bioinspired Electrospinning Silk Fibroin Nanofibers Modified By Graphene Oxide.”, *ACS Omega*, Vol. 3, No. 1, pp. 406–413, 2017.

172. Shao, W., J. He, Q. Wang, S. Cui, and B. Ding, “Biomineralized Poly(L -Lactic-Co-Glycolic Acid)/Graphene Oxide/Tussah Silk Fibroin Nanofiber Scaffolds With Multiple Orthogonal Layers Enhance Osteoblastic Differentiation Of Mesenchymal Stem Cells.”, *ACS Biomaterials Science and Engineering*, Vol. 3, No. 7, pp. 1370–1380, 2017.

173. Mauro, N., C. Scialabba, G. Pitarresi, and G. Giammona, “Enhanced Adhesion And In Situ Photothermal Ablation Of Cancer Cells In Surface-Functionalized Electrospun Microfiber Scaffold With Graphene Oxide.”, *International Journal of Pharmaceutics*, Vol. 526, No. 1–2, pp. 167–177, 2017.

174. Gentry, L. O, G. Rodriguez-Gomez, H. Mexico, S. Jose, and C. Rica, “Randomized Comparison Of Cefepime And Ceftazidime For Treatment Of Skin, Surgical Wound, And Complicated Urinary Tract Infections In Hospitalized Subjects.”, *Antimicrobial Agents and Chemotherapy*, Vol. 35, No. 11, pp. 2371–2374, 1991.

175. Li, C., R. Ye, J. Bouckaert, A. Zurutuza, D. Drider, T. Dumych, S. Paryzhak, V. Vovk, R.O. Bilyy, S. Melinte, M. Li, R. Boukherroub, and S. Szunerits, “Flexible Nanoholey Patches For Antibiotic-Free Treatments Of Skin Infections.”, *ACS Applied Materials and Interfaces*, Vol. 9, No. 42, pp. 36665–36674, 2017.

176. Teodorescu, F., Y. Oz, G. Quéniat, A. Abderrahmani, C. Foulon, M. Lecoeur, R. Sanyal, A. Sanyal, R. Boukherroub, and S. Szunerits, “Photothermally Triggered On-Demand Insulin Release From Reduced Graphene Oxide Modified Hydrogels.”, *Journal of Controlled Release*, Vol. 246, pp. 164–173, 2017.

177. Boulahneche, S., R. Jijie, A. Barras, F. Chekin, S.K. Singh, J. Bouckaert, M.S. Medjram, S. Kurungot, R. Boukherroub, and S. Szunerits, “On Demand Electrochemical Release Of Drugs From Porous Reduced Graphene Oxide Modified Flexible Electrodes.”, *Journal of Materials Chemistry B*, Vol. 5, No. 32, pp. 6557–6565, 2017.

178. Koenig, J.L., and A.C. Angood, “Raman Spectra Of Poly(Ethylene Glycols) In Solution.”, *Journal of Polymer Science Part A-2: Polymer Physics*, Vol. 8, No. 10, pp. 1787–1796, 1970.

179. Li, L., and Y. Lo Hsieh, “Ultra-Fine Polyelectrolyte Fibers From Electrospinning Of Poly(Acrylic Acid).”, *Polymer*, Vol. 46, No. 14, pp. 5133–5139, 2005.

180. Wiśniewska, M., T. Urban, E. Grządka, V.I. Zarko, and V.M. Gun'ko, "Comparison Of Adsorption Affinity Of Polyacrylic Acid For Surfaces Of Mixed Silica–Alumina.", *Colloid and Polymer Science*, Vol. 292, No. 3, p. 699, 2014.

181. Mölne, L., and A. Tarkowski, "An Experimental Model Of Cutaneous Infection Induced By Superantigen-Producing Staphylococcus Aureus.", *Journal of Investigative Dermatology*, Vol. 114, No. 6, pp. 1120–1125, 2000.

182. Dai, T., G.P. Tegos, T. Zhiyentayev, E. Mylonakis, and M.R. Hamblin, "Photodynamic Therapy For Methicillin-Resistant Staphylococcus Aureus Infection In A Mouse Skin Abrasion Model.", *Lasers in Surgery and Medicine*, Vol. 42, No. 1, pp. 38–44, 2010.

183. Kugelberg, E., T. Norström, T.K. Petersen, T. Duvold, D.I. Andersson, and D. Hughes, "Establishment Of A Superficial Skin Infection Model In Mice By Using Staphylococcus Aureus And Streptococcus Pyogenes.", *Antimicrobial Agents and Chemotherapy*, Vol. 49, No. 8, pp. 3435–3441, 2005.

184. Altinbasak, I., S. Kocak, A.H. Colby, Y. Alp, R. Sanyal, M.W. Grinstaff, and A. Sanyal, "PH-Responsive Nanofiber Buttresses As Local Drug Delivery Devices.", *Biomaterials Science,* Advanced Article, 2022.

185. Hoffman, A.S., "Stimuli-Responsive Polymers: Biomedical Applications And Challenges For Clinical Translation.", *Advanced Drug Delivery Reviews*, Vol. 65, No. 1, pp. 10–16, 2013.

186. Roy, D., J.N. Cambre, and B.S. Sumerlin, "Future Perspectives And Recent Advances In Stimuli-Responsive Materials.", *Progress in Polymer Science*, Vol. 35, No. 1–2, pp. 278–301, 2010.

187. Kakkar, A., G. Traverso, O.C. Farokhzad, R. Weissleder, and R. Langer, "Evolution Of Macromolecular Complexity In Drug Delivery Systems.", *Nature Reviews Chemistry*, Vol. 1, No. 8, pp. 0063, 2017.

188. Dong, X., R.K. Brahma, C. Fang, and S.Q. Yao, “Stimulus-Responsive Self-Assembled Prodrugs In Cancer Therapy.”, *Chemical Science*, Vol. 13, No. 15, pp. 4239–4269, 2022.

189. Falde, E.J., S.T. Yohe, Y.L. Colson, and M.W. Grinstaff, “Superhydrophobic Materials For Biomedical Applications.”, *Biomaterials*, Vol. 104, pp. 87–103, 2016.

190. Jochum, F.D., and P. Theato, “Temperature- And Light-Responsive Smart Polymer Materials.”, *Chemical Society Reviews*, Vol. 42, No. 17, pp. 7468–7483, 2013.

191. Chambre, L., L. Rosselle, A. Barras, D. Aydin, A. Loczechin, S. Gunbay, R. Sanyal, N. Skandrani, N. Metzler-Nolte, J.E. Bandow, R. Boukherroub, S. Szunerits, and A. Sanyal, “Photothermally Active Cryogel Devices For Effective Release Of Antimicrobial Peptides: On-Demand Treatment Of Infections.”, *ACS Applied Materials and Interfaces*, Vol. 12, No. 51, pp. 56805–56814, 2020.

192. Rosselle, L., A.R. Cantelmo, A. Barras, N. Skandrani, M. Pastore, D. Aydin, L. Chambre, R. Sanyal, A. Sanyal, R. Boukherroub, and S. Szunerits, “An ‘On-Demand’ Photothermal Antibiotic Release Cryogel Patch: Evaluation Of Efficacy On An Ex Vivo Model For Skin Wound Infection.”, *Biomaterials Science*, Vol. 8, No. 21, pp. 5911–5919, 2020.

193. Kotsuchibashi, Y., “Recent Advances In Multi-Temperature-Responsive Polymeric Materials.”, *Polymer Journal*, Vol. 52, No. 7, pp. 681–689, 2020.

194. Tang, H., W. Zhao, J. Yu, Y. Li, and C. Zhao, “Recent Development Of PH-Responsive Polymers For Cancer Nanomedicine.”, *Molecules*, Vol. 24, No. 1, p. 4, 2018.

195. Thévenot, J., H. Oliveira, O. Sandre, and S. Lecommandoux, “Magnetic Responsive Polymer Composite Materials.”, *Chemical Society Reviews*, Vol. 42, No. 17, p. 7099, 2013.

196. Huo, M., J. Yuan, L. Tao, and Y. Wei, “Redox-Responsive Polymers For Drug Delivery: From Molecular Design To Applications.”, *Polymer Chemistry*, Vol. 5, No. 5, pp. 1519–1528, 2014.

197. Arslan, M., R. Sanyal, and A. Sanyal, “Thiol-Reactive Thiosulfonate Group Containing Copolymers: Facile Entry To Disulfide-Mediated Polymer Conjugation And Redox-Responsive Functionalizable Networks.”, *Polymer Chemistry*, Vol. 11, No. 10, pp. 1763–1773, 2020.

198. Ojugo, A.S.E., P.M.J. McSheehy, D.J.O. McIntyre, C. McCoy, M. Stubbs, M.O. Leach, I.R. Judson, and J.R. Griffiths, “Measurement Of The Extracellular PH Of Solid Tumours In Mice By Magnetic Resonance Spectroscopy: A Comparison Of Exogenous 19F And 31P Probes.”, *NMR in Biomedicine*, Vol. 12, No. 8, pp. 495–504, 1999.

199. Zhang, X., Y. Lin, and R.J. Gillies, “Tumor PH And Its Measurement.”, *Journal of Nuclear Medicine*, Vol. 51, No. 8, pp. 1167–1170, 2010.

200. Estrella, V., T. Chen, M. Lloyd, J. Wojtkowiak, H.H. Cornnell, A. Ibrahim-Hashim, K. Bailey, Y. Balagurunathan, J.M. Rothberg, B.F. Sloane, J. Johnson, R.A. Gatenby, and R.J. Gillies, “Acidity Generated By The Tumor Microenvironment Drives Local Invasion.”, *Cancer Research*, Vol. 73, No. 5, pp. 1524–1535, 2013.

201. Som, A., S. Bloch, J.E. Ippolito, and S. Achilefu, “Acidic Extracellular PH Of Tumors Induces Octamer-Binding Transcription Factor 4 Expression In Murine Fibroblasts In Vitro And In Vivo.”, *Scientific Reports*, Vol. 6, No. 1, p. 27803, 2016.

202. Kumar, A., C. Montemagno, and H.-J. Choi, “Smart Microparticles With A PH-Responsive Macropore For Targeted Oral Drug Delivery.”, *Scientific Reports*, Vol. 7, No. 1, p. 3059, 2017.

203. Gao, W., J.M. Chan, and O.C. Farokhzad, “PH-Responsive Nanoparticles For Drug Delivery.”, *Molecular Pharmaceutics*, Vol. 7, No. 6, pp. 1913–1920, 2010.

204. Kilic, R., and A. Sanyal, “Self-Healing Hydrogels Based On Reversible Covalent Linkages: A Survey Of Dynamic Chemical Bonds In Network Formation.”, *Advances in Polymer Science*, Vol. 285, pp. 243–294, 2020.

205. Aydin, D., M. Arslan, A. Sanyal, and R. Sanyal, “Hooked On Cryogels: A Carbamate Linker Based Depot For Slow Drug Release.”, *Bioconjugate Chemistry*, Vol. 28, No. 5, pp. 1443–1451, 2017.

206. Mendes, P.M., “Stimuli-Responsive Surfaces For Bio-Applications.”, *Chemical Society Reviews*, Vol. 37, No. 11, p. 2512, 2008.

207. Schoeller, J., F. Itel, K. Wuertz-Kozak, G. Fortunato, and R.M. Rossi, “PH-Responsive Electrospun Nanofibers And Their Applications.”, *Polymer Reviews*, Vol. 62, No. 2, pp. 351–399, 2022.

208. Qi, Y., H. Min, A. Mujeeb, Y. Zhang, X. Han, X. Zhao, G.J. Anderson, Y. Zhao, and G. Nie, “Injectable Hexapeptide Hydrogel For Localized Chemotherapy Prevents Breast Cancer Recurrence.”, *ACS Applied Materials and Interfaces*, Vol. 10, No. 8, pp. 6972–6981, 2018.

209. Kaplan, J.A., R. Liu, J.D. Freedman, R. Padera, J. Schwartz, Y.L. Colson, and M.W. Grinstaff, “Prevention Of Lung Cancer Recurrence Using Cisplatin-Loaded Superhydrophobic Nanofiber Meshes.”, *Biomaterials*, Vol. 76, pp. 273–281, 2016.

210. Zhang, Z., S. Liu, Y. Qi, D. Zhou, Z. Xie, X. Jing, X. Chen, and Y. Huang, “Time-Programmed DCA And Oxaliplatin Release By Multilayered Nanofiber Mats In Prevention Of Local Cancer Recurrence Following Surgery.”, *Journal of Controlled Release*, Vol. 235, pp. 125–133, 2016.

211. Kalaoglu-Altan, O.I., R. Sanyal, and A. Sanyal, “‘Clickable’ Polymeric Nanofibers Through Hydrophilic-Hydrophobic Balance: Fabrication Of Robust Biomolecular Immobilization Platforms.”, *Biomacromolecules*, Vol. 16, No. 5, pp. 1590–1597, 2015.

212. Zhou, F.-L., R.-H. Gong, and I. Porat, “Mass Production Of Nanofibre Assemblies By Electrostatic Spinning.”, *Polymer International*, Vol. 58, No. 4, pp. 331–342, 2009.

213. Persano, L., A. Camposeo, C. Tekmen, and D. Pisignano, “Industrial Upscaling Of Electrospinning And Applications Of Polymer Nanofibers: A Review.”, *Macromolecular Materials and Engineering*, Vol. 298, No. 5, pp. 504–520, 2013.

214. Hu, J., H.-Y. Li, G.R. Williams, H.-H. Yang, L. Tao, and L.-M. Zhu, “Electrospun Poly(N-Isopropylacrylamide)/Ethyl Cellulose Nanofibers As Thermoresponsive Drug Delivery Systems.”, *Journal of Pharmaceutical Sciences*, Vol. 105, No. 3, pp. 1104–1112, 2016.

215. Demirci, S., A. Celebioglu, Z. Aytac, and T. Uyar, “pH-Responsive Nanofibers With Controlled Drug Release Properties.”, *Polymer Chemistry*, Vol. 5, No. 6, pp. 2050–2056, 2014.

216. Altinbasak, I., R. Jijie, A. Barras, B. Golba, R. Sanyal, J. Bouckaert, D. Drider, R. Bilyy, T. Dumych, S. Paryzhak, V. Vovk, R. Boukherroub, A. Sanyal, and S. Szunerits, “Reduced Graphene-Oxide-Embedded Polymeric Nanofiber Mats: An ‘On-Demand’ Photothermally Triggered Antibiotic Release Platform.”, *ACS Applied Materials & Interfaces*, Vol. 10, No. 48, pp. 41098–41106, 2018.

217. Yohe, S.T., J.A. Kopechek, T.M. Porter, Y.L. Colson, and M.W. Grinstaff, “Triggered Drug Release From Superhydrophobic Meshes Using High-Intensity Focused Ultrasound.”, *Advanced Healthcare Materials*, Vol. 2, No. 9, pp. 1204–1208, 2013.

218. Altinbasak, I., M. Arslan, R. Sanyal, and A. Sanyal, “Pyridyl Disulfide-Based Thiol–Disulfide Exchange Reaction: Shaping The Design Of Redox-Responsive Polymeric Materials.”, *Polymer Chemistry*, Vol. 11, No. 48, pp. 7603–7624, 2020.

219. Abdalkarim, S.Y.H., H. Yu, C. Wang, Y. Chen, Z. Zou, L. Han, J. Yao, and K.C. Tam, “Thermo And Light-Responsive Phase Change Nanofibers With High Energy Storage Efficiency For Energy Storage And Thermally Regulated On–Off Drug Release

Devices.”, *Chemical Engineering Journal*, Vol. 375, p. 121979, 2019.

220. Singh, B., N. Shukla, J. Kim, K. Kim, and M.-H. Park, “Stimuli-Responsive Nanofibers Containing Gold Nanorods For On-Demand Drug Delivery Platforms.”, *Pharmaceutics*, Vol. 13, No. 8, p. 1319, 2021.

221. Gong, T., T. Liu, L. Zhang, W. Ye, X. Guo, L. Wang, L. Quan, and C. Pan, “Design Redox-Sensitive Drug-Loaded Nanofibers For Bone Reconstruction.”, *ACS Biomaterials Science and Engineering*, Vol. 4, No. 1, pp. 240–247, 2018.

222. Contreras-Cáceres, R., L. Cabeza, G. Perazzoli, A. Díaz, J.M. López-Romero, C. Melguizo, and J. Prados, “Electrospun Nanofibers: Recent Applications In Drug Delivery And Cancer Therapy.”, *Nanomaterials*, Vol. 9, No. 4, p. 656, 2019.

223. Cui, W., M. Qi, X. Li, S. Huang, S. Zhou, and J. Weng, “Electrospun Fibers Of Acid-Labile Biodegradable Polymers With Acetal Groups As Potential Drug Carriers.”, *International Journal of Pharmaceutics*, Vol. 361, No. 1–2, pp. 47–55, 2008.

224. Gillies, E.R., and J.M.J. Fréchet, “PH-Responsive Copolymer Assemblies For Controlled Release Of Doxorubicin.”, *Bioconjugate Chemistry*, Vol. 16, No. 2, pp. 361–368, 2005.

225. Herrera, V.L., A.H. Colby, G. Al Tan, A.M. Moran, M.J. O’Brien, Y.L. Colson, N. Ruiz-Opazo, and M.W. Grinstaff, “Evaluation Of Expansile Nanoparticle Tumor Localization And Efficacy In A Cancer Stem Cell-Derived Model Of Pancreatic Peritoneal Carcinomatosis.”, *Nanomedicine*, Vol. 11, No. 9, pp. 1001–1015, 2016.

226. Griset, A.P., J. Walpole, R. Liu, A. Gaffey, Y.L. Colson, and M.W. Grinstaff, “Expansile Nanoparticles: Synthesis, Characterization, And In Vivo Efficacy Of An Acid-Responsive Polymeric Drug Delivery System.”, *Journal of the American Chemical Society*, Vol. 131, No. 7, pp. 2469–2471, 2009.

227. Stolzoff, M., I. Ekladious, A.H. Colby, Y.L. Colson, T.M. Porter, and M.W. Grinstaff,

"Synthesis And Characterization Of Hybrid Polymer/Lipid Expansile Nanoparticles: Imparting Surface Functionality For Targeting And Stability.", *Biomacromolecules*, Vol. 16, No. 7, pp. 1958–1966, 2015.

228. Zubris, K.A. V., R. Liu, A. Colby, M.D. Schulz, Y.L. Colson, and M.W. Grinstaff, "In Vitro Activity Of Paclitaxel-Loaded Polymeric Expansile Nanoparticles In Breast Cancer Cells.", *Biomacromolecules*, Vol. 14, No. 6, pp. 2074–2082, 2013.

229. Zubris, K.A. V., Y.L. Colson, and M.W. Grinstaff, "Hydrogels As Intracellular Depots For Drug Delivery.", *Molecular Pharmaceutics*, Vol. 9, No. 1, pp. 196–200, 2012.

230. Colby, A.H., N.H. Oberlies, C.J. Pearce, V.L.M. Herrera, Y.L. Colson, and M.W. Grinstaff, "Nanoparticle Drug-delivery Systems For Peritoneal Cancers: A Case Study Of The Design, Characterization And Development Of The Expansile Nanoparticle.", *WIREs Nanomedicine and Nanobiotechnology*, Vol. 9, No. 3, p. e1451, 2017.

231. Colby, A.H., S.M. Berry, A.M. Moran, K.A. Pasion, R. Liu, Y.L. Colson, N. Ruiz-Opazo, M.W. Grinstaff, and V.L.M. Herrera, "Highly Specific And Sensitive Fluorescent Nanoprobes For Image-Guided Resection Of Sub-Millimeter Peritoneal Tumors.", *ACS Nano*, Vol. 11, No. 2, pp. 1466–1477, 2017.

232. Colby, A.H., R. Liu, M.D. Schulz, R.F. Padera, Y.L. Colson, and M.W. Grinstaff, "Two-Step Delivery: Exploiting The Partition Coefficient Concept To Increase Intratumoral Paclitaxel Concentrations In Vivo Using Responsive Nanoparticles.", *Scientific Reports*, Vol. 6, No. 1, p. 18720, 2016.

233. Colson, Y.L., R. Liu, E.B. Southard, M.D. Schulz, J.E. Wade, A.P. Griset, K.A. V. Zubris, R.F. Padera, and M.W. Grinstaff, "The Performance Of Expansile Nanoparticles In A Murine Model Of Peritoneal Carcinomatosis.", *Biomaterials*, Vol. 32, No. 3, pp. 832–840, 2011.

234. Gilmore, D., M. Schulz, R. Liu, K.A. V. Zubris, R.F. Padera, P.J. Catalano, M.W. Grinstaff, and Y.L. Colson, "Cytoreductive Surgery And Intraoperative

Administration Of Paclitaxel-Loaded Expansile Nanoparticles Delay Tumor Recurrence In Ovarian Carcinoma.", *Annals of Surgical Oncology*, Vol. 20, No. 5, pp. 1684–93, 2013.

235. Colby, A.H., R. Liu, R.P. Doyle, A. Merting, H. Zhang, N. Savage, N.-Q. Chu, B.A. Hollister, W. McCulloch, J.E. Burdette, C.J. Pearce, K. Liu, N.H. Oberlies, Y.L. Colson, and M.W. Grinstaff, "Pilot-Scale Production Of Expansile Nanoparticles: Practical Methods For Clinical Scale-Up.", *Journal of Controlled Release*, Vol. 337, pp. 144–154, 2021.

236. Colby, A.H., Y.L. Colson, and M.W. Grinstaff, "Microscopy And Tunable Resistive Pulse Sensing Characterization Of The Swelling Of PH-Responsive, Polymeric Expansile Nanoparticles.", *Nanoscale*, Vol. 5, No. 8, pp. 3496–3504, 2013.

237. Hanahan, D., and R.A. Weinberg, "Hallmarks Of Cancer: The Next Generation.", *Cell*, Vol. 144, No. 5, pp. 646–674, 2011.

238. Estrella, V., T. Chen, M. Lloyd, J. Wojtkowiak, H.H. Cornnell, A. Ibrahim-Hashim, K. Bailey, Y. Balagurunathan, J.M. Rothberg, B.F. Sloane, J. Johnson, R.A. Gatenby, and R.J. Gillies, "Acidity Generated By The Tumor Microenvironment Drives Local Invasion.", *Cancer Research*, Vol. 73, No. 5, pp. 1524–1535, 2013.

239. Altinbasak, I., S. Kocak, R. Sanyal, and A. Sanyal, "Fast-Forming Dissolvable Redox-Responsive Hydrogels: Exploiting The Orthogonality Of Thiol–Maleimide And Thiol–Disulfide Exchange Chemistry.", *Biomacromolecules*, Vol. 23, No. 9, pp. 3525–3534, 2022.

240. Hoque, J., R.G. Prakash, K. Paramanandham, B.R. Shome, and J. Haldar, "Biocompatible Injectable Hydrogel With Potent Wound Healing And Antibacterial Properties.", *Molecular Pharmaceutics*, Vol. 14, No. 4, pp. 1218–1230, 2017.

241. Yan, X., W.-W. Fang, J. Xue, T.-C. Sun, L. Dong, Z. Zha, H. Qian, Y.-H. Song, M. Zhang, X. Gong, Y. Lu, and T. He, "Thermoresponsive *In Situ* Forming Hydrogel

With Sol–Gel Irreversibility For Effective Methicillin-Resistant *Staphylococcus Aureus* Infected Wound Healing.", *ACS Nano*, Vol. 13, No. 9, pp. 10074–10084, 2019.

242. Oelker, A.M., J.A. Berlin, M. Wathier, and M.W. Grinstaff, "Synthesis And Characterization Of Dendron Cross-Linked PEG Hydrogels As Corneal Adhesives.", *Biomacromolecules*, Vol. 12, No. 5, pp. 1658–1665, 2011.

243. Huang, W., Y. Wang, Z. Huang, X. Wang, L. Chen, Y. Zhang, and L. Zhang, "On-Demand Dissolvable Self-Healing Hydrogel Based On Carboxymethyl Chitosan And Cellulose Nanocrystal For Deep Partial Thickness Burn Wound Healing.", *ACS Applied Materials & Interfaces*, Vol. 10, No. 48, pp. 41076–41088, 2018.

244. Li, Ziyi, F. Zhou, Zhiyong Li, S. Lin, L. Chen, L. Liu, and Y. Chen, "Hydrogel Cross-Linked With Dynamic Covalent Bonding And Micellization For Promoting Burn Wound Healing.", *ACS Applied Materials and Interfaces*, Vol. 10, No. 30, pp. 25194–25202, 2018.

245. Altinbasak, I., R. Sanyal, and A. Sanyal, "Best Of Both Worlds: Diels–Alder Chemistry Towards Fabrication Of Redox-Responsive Degradable Hydrogels For Protein Release.", *RSC Advances*, Vol. 6, No. 78, pp. 74757–74764, 2016.

246. Gregoritza, M., V. Messmann, K. Abstiens, F.P. Brandl, and A.M. Goepferich, "Controlled Antibody Release From Degradable Thermoresponsive Hydrogels Cross-Linked By Diels–Alder Chemistry.", *Biomacromolecules*, Vol. 18, No. 8, pp. 2410–2418, 2017.

247. Konieczynska, M.D., J.C. Villa-Camacho, C. Ghobril, M. Perez-Viloria, K.M. Tevis, W.A. Blessing, A. Nazarian, E.K. Rodriguez, and M.W. Grinstaff, "On-Demand Dissolution Of A Dendritic Hydrogel-Based Dressing For Second-Degree Burn Wounds Through Thiol-Thioester Exchange Reaction.", *Angewandte Chemie International Edition*, Vol. 55, No. 34, pp. 9984–9987, 2016.

248. Atchison, N.E., P.F. Osgood, D.B. Carr, and S.K. Szyfelbein, "Pain During Burn

Dressing Change In Children: Relationship To Burn Area, Depth And Analgesic Regimens.", *Pain*, Vol. 47, No. 1, pp. 41–45, 1991.

249. Konieczynska, M.D., and M.W. Grinstaff, "On-Demand Dissolution Of Chemically Cross-Linked Hydrogels.", *Accounts of Chemical Research*, Vol. 50, No. 2, pp. 151–160, 2017.

250. Pradhan, K., G. Das, J. Khan, V. Gupta, S. Barman, A. Adak, and S. Ghosh, "Neuro-Regenerative Choline-Functionalized Injectable Graphene Oxide Hydrogel Repairs Focal Brain Injury.", *ACS Chemical Neuroscience*, Vol. 10, No. 3, pp. 1535–1543, 2019.

251. Baldwin, A.D., and K.L. Kiick, "Reversible Maleimide-Thiol Adducts Yield Glutathione-Sensitive Poly(Ethylene Glycol)-Heparin Hydrogels.", *Polymer Chemistry*, Vol. 4, No. 1, pp. 133–143, 2013.

252. Kharkar, P.M., A.M. Kloxin, and K.L. Kiick, "Dually Degradable Click Hydrogels For Controlled Degradation And Protein Release.", *Journal of Material Chemistry B*, Vol. 2, No. 34, pp. 5511–5521, 2014.

253. Kim, Y.-M., M.-R. Park, and S.-C. Song, "Injectable Polyplex Hydrogel For Localized And Long-Term Delivery Of SiRNA.", *ACS Nano*, Vol. 6, No. 7, pp. 5757–5766, 2012.

254. Chen, Y.-Y., H.-C. Wu, J.-S. Sun, G.-C. Dong, and T.-W. Wang, "Injectable And Thermoresponsive Self-Assembled Nanocomposite Hydrogel For Long-Term Anticancer Drug Delivery.", *Langmuir*, Vol. 29, No. 11, pp. 3721–3729, 2013.

255. Jiang, H., S. Qin, H. Dong, Q. Lei, X. Su, R. Zhuo, and Z. Zhong, "An Injectable And Fast-Degradable Poly(Ethylene Glycol) Hydrogel Fabricated Via Bioorthogonal Strain-Promoted Azide–Alkyne Cycloaddition Click Chemistry.", *Soft Matter*, Vol. 11, No. 30, pp. 6029–6036, 2015.

256. Bai, X., S. Lü, Z. Cao, B. Ni, X. Wang, P. Ning, D. Ma, H. Wei, and M. Liu, “Dual Crosslinked Chondroitin Sulfate Injectable Hydrogel Formed Via Continuous Diels-Alder (DA) Click Chemistry For Bone Repair.”, *Carbohydrate Polymers*, Vol. 166, pp. 123–130, 2017.

257. Grover, G.N., J. Lam, T.H. Nguyen, T. Segura, and H.D. Maynard, “Biocompatible Hydrogels By Oxime Click Chemistry.”, *Biomacromolecules*, Vol. 13, No. 10, pp. 3013–3017, 2012.

258. Liu, M., X. Zeng, C. Ma, H. Yi, Z. Ali, X. Mou, S. Li, Y. Deng, and N. He, “Injectable Hydrogels For Cartilage And Bone Tissue Engineering.”, *Bone Research*, Vol. 5, No. 1, p. 17014, 2017.

259. Jin, R., L.S. Moreira Teixeira, A. Krouwels, P.J. Dijkstra, C.A. van Blitterswijk, M. Karperien, and J. Feijen, “Synthesis And Characterization Of Hyaluronic Acid–Poly(Ethylene Glycol) Hydrogels Via Michael Addition: An Injectable Biomaterial For Cartilage Repair.”, *Acta Biomaterialia*, Vol. 6, No. 6, pp. 1968–1977, 2010.

260. Lin, C., P. Zhao, F. Li, F. Guo, Z. Li, and X. Wen, “Thermosensitive In Situ-Forming Dextran–Pluronic Hydrogels Through Michael Addition.”, *Materials Science and Engineering: C*, Vol. 30, No. 8, pp. 1236–1244, 2010.

261. Yu, Y., C. Deng, F. Meng, Q. Shi, J. Feijen, and Z. Zhong, “Novel Injectable Biodegradable Glycol Chitosan-Based Hydrogels Crosslinked By Michael-Type Addition Reaction With Oligo(Acryloyl Carbonate)-B-Poly(Ethylene Glycol)-B-Oligo(Acryloyl Carbonate) Copolymers.”, *Journal of Biomedical Materials Research Part A*, Vol. 99A, No. 2, pp. 316–326, 2011.

262. Phelps, E.A., N.O. Enemchukwu, V.F. Fiore, J.C. Sy, N. Murthy, T.A. Sulchek, T.H. Barker, and A.J. García, “Maleimide Cross-Linked Bioactive PEG Hydrogel Exhibits Improved Reaction Kinetics And Cross-Linking For Cell Encapsulation And In Situ Delivery.”, *Advanced Materials*, Vol. 24, No. 1, pp. 64–70, 2012.

263. Dunn, S.S., S. Tian, S. Blake, J. Wang, A.L. Galloway, A. Murphy, P.D. Pohlhaus, J.P. Rolland, M.E. Napier, and J.M. DeSimone, “Reductively Responsive SiRNA-Conjugated Hydrogel Nanoparticles For Gene Silencing.”, *Journal of the American Chemical Society*, Vol. 134, No. 17, pp. 7423–7430, 2012.

264. Schafer, F.Q., and G.R. Buettner, “Redox Environment Of The Cell As Viewed Through The Redox State Of The Glutathione Disulfide/Glutathione Couple.”, *Free Radical Biology and Medicine*, Vol. 30, No. 11, pp. 1191–1212, 2001.

265. Altinbasak, I., M. Arslan, R. Sanyal, and A. Sanyal, “Pyridyl Disulfide-Based Thiol–Disulfide Exchange Reaction: Shaping The Design Of Redox-Responsive Polymeric Materials.”, *Polymer Chemistry*, Vol. 11, No. 48, pp. 7603–7624, 2020.

266. Saha, B., S. Bhattacharyya, S. Mete, A. Mukherjee, and P. De, “Redox-Driven Disassembly Of Polymer-Chlorambucil Polyprodrug: Delivery Of Anticancer Nitrogen Mustard And DNA Alkylation.”, *ACS Applied Polymer Materials*, Vol. 1, No. 9, pp. 2503–2515, 2019.

267. Baldwin, A.D., K.G. Robinson, J.L. Militar, C.D. Derby, K.L. Kiick, and R.E. Akins, “In Situ Crosslinkable Heparin-Containing Poly(Ethylene Glycol) Hydrogels For Sustained Anticoagulant Release.”, *Journal of Biomedical Materials Research Part A*, Vol. 100A, No. 8, pp. 2106–2118, 2012.

268. Neubert, B.J., and B.B. Snider, “Synthesis Of (±)-Phloeodictine A1.”, *Organic Letters*, Vol. 5, No. 5, pp. 765–768, 2003.

269. Dübner, M., T.N. Gevrek, A. Sanyal, N.D. Spencer, and C. Padeste, “Fabrication Of Thiol-Ene ‘Clickable’ Copolymer-Brush Nanostructures On Polymeric Substrates Via Extreme Ultraviolet Interference Lithography.”, *ACS Applied Materials and Interfaces*, Vol. 7, No. 21, pp. 11337–11345, 2015.

270. Hershberger, K.K., A.J. Gauger, and L.M. Bronstein, “Utilizing Stimuli Responsive Linkages To Engineer And Enhance Polymer Nanoparticle-Based Drug Delivery

Platforms.", *ACS Applied Bio Materials*, Vol. 4, No. 6, pp. 4720–4736, 2021.

271. Ko, N.R., and J.K. Oh, "Glutathione-Triggered Disassembly Of Dual Disulfide Located Degradable Nanocarriers Of Polylactide-Based Block Copolymers For Rapid Drug Release.", *Biomacromolecules*, Vol. 15, No. 8, pp. 3180–3189, 2014.

272. Kalepu, S., and V. Nekkanti, "Improved Delivery Of Poorly Soluble Compounds Using Nanoparticle Technology: A Review.", *Drug Delivery and Translational Research*, Vol. 6, No. 3, pp. 319–332, 2016.

273. Griset, A.P., J. Walpole, R. Liu, A. Gaffey, Y.L. Colson, and M.W. Grinstaff, "Expansile Nanoparticles: Synthesis, Characterization, And In Vivo Efficacy Of An Acid-Responsive Polymeric Drug Delivery System.", *Journal of the American Chemical Society*, Vol. 131, No. 7, pp. 2469–2471, 2009.

274. Ejderyan, N., R. Sanyal, and A. Sanyal, "Stimuli-Responsive Polymer-Coated Iron Oxide Nanoparticles As Drug Delivery Platforms.", *Stimuli-Responsive Nanocarriers*, pp. 133–169, 2022.

275. Kwon, G.S., and T. Okano, "Polymeric Micelles As New Drug Carriers.", *Advanced Drug Delivery Reviews*, Vol. 21, No. 2, pp. 107–116, 1996.

276. Wilczewska, A.Z., K. Niemirowicz, K.H. Markiewicz, and H. Car, "Nanoparticles As Drug Delivery Systems.", *Pharmacological Reports*, Vol. 64, No. 5, pp. 1020–1037, 2012.

277. Nayak, S., and L. Andrew Lyon, "Soft Nanotechnology With Soft Nanoparticles.", *Angewandte Chemie - International Edition*, Vol. 44, No. 47, pp. 7686–7708, 2005.

278. Hui, Y., X. Yi, F. Hou, D. Wibowo, F. Zhang, D. Zhao, H. Gao, and C.X. Zhao, "Role Of Nanoparticle Mechanical Properties In Cancer Drug Delivery.", *ACS Nano*, Vol. 13, No. 7, pp. 7410–7424, 2019.

279. Latreille, P.-L., V. Adibnia, A. Nour, J.-M. Rabanel, A. Lalloz, J. Arlt, W.C.K. Poon, P. Hildgen, V.A. Martinez, and X. Banquy, “Spontaneous Shrinking Of Soft Nanoparticles Boosts Their Diffusion In Confined Media.”, *Nature Communications*, Vol. 10, No. 1, p. 4294, 2019.

280. Anselmo, A.C., M. Zhang, S. Kumar, D.R. Vogus, S. Menegatti, M.E. Helgeson, and S. Mitragotri, “Elasticity Of Nanoparticles Influences Their Blood Circulation, Phagocytosis, Endocytosis, And Targeting.”, *ACS Nano*, Vol. 9, No. 3, pp. 3169–3177, 2015.

281. Chacko, R.T., J. Ventura, J. Zhuang, and S. Thayumanavan, “Polymer Nanogels: A Versatile Nanoscopic Drug Delivery Platform.”, *Advanced Drug Delivery Reviews*, Vol. 64, No. 9, pp. 836–851, 2012.

282. Zhang, H., Y. Zhai, J. Wang, and G. Zhai, “New Progress And Prospects: The Application Of Nanogel In Drug Delivery.”, *Materials Science and Engineering: C*, Vol. 60, pp. 560–568, 2016.

283. Pinelli, F., Ó.F. Ortolà, P. Makvandi, G. Perale, and F. Rossi, “In Vivo Drug Delivery Applications Of Nanogels: A Review.”, *Nanomedicine*, Vol. 15, No. 27, pp. 2707–2727, 2020.

284. Matsumoto, N.M., D.C. González-Toro, R.T. Chacko, H.D. Maynard, and S. Thayumanavan, “Synthesis Of Nanogel–Protein Conjugates.”, *Polymer Chemistry*, Vol. 4, No. 8, pp. 2464–2469, 2013.

285. Ryu, J.H., S. Jiwpanich, R. Chacko, S. Bickerton, and S. Thayumanavan, “Surface-Functionalizable Polymer Nanogels With Facile Hydrophobic Guest Encapsulation Capabilities.”, *Journal of the American Chemical Society*, Vol. 132, No. 24, pp. 8246–8247, 2010.

286. Maeda, H., “Polymer Therapeutics And The EPR Effect.”, *Journal of Drug Targeting*, Vol. 25, No. 9–10, pp. 781–785, 2017.

287. Chen, J., J. Ding, W. Xu, T. Sun, H. Xiao, X. Zhuang, and X. Chen, “Receptor And Microenvironment Dual-Recognizable Nanogel For Targeted Chemotherapy Of Highly Metastatic Malignancy.”, *Nano Letters*, Vol. 17, No. 7, pp. 4526–4533, 2017.

288. He, H., A.W. Cattran, T. Nguyen, A.L. Nieminen, and P. Xu, “Triple-Responsive Expansile Nanogel For Tumor And Mitochondria Targeted Photosensitizer Delivery.”, *Biomaterials*, Vol. 35, No. 35, pp. 9546–9553, 2014.

289. Maya, S., B. Sarmento, A. Nair, N. Rejinold, S. Nair, and R. Jayakumar, “Smart Stimuli Sensitive Nanogels In Cancer Drug Delivery And Imaging: A Review.”, *Current Pharmaceutical Design*, Vol. 19, No. 41, pp. 7203–7218, 2013.

290. Jung, K.O., D.J. Siegwart, H. Il Lee, G. Sherwood, L. Peteanu, J.O. Hollinger, K. Kataoka, and K. Matyjaszewski, “Biodegradable Nanogels Prepared By Atom Transfer Radical Polymerization As Potential Drug Delivery Carriers: Synthesis, Biodegradation, In Vitro Release, And Bioconjugation.”, *Journal of the American Chemical Society*, Vol. 129, No. 18, pp. 5939–5945, 2007.

291. Chambre, L., W.S. Saw, G. Ekineker, L.V. Kiew, W.Y. Chong, H.B. Lee, L.Y. Chung, Y. Bretonnière, F. Dumoulin, and A. Sanyal, “Surfactant-Free Direct Access To Porphyrin-Cross-Linked Nanogels For Photodynamic And Photothermal Therapy.”, *Bioconjugate Chemistry*, Vol. 29, No. 12, pp. 4149–4159, 2018.

292. Mitra, S., U. Gaur, P.C. Ghosh, and A.N. Maitra, “Tumour Targeted Delivery Of Encapsulated Dextran–Doxorubicin Conjugate Using Chitosan Nanoparticles As Carrier.”, *Journal of Controlled Release*, Vol. 74, No. 1–3, pp. 317–323, 2001.

293. Daniel-da-Silva, A.L., L. Ferreira, A.M. Gil, and T. Trindade, “Synthesis And Swelling Behavior Of Temperature Responsive κ-Carrageenan Nanogels.”, *Journal of Colloid and Interface Science*, Vol. 355, No. 2, pp. 512–517, 2011.

294. Messager, L., N. Portecop, E. Hachet, V. Lapeyre, I. Pignot-Paintrand, B. Catargi, R. Auzély-Velty, and V. Ravaine, “Photochemical Crosslinking Of Hyaluronic Acid

Confined In Nanoemulsions: Towards Nanogels With A Controlled Structure.", *Journal of Materials Chemistry B*, Vol. 1, No. 27, pp. 3369–3379, 2013.

295. Zha, L., B. Banik, and F. Alexis, "Stimulus Responsive Nanogels For Drug Delivery.", *Soft Matter*, Vol. 7, No. 13, pp. 5908–5916, 2011.

296. Zhang, R., T. Nie, Y. Fang, H. Huang, and J. Wu, "Poly(Disulfide)S: From Synthesis To Drug Delivery.", *Biomacromolecules*, Vol. 23, No. 1, pp. 1–19, 2022.

297. Altinbasak, I., M. Arslan, R. Sanyal, and A. Sanyal, "Pyridyl Disulfide-Based Thiol–Disulfide Exchange Reaction: Shaping The Design Of Redox-Responsive Polymeric Materials.", *Polymer Chemistry*, Vol. 11, No. 48, pp. 7603–7624, 2020.

298. Wang, H., L. Gao, T. Fan, C. Zhang, B. Zhang, O.A. Al-Hartomy, A. Al-Ghamdi, S. Wageh, M. Qiu, and H. Zhang, "Strategic Design Of Intelligent-Responsive Nanogel Carriers For Cancer Therapy.", *ACS Applied Materials and Interfaces*, Vol. 13, No. 46, pp. 54621–54647, 2021.

299. Hoffman, A.S., P.S. Stayton, M.E.H. El-Sayed, N. Murthy, V. Bulmus, C. Lackey, and C. Cheung, "Design Of 'Smart' Nano-Scale Delivery Systems For Biomolecular Therapeutics.", *Journal of Biomedical Nanotechnology*, Vol. 3, No. 3, pp. 213–217, 2007.

300. Bauri, K., M. Nandi, and P. De, "Amino Acid-Derived Stimuli-Responsive Polymers And Their Applications.", *Polymer Chemistry*, Vol. 9, p. 1257, 2018.

301. Bej, R., K. Achazi, R. Haag, and S. Ghosh, "Polymersome Formation By Amphiphilic Polyglycerol- B-Polydisulfide- B-Polyglycerol And Glutathione-Triggered Intracellular Drug Delivery.", *Biomacromolecules*, Vol. 21, No. 8, pp. 3353–3363, 2020.

302. Deshpande, N.U., and M. Jayakannan, "Biotin-Tagged Polysaccharide Vesicular Nanocarriers For Receptor-Mediated Anticancer Drug Delivery In Cancer Cells.",

Biomacromolecules, Vol. 19, No. 8, pp. 3572–3585, 2018.

303. Torchilin, V.P., "Multifunctional, Stimuli-Sensitive Nanoparticulate Systems For Drug Delivery.", *Nature Reviews Drug Discovery*, Vol. 13, No. 11, pp. 813–827, 2014.

304. Ghosh, S., S. Basu, and S. Thayumanavan, "Simultaneous And Reversible Functionalization Of Copolymers For Biological Applications.", *Macromolecules*, Vol. 39, No. 17, pp. 5595–5597, 2006.

305. Ekkelenkamp, A.E., M.R. Elzes, J.F.J. Engbersen, and J.M.J. Paulusse, "Responsive Crosslinked Polymer Nanogels For Imaging And Therapeutics Delivery.", *Journal of Materials Chemistry B*, Vol. 6, No. 2, pp. 210–235, 2018.

306. Griset, A.P., J. Walpole, R. Liu, A. Gaffey, Y.L. Colson, and M.W. Grinstaff, "Expansile Nanoparticles: Synthesis, Characterization, And In Vivo Efficacy Of An Acid-Responsive Polymeric Drug Delivery System.", *Journal of the American Chemical Society*, Vol. 131, No. 7, pp. 2469–2471, 2009.

307. Li, Y., Q.N. Bui, L.T.M. Duy, H.Y. Yang, and D.S. Lee, "One-Step Preparation Of PH-Responsive Polymeric Nanogels As Intelligent Drug Delivery Systems For Tumor Therapy.", *Biomacromolecules*, Vol. 19, No. 6, pp. 2062–2071, 2018.

308. Alkanawati, M.S., M. Machtakova, K. Landfester, and H. Thérien-Aubin, "Bio-Orthogonal Nanogels For Multiresponsive Release.", *Biomacromolecules*, Vol. 22, No. 7, pp. 2976–2984, 2021.

309. Huang, J., C. Zheng, H. Xiao, H. Huang, Yiyao Wang, M. Lin, J. Pang, Yong Wang, Y. Yuan, and X. Shuai, "A Polymer-calcium Phosphate Nanocapsule For RNAi-Induced Oxidative Stress And Cascaded Chemotherapy.", *Journal of Controlled Release*, Vol. 340, pp. 259–270, 2021.

310. Zhang, Y., D. Zhang, J.T. Wang, X. Zhang, and Y. Yang, "Fabrication Of Stimuli-Responsive Nanogels For Protein Encapsulation And Traceless Release Without

Introducing Organic Solvents, Surfactants, Or Small-Molecule Cross-Linkers.", *Polymer Chemistry*, Vol. 12, No. 4, pp. 554–563, 2021.

311. Syrett, J.A., D.M. Haddleton, M.R. Whittaker, T.P. Davis, and C. Boyer, "Functional, Star Polymeric Molecular Carriers, Built From Biodegradable Microgel/Nanogel Cores.", *Chemical Communications*, Vol. 47, pp. 1449–1451, 2011.

312. Boehnke, Natalie, Jacquelin K Kammeyer, Robert Damoiseaux, H.D. Maynard, N Boehnke, J K Kammeyer, D. Maynard, and R Damoiseaux, "Stabilization Of Glucagon By Trehalose Glycopolymer Nanogels.", *Advanced Functional Materials*, Vol. 28, No. 10, p. 1705475, 2018.

313. Degirmenci, A., R. Sanyal, M. Arslan, and A. Sanyal, "Benzothiazole-Disulfide Based Redox-Responsive Polymers: Facile Access To Reversibly Functionalizable Polymeric Coatings.", *Polymer Chemistry*, Vol. 13, No. 18, pp. 2595–2607, 2022.

314. Kilic Boz, R., D. Aydin, S. Kocak, B. Golba, R. Sanyal, and A. Sanyal, "Redox-Responsive Hydrogels For Tunable And 'On-Demand' Release Of Biomacromolecules.", *Bioconjugate Chemistry*, Vol. 33, p. 847, 2022.

315. Gok, O., P. Erturk, B. Sumer Bolu, T.N. Gevrek, R. Sanyal, and A. Sanyal, "Dendrons And Multiarm Polymers With Thiol-Exchangeable Cores: A Reversible Conjugation Platform For Delivery.", *Biomacromolecules*, Vol. 18, No. 8, pp. 2463–2477, 2017.

316. Altinbasak, I., R. Sanyal, and A. Sanyal, "Best Of Both Worlds: Diels–Alder Chemistry Towards Fabrication Of Redox-Responsive Degradable Hydrogels For Protein Release.", *RSC Advances*, Vol. 6, No. 78, pp. 74757–74764, 2016.

317. Santra, S., S. Kolay, S. Sk, D. Ghosh, A. Mishra, L. Roy, K. Sarkar, and M.R. Molla, "Supramolecularly Cross-Linked Nanoassemblies Of Self-Immolative Polyurethane From Recycled Plastic Waste: High Encapsulation Stability And The Triggered Release Of Guest Molecules.", *Polymer Chemistry*, Vol. 13, No. 22, pp. 3294–3303, 2022.

318. Arslan, M., R. Sanyal, and A. Sanyal, “Thiol-Reactive Thiosulfonate Group Containing Copolymers: Facile Entry To Disulfide-Mediated Polymer Conjugation And Redox-Responsive Functionalizable Networks.”, *Polymer Chemistry*, Vol. 11, No. 10, pp. 1763–1773, 2020.

319. Jiang, Z., and S. Thayumanavan, “Disulfide-Containing Macromolecules For Therapeutic Delivery.”, *Israel Journal of Chemistry*, Vol. 60, No. 1–2, pp. 132–139, 2020.

320. Phillips, D.J., and M.I. Gibson, “Redox-Sensitive Materials For Drug Delivery: Targeting The Correct Intracellular Environment, Tuning Release Rates, And Appropriate Predictive Systems.”, *Antioxidants & Redox Signaling*, Vol. 21, No. 5, pp. 786–803, 2014.

321. Bej, R., J. Sarkar, and S. Ghosh, “Structural Diversity In Poly(Disulfide)S.”, *Journal of Polymer Science Part A: Polymer Chemistry*, Vol. 56, No. 2, pp. 194–202, 2018.

322. Chambre, L., A. Degirmenci, R. Sanyal, and A. Sanyal, “Multi-Functional Nanogels As Theranostic Platforms: Exploiting Reversible And Nonreversible Linkages For Targeting, Imaging, And Drug Delivery.”, *Bioconjugate Chemistry*, Vol. 29, No. 6, pp. 1885–1896, 2018.

323. Aktan, B., L. Chambre, R. Sanyal, and A. Sanyal, “‘Clickable’ Nanogels Via Thermally Driven Self-Assembly Of Polymers: Facile Access To Targeted Imaging Platforms Using Thiol-Maleimide Conjugation.”, *Biomacromolecules*, Vol. 18, No. 2, pp. 490–497, 2017.

324. Nair, D.P., M. Podgórski, S. Chatani, T. Gong, W. Xi, C.R. Fenoli, and C.N. Bowman, “The Thiol-Michael Addition Click Reaction: A Powerful And Widely Used Tool In Materials Chemistry.”, *Chemistry of Materials*, Vol. 26, No. 1, pp. 724–744, 2014.

325. Hoyle, C.E., A.B. Lowe, and C.N. Bowman, “Thiol -Click Chemistry: A Multifaceted Toolbox For Small Molecule And Polymer Synthesis.”, *Chemical Society Reviews*,

Vol. 39, No. 4, pp. 1355–1387, 2010.

326. Oz, Y., and A. Sanyal, “The Taming Of The Maleimide: Fabrication Of Maleimide-Containing ‘Clickable’ Polymeric Materials.”, *The Chemical Record*, Vol. 18, No. 6, pp. 570–586, 2018.

327. Arslan, M., B.S. Bolu, R. Sanyal, and A. Sanyal, “A Modular And Orthogonally Reactive Platform For Fabrication Of Polymer–Drug Conjugates For Targeted Delivery.”, *Polymer Chemistry*, Vol. 11, No. 45, pp. 7137–7146, 2020.

328. Chambre, L., H. Maouati, Y. Oz, R. Sanyal, and A. Sanyal, “Thiol-Reactive Clickable Cryogels: Importance Of Macroporosity And Linkers On Biomolecular Immobilization.”, *Bioconjugate Chemistry*, Vol. 31, No. 9, pp. 2116–2124, 2020.

329. Cengiz, N., T.N. Gevrek, R. Sanyal, R. Sanyal, A. Sanyal, and A. Sanyal, “Fabrication Of Patterned Hydrogel Interfaces: Exploiting The Maleimide Group As A Dual Purpose Handle For Cross-Linking And Bioconjugation.”, *Bioconjugate Chemistry*, Vol. 31, No. 5, pp. 1382–1391, 2020.

330. Oz, Y., M. Arslan, T.N. Gevrek, R. Sanyal, and A. Sanyal, “Modular Fabrication Of Polymer Brush Coated Magnetic Nanoparticles: Engineering The Interface For Targeted Cellular Imaging.”, *ACS Applied Materials and Interfaces*, Vol. 8, No. 30, pp. 19813–19826, 2016.

331. Baldwin, A.D., and K.L. Kiick, “Tunable Degradation Of Maleimide-Thiol Adducts In Reducing Environments.”, *Bioconjugate Chemistry*, Vol. 22, No. 10, pp. 1946–1953, 2011.

332. Klibanov, A.L., K. Maruyama, V.P. Torchilin, and L. Huang, “Amphipathic Polyethyleneglycols Effectively Prolong The Circulation Time Of Liposomes.”, *FEBS Letters*, Vol. 268, No. 1, pp. 235–237, 1990.

333. Torchilin, V.P., and V.S. Trubetskoy, “Which Polymers Can Make Nanoparticulate

Drug Carriers Long-Circulating?", *Advanced Drug Delivery Reviews*, Vol. 16, No. 2–3, pp. 141–155, 1995.

334. Xu, X., T. Li, and K. Jin, "Bioinspired And Biomimetic Nanomedicines For Targeted Cancer Therapy.", *Pharmaceutics*, Vol. 14, No. 5, pp. 1109, 2022.

335. Gavas, S., S. Quazi, and T.M. Karpiński, "Nanoparticles For Cancer Therapy: Current Progress And Challenges.", *Nanoscale Research Letters*, Vol. 16, No. 1, pp. 173, 2021.

336. Hobbs, S.K., W.L. Monsky, F. Yuan, W.G. Roberts, L. Griffith, V.P. Torchilin, and R.K. Jain, "Regulation Of Transport Pathways In Tumor Vessels: Role Of Tumor Type And Microenvironment.", *Proceedings of the National Academy of Sciences of the United States of America*, Vol. 95, No. 8, pp. 4607–4612, 1998.

337. Jain, R.K., "Transport Of Molecules, Particles, And Cells In Solid Tumors.", *Annual Review of Biomedical Engineering*, Vol. 1, No. 1, pp. 241–263, 1999.

338. Subhan, M.A., S.S.K. Yalamarty, N. Filipczak, F. Parveen, and V.P. Torchilin, "Recent Advances In Tumor Targeting Via EPR Effect For Cancer Treatment.", *Journal of Personalized Medicine*, Vol. 11, No. 6, p. 571, 2021.

339. Fitzmaurice, O., M. Bartkowski, and S. Giordani, "Molecular Switches—Tools For Imparting Control In Drug Delivery Systems.", *Frontiers in Chemistry*, Vol. 10, p. 284, 2022.

340. Kaushik, N., S.B. Borkar, S.K. Nandanwar, P.K. Panda, E.H. Choi, and N.K. Kaushik, "Nanocarrier Cancer Therapeutics With Functional Stimuli-Responsive Mechanisms.", *Journal of Nanobiotechnology*, Vol. 20, No. 1, pp. 1–23, 2022.

341. Chen, J., Z. Jiang, Y.S. Zhang, J. Ding, and X. Chen, "Smart Transformable Nanoparticles For Enhanced Tumor Theranostics.", *Applied Physics Reviews*, Vol. 8, No. 4, p. 041321, 2021.

342. Kataoka, K., A. Harada, and Y. Nagasaki, “Block Copolymer Micelles For Drug Delivery: Design, Characterization And Biological Significance.”, *Advanced Drug Delivery Reviews*, Vol. 47, No. 1, pp. 113–131, 2001.

343. Hwang, D., J.D. Ramsey, and A. V. Kabanov, “Polymeric Micelles For The Delivery Of Poorly Soluble Drugs: From Nanoformulation To Clinical Approval.”, *Advanced Drug Delivery Reviews*, Vol. 156, pp. 80–118, 2020.

344. Kaur, J., M. Gulati, N.K. Jha, J. Disouza, V. Patravale, K. Dua, and S.K. Singh, “Recent Advances In Developing Polymeric Micelles For Treating Cancer: Breakthroughs And Bottlenecks In Their Clinical Translation.”, *Drug Discovery Today*, Vol. 27, No. 5, pp. 1495–1512, 2022.

345. Torchilin, V., “Tumor Delivery Of Macromolecular Drugs Based On The EPR Effect.”, *Advanced Drug Delivery Reviews*, Vol. 63, No. 3, pp. 131–135, 2011.

346. Shin, D.H., Y.T. Tam, and G.S. Kwon, “Polymeric Micelle Nanocarriers In Cancer Research.”, *Frontiers of Chemical Science and Engineering*, Vol. 10, No. 3, pp. 348–359, 2016.

347. Wang, J., W. Mao, L.L. Lock, J. Tang, M. Sui, W. Sun, H. Cui, D. Xu, and Y. Shen, “The Role Of Micelle Size In Tumor Accumulation, Penetration, And Treatment.”, *ACS Nano*, Vol. 9, No. 7, pp. 7195–7206, 2015.

348. Prencipe, F., C. Diaferia, F. Rossi, L. Ronga, and D. Tesauro, “Forward Precision Medicine: Micelles For Active Targeting Driven By Peptides.”, *Molecules*, Vol. 26, No. 13, p. 4049, 2021.

349. Shi, C., Z. Zhang, F. Wang, and Y. Luan, “Active-Targeting Docetaxel-Loaded Mixed Micelles For Enhancing Antitumor Efficacy.”, *Journal of Molecular Liquids*, Vol. 264, pp. 172–178, 2018.

350. Guo, Xing, Lin Wang, Kayla Duval, Jing Fan, Shaobing Zhou, Zi Chen, X Guo, L

Wang, K Duval, Z Chen, S Zhou, and J Fan, “Dimeric Drug Polymeric Micelles With Acid-Active Tumor Targeting And FRET-Traceable Drug Release.”, *Advanced Materials*, Vol. 30, No. 3, p. 1705436, 2018.

351. Bolu, B.S., B. Golba, N. Boke, A. Sanyal, and R. Sanyal, “Designing Dendron-Polymer Conjugate Based Targeted Drug Delivery Platforms With A ‘Mix-And-Match’ Modularity.”, *Bioconjugate Chemistry*, Vol. 28, No. 12, pp. 2962–2975, 2017.

352. Unsal, H., S. Onbulak, F. Calik, M. Er-Rafik, M. Schmutz, A. Sanyal, and J. Rzayev, “Interplay Between Molecular Packing, Drug Loading, And Core Cross-Linking In Bottlebrush Copolymer Micelles.”, *Macromolecules*, Vol. 50, No. 4, pp. 1342–1352, 2017.

353. Sumer Bolu, B., E. Manavoglu Gecici, and R. Sanyal, “Combretastatin A-4 Conjugated Antiangiogenic Micellar Drug Delivery Systems Using Dendron-Polymer Conjugates.”, *Molecular Pharmaceutics*, Vol. 13, No. 5, pp. 1482–1490, 2016.

354. Pang, X., Y. Jiang, Q. Xiao, A.W. Leung, H. Hua, and C. Xu, “PH-Responsive Polymer-Drug Conjugates: Design And Progress.”, *Journal of Controlled Release*, Vol. 222, pp. 116–129, 2016.

355. Arslan, M., B.S. Bolu, R. Sanyal, and A. Sanyal, “A Modular And Orthogonally Reactive Platform For Fabrication Of Polymer–Drug Conjugates For Targeted Delivery.”, *Polymer Chemistry*, Vol. 11, No. 45, pp. 7137–7146, 2020.

356. Lv, S., Z. Tang, D. Zhang, W. Song, M. Li, J. Lin, H. Liu, and X. Chen, “Well-Defined Polymer-Drug Conjugate Engineered With Redox And PH-Sensitive Release Mechanism For Efficient Delivery Of Paclitaxel.”, *Journal of Controlled Release*, Vol. 194, pp. 220–227, 2014.

357. Chau, Y., R.F. Padera, N.M. Dang, and R. Langer, “Antitumor Efficacy Of A Novel Polymer–Peptide–Drug Conjugate In Human Tumor Xenograft Models.”, *International Journal of Cancer*, Vol. 118, No. 6, pp. 1519–1526, 2006.

358. Chen, L., T. Jiang, C. Cai, L. Wang, J. Lin, and X. Cao, “Polypeptide-Based ‘Smart’ Micelles For Dual-Drug Delivery: A Combination Study Of Experiments And Simulations.”, *Advanced Healthcare Materials*, Vol. 3, No. 9, pp. 1508–1517, 2014.

359. Janinis, J., M. Papadakou, G. Panagos, A. Panousaki, V. Georgoulias, D. Hatzidaki, D. Lefantzis, and G. Dokianakis, “Sequential Chemoradiotherapy With Docetaxel, Cisplatin, And 5-Fluorouracil In Patients With Locally Advanced Head And Neck Cancer.”, *American Journal of Clinical Oncology*, Vol. 24, No. 3, pp. 227-231, 2001.

360. Schrijvers, D., C. Van Herpen, J. Kerger, E. Joosens, C. Van Laer, A. Awada, D. Van den Weyngaert, H. Nguyen, C. Le Bouder, J.A. Castelijns, J. Kaanders, P. De Mulder, and J.B. Vermorken, “Docetaxel, Cisplatin And 5-Fluorouracil In Patients With Locally Advanced Unresectable Head And Neck Cancer: A Phase I–II Feasibility Study.”, *Annals of Oncology*, Vol. 15, No. 4, pp. 638–645, 2004.

361. Yamamoto, S., J. Kurebayashi, M. Kurosumi, H. Kunisue, T. Otsuki, K. Tanaka, and H. Sonoo, “Combined Effects Of Docetaxel And Fluoropyrimidines On Tumor Growth And Expression Of Interleukin-6 And Thymidine Phosphorylase In Breast Cancer Xenografts.”, *Cancer Chemotherapy and Pharmacology*, Vol. 48, No. 4, pp. 283–288, 2001.

362. Yoshida, K., M. Ninomiya, N. Takakura, N. Hirabayashi, W. Takiyama, Y. Sato, S. Todo, M. Terashima, M. Gotoh, J. Sakamoto, and M. Nishiyama, “Phase II Study Of Docetaxel And S-1 Combination Therapy For Advanced Or Recurrent Gastric Cancer.”, *Clinical Cancer Research*, Vol. 12, No. 11, pp. 3402–3407, 2006.

363. Lee, N.J., C.S. Ha, and W.J. Cho, “Syntheses And Toxicity Of Monomers And Polymers Containing 5-Fluorouracil.”, *Journal of Macromolecular Science, Part A*, Vol. 29, No. 2, pp. 161–172, 1992.

364. Ozaki, S., J. Ohnishi, T. Akiyama, T. Nagase, N. Uehara, and A. Hosm, “Preparation Of Antitumor Active Vinyl Polymers Containing 5-Fluorouracil As A Componentt.”, *Polymer Journal*, Vol. 22, No. 8, pp. 689–695, 1990.

365. Liu, Z., and S. Rimmer, “Synthesis And Release Of 5-Fluorouracil From Poly(N-Vinylpyrrolidinone) Bearing 5-Fluorouracil Derivatives.”, *Journal of Controlled Release*, Vol. 81, No. 1–2, pp. 91–99, 2002.

366. Jung, E.-Y., I.-D. Chung, N.-J. Lee, J.-S. Park, C.-S. Ha, and W.-J. Cho, “Syntheses, Antitumor Activities, And Antiangiogenesis Of A Monomer And Its Medium Molecular Weight Polymers: Maleimidoethanoyl-5-Fluorouracil And Its Polymers.”, *Journal of Polymer Science A: Polymer Chemistry*, Vol. 38, p. 1247–1256, 2000.

367. Akashi, M., K. Beppu, I. Kikuchi, and N. Miyauchi, “Synthesis And Properties Of Hydrophilic Copolymers Containing 5-Fluorouracil, Thymine, Or Adenine.”, *Journal of Macromolecular Science: Part A - Chemistry*, Vol. 23, No. 10, pp. 1233–1249, 1986.

368. Wada, Y., K. Yoshida, T. Suzuki, H. Mizuiri, K. Konishi, K. Ukon, K. Tanabe, Y. Sakata, and M. Fukushima, “Synergistic Effects Of Docetaxel And S-1 By Modulating The Expression Of Metabolic Enzymes Of 5-Fluorouracil In Human Gastric Cancer Cell Lines.”, *International Journal of Cancer*, Vol. 119, No. 4, pp. 783–791, 2006.

369. Tamatani, T., T. Ferdous, N. Takamaru, K. Hara, M. Kinouchi, N. Kuribayashi, G. Ohe, D. Uchida, H. Nagai, K. Fujisawa, and Y. Miyamoto, “Antitumor Efficacy Of Sequential Treatment With Docetaxel And 5-Fluorouracil Against Human Oral Cancer Cells.”, *International Journal of Oncology*, Vol. 41, No. 3, pp. 1148–1156, 2012.

370. Liu, J., Y. Huang, A. Kumar, A. Tan, S. Jin, A. Mozhi, and X.J. Liang, “PH-Sensitive Nano-Systems For Drug Delivery In Cancer Therapy.”, *Biotechnology Advances*, Vol. 32, No. 4, pp. 693–710, 2014.

APPENDIX A: ADDITIONAL DATA

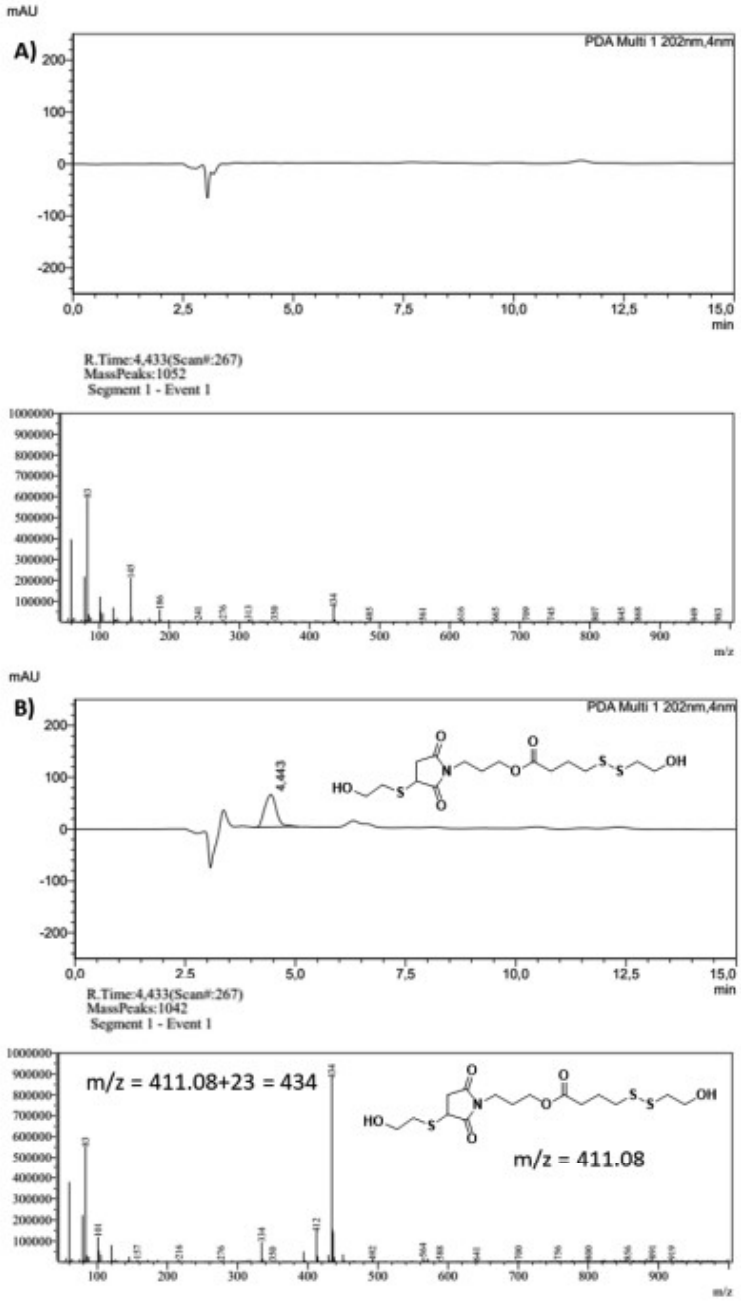

Figure A.1. LC-MS characterization of the solution of the reaction between maleimide-disulfide terminated PEG with (a) the stoichiometric equivalent of 2-mercaptoethanol and (b) four equivalent of 2-mercaptoethanol.

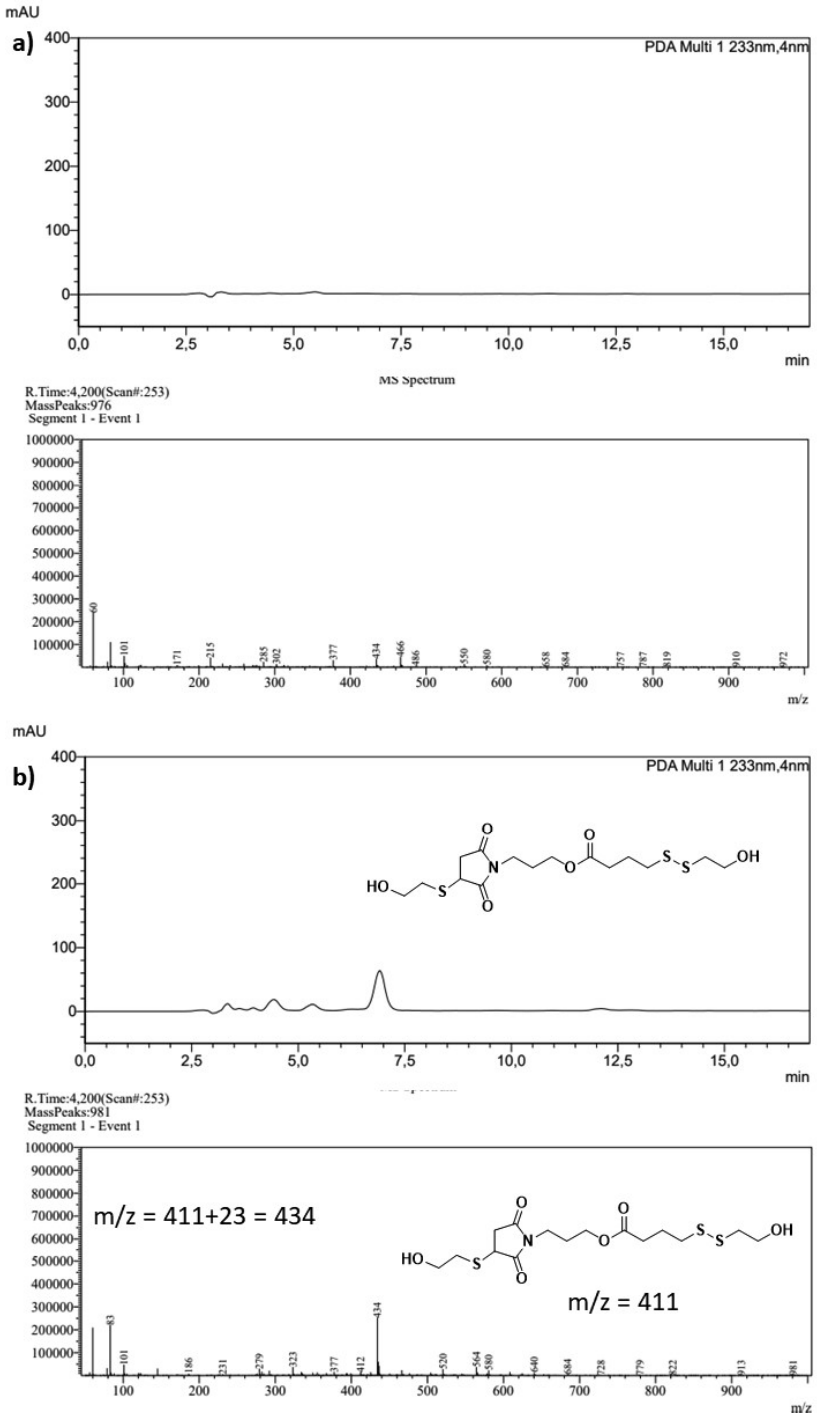

Figure A.2. LC-MS characterization of the solution of the reaction between copolymer with (a) the stoichiometric equivalent of 2-mercaptoethanol and (b) four equivalent of 2-mercaptoethanol.

APPENDIX B: COPYRIGHT NOTICES

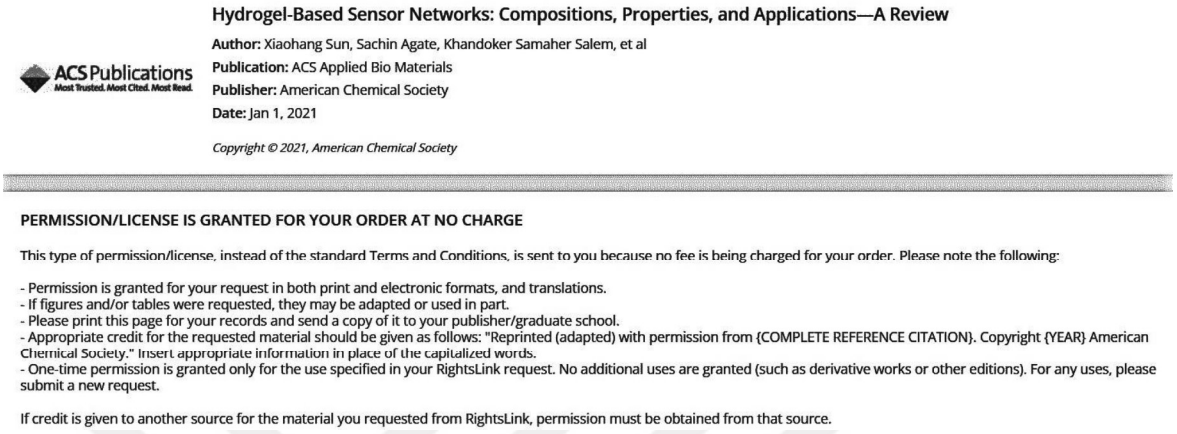

Hydrogel-Based Sensor Networks: Compositions, Properties, and Applications—A Review

Author: Xiaohang Sun, Sachin Agate, Khandoker Samaher Salem, et al
Publication: ACS Applied Bio Materials
Publisher: American Chemical Society
Date: Jan 1, 2021

Copyright © 2021, American Chemical Society

PERMISSION/LICENSE IS GRANTED FOR YOUR ORDER AT NO CHARGE

This type of permission/license, instead of the standard Terms and Conditions, is sent to you because no fee is being charged for your order. Please note the following:

- Permission is granted for your request in both print and electronic formats, and translations.
- If figures and/or tables were requested, they may be adapted or used in part.
- Please print this page for your records and send a copy of it to your publisher/graduate school.
- Appropriate credit for the requested material should be given as follows: "Reprinted (adapted) with permission from {COMPLETE REFERENCE CITATION}. Copyright {YEAR} American Chemical Society." Insert appropriate information in place of the capitalized words.
- One-time permission is granted only for the use specified in your RightsLink request. No additional uses are granted (such as derivative works or other editions). For any uses, please submit a new request.

If credit is given to another source for the material you requested from RightsLink, permission must be obtained from that source.

Figure B.1. Permission for Figure 1.2 from Ref [21].

Order Date	06-Dec-2022	**Type of Use**	Republish in a thesis/dissertation
Order License ID	1297652-1	**Publisher**	John Wiley & Sons
ISSN	2196-7350	**Portion**	Image/photo/illustration

LICENSED CONTENT

Publication Title	Advanced Materials Interfaces	**Rightsholder**	John Wiley & Sons - Books
Article Title	Recent Advances on Designs and Applications of Hydrogel Adhesives	**Publication Type**	e-Journal
		Start Page	2101038
Date	01/01/2014	**Issue**	2
Language	English	**Volume**	9
Country	Germany		

REQUEST DETAILS

Portion Type	Image/photo/illustration	**Distribution**	Worldwide
Number of Images / Photos / Illustrations	1	**Translation**	Original language of publication
Format (select all that apply)	Print	**Copies for the Disabled?**	No
Who Will Republish the Content?	Academic institution	**Minor Editing Privileges?**	No
Duration of Use	Life of current edition	**Incidental Promotional Use?**	No
Lifetime Unit Quantity	Up to 499	**Currency**	USD
Rights Requested	Main product		

NEW WORK DETAILS

Title	SYNTHESIS AND APPLICATION OF STIMULI-RESPONSIVE POLYMERIC MATERIALS FOR DRUG DELIVERY	**Institution Name**	boğaziçi üniversitesi
		Expected Presentation Date	2023-02-15
Instructor Name	ismail altinbasak		

ADDITIONAL DETAILS

The Requesting Person/Organization to Appear on the License	ismail altinbasak

REUSE CONTENT DETAILS

Title, Description or Numeric Reference of the Portion(s)	Figure 1	**Title of the Article/Chapter the Portion Is From**	Recent Advances on Designs and Applications of Hydrogel Adhesives
Editor of Portion(s)	Liu, Xiaowei; Yu, Haojie; Wang, Li; Huang, Zhikun; Haq, Fazal; Teng, Lisong; Jin, Meijin; Ding, Binbin	**Author of Portion(s)**	Liu, Xiaowei; Yu, Haojie; Wang, Li; Huang, Zhikun; Haq, Fazal; Teng, Lisong; Jin, Meijin; Ding, Binbin
Volume of Serial or Monograph	9	**Publication Date of Portion**	2022-01-14
Page or Page Range of Portion	2101038		

Figure B.2. Permission for Figure 1.3 from Ref [28].



1. RSC advances

Billing Status: Open

Article: Best of both worlds: Diels–Alder chemistry towards fabrication of redox-responsive degradable hydroge...

Print License

Order License ID	1297653-1	Type of use	Republish in a thesis/dissert...
Order detail status	Completed	Publisher	RSC Publishing
ISSN	2046-2069	Portion	Image/photo/illustration

0.00 USD

Hide Details

Republication Permission

LICENSED CONTENT

Publication Title	RSC advances	Publication Type	e-Journal
Article Title	Best of both worlds: Diels–Al...	Start Page	74757
Date	01/01/2011	End Page	74764
Language	English	Issue	78
Country	United Kingdom of Great Bri...	Volume	6
Rightsholder	Royal Society of Chemistry	URL	http://pubs.rsc.org/en/Journ...

REQUEST DETAILS

Portion Type	Image/photo/illustration	Distribution	Worldwide
Number of Images / Photos / Illustrations	1	Translation	Original language of publica...
Format (select all that apply)	Print	Copies for the Disabled?	No
Who Will Republish the Content?	Academic institution	Minor Editing Privileges?	No
Duration of Use	Life of current edition	Incidental Promotional Use?	No
Lifetime Unit Quantity	Up to 499	Currency	USD
Rights Requested	Main product		

NEW WORK DETAILS

Title	Best Of Both Worlds: Diels–...	Institution Name	Bogazici University
Instructor Name	ismail altinbasak	Expected Presentation Date	2023-02-15

ADDITIONAL DETAILS

The Requesting Person/Organization to Appear on the License	ismail altınbaşak

REUSE CONTENT DETAILS

Title, Description or Numeric Reference of the Portion(s)	Figure 1	Title of the Article/Chapter the Portion Is From	Best of both worlds: Diels–Al...
Editor of Portion(s)	Altinbasak, Ismail; Sanyal, R...	Author of Portion(s)	Altinbasak, Ismail; Sanyal, R...
Volume of Serial or Monograph	6	Issue, if Republishing an Article From a Serial	78
Page or Page Range of Portion	74757-74764	Publication Date of Portion	2016-08-18

Figure B.3. Permission for Figure 1.4 from Ref [49].

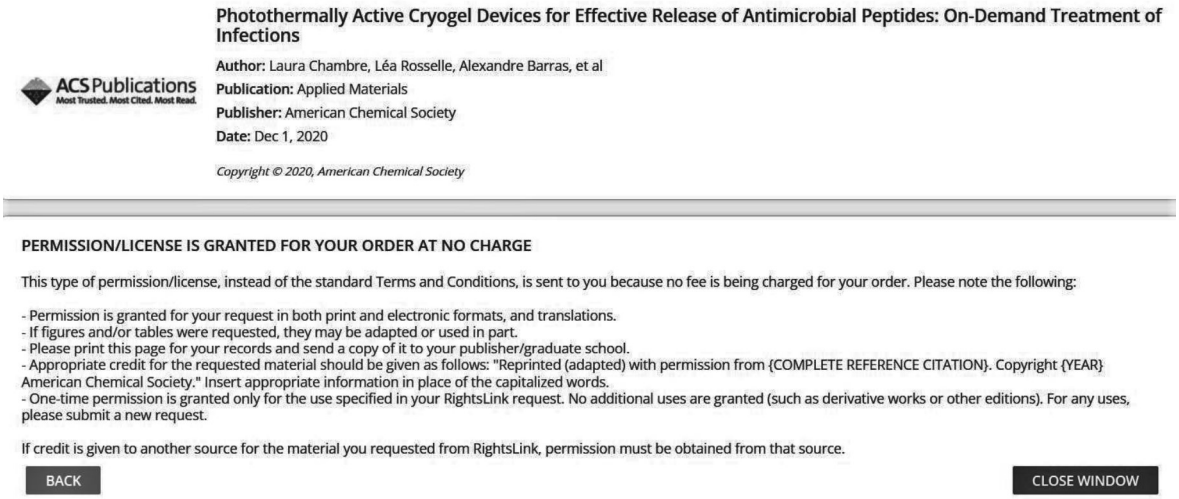

Photothermally Active Cryogel Devices for Effective Release of Antimicrobial Peptides: On-Demand Treatment of Infections

Author: Laura Chambre, Léa Rosselle, Alexandre Barras, et al
Publication: Applied Materials
Publisher: American Chemical Society
Date: Dec 1, 2020

Copyright © 2020, American Chemical Society

PERMISSION/LICENSE IS GRANTED FOR YOUR ORDER AT NO CHARGE

This type of permission/license, instead of the standard Terms and Conditions, is sent to you because no fee is being charged for your order. Please note the following:

- Permission is granted for your request in both print and electronic formats, and translations.
- If figures and/or tables were requested, they may be adapted or used in part.
- Please print this page for your records and send a copy of it to your publisher/graduate school.
- Appropriate credit for the requested material should be given as follows: "Reprinted (adapted) with permission from {COMPLETE REFERENCE CITATION}. Copyright {YEAR} American Chemical Society." Insert appropriate information in place of the capitalized words.
- One-time permission is granted only for the use specified in your RightsLink request. No additional uses are granted (such as derivative works or other editions). For any uses, please submit a new request.

If credit is given to another source for the material you requested from RightsLink, permission must be obtained from that source.

BACK CLOSE WINDOW

Figure B.4. Permission for Figure 1.5 from Ref [57].

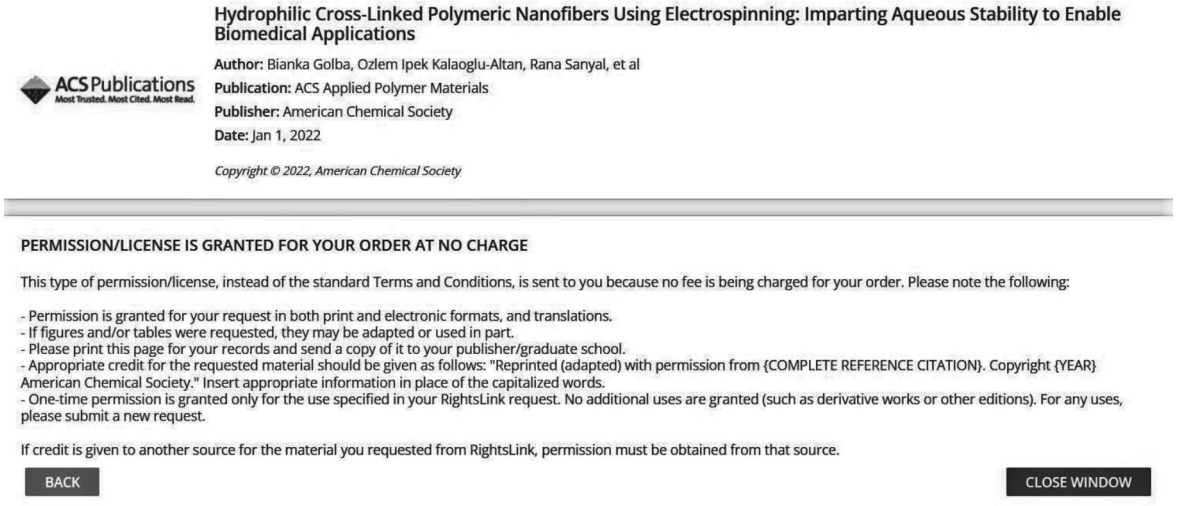

Hydrophilic Cross-Linked Polymeric Nanofibers Using Electrospinning: Imparting Aqueous Stability to Enable Biomedical Applications

Author: Bianka Golba, Ozlem Ipek Kalaoglu-Altan, Rana Sanyal, et al
Publication: ACS Applied Polymer Materials
Publisher: American Chemical Society
Date: Jan 1, 2022

Copyright © 2022, American Chemical Society

PERMISSION/LICENSE IS GRANTED FOR YOUR ORDER AT NO CHARGE

This type of permission/license, instead of the standard Terms and Conditions, is sent to you because no fee is being charged for your order. Please note the following:

- Permission is granted for your request in both print and electronic formats, and translations.
- If figures and/or tables were requested, they may be adapted or used in part.
- Please print this page for your records and send a copy of it to your publisher/graduate school.
- Appropriate credit for the requested material should be given as follows: "Reprinted (adapted) with permission from {COMPLETE REFERENCE CITATION}. Copyright {YEAR} American Chemical Society." Insert appropriate information in place of the capitalized words.
- One-time permission is granted only for the use specified in your RightsLink request. No additional uses are granted (such as derivative works or other editions). For any uses, please submit a new request.

If credit is given to another source for the material you requested from RightsLink, permission must be obtained from that source.

BACK CLOSE WINDOW

Figure B.5. Permission for Figure 1.6 from Ref [58].

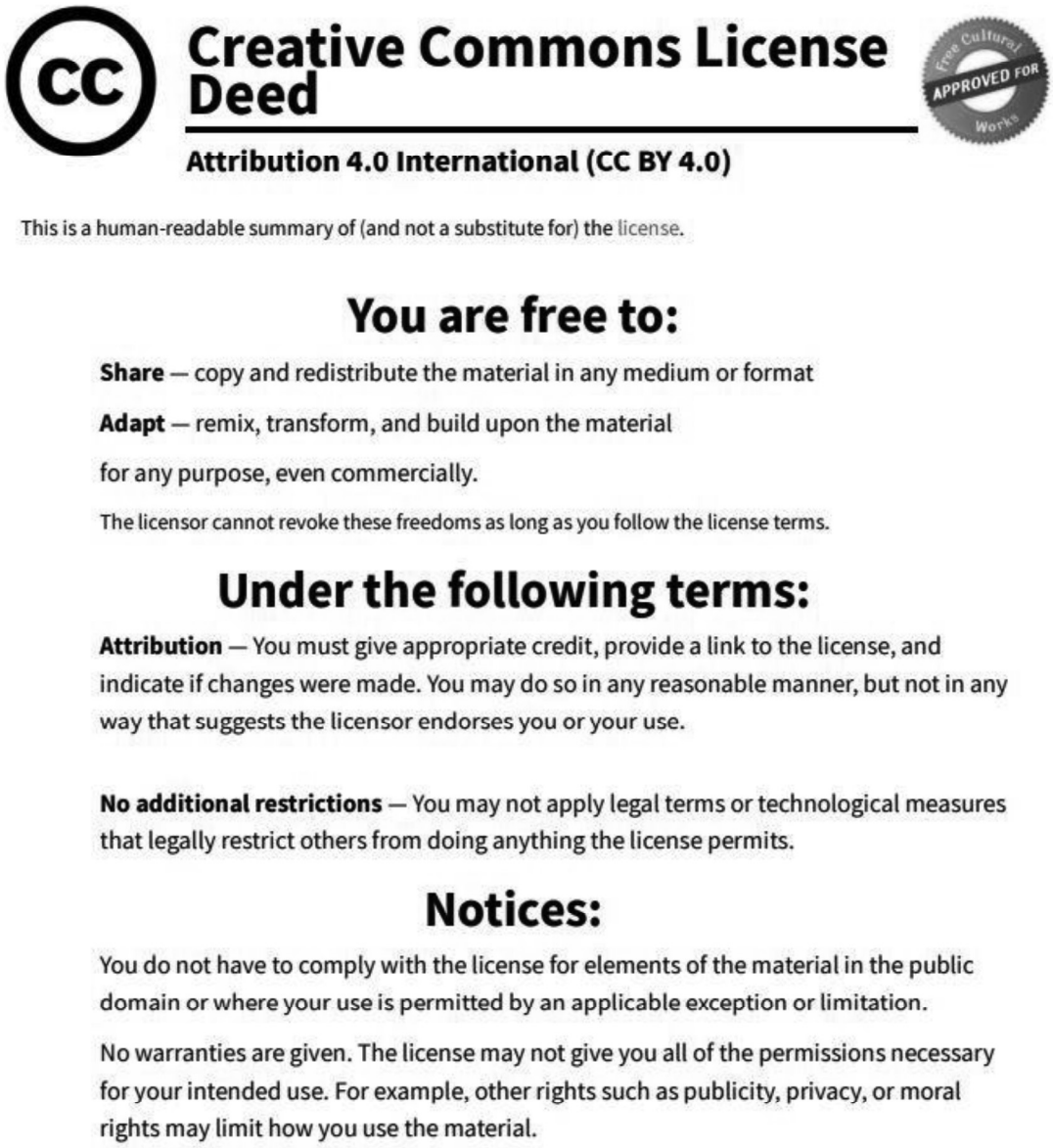

Creative Commons License Deed

Attribution 4.0 International (CC BY 4.0)

This is a human-readable summary of (and not a substitute for) the license.

You are free to:

Share — copy and redistribute the material in any medium or format

Adapt — remix, transform, and build upon the material

for any purpose, even commercially.

The licensor cannot revoke these freedoms as long as you follow the license terms.

Under the following terms:

Attribution — You must give appropriate credit, provide a link to the license, and indicate if changes were made. You may do so in any reasonable manner, but not in any way that suggests the licensor endorses you or your use.

No additional restrictions — You may not apply legal terms or technological measures that legally restrict others from doing anything the license permits.

Notices:

You do not have to comply with the license for elements of the material in the public domain or where your use is permitted by an applicable exception or limitation.

No warranties are given. The license may not give you all of the permissions necessary for your intended use. For example, other rights such as publicity, privacy, or moral rights may limit how you use the material.

Figure B.6. Permission for Figure 1.7 from Ref [75].



Electrospinning polyaniline-contained gelatin nanofibers for tissue engineering applications

Author: Mengyan Li,Yi Guo,Yen Wei,Alan G. MacDiarmid,Peter I. Lelkes
Publication: Biomaterials
Publisher: Elsevier
Date: May 2006

Copyright © 2005 Elsevier Ltd. All rights reserved.

Order Completed

Thank you for your order.

This Agreement between Bogazici University -- ismail altinbasak ("You") and Elsevier ("Elsevier") consists of your license details and the terms and conditions provided by Elsevier and Copyright Clearance Center.

Your confirmation email will contain your order number for future reference.

Printable Details

License Number	5443020197750
License date	Dec 06, 2022

Licensed Content

Licensed Content Publisher	Elsevier
Licensed Content Publication	Biomaterials
Licensed Content Title	Electrospinning polyaniline-contained gelatin nanofibers for tissue engineering applications
Licensed Content Author	Mengyan Li,Yi Guo,Yen Wei,Alan G. MacDiarmid,Peter I. Lelkes
Licensed Content Date	May 1, 2006
Licensed Content Volume	27
Licensed Content Issue	13
Licensed Content Pages	11

Order Details

Type of Use	reuse in a thesis/dissertation
Portion	figures/tables/illustrations
Number of figures/tables/illustrations	1
Format	print
Are you the author of this Elsevier article?	No
Will you be translating?	No

Figure B.7. Permission for Figure 1.8 from Ref [77].

ACS Publications
Most Trusted. Most Cited. Most Read.

Multireactive Poly(2-oxazoline) Nanofibers through Electrospinning with Crosslinking on the Fly

Author: Ozlem I. Kalaoglu-Altan, Bart Verbraeken, Kathleen Lava, et al
Publication: ACS Macro Letters
Publisher: American Chemical Society
Date: Jun 1, 2016

Copyright © 2016, American Chemical Society

PERMISSION/LICENSE IS GRANTED FOR YOUR ORDER AT NO CHARGE

This type of permission/license, instead of the standard Terms and Conditions, is sent to you because no fee is being charged for your order. Please note the following:

- Permission is granted for your request in both print and electronic formats, and translations.
- If figures and/or tables were requested, they may be adapted or used in part.
- Please print this page for your records and send a copy of it to your publisher/graduate school.
- Appropriate credit for the requested material should be given as follows: "Reprinted (adapted) with permission from {COMPLETE REFERENCE CITATION}. Copyright {YEAR} American Chemical Society." Insert appropriate information in place of the capitalized words.
- One-time permission is granted only for the use specified in your RightsLink request. No additional uses are granted (such as derivative works or other editions). For any uses, please submit a new request.

If credit is given to another source for the material you requested from RightsLink, permission must be obtained from that source.

BACK CLOSE WINDOW

Figure B.8. Permission for Figure 1.9 from Ref [79].

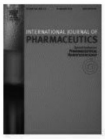

Electrospun fibers of acid-labile biodegradable polymers with acetal groups as potential drug carriers

Author: Wenguo Cui,Mingbo Qi,Xiaohong Li,Shaozhou Huang,Shaobing Zhou,Jie Weng
Publication: International Journal of Pharmaceutics
Publisher: Elsevier
Date: 1 September 2008

Copyright © 2008 Elsevier B.V. All rights reserved.

Review Order

Please review the order details and the associated terms and conditions.

No royalties will be charged for this reuse request although you are required to obtain a license and comply with the license terms and conditions. To obtain the license, click the Accept button below.

Licensed Content

Licensed Content Publisher	Elsevier
Licensed Content Publication	International Journal of Pharmaceutics
Licensed Content Title	Electrospun fibers of acid-labile biodegradable polymers with acetal groups as potential drug carriers
Licensed Content Author	Wenguo Cui,Mingbo Qi,Xiaohong Li,Shaozhou Huang,Shaobing Zhou,Jie Weng
Licensed Content Date	1 September 2008
Licensed Content Volume	361
Licensed Content Issue	1-2
Licensed Content Pages	9

Order Details

Type of Use	reuse in a thesis/dissertation
Portion	figures/tables/illustrations
Number of figures/tables/illustrations	1
Format	print
Are you the author of this Elsevier article?	No
Will you be translating?	No

About Your Work

Title	SYNTHESIS AND APPLICATION OF STIMULI-RESPONSIVE POLYMERIC MATERIALS FOR DRUG DELIVERY
Institution name	bogazici university
Expected presentation date	Feb 2023

Additional Data

Order reference number	ismail altinbasak
Portions	Figure 6

Figure B.9. Permission for Figure 1.10 from Ref [84].

Utilizing Inverse Emulsion Polymerization To Generate Responsive Nanogels for Cytosolic Protein Delivery

Author: Kishore Raghupathi, Scott J. Eron, Francesca Anson, et al
Publication: Molecular Pharmaceutics
Publisher: American Chemical Society
Date: Dec 1, 2017

Copyright © 2017, American Chemical Society

PERMISSION/LICENSE IS GRANTED FOR YOUR ORDER AT NO CHARGE

This type of permission/license, instead of the standard Terms and Conditions, is sent to you because no fee is being charged for your order. Please note the following:

- Permission is granted for your request in both print and electronic formats, and translations.
- If figures and/or tables were requested, they may be adapted or used in part.
- Please print this page for your records and send a copy of it to your publisher/graduate school.
- Appropriate credit for the requested material should be given as follows: "Reprinted (adapted) with permission from {COMPLETE REFERENCE CITATION}. Copyright {YEAR} American Chemical Society." Insert appropriate information in place of the capitalized words.
- One-time permission is granted only for the use specified in your RightsLink request. No additional uses are granted (such as derivative works or other editions). For any uses, please submit a new request.

If credit is given to another source for the material you requested from RightsLink, permission must be obtained from that source.

BACK CLOSE WIN

Figure B.10. Permission for Figure 1.12 from Ref [99].

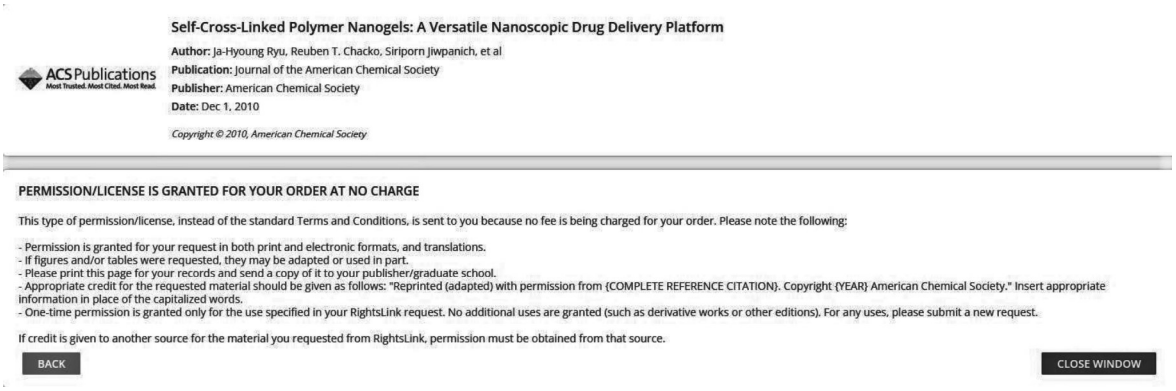

Self-Cross-Linked Polymer Nanogels: A Versatile Nanoscopic Drug Delivery Platform

Author: Ja-Hyoung Ryu, Reuben T. Chacko, Siriporn Jiwpanich, et al
Publication: Journal of the American Chemical Society
Publisher: American Chemical Society
Date: Dec 1, 2010

Copyright © 2010, American Chemical Society

PERMISSION/LICENSE IS GRANTED FOR YOUR ORDER AT NO CHARGE

This type of permission/license, instead of the standard Terms and Conditions, is sent to you because no fee is being charged for your order. Please note the following:

- Permission is granted for your request in both print and electronic formats, and translations.
- If figures and/or tables were requested, they may be adapted or used in part.
- Please print this page for your records and send a copy of it to your publisher/graduate school.
- Appropriate credit for the requested material should be given as follows: "Reprinted (adapted) with permission from {COMPLETE REFERENCE CITATION}. Copyright {YEAR} American Chemical Society." Insert appropriate information in place of the capitalized words.
- One-time permission is granted only for the use specified in your RightsLink request. No additional uses are granted (such as derivative works or other editions). For any uses, please submit a new request.

If credit is given to another source for the material you requested from RightsLink, permission must be obtained from that source.

BACK CLOSE WINDOW

Figure B.11. Permission for Figure 1.13 from Ref [103].



LICENSED CONTENT

Publication Title	Wiley interdisciplinary reviews. Nanomedicine and nanobiotechnology	**Publication Type**	Journal
Article Title	Applications of polymer micelles for imaging and drug delivery.	**Start Page**	691
Date	01/01/2008	**End Page**	707
Language	English	**Issue**	5
Country	United States of America	**Volume**	7
Rightsholder	John Wiley & Sons - Books		

REQUEST DETAILS

Portion Type	Image/photo/illustration	**Distribution**	Worldwide
Number of Images / Photos / Illustrations	1	**Translation**	Original language of publication
Format (select all that apply)	Print	**Copies for the Disabled?**	No
Who Will Republish the Content?	Academic institution	**Minor Editing Privileges?**	No
Duration of Use	Life of current edition	**Incidental Promotional Use?**	No
Lifetime Unit Quantity	Up to 499	**Currency**	USD
Rights Requested	Main product		

NEW WORK DETAILS

Title	TARGETED AND CONTROLLED DELIVERY OF DRUGS USING NANO AND MACRO POLYMERIC MATERIALS: HYDROGELS, NANOFIBERS, NANOGELS AND MICELLES	**Institution Name**	bogazici university
		Expected Presentation Date	2023-02-15
Instructor Name	ismail altinbasak		

ADDITIONAL DETAILS

The Requesting Person/Organization to Appear on the License	ismail altinbasak

REUSE CONTENT DETAILS

Title, Description or Numeric Reference of the Portion(s)	Figure 1	**Title of the Article/Chapter the Portion Is From**	Applications of polymer micelles for imaging and drug delivery.
Editor of Portion(s)	Movassaghian, Sara; Merkel, Olivia M.; Torchilin, Vladimir P.	**Author of Portion(s)**	Movassaghian, Sara; Merkel, Olivia M.; Torchilin, Vladimir P.
Volume of Serial or Monograph	7	**Publication Date of Portion**	2015-09-01
Page or Page Range of Portion	691-707		

Figure B.12. Permission for Figure 1.14 from Ref [112].

1. Biomaterials science **0.00 USD**

Article: Trastuzumab targeted micellar delivery of docetaxel using dendron-polymer conjugates.

ISSN	2047-4830	**Publisher**	Royal Society of Chemistry
Type of Use	Republish in a thesis/dissertation	**Portion**	Image/photo/illustration

Hide Details

LICENSED CONTENT

Publication Title	Biomaterials science	**Rightsholder**	Royal Society of Chemistry
Article Title	Trastuzumab targeted micellar delivery of docetaxel using dendron-polymer conjugates.	**Publication Type**	Journal
		Start Page	2600
Author/Editor	Kyōto Daigaku.Busshitsu-Saibō Tōgō Shisutemu Kyoten, Royal Society of Chemistry (Great Britain)	**End Page**	2610
		Issue	9
		Volume	8
Date	01/01/2013		
Language	English		
Country	United Kingdom of Great Britain and Northern Ireland		

REQUEST DETAILS

Portion Type	Image/photo/illustration	**Distribution**	Worldwide
Number of Images / Photos / Illustrations	1	**Translation**	Original language of publication
		Copies for the Disabled?	No
Format (select all that apply)	Print	**Minor Editing Privileges?**	No
Who Will Republish the Content?	Academic institution	**Incidental Promotional Use?**	No
Duration of Use	Life of current edition	**Currency**	USD
Lifetime Unit Quantity	Up to 499		
Rights Requested	Main product		

NEW WORK DETAILS

Title	TARGETED AND CONTROLLED DELIVERY OF DRUGS USING NANO AND MACRO POLYMERIC MATERIALS: HYDROGELS, NANOFIBERS, NANOGELS AND MICELLES	**Institution Name**	Bogazici University
		Expected Presentation Date	2023-02-15
Instructor Name	ismail altinbasak		

Figure B.13. Permission for Figure 1.15 from Ref [119].

Dendron–Polymer Conjugate Based Cross-Linked Micelles: A Robust and Versatile Nanosystem for Targeted Delivery

Author: Filiz Calik, Aysun Degirmenci, Melike Eceoglu, et al
Publication: Bioconjugate Chemistry
Publisher: American Chemical Society
Date: Apr 1, 2019

Copyright © 2019, American Chemical Society

PERMISSION/LICENSE IS GRANTED FOR YOUR ORDER AT NO CHARGE

This type of permission/license, instead of the standard Terms and Conditions, is sent to you because no fee is being charged for your order. Please note the following:

- Permission is granted for your request in both print and electronic formats, and translations.
- If figures and/or tables were requested, they may be adapted or used in part.
- Please print this page for your records and send a copy of it to your publisher/graduate school.
- Appropriate credit for the requested material should be given as follows: "Reprinted (adapted) with permission from {COMPLETE REFERENCE CITATION}. Copyright {YEAR} American Chemical Society." Insert appropriate information in place of the capitalized words.
- One-time permission is granted only for the use specified in your RightsLink request. No additional uses are granted (such as derivative works or other editions). For any uses, please submit a new request.

If credit is given to another source for the material you requested from RightsLink, permission must be obtained from that source.

BACK CLOSE WINDOW

Figure B.14. Permission for Figure 1.16 from Ref [123].

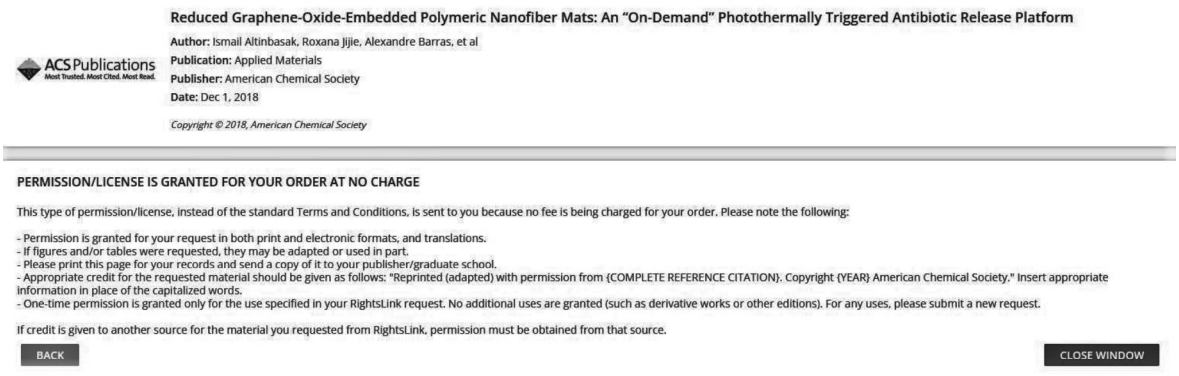

Reduced Graphene-Oxide-Embedded Polymeric Nanofiber Mats: An "On-Demand" Photothermally Triggered Antibiotic Release Platform

Author: Ismail Altinbasak, Roxana Jijie, Alexandre Barras, et al
Publication: Applied Materials
Publisher: American Chemical Society
Date: Dec 1, 2018

Copyright © 2018, American Chemical Society

PERMISSION/LICENSE IS GRANTED FOR YOUR ORDER AT NO CHARGE

This type of permission/license, instead of the standard Terms and Conditions, is sent to you because no fee is being charged for your order. Please note the following:

- Permission is granted for your request in both print and electronic formats, and translations.
- If figures and/or tables were requested, they may be adapted or used in part.
- Please print this page for your records and send a copy of it to your publisher/graduate school.
- Appropriate credit for the requested material should be given as follows: "Reprinted (adapted) with permission from {COMPLETE REFERENCE CITATION}. Copyright {YEAR} American Chemical Society." Insert appropriate information in place of the capitalized words.
- One-time permission is granted only for the use specified in your RightsLink request. No additional uses are granted (such as derivative works or other editions). For any uses, please submit a new request.

If credit is given to another source for the material you requested from RightsLink, permission must be obtained from that source.

BACK CLOSE WINDOW

Figure B.15. Permission for Chapter 3 from Ref [129].



Request ID	600105187	**Request Date**	12 Dec 2022
Request Status	Accepted	**Price**	0.00 USD

ALL DETAILS

ISSN:	2047-4830	**Publisher:**	Royal Society of Chemistry
Type of Use:	Republish in a thesis/dissertation	**Portion:**	Chapter/article

LICENSED CONTENT

Publication Title	Biomaterials science	**Language**	English
Article Title	pH-Responsive Nanofiber Buttresses a...	**Country**	United Kingdom of Great Britain and N...
Author/Editor	Kyōto Daigaku.Busshitsu-Saibō Tōgō S...	**Rightsholder**	Royal Society of Chemistry
Date	01/01/2013	**Publication Type**	Journal

REQUEST DETAILS

Page Range(s)	1-9	**Distribution**	Worldwide
Total Number of Pages	9	**Translation**	Original language of publication
Format (select all that apply)	Print	**Copies for the Disabled?**	No
Who Will Republish the Content?	Author of requested content	**Minor Editing Privileges?**	No
Duration of Use	Life of current edition	**Incidental Promotional Use?**	No
Lifetime Unit Quantity	Up to 499	**Currency**	USD
Rights Requested	Main product		

NEW WORK DETAILS

Title	TARGETED AND CONTROLLED DELIVER...	**Institution Name**	Bogazici University
Instructor Name	ismail altinbasak	**Expected Presentation Date**	2023-02-15

ADDITIONAL DETAILS

The Requesting Person/Organization to Appear on the License	ismail altinbasak

REUSE CONTENT DETAILS

Title, Description or Numeric Reference of the Portion(s)	full article	**Title of the Article/Chapter the Portion Is From**	pH-Responsive Nanofiber Buttresses a...
Editor of Portion(s)	Altinbasak, Ismail; Kocak, Salli; Colby, A...	**Author of Portion(s)**	Altinbasak, Ismail; Kocak, Salli; Colby, A...
Volume of Serial or Monograph	N/A	**Publication Date of Portion**	2023-01-01
Page or Page Range of Portion	1-9		

Figure B.16. Permission for Chapter 4 from Ref [184].

American Chemical Society's Policy on Theses and Dissertations

This policy addresses permission to include **your article**(s) or portions of text from **your article**(s) in your thesis.

Reuse/Republication of the Entire Work in Theses or Collections: Authors may reuse all or part of the Submitted, Accepted or Published Work in a thesis or dissertation that the author writes and is required to submit to satisfy the criteria of degree-granting institutions. Such reuse is permitted subject to the ACS' "Ethical Guidelines to Publication of Chemical Research". Appropriate citation of the Published Work must be made as follows

"Reprinted with permission from [COMPLETE REFERENCE CITATION]. Copyright [YEAR] American Chemical Society." Insert the appropriate wording in place of the capitalized words. Citation information may be found after the "Cite this:" heading below the title of the online version and at the bottom of **the first page of the pdf or print version of your ACS journal article**.

If the thesis or dissertation to be published is in electronic format, a direct link to the Published Work must also be included using the ACS Articles on Request author-directed link.

If your university requires written permission and your manuscript has not yet received a DOI (published ASAP), send a request to copyright@acs.org that includes the manuscript number, the name of the ACS journal, and the date that you need to receive our reply.

If your university requires you to obtain permission for manuscripts in ASAP status or final published articles, you must use the RightsLink permission system. **See RightsLink instructions at http://pubs.acs.org/page/copyright/permissions.html and make requests at the "Rights & Permissions" link under the title of the online version of the article.**

Submission to a Dissertation Distributor: If you plan to submit your thesis to UMI or to another dissertation distributor, you should not include the unpublished ACS paper in your thesis if the thesis will be disseminated electronically, until ACS has published your paper. After publication of the paper by ACS, you may release the entire thesis (**not the individual ACS article by itself**) for electronic dissemination through the distributor; ACS's copyright credit line should be printed on the first page of the ACS paper.

Updated: 07/2021

Figure B.17. Permission for Chapter 5 from Ref [239].